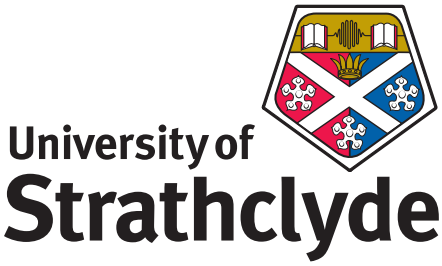

Refinable Stable Local Bivariate Spline Bases on Powell-Sabin-12 Triangulations

Wee Ping Yeo

Department of Mathematics and Statistics

University of Strathclyde

Glasgow, UK

December 2013

This thesis is submitted to the University of Strathclyde for the degree of Doctor of Philosophy in the Faculty of Science.

Acknowledgements

First of all, I wish to express my sincere thanks and appreciation to my supervisor Dr Oleg Davydov, for his valuable guidance, encouragement and generous support. Without him, this thesis would not have been completed.

I also thank my friends Abid, HongRui, Gaelle, Fabi, Omer, Richard, Eusebio and Marita for their supports and various kinds of help.

I would also like to acknowledge the Government of Brunei Darussalam for providing the scholarship for my studies.

Finally, I am grateful to my parents, my wife Jenny and daughter Adrienna for their love, support and encouragement throughout the period of my studies.

Abstract

In this thesis, we investigate the hierarchical bases of C^1 quadratic spline functions on Powell-Sabin-12 triangulations and their applications to surface compression and numerical solutions of the biharmonic equation. We also construct C^2 quintic refinable spaces of spline functions on the Powell-Sabin-12 triangulations.

We first show that a nested sequence of C^r macro-element spline spaces on quasi-uniform triangulations gives rise to hierarchical Riesz bases of Sobolev spaces $H^s(\Omega)$, $1 < s < r + \frac{3}{2}$, and $H_0^s(\Omega)$, $1 < s < \sigma + \frac{3}{2}$, $s \notin \mathbb{Z} + \frac{1}{2}$, as soon as there is a nested sequence of Lagrange interpolation sets with uniformly local and bounded basis functions, and, in case of $H_0^s(\Omega)$, the nodal interpolation operators associated with the macro-element spaces are boundary conforming of order $\sigma \leq r$.

Starting with a nested sequence of C^1 piecewise quadratic macro-element spaces which is generated by uniform refinements and combined Powell-Sabin-6 and -12 splits on arbitrary polygonal domains $\Omega \subset \mathbb{R}^2$ we construct hierarchical bases of Lagrange type. Properly normalised, these bases are Riesz bases for Sobolev spaces $H^s(\Omega)$, with $s \in (1, \frac{5}{2})$ and $H_0^s(\Omega)$ for $s \in (1, 3/2) \cup (3/2, 5/2)$. Compared to the previously constructed C^1 Lagrange hierarchical bases of [21, 41] which require some special partitions of the initial triangulations, our bases are constructed on general triangulations. Our bases have larger stability range for $H^s(\Omega)$ compared to the C^1 wavelet bases of [33] and the C^1 Hermite type hierarchical bases of [14, 49].

Numerical results are presented to show the advantages of our Lagrange hierarchical basis in compressing surfaces. Since this basis is a Riesz basis for the space

$H_0^2(\Omega)$, we also investigate the use of the hierarchical basis as a preconditioner for solving the biharmonic equation.

In addition, we propose a construction of refinable spaces of C^2 macro-elements of degree 5 on triangulations of a polygonal domain obtained by uniform refinements of an initial triangulation and a Powell-Sabin-12 split. The new refinable macro-elements have stable local minimal determining sets (MDS). Therefore they can be used to construct nested spline spaces which possess stable local bases and also achieve optimal approximation power.

Contents

Chapter 1

Introduction

1.1 Introduction

Let Δ be a triangulation of a domain in $\mathbb{R}^2$. Given integers $0 \leq r < d$, we write the space of splines

$$S_d^r(\Delta) := \{s \in C^r(\Omega) : s|_T \in \mathbb{P}_d \text{ for all } T \in \Delta\},$$

where $\mathbb{P}_d$ is the space of polynomials of degree d. Spline functions are well known as highly effective tools in approximation theory, computer aided geometric design, image analysis and numerical analysis. The application of $S_d^r(\Delta)$ splines in numerical computations usually requires stable local bases for the space $S_d^r(\Delta)$ or its subspaces. It is well known that the space $S_d^r(\Delta)$ possesses stable local bases for any regular triangulation only if $d \geq 3r+2$, see [20]. In order to obtain a spline space with C^1 smoothness we need to consider either C^1 quintic polynomials with 21 degrees of freedom on each triangle or to use lower degree macro-element spaces that subdivide each triangle into a number of subtriangles. For example, the well-known macro-element spaces are the Clough-Tocher, Powell-Sabin-6 and -12 macro-element spaces.

Let $S(\Delta_R)$ be a subspace of $S_d^r(\Delta)$ where Δ_R is a refinement of Δ obtained by applying a given splitting procedure to each triangle of Δ. Suppose in addition

that every spline $s \in S(\Delta_R)$ is uniquely determined by the values of s and its derivatives at some collection of points in Ω. Then $S(\Delta_R)$ is called a *macro-element space* provided that for each triangle in Δ, $s|_T$ is uniquely determined by the data at points in T. There are many examples of macro-element spaces. For a comprehensive study of macro-element spaces, see Lai and Schumaker [36]. Macro-element spaces are particularly important in applications since they are available on arbitrary polygonal domains, they generally have stable local bases and have full approximation power. This means that they approximate sufficiently smooth functions to $\mathcal{O}(h_\Delta^{d+1})$, where h_Δ is the mesh size of Δ, that is, the length of the longest edge in Δ. In this work we are interested in the case where Δ_R is obtained by applying Powell-Sabin splits [53] to each of the triangles in Δ, in particular the Powell-Sabin-12 split (Δ_{PS12}), see Fig.1.1. Here each triangle is divided into 12 subtriangles by connecting each vertex of the triangle to the midpoint of the opposite edge and connecting the midpoints. Given function values and gradients at the vertices of a triangle and normal derivatives at the midpoints of edges, a unique C^1 quadratic spline which interpolates this data is determined [53]. We call the resulting spline space $S(\Delta_{PS12})$ the C^1 *Powell-Sabin-12 macro-element space*. A spline $s \in S(\Delta_{PS12})$ can be represented piecewise using a Bernstein-

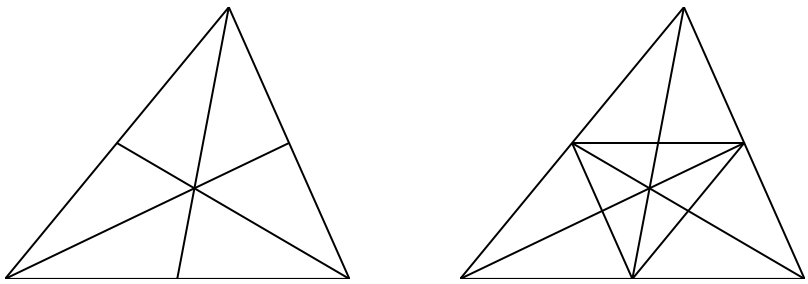

Figure 1.1: Left: Powell-Sabin-6 split, and right: Powell-Sabin-12 split.

Bézeir representation on each triangle in Δ_{PS12} and it can be easily evaluated using the de Casteljau Algorithm [36]. Alternatively, a subdivision scheme based on Hermite interpolation for the Powell-Sabin-12 split introduced by Dyn and

Lyche in [26] can be used to evaluate a C^1 quadratic Powell-Sabin-12 spline on an arbitrary triangulation. In applications, and in particular for scattered data fitting and the solution of boundary-value problems by the finite element method, it is advantageous to work with macro-element spaces that produce a given order of approximation while involving the least number of degrees of freedom. In [2] Alfeld *et al.* show that certain degrees of freedom can be removed from the C^1 Powell-Sabin-12 macro-element without losing any approximation power. The C^1 *reduced* macro-element space was constructed by requiring the normal derivatives at the midpoints of edges be linear rather than piecewise linear. This reduced space is then uniquely defined with only function values and gradients at the vertices. They also showed that the space has a stable local nodal minimal determining set and full approximation power. See also the paper [9] of Chui and He for discussions on Powell-Sabin macro-element spaces. There is also a recent paper [10] by Cohen *et al.* where a simplex spline basis for C^1 Powell-Sabin-12 macro-element is introduced. For higher smoothness Powell-Sabin-12 elements, see the paper [54] of Schumaker and Sorokina.

In our work we are particularly interested in refinable spline spaces. Given a sequence of triangulations $\Delta_0, \Delta_1, \ldots, \Delta_n, \ldots$, such that Δ_n is a refinement of Δ_{n-1} for each n, suppose that $S_0, S_1, \ldots, S_n, \ldots$, is a sequence of spline spaces defined on these triangulations. If $S_{n-1} \subset S_n$ for each n, then we say that the sequence of spline spaces is *refinable* or *nested*. Nested sequences of splines play an important role in the numerical solution of partial differential equations, see [49, 14, 37]. They have also been used for surface compression in [32, 42]. The spaces $S_d^r(\Delta)$ are nested for any choice of $0 \leq r < d$. However, many other sequences of spline spaces are not nested. For example, the superspline subspaces [36, Definition 5.6] of $S_d^r(\Delta)$ are not nested since a given superspline on level n will not have the needed "supersmoothness" at the vertices of the macro triangles to belong to space of level $n+1$. Now we would like to note that Powell-Sabin-12 split has the refinability property if we subdivide a triangle in $T \in \Delta$ into four

similar subtriangles by connecting midpoints of edges. Then applying the Powell-Sabin-12 split on each of the subtriangles we obtain a spline space of C^1 piecewise quadratic polynomials which contains the spline space of C^1 piecewise quadratic polynomials defined on the Powell-Sabin-12 split of T as a subspace. This shows that the space $S(\Delta_{PS12})$ is *refinable* and therefore nested spline spaces with stable local bases can be constructed. The nested spaces are therefore suitable for the multiresolution analysis [12, 13, 14, 17, 19, 21, 22, 24, 29, 33, 49, 50], with applications in particular to multilevel methods in numerical partial differential equations and surface modelling. Recently, Jia and Liu in [33] introduced a refinable space of C^1 piecewise quadratic polynomials on combination of Powell-Sabin-6 and Powell-Sabin-12 splits. The refinable space in [33] was employed to construct spline wavelets. Besides C^1 piecewise quadratic Powell-Sabin-12 element, there are other notable approaches to constructing refinable C^1 spline spaces. They are cubic Fraeijs de Veubeke-Sanders C^1 macro-elements, see [21, 32] and C^1 quadratic macro-element on Powell-Sabin-6 triangulations, see [11, 41, 42, 43]. For recent survey of refinable multivariate spline functions, see the paper [29] of Goodman and Hardin.

Starting with a nested sequence of spline spaces one can now build a multilevel basis for it. The idea is to construct them recursively by adding to the basis from the previous space a set of locally supported functions spanning a complement space such that the union is a basis of the current space. In particular, in this work we will use *hierarchical bases* meaning that the functions that are added are just a subset of a *single level* basis for the space of the current level. For piecewise linear functions on general triangulations, Yserentant [58] constructed hierarchical bases and introduced the idea to use hierarchical bases as preconditioners in the finite element application to solve second order elliptic boundary value problems when using the conjugate gradient method. The hierarchical bases of [58] give rise to *Riesz* (stable) bases for the Sobolev spaces $H^s(\Omega), s \in (1, 3/2)$, in 2D with a suboptimal stability result for the case $s = 1$, leading to logarithmically growing

condition numbers of the related stiffness matrices. In [49] Oswald constructed hierarchical bases on general triangulations using refinable C^1 quadratic and cubic Powell-Sabin-12 macro-element spline spaces. The hierarchical bases are of Hermite type which means that they are derived from the Hermite interpolation functionals. The hierarchical bases studied in [49] are introduced for preconditioning the finite element equations for fourth-order elliptic boundary value problems. Motivated by the same problem, [14] constructed hierarchical bases of C^1 quintics splines, which are also of Hermite type. These C^1 hierarchical bases are Riesz bases for the Sobolev spaces $H^s(\Omega)$ with $s \in (2, 5/2)$, with a suboptimal stability result for the case $s = 2$. That is using the associated hierarchical bases as preconditioners will lead to logarithmically growing condition numbers of stiffness matrices related to fourth order elliptic equations. These C^1 hierarchical bases are of Hermite type, which restricts the range of stability to values $s > 2$, since, by the Sobolev embedding theorem, the corresponding Hermite interpolation operator is only well defined for functions in $H^s(\Omega), s > 2$. Taking that into consideration, the construction of hierarchical bases based on C^1 macro-elements of Lagrange type instead of Hermite type allows to enlarge the range of stability from $s \in (2, 5/2)$ to $s \in (1, 5/2)$.

Hierarchical bases are employed for surface compression. Surface compression using C^2 quadratic wavelets of certain box-spline spaces was studied in [25]. The application of hierarchical bases in surface compression was first proposed by Hong and Schumaker in [32]. In [32] a surface compression method was constructed for the space of C^1 cubic splines defined on triangulations obtained from convex quadrangulations. Later Maes and Bultheel [42] construct a compression method for the space of C^1 quadratic splines on Powell-Sabin-6 triangulations. The hierarchical basis of [32] is of Hermite type and the hierarchical basis of [42] is constructed using quasi-interpolation schemes.

Lagrange bases with local support were constructed in [44, 45, 46] for C^1 cubic splines on triangulation generated by triangulated quadrangulations and for

C^1 quadratic Powell-Sabin-6 macro-element spaces in [47]. In [21] Davydov and Stevenson constructed the first C^1 hierarchical bases of Lagrange type where the nested spline spaces are macro-element spaces of C^1 piecewise cubic polynomials [36, Section 6.5] on certain triangulations obtained from checkerboard quadrangulations of any polygonal domain and the nestedness of the space is obtained by a *triadic* refinement scheme. The Lagrange interpolation points are chosen so that the sequence of Lagrange interpolation sets $\{\Xi_n\}_{n=0}^{\infty}$ for the corresponding spaces S_n is *nested*, that is $\Xi_0 \subset \Xi_1 \subset \ldots \subset \Xi_n \subset \ldots$ and hence a corresponding hierarchical basis can be constructed. The C^1 Lagrange hierarchical bases of [21] generate Riesz bases for Sobolev space $H^s(\Omega), s \in (1, 5/2)$, which is an optimal result for $s = 2$. Later, Maes and Butheel in [41] also constructed a C^1 hierarchical basis of Lagrange type. The nested spline spaces are C^1 Powell-Sabin-6 macro-elements and the nested sequence of triangulations is obtained by a triadic refinement of the Powell-Sabin-6 split. Here an initial triangulation is obtained from a certain checkerboard quadrangulation of the polygonal domain. We note that the constructions of C^1 hierarchical bases of Lagrange type in [21, 41] require some special partitions of the initial triangulations of polygonal domains. Furthermore, the construction in [41] only leads to Riesz bases under the assumption that the resulting nested family of triangulations is regular. We say a sequence of triangulations is regular if the minimum angle of all triangulations in the sequence of triangulations remains bounded below by a positive constant $\beta > 0$ independent on the refinement level n. This is a standard property required in the multilevel methods. Although not shown in [21], the sequence of triangulations suggested there is always regular as we verify in Chapter 2 Proposition 2.12. Besides the hierarchical Riesz bases, there are also Riesz bases of wavelet type. On general triangulations of polygonal domains, Jia and Liu [33] constructed cubic spline wavelet bases based on orthogonal projection operators which lead to Riesz bases for $H^s(\Omega), s \in (1.618, 5/2)$. On unit square, Jia and Zhao [34] constructed bicubic splines wavelet bases which lead to Riesz bases for $H^s(\Omega), s \in (1, 5/2)$.

As a central result of this work, in Chapter 3, we construct C^1 Lagrange hierarchical Riesz bases for the Sobolev spaces $H^s(\Omega)$ for $s \in (1, 5/2)$ and $H_0^s(\Omega)$ for $s \in (1, 3/2) \cup (3/2, 5/2)$ on general triangulations of arbitrary polygonal domains $\Omega \in \mathbb{R}^2$. We note that our construction gives a larger range of stability compared to [33]. Our method can be applied to any polygonal domain in contrast to [34] where the method is only available on the unit square. We also would like to note that no numerical results are available for the numerical schemes based on the hierarchical bases of Lagrange type [21, 41] and wavelet bases of [33]. We have implemented our method and numerical results are presented in Chapter 4.

We have seen from the above discussion the effectiveness of using hierarchical basis as a preconditioner is related to the Riesz basis (or "stability") property of this hierarchical basis in the Sobolev spaces $H^s(\Omega)$, and $H_0^s(\Omega)$ in the case of homogeneous boundary conditions. In [34], Jia and Zhao developed a general theory for multilevel Riesz bases of Hilbert spaces. Under the guidance of the general theory, they were able to construct wavelet bases for Sobolev spaces on the unit square. The similar theory is also studied in [33]. The key ingredient for establishing the stability properties is the norm equivalence of the form

$$\|f\|_{H_s} \sim \inf_{f_n \in S_n:\, f=\sum_{n=0}^{\infty} f_n} \Big(\sum_{n=0}^{\infty} \big[\rho^{ns} \|f_n\|_{L_2(\Omega)}\big]^2 \Big)^{1/2}, \qquad f \in H_s. \tag{1.1.1}$$

with $H_s = H^s(\Omega)$ or $H_0^s(\Omega)$ and ρ being the refinement factor. The norm equivalence can be established using the arguments similar to those in Oswald [50], Theorem 6 and [13]. The following *Jackson inequality* of the form

$$\inf_{g \in S_n} \|f - g\|_{L_2(\Omega)} \lesssim \rho^{-n(k+1)} |f|_{H^{k+1}(\Omega)}, \quad f \in H^{k+1}(\Omega), \quad r < k \le d, \tag{1.1.2}$$

plays an important role in getting the estimate (1.1.1). The Jackson inequality (1.1.2) can be obtained by using quasi-interpolation operators for any spline space S with a stable local basis, see [18] and [36]. However, if one has to establish (1.1.1) for $H_s = H_0^s$ one would first require the Jackson estimate (1.1.2) to hold for all $f \in H_0^{k+1}$. But this can be established if the interpolation operators Π_n associated

with the spline spaces S_n are boundary conforming of order r in the sense that for any function f vanishing on the boundary of Ω together with its derivatives up to order r, the interpolants $\Pi_n f$ satisfy the same property. This is normally true for macro-element spaces. We note that the results for spaces $H_0^s(\Omega)$ have not been established before. In Chapter 2, with the focus on the macro-element spaces due to the availability of boundary conforming interpolation operators that allow appropriate treatment of subspaces with zero boundary conditions, we present general conditions for the nested sequences of macro-element spline spaces to give rise to Riesz basis in $H^s(\Omega)$ and $H_0^s(\Omega)$.

We have already mentioned some examples of macro-element spaces, in particular the refinable macro-element spaces which are of our interest in this work. We note that refinable macro-element spaces we have seen so far are of C^1 smoothness. In fact refinable macro-element spaces of higher smoothness have not been known yet. Constructing such spaces is non-trivial, and depending on the nature of the type of split Δ_R used. Usually one would require working with supersplines, that means that the splines space will need to satisfy certain smoothness conditions at the vertices higher than the degree of smoothness enforced across the edges. We know that supersplines are usually not refinable because of the supersmoothness conditions at the vertices. For a construction of refinable sequences of special superspline spaces, see [17]. As the last part of this work, in Chapter 5, we present a construction of C^2 refinable macro-element spaces on Powell-Sabin-12 triangulations, whose degree 5 is substantially lower than the degree 8 of the C^2 spline spaces of [20] and degree 9 of the refinable C^2 superspline spaces of [17]. The nestedness of the spaces is achieved by relaxing the C^3 smoothness conditions at the vertices of macro-triangles, which allows to break the 'super-smoothness disks' at the vertices into half-disks.

1.2 Organisation of this Thesis

Here is the outline of this thesis.

In **Chapter 2** we study the general conditions for the nested sequences of macro-element spline spaces to give rise to Riesz bases in $H^s(\Omega)$ and $H_0^s(\Omega)$. We first establish the Bernstein inequality for spline spaces with stable local bases. We then proceed to derive the Jackson inequality for macro-element spline spaces where we only assume that the nodal basis is uniformly bounded. We then present a general theory which shows that a nested sequence of C^r macro-element spaces with nested Lagrange interpolation sets and uniformly bounded and local basis functions, generates hierarchical Riesz bases for the Sobolev spaces $H^s(\Omega)$ for $s \in (1, r + 5/2)$, and for $H_0^s(\Omega)$ for $s \in (1, \sigma + 3/2) \setminus (\mathbb{Z} + 1/2)$ when the nodal interpolation operators related to the macro-elements are boundary conforming of order σ. In the last part of the chapter, we review the existing constructions of C^1 Lagrange type hierarchical Riesz bases for Sobolev spaces. In particular, we verify that the triadic refinement underlying the construction of [21] leads to quasi-uniform triangulations.

In **Chapter 3** we construct Lagrange bases for the spaces of C^1 piecewise quadratic polynomials on the combination of Powell-Sabin-6 and Powell-Sabin-12 triangulations introduced in [33]. We prove that the Lagrange bases are uniformly stable and local. We then consider the multilevel setting and construct hierarchical bases of Lagrange basis functions and prove that they form Riesz (stable) bases for the Sobolev spaces $H^s(\Omega), s \in (1, 5/2)$ and $H_0^s(\Omega)$, $s \in (1, 3/2) \cup (3/2, 5/2)$ using the general theory developed in Chapter 2.

In **Chapter 4** we first investigate the performance of our hierarchical bases constructed in Chapter 3 for surface compression. Numerical test results show the advantages of the Lagrange hierarchical bases for this application. The last part of this chapter is devoted to solving the biharmonic equation $\Delta^2 u = f$. We numerically compare the multilevel preconditioners of hierarchical and BPX type

based on both Lagrange and Hermite basis functions.

In **Chapter 5** we propose a construction of refinable C^2 macro-elements of degree 5 on Powell-Sabin-12 triangulations. We show that the macro-element spaces have stable local minimal determining sets (MDS) and also stable local nodal minimal determining sets (NMDS). We also provide explicit formulas for all B-coefficients which are not computed directly by the standard smoothness conditions so that the proposed macro-elements can be easily implemented in the framework of the Bernstein-Bézier techniques.

Chapter 6 provides a conclusion and indicates possible directions for future research.

Throughout we employ the usual notation $a \lesssim b$ and $a \sim b$ to indicate that the inequality (respectively, the double inequality) includes bounding constants which are not of interest. The parameters on which these constants may depend are either explicitly mentioned or clear from the context.

1.3 Preliminaries

The aim of this section is to introduce standard definitions from the theory of bivariate piecewise polynomial splines as described in the book of Lai and Schumaker [36], which will be used throughout the thesis.

1.3.1 Sobolev spaces

Let Ω be a bounded domain in $\mathbb{R}^2$. Suppose $1 \leq p \leq \infty$ and $k \in \mathbb{N}$. Then *Sobolev space* is defined by

$$W_p^k(\Omega) = \{f : \|f\|_{W_p^k(\Omega)} < \infty\},$$

where

$$\|f\|_{W_p^k(\Omega)} = \begin{cases} \left(\sum_{i=0}^{k} |f|^p_{W_p^i(\Omega)} \right)^{1/p}, & 1 \leq p < \infty, \\ \sum_{i=0}^{k} |f|_{W_\infty^i(\Omega)}, & p = \infty, \end{cases}$$

with

$$|f|_{W_p^i(\Omega)} = \begin{cases} \left(\sum_{\nu+\mu=i} \|D_x^\nu D_y^\mu f\|^p_{L_p(\Omega)} \right)^{1/p}, & 1 \leq p < \infty, \\ \max_{\nu+\mu=i} \|D_x^\nu D_y^\mu f\|_{L_\infty(\Omega)}, & p = \infty. \end{cases}$$

Thus the space W_p^k consists of all functions f in $L_p(\Omega)$ whose partial derivatives of order less than or equal to k belong to $L_p(\Omega)$. For a good reference work concerning Sobolev spaces, see [1].

1.3.2 Bivariate Spline Functions on Triangulations

Let Ω be a polygonal domain in $\mathbb{R}^2$ and Δ a finite collection of triangles whose union coincides with Ω. We assume that the intersection of any two triangles in Δ is empty, or a common vertex, or a common edge of them. Then Δ is a *triangulation* of Ω. The length of an edge e of Δ is denoted by $|e|$. Let ξ be the set of all edges of Δ. The maximum length of the edges of Δ, denoted by

$h = h_\Delta = \sup_{e\in\xi} |e|$, is called the *diameter* or *mesh size* of Δ. Given a triangle $T \in \Delta$, we denote the *diameter* of T by $\mathrm{diam}(T)$, which refers to the length of its longest edge. We denote the smallest angle of the triangles $T \in \Delta$ by β_Δ, and set

$$\gamma_\Delta = \min\{\mathrm{diam}(T) : T \in \Delta\}/h_\Delta.$$

A family of triangulations is called *regular* if $\beta_\Delta \geq \beta > 0$ for every Δ in the family. A regular family is said to be *quasi-uniform* if $\gamma_\Delta \geq \gamma > 0$ for every Δ.

For any positive integer d, let $S_d(\Delta)$ denote the space of all piecewise polynomials of degree d with respect to Δ. In other words, $s \in S_d(\Delta)$ if and only if, on each triangle $T \in \Delta$, s agrees with a polynomial in $\mathbb{P}_d$, the space of all bivariate polynomials of total degree at most d. For any $r = 0, 1, \ldots, d-1$, let

$$S_d^r(\Delta) := S_d(\Delta) \cap C^r(\Omega)$$

be the space of all piecewise polynomials of degree d and smoothness r with respect to Δ.

Let $\{s_1, \ldots, s_N\}$ be a basis for a linear space $S \subset S_d(\Delta)$. We say that the basis is *m-local* if for each $i = 1, \ldots, N$ there is a triangle $T_i \in \Delta$ such that $\mathrm{supp}\, s_i \subset \mathrm{star}^m(T_i)$. Here $\mathrm{star}^k(T) := \mathrm{star}(\mathrm{star}^{k-1}(T))$ for $k \geq 2$, where if U is the union of a cluster of triangles, then $\mathrm{star}(U) = \mathrm{star}^1(U)$ is the union of all triangles in Δ that have a non-empty intersection with U. A basis is called *local* if it is m-local for some m.

Suppose that $\{\lambda_1, \ldots, \lambda_N\} \subset S^*$ is the dual basis, that is,

$$\lambda_i s_j = \begin{cases} 1, & i = j, \\ 0, & \text{otherwise.} \end{cases}$$

A basis $\{s_1, \ldots, s_N\}$ for $S \subset S_d(\Delta)$ is said to be a *stable local basis* [16] if for an integer m and positive constants C_1, C_2,

(a) $\{s_1, \ldots, s_N\}$ is m-local,

(b) $|\lambda_i s| \leq C_1 \|s\|_{L_\infty(\mathrm{star}^m(T_i))}$ for all $s \in S$, $i = 1, \ldots, N$, and

(c) $\|s_i\|_{L_\infty(\Omega)} \le C_2$, $i = 1, \ldots, N$.

Any stable local basis is *L_p-stable* for all $1 \le p \le \infty$ after appropriate renorming, that is, for any $\alpha = (\alpha_1, \ldots, \alpha_N) \in \mathbb{R}^N$,

$$k_1 C_2^{-1} \|\alpha\|_{l_p} \le \Big\| \sum_{i=1}^{N} \alpha_i \frac{s_i}{|\operatorname{supp} s_i|^{1/p}} \Big\|_{L_p(\Omega)} \le k_2 C_1 \|\alpha\|_{l_p}, \quad 1 \le p \le \infty,$$

where k_1, k_2 are some constants depending only on p, r, d and m, and $|M|$ denotes the area of a set $M \subset \mathbb{R}^2$.

1.3.3 Bernstein-Bézier techniques

Given a nondegenerate triangle T (one with nonzero area) in $\mathbb{R}^2$ with vertices $v_i := (x_i, y_i)$, $i = 1, 2, 3$. Let v be any arbitraty point in $\mathbb{R}^2$ with Cartesian coordinates (x, y). We define the *barycentric coordinates* b_1, b_2, b_3 of v with respect to T as the unique solution of the system

$$\begin{bmatrix} 1 & 1 & 1 \\ x_1 & x_2 & x_3 \\ y_1 & y_2 & y_3 \end{bmatrix} \begin{bmatrix} b_1 \\ b_2 \\ b_3 \end{bmatrix} = \begin{bmatrix} 1 \\ x \\ y \end{bmatrix}.$$

Any bivariate polynomial p of total degree d on T can be uniquely represented in the form

$$p = \sum_{i+j+k=d} c_{ijk} B_{ijk}^{T,d}, \tag{1.3.1}$$

with

$$B_{ijk}^{T,d} = \frac{d!}{i!j!k!} b_1^i b_2^j b_3^k$$

the *Bernstein basis polynomials* of degree d associated with T. We refer to the representation (1.3.1) as the *B-form* of p related to T. The c_{ijk}'s are called the *B-coefficients* of p, and the associated set of *domain points* is defined by

$$\mathcal{D}_{d,T} := \left\{ \xi_{ijk} := \frac{i v_1 + j v_2 + k v_3}{d} \right\}_{i+j+k=d}. \tag{1.3.2}$$

Given a triangulation $\Delta = \{T_i\}_{i=1}^N$ of a bounded connected polygonal domain $\Omega \subseteq \mathbb{R}^2$ and a positive integer d, we define the corresponding set of domain points

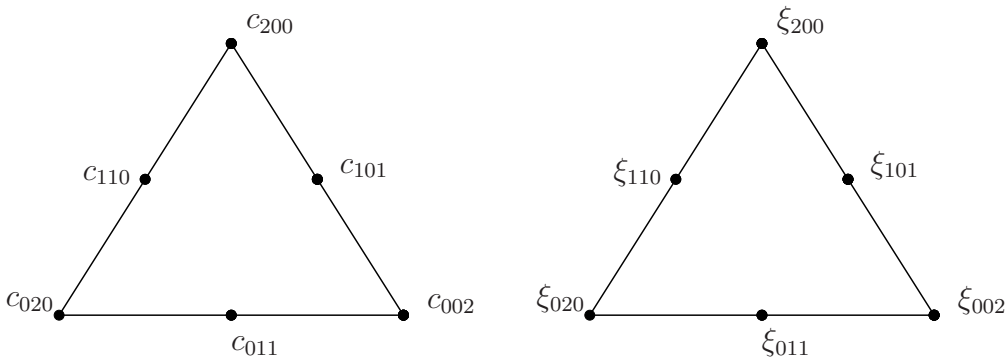

Figure 1.2: Domain points ξ_{ijk} and B-coefficients c_{ijk} of a quadratic polynomial.

by

$$\mathcal{D}_{d,\Delta} := \bigcup_{T\in\Delta} D_{d,T}.$$

Given $s \in S_d^0(\Delta)$ and $T \in \Delta$, there exists a unique set of coefficients $\{c_\xi\}_{\xi\in\mathcal{D}_{d,T}}$ such that

$$s|_T = \sum_{\xi\in\mathcal{D}_{d,T}} c_\xi B_\xi^{T,d},$$

and each spline in $S_d^0(\Delta)$ is uniquely determined by its set of B-coefficients $\{c_\xi\}_{\xi\in\mathcal{D}_{d,\Delta}}$.

Given $0 \le m \le d$ and $T := \langle v_1, v_2, v_3\rangle$, we say that a domain point ξ_{ijk} is at a *distance* $\mathrm{dist}(\xi, v_1) = d-i$ from the vertex v_1 and at a distance $\mathrm{dist}(\xi, e_1) = i$ from the edge $e_1 = \langle v_2, v_3\rangle$ opposite to v_1. Furthermore, we refer to the set of domain points $R_m^T(v_1) := \{\xi_{d-m,j,m-j}\}_{j=0}^m$ as the *ring* of radius m around the vertex v_1. We refer to the set $D_m^T(v_1) := \bigcup_{n=0}^m R_n^T(v_1)$ as the *disk* of radius m around the vertex v_1. The rings and disks around v_2 and v_3 are defined similarly. If v is a vertex of Δ with triangles $T_1, \ldots, T_k$ attached to it, then the ring and the disk of radius m around v are defined by $R_m(v) = \bigcup_{i=1}^k R_m^{T_i}(v)$ and $D_m(v) = \bigcup_{i=1}^k D_m^{T_i}(v)$, respectively.

Suppose now that S is a linear subspace of $S_d^0(\Delta)$ defined by enforcing some set of smoothness conditions across the edges of the triangulation Δ. Then a *determining set* for S is a subset M of the set of domain points $\mathcal{D}_{d,\Delta}$ such that if we set the B-coefficients c_ξ of some spline $s \in S$ to zero for all $\xi \in M$, then $s \equiv 0$. If M is a determining set for a spline space S and M has the smallest cardinality

among all possible determining sets for S, then we call M *a minimal determining set* (MDS) for S. It is known that M is a MDS for S if and only if every spline $s \in S$ is uniquely determined by its set of B-coefficients $\{c_\xi\}_{\xi \in M}$.

An MDS M is called *local* provided that there is an integer ℓ such that for every $\xi \in \mathcal{D}_{d,\Delta} \cap T$ and every $T \in \Delta$, the B-coefficient c_ξ of a spline $s \in S$ is a linear combination of $\{c_\eta\}_{\eta \in \Gamma_\xi}$ where Γ_ξ is a subset of M with $\Gamma_\xi \subset \text{star}^\ell(T)$. Moreover, M is said to be *stable* provided that there is a constant K depending only on d and the smallest angle in Δ such that

$$|c_\xi| \leq K \max_{\eta \in \Gamma_\xi} |c_\eta|, \qquad \text{for all } \xi \in \mathcal{D}_{d,\Delta}.$$

We say that a spline $s \in S_d^0(\Delta)$ is C^ρ smooth at the vertex v provided that all polynomials $s|_T$ such that T is a triangle with vertex at v have common partial derivatives up to order ρ at the point v. In this case we write $s \in C^\rho(v)$.

Smoothness across an edge is described with the help of smoothness functionals defined as follows. Let $T = \langle v_1, v_2, v_3 \rangle$ and $\tilde{T} = \langle v_4, v_3, v_2 \rangle$ be two adjoining triangles which share the edge $e = \langle v_2, v_3 \rangle$, and let c_{ijk} and $\tilde{c}_{ijk}$ be the coefficients of the B-representations of s_T and $s_{\tilde{T}}$, respectively. Then for any $n \leq m \leq d$, let $\tau_{e,m}^n$ be the linear functional defined on $S_d^0(\Delta)$ by

$$\tau_{e,m}^n s = \tilde{c}_{n,m-n,d-m} - \sum_{i+j+k=n} c_{i,j+d-m,k+m-n} B_{ijk}^{T,n}(v_4). \tag{1.3.3}$$

In terms of these linear functionals, the condition that s be C^r smooth across the edge e is equivalent to

$$\tau_{e,m}^n s = 0, \quad n \leq m \leq d, \ 0 \leq n \leq r.$$

1.3.4 Macro-Element Spline Spaces

A linear functional λ is called a *nodal functional* provided λf is a scalar multiple of the value of f or its (directional) partial derivative at some point $\eta = \eta(\lambda) \in \mathbb{R}^2$, that is $\lambda f = \gamma \frac{\partial^{\nu+\mu} f}{\partial \sigma^\nu \partial \tau^\mu}(\eta)$, for suitable $\nu, \mu \in \mathbb{Z}_+$, $\eta \in \Omega$, unit vectors σ, τ, and a scaling coefficient $\gamma \in \mathbb{R}$. The number $\kappa(\lambda) = \nu + \mu$ is called the *order* of λ.

A collection $\mathcal{N} = \{\lambda_i\}_{i=1}^N$ is called a *nodal determining set* for a spline space $S \subset S_d(\Delta)$ if every $s \in S$ is $\kappa(\lambda)$ times continuously differentiable at $\eta(\lambda)$, and $\lambda s = 0$ for all $\lambda \in \mathcal{N}$ implies $s \equiv 0$. $\mathcal{N}$ is called a *nodal minimal determining set* (NMDS) for S if there is no smaller nodal determining set. In other words, $\mathcal{N}$ is an NMDS if it is a basis for the dual S^* of S. Let $\{s_i\}_{i=1}^N$ be the basis of S dual to $\mathcal{N}$, called the *nodal basis*.

We will work with spaces of splines that are defined on triangulations $\Delta_R = \bigcup_{K\in\Delta} K_R$ obtained from a given partition Δ of Ω into polygonal cells K by applying some refinement process to each $K \in \Delta$. Examples are provided by well-known Clough-Tocher and Powell-Sabin splits of the triangles of a triangulation Δ of Ω. We assume that each K is star-shaped with respect to a disk. We denote by χ_K the *chunkiness parameter* $\operatorname{diam} K/\rho_{\max}$ of K, where $\rho_{\max}$ is the maximum radius of disks with respect to which K is star-shaped [7, Section 4.3]. Recall that χ_K is bounded in terms of the minimum angle of K if K is a triangle. We set $\chi_\Delta := \max_{K\in\Delta} \chi_K$.

For each cell $K \in \Delta$, we define

$$\mathcal{N}_K = \{\lambda \in \mathcal{N} : \eta(\lambda) \in K\}.$$

We call $S \subset S_d(\Delta_R)$ a *macro-element space* provided there is a NMDS $\mathcal{N}$ for S such that for each $K \in \Delta$, $S|_K$ is uniquely determined from the values $\{\lambda s\}_{\lambda\in\mathcal{N}_K}$. It is easy to see that the support of a basis function s_i in a macro-element space is contained in the union of all $K \in \Delta$ containing $\eta(\lambda_i)$. For each $\lambda_i \in \mathcal{N}$, we choose the scaling coefficient γ to be equal to $\gamma_i = \operatorname{diam}(T_i)^{\kappa(\lambda_i)}$, where $T_i \in \Delta_R$ is a triangle containing $\eta(\lambda_i)$. Note that $\operatorname{diam}(T_i) \sim \operatorname{diam}(T')$ for any other triangle $T' \in \Delta_R$ sharing a vertex with T_i, with the constant of equivalence depending only on β_{Δ_R}, see [36, Section 4.7], and $\operatorname{diam}(T_i) \sim \operatorname{diam}(K)$, where $T_i \subset K \in \Delta$, and the constant of equivalence depends only on β_{Δ_R} and $\nu_{\Delta_R} := \max_{K\in\Delta} |K_R|$. Then by Markov inequality [36, Theorem 2.32] $|\lambda_i s| \le C_1 \|s\|_{L_\infty(T_i)}$ for any $s \in S$, where C_1 depends only on d, $\kappa(S) := \max_i \kappa(\lambda_i)$ and β_{Δ_R}. It follows that $\{s_i\}_{i=1}^N$ is a

stable local basis for S with parameters depending only on d, $\kappa(S)$, β_{Δ_R} and ν_{Δ_R} as soon as $\|s_i\|_{L_\infty(\Omega)} \le C_2$, $i = 1, \dots, N$, for some constant C_2.

The interpolation operator $\Pi : C^{\kappa(S)}(\Omega) \to S$ is defined by

$$\Pi f = \sum_{i=1}^{N} \lambda_i(f) s_i. \tag{1.3.4}$$

By the duality of the basis functions s_i, it is clear that $\Pi s = s$ for all $s \in S$. In particular, Π reproduces polynomials of degree at most k if $\mathbb{P}_k \subset S$. The definition of the macro-element space implies that the *local interpolation operators* $\Pi_K : C^{\kappa(S)}(K) \to S|_K$,

$$\Pi_K f = \sum_{i:\, \eta(\lambda_i) \in K} \lambda_i(f) s_i$$

satisfy $\Pi_K f = (\Pi f)|_K$ for $f \in C^{\kappa(S)}(\Omega)$.

We say that the interpolation operator Π is *boundary conforming* of order σ if the homogeneous boundary conditions of order σ are preserved by the interpolant, that is, if

$$\frac{\partial^{\nu+\mu} f}{\partial x^\nu \partial y^\mu} = 0 \quad \text{on } \partial\Omega, \qquad \text{for all} \quad \nu, \mu \ge 0, \quad \nu + \mu \le \sigma,$$

implies

$$\Pi f \in S_{0,\sigma} := \{ s \in S : \frac{\partial^{\nu+\mu} s}{\partial x^\nu \partial y^\mu} = 0 \text{ on } \partial\Omega, \text{ for all } \nu, \mu \ge 0,\ \nu + \mu \le \sigma \}.$$

Using the Bernstein-Bézeir techniques, we say a NMDS $\mathcal{N}$ is *local* provided that there exists an integer l not depending on Δ such that for every $s \in S$, $K \in \Delta$, and $\xi \in \mathcal{D}_{d,K}$ the B-coefficients c_ξ of s can be computed from the nodal data at points in $\mathrm{star}^l(K)$. Moreover, $\mathcal{N}$ is said to be *stable* provided there exists a constant $\mathcal{K}$ depending on l and the smallest angle in Δ such that for every $s \in S$, $K \in \Delta$, and $\xi \in \mathcal{D}_{d,K}$,

$$|c_\xi| \le \mathcal{K} \sum_{\nu=0}^{\kappa(S)} \mathrm{diam}(K)^\nu |s|_{W^\nu_\infty(\mathrm{star}^l(K))},$$

where $|\cdot|_{W^{\nu}_{\infty}(\mathrm{star}^l(K))}$ denotes the standard Sobolev semi-norm. Given a stable local NMDS for spline space S, the corresponding *nodal basis* $\{s_i\}_{i=1}^N$ is a stable local basis for S, see [36, pp. 144], in the sense of the definition in Section 1.3.2.

The following result gives an error bound for (Hemite) nodal interpolation with a spline space S possessing a stable local NMDS.

Theorem 1.1. *[36, Theorem 5.26] Suppose $\mathcal{N}$ is a stable local nodal minimal determining set for a spline space S. Let Π be the associated (Hermite) nodal interpolation operator defined in* (1.3.4)*. Then there exists a constant $\mathcal{K}$ depending only on d, l and the smallest angle in Δ such that for every $f \in C^r(\Omega)$ with $\kappa(S) \leq r \leq d+1$,*

$$\|D_x^{\alpha} D_y^{\beta}(f - \Pi f)\|_{L_\infty(\Omega)} \leq \mathcal{K} h_{\Delta}^{r-\alpha-\beta} |f|_{W^r_\infty(\Omega)}$$

for all $0 \leq \alpha + \beta \leq r - 1$.

1.3.5 Hierarchical Bases

Given a nested sequence of finite dimensional spaces of real-valued functions

$$S_0 \subset S_1 \subset S_2 \subset \ldots S_n.$$

Each of the space S_n has a finite basis and then a set of functions

$$\Phi := \bigcup_{k=0}^{n} \{\phi_i^{(k)}\}_{i=1}^{n_k}$$

is said to be a *hierarchical basis* for S_n given that

$$\Phi_m := \bigcup_{k=0}^{m} \{\phi_i^{(k)}\}_{i=1}^{n_k}$$

is a basis for S_m for each $m = 0, 1, \ldots, n$. Then every $s \in S_n$ can be written in the form

$$s = \sum_{m=0}^{n} \sum_{i=1}^{n_m} c_i^{(m)} \phi_i^{(m)}, \tag{1.3.5}$$

and the partial sums

$$s_k = \sum_{m=0}^{k} \sum_{i=1}^{n_m} c_i^{(m)} \phi_i^{(m)}$$

are functions in the space S_k for each $k = 0, 1, \ldots, n$.

Chapter 2

Macro-Element Hierarchical Riesz Bases

2.1 Introduction

Given a sequence of nested spline spaces $S_0 \subset S_1 \subset \cdots \subset S_n \subset \cdots$, and corresponding nested interpolation sets $\Xi_0 \subset \Xi_1 \subset \cdots \subset \Xi_n \subset \cdots$ with Lagrange bases $\{B_\xi^{(n)}\}_{\xi\in\Xi_n}$, *hierarchical bases* are obtained from the appropriately re-scaled functions

$$B_\xi^{(n)}, \quad \xi \in \Xi_n \setminus \Xi_{n-1}, \qquad n = 0, 1, \ldots \ (\Xi_{-1} := \emptyset).$$

The most famous example is given by the piecewise linear basis functions (hat functions), where the hierarchical basis is used for the multilevel preconditioning of the discretised second order elliptic equations [57]. The effectiveness of this method is related to the Riesz basis (or "stability") property of this hierarchical basis in the Sobolev spaces $H^s(\Omega)$ and $H_0^s(\Omega)$, $1 < s < \frac{3}{2}$. For elliptic equations of fourth order, stability in $H^2(\Omega)$ and $H_0^2(\Omega)$ is needed, and this can be achieved by C^1 hierarchical bases [21] that are Riesz bases in the range $1 < s < \frac{5}{2}$. In fact, as noted in [39], bases with stability in $H^s(\Omega)$ with as large as possible range of s is advantageous, in particular when an elliptic operator includes parts of different

order. Moreover, a good preconditioning effect is expected when s corresponding to a given variational problem lies in the central part of the stability interval, see [39].

In this chapter we study general conditions for the nested sequences of macro-element spline spaces to give rise to Riesz bases in $H^s(\Omega)$ and $H_0^s(\Omega)$. The main result (see Theorem 2.11) shows that the stability range $1 < s < r + \frac{3}{2}$ in $H^s(\Omega)$ is guaranteed for refinable C^r macro-elements on quasi-uniform triangulations in $\mathbb{R}^2$ if the Lagrange bases $\{B_\xi^{(n)}\}_{\xi\in\Xi_n}$ are uniformly local and bounded, and the nodal bases of the macro-element spaces are also uniformly bounded. Moreover, the same stability range (up to the half-integer values) is obtained in $H_0^s(\Omega)$ if the macro-element nodal (Hermite) interpolation operators Π_n are *boundary conforming* of order r in the sense that for any function f vanishing on the boundary of Ω together with its derivatives up to order r, the interpolants $\Pi_n f$ have the same property. These results are published in the paper [23].

In Section 2.2 we list some auxiliary results on K-functionals, interpolation spaces and Sobolev spaces $H^s(\Omega)$ and $H_0^s(\Omega)$. Section 2.3 is devoted to Bernstein and Jackson inequalities for bivariate splines, including the Bernstein inequality in $H^s(\Omega)$ for spline spaces possessing stable local bases, and error bounds for the macro-element nodal interpolation of functions in Sobolev spaces of integer order. General results on hierarchical bases of Lagrange type are given in Section 2.4, whereas C^1 macro-element spaces where such bases are known are reviewed in Section 2.5. In particular, we verify that the sequence of nested triangulations suggested in [21] is quasi-uniform.

2.2 Preliminaries

We denote by $W_p^k(\Omega)$, $k \in \mathbb{N}$, $1 \le p \le \infty$, the usual Sobolev spaces on a bounded Lipschitz domain $\Omega \subset \mathbb{R}^n$. The space $C^k(\Omega) \subset W_\infty^k(\Omega)$ consists of all k times continuously differentiable functions f on the closure of Ω, with $\|f\|_{C^k(\Omega)} = \|f\|_{W_\infty^k(\Omega)}$.

The space $W_2^k(\Omega)$ is also denoted by $H^k(\Omega)$, with $H^0(\Omega) := L_2(\Omega)$. It is a Hilbert space with inner product

$$\langle f, g\rangle_{H^k(\Omega)} = \langle f, g\rangle_{L_2(\Omega)} + \sum_{|\alpha|=k} \left\langle \frac{\partial^\alpha f}{\partial x^\alpha}, \frac{\partial^\alpha g}{\partial x^\alpha} \right\rangle_{L_2(\Omega)},$$

where $\alpha = (\alpha_1, \ldots, \alpha_n) \in \mathbb{Z}_+^n$ is a multi-index, with $|\alpha| := \alpha_1 + \cdots + \alpha_n$.

Let X and $Y \subset X$ be two Hilbert spaces with norms $\|\cdot\|_X$ and $\|\cdot\|_Y = \|\cdot\|_X + |\cdot|_Y$, respectively, where $|\cdot|_Y$ is a seminorm. The K-functional is defined for each $f \in X$ and $t > 0$ by

$$K_{XY}(f, t) := \inf_{g \in Y} \|f - g\|_X + t|g|_Y,$$

or equivalently (see [40, Remark 4.8]) by the same expression with $|g|_Y$ replaced by $\|g\|_Y$.

One of the key properties of the K-functional is the following Jackson type inequality.

Lemma 2.1. *Let S be linear subspace of X. Suppose that for some $t > 0$,*

$$\inf_{s \in S} \|g - s\|_X \le t|g|_Y, \quad \textit{for all} \quad g \in Y.$$

Then for any $f \in X$,

$$\inf_{s \in S} \|f - s\|_X \le K_{XY}(f, t).$$

Proof. Indeed,

$$\inf_{s \in S} \|f - s\|_X \le \inf_{g \in Y} \inf_{s \in S} (\|f - g\|_X + \|g - s\|_X) \le K_{XY}(f, t)$$

if the assumption holds. □

According to the K-method [3], the interpolation space $[X, Y]_\theta$, $0 < \theta < 1$, consists of all $f \in X$ for which the functional

$$|f|_{\theta;K} = \left(\int_0^\infty \left(t^{-\theta} K_{XY}(f, t) \right)^2 \frac{dt}{t} \right)^{1/2} \tag{2.2.1}$$

is finite.

For each $f \in X$, by taking $g = 0$, we obtain

$$K_{XY}(f,t) \le \|f\|_X.$$

Hence

$$\int_1^\infty \left(t^{-\theta} K_{XY}(f,t)\right)^2 \frac{dt}{t} \le \|f\|_X^2 \int_1^\infty \frac{dt}{t^{1+2\theta}} = \frac{1}{2\theta}\|f\|_X^2.$$

Given a number $\alpha > 1$, obviously

$$K_{XY}(f,\alpha^{-(n+1)}) \le K_{XY}(f,t) \le K_{XY}(f,\alpha^{-n}) \qquad \text{for all} \quad t \in [\alpha^{-(n+1)}, \alpha^{-n}],$$

and $K_{XY}(f,\alpha t) \le \alpha K_{XY}(f,t)$. Hence

$$\begin{aligned}
\int_0^1 \left(t^{-\theta} K_{XY}(f,t)\right)^2 \frac{dt}{t} &= \sum_{n=0}^\infty \int_{\alpha^{-(n+1)}}^{\alpha^{-n}} \left(t^{-\theta} K_{XY}(f,t)\right)^2 \frac{dt}{t} \\
&\sim \sum_{n=0}^\infty K_{XY}^2(f,\alpha^{-n}) \int_{\alpha^{-(n+1)}}^{\alpha^{-n}} \left(t^{-\theta}\right)^2 \frac{dt}{t} \\
&= \sum_{n=0}^\infty K_{XY}^2(f,\alpha^{-n}) \frac{\alpha^{2n\theta}(\alpha^{2\theta}-1)}{2\theta} \\
&\sim \sum_{n=0}^\infty \alpha^{2n\theta} K_{XY}^2(f,\alpha^{-n}).
\end{aligned}$$

It follows that

$$|f|_{\theta;K} \sim \Big(\sum_{n=0}^\infty \left[\alpha^{n\theta} K_{XY}(f,\alpha^{-n})\right]^2\Big)^{1/2}, \tag{2.2.2}$$

where the constants of equivalence depend only on θ and α.

The *k-th modulus of smoothness* of $f \in L_p(\Omega)$, $0 < p \le \infty$, is defined by

$$\omega_k(f,t)_p = \sup_{|\delta|<t} \|\Delta_\delta^k f\|_{L_p(\Omega_{k\delta})},$$

where $|\delta|$ denotes the Euclidean length of $\delta \in \mathbb{R}^n$, $\Omega_{k\delta} := \{x \in \Omega : x + j\delta \in \Omega,\ j = 0,\dots,k\}$, and

$$(\Delta_\delta^k f)(x) := \sum_{j=0}^k \binom{k}{j} (-1)^{k-j} f(x+j\delta), \quad x \in \mathbb{R}^n,$$

is the usual difference operator. By [50, Theorem 1], the modulus of smoothness is equivalent to the K-functional,

$$\omega_k(f,t)_2 \sim K_{L_2,H^k}(f,t^k), \qquad t > 0. \tag{2.2.3}$$

Therefore, in view of Lemma 2.1, error bounds for functions in Sobolev spaces immediately lead to Jackson type estimates in terms of the modulus of smoothness.

The Sobolev spaces $H^s(\Omega)$ of a fractional order $s > 0$ can be defined as interpolation spaces

$$H^s(\Omega) = \big[L_2(\Omega),\ H^k(\Omega)\big]_\theta,$$

where $s = k\theta$, k integer, $0 < \theta < 1$. In view of (2.2.1) and (2.2.3),

$$|f|_{H^s(\Omega)} \sim \Big(\int_0^\infty (t^{-s}\omega_k(f,t)_2)^2 \, \frac{dt}{t} \Big)^{1/2}. \tag{2.2.4}$$

Let $C_c^\infty(\Omega)$ be the linear space of all infinitely differentiable functions on Ω with compact support contained in Ω. We use $H_0^s(\Omega)$ to denote the closure of $C_c^\infty(\Omega)$ in $H^s(\Omega)$. It is well known [38] that $C_c^\infty(\Omega)$ is dense in $H^s(\Omega)$ if and only if $s \le \frac{1}{2}$. If $s > \frac{1}{2}$ and the boundary of Ω is smooth, then $H_0^s(\Omega)$ is a proper subspace of $H^s(\Omega)$ given by

$$H_0^s(\Omega) = \Big\{ u \in H^s(\Omega) : \frac{\partial^\alpha u}{\partial x^\alpha} = 0 \text{ on } \partial\Omega, \text{ for all } 0 \le |\alpha| < s - \frac{1}{2},\ \alpha \in \mathbb{Z}^n \Big\},$$

see [38, Theorem 11.5]. Hence, $H_0^s(\Omega) = H^s(\Omega)$ if $s \le \frac{1}{2}$ and $H_0^s(\Omega) = H^s(\Omega) \cap H_0^{s_0}(\Omega)$, where $s_0 = \lceil s - \frac{1}{2} \rceil$ if $s > \frac{1}{2}$. According to [38, Theorem 11.6] the spaces $H_0^s(\Omega)$ of fractional order $s \notin \mathbb{Z} + \frac{1}{2}$ can be obtained from the integer order spaces $H_0^k(\Omega)$, $k > s$, by interpolation

$$H_0^s(\Omega) = \big[L_2(\Omega), H_0^k(\Omega)\big]_\theta, \quad \theta = \frac{s}{k}, \quad s \notin \mathbb{Z} + \frac{1}{2}. \tag{2.2.5}$$

For $s \in \mathbb{Z} + \frac{1}{2}$ a description of the interpolation spaces $H_{00}^s(\Omega) := \big[L_2(\Omega), H_0^k(\Omega)\big]_\theta$, $\theta = \frac{s}{k}$, can be found in [38, Theorem 11.7].

For a domain $\Omega \subset \mathbb{R}^2$ with piecewise smooth boundary in the sense of [31, p. 34], which includes the case of Lipschitz polygonal domains, the interpolation property (2.2.5) has been shown in [59]. As shown in [31], $H_0^s(\Omega)$, $s \notin \mathbb{Z} + \frac{1}{2}$, in this case coincides with the space $\tilde{H}^s(\Omega)$ of all those functions $f \in H^s(\Omega)$ whose extension to $\mathbb{R}^2$ by zero belongs to $H^s(\mathbb{R}^2)$. See also [5] for (2.2.5) in the case of a bounded Lipschitz domain in any space dimensions and integer s.

2.3 Bernstein and Jackson inequalities for bivariate splines

2.3.1 Bernstein inequality

We first recall some notations introduced in Section 1.3.2. Let Ω be a polygonal domain in $\mathbb{R}^2$. For a triangulation Δ of Ω, then h_Δ denotes the mesh size of Δ, β_Δ denotes the smallest angle of the triangles $T \in \Delta$, and the shape parameter is denoted by $\gamma_\Delta = \min\{\mathrm{diam}(T) : T \in \Delta\}/h_\Delta$. In this section we show that functions in subspaces of $S_d^r(\Delta)$ possessing a stable local basis satisfy a Bernstein type inequality in the norm of $H^s(\Omega)$ for all $0 < s < r + \frac{3}{2}$ (see Theorem 2.5). We begin by providing some auxiliary results.

Lemma 2.2. *Fix $T \in \Delta$ and set $T_\mu = T + \mu$, $\mu \in \mathbb{R}^2$. We denote by $\{T_j\}_{j\in J} \subset \Delta$ the set of all triangles $T_j \in \Delta$ such that $T_j \cap T_\mu \neq \emptyset$. Then the cardinality of J satisfy*

$$\#J \leq N_1$$

for some constant N_1 dependent only on β_Δ and γ_Δ.

Proof. Let $D \subset \Omega$ be a disk with centre of D at the barycentre of T_μ such that

$$T_j \subset D \text{ for all } j \in J.$$

Let $|D|$ denote the area of the disk D and denote by $|T_j|$ the area of the triangle T_j. Then it is easy to see that

$$\#J \cdot \min_{j\in J} |T_j| \leq |D|.$$

It is also clear that

$$\min_{j\in J} |T_j| \geq k_1 h_\Delta^2,$$

where the constant k_1 depends only on β_Δ and γ_Δ.

Let $T_k \in \{T_j\}_{j\in J}$ be a triangle with a vertex v_1 on the boundary of D and another vertex v_2 on the edge of T_μ as shown in Fig.2.1. Let d_1 denote the distance

of v_2 from the centre of D and d_2 denote the distance between v_1 and v_2. Let r be the radius of the disk. Then we see that

$$r \leq d_1 + d_2 \leq 2h_\Delta$$

since $d_1 \leq h_\Delta$ and $d_2 \leq h_\Delta$.

Thus the area of the disk D satisfies

$$|D| = \pi r^2 \leq 4\pi h_\Delta^2,$$

and hence we obtain

$$\#J \leq \frac{4\pi}{k_1}.$$

□

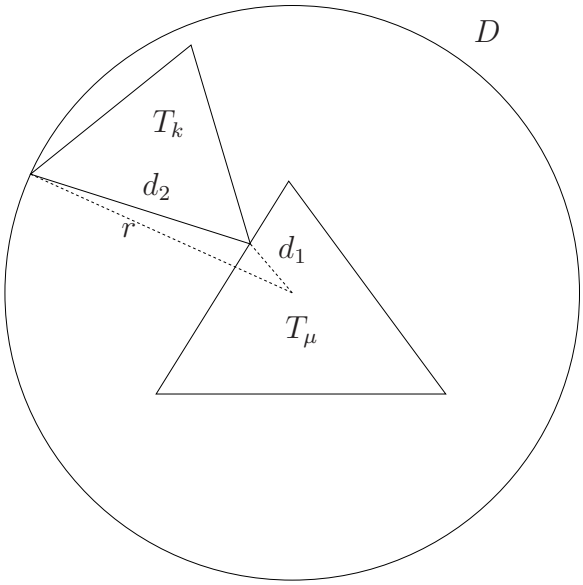

Figure 2.1: Radius of Disk.

Lemma 2.3. *Suppose that $S \subset S_d(\Delta)$ has an m-local basis $\{\phi_i\}_{i\in I}$. Fix $T \in \Delta$ and also fix an integer k and $\delta \in \mathbb{R}^2$. Consider*

$$I_T = \{i \in I : \Delta_\delta^k \phi_i|_T \neq 0\} = \{i \in I : T \subset \mathrm{supp}(\Delta_\delta^k \phi_i)\}.$$

Then the cardinality of I_T satisfies

$$\#I_T \leq N_2$$

for some N_2 dependent only on $k, \beta_\Delta, \gamma_\Delta, d$ and m.

Proof. Let $i \in I$. Then for some $l \in \{0, 1, \ldots, k\}$,

$$T \cap \operatorname{supp} \phi_i(x + l\delta) \neq \emptyset.$$

For a fixed l, we denote

$$I_{T,l} = \{i \in I : T \cap \operatorname{supp} \phi_i(x + l\delta) \neq \emptyset\}.$$

Then

$$I_T \subset \cup_{l=0}^{k} I_{T,l}$$

and

$$\#I_T \leq \sum_{l=0}^{k} \#I_{T,l}.$$

Take $l = 0$, that is

$$I_{T,0} = \{i \in I : T \cap \operatorname{supp} \phi_i \neq \emptyset\},$$

where $\operatorname{supp} \phi_i \subset \operatorname{star}^m(T_i)$ for some triangle $T_i \in \Delta$ and $\operatorname{star}^m(T_i) \subset \operatorname{star}^{m+1}(v_i)$ where v_i is a vertex of T_i. Then it is known that [16, 35]

$$\#\{T \in \Delta : T \subset \operatorname{star}^{m+1}(v_i)\} \leq K_1$$

where K_1 depends only on $\beta_\Delta, \gamma_\Delta$ and m.

Since the cardinality $\#I_{T,0}$ does not exceed the dimension of the space of all polynomials of degree d on $\operatorname{star}^m(T_i)$ [16], that is,

$$\#I_{T,0} \leq K_2 \binom{d+2}{2} \tag{2.3.1}$$

where K_2 is the number of triangles of Δ lying in $\operatorname{star}^m(T_i)$, and K_2 is bounded by K_1.

Now take $l \geq 1$. We note that $I_{T,l}$ can also be written as

$$I_{T,l} = \{i \in I : (T - l\delta) \cap \operatorname{supp} \phi_i \neq \emptyset\}$$

and $T_{l\delta} = T - l\delta \subset \bigcup_{j\in J} T_j$ where $\{T_j\}_{j\in J} \subset \Delta$ the set of all triangles $T_j \in \Delta$ such that $T_j \cap T_{l\delta} \neq \emptyset$.

Since

$$\#I_{T,l} \leq \sum_{j\in J} \#I_{T_j,0}, \quad l \geq 1,$$

then by Lemma 2.2 and (2.3.1), we obtain

$$\#I_{T,l} \leq N_1 \cdot K_2 \binom{d+2}{2}$$

because $\#J \leq N_1$ and hence

$$\sum_{l=0}^{k} \#I_{T,l} \leq (k+1) \cdot N_1 \cdot K_2 \binom{d+2}{2}.$$

Thus we get

$$\#I_T \leq N_2$$

where $N_2 = (k+1) \cdot N_1 \cdot K_2 \binom{d+2}{2}$. □

Lemma 2.4. *Suppose that $S \subset S_d(\Delta)$ has an m-local basis $\{\phi_i\}_{i\in I}$. Then for any $f = \sum_{i\in I} c_i\phi_i \in S$ where $c_i \in \mathbb{R}$,*

$$I_k(f,\delta)^2 \lesssim \sum_{i\in I} c_i^2 I_k(\phi_i,\delta)^2, \qquad \delta \in \mathbb{R}^2,$$

where the bounding constant is dependent only on $k, \beta_\Delta, \alpha_\Delta, d$ and m.

Proof. Fix $\delta \in \mathbb{R}^2$ and fix an integer k,

$$\begin{aligned} I_k(f,\delta)^2 = \|\Delta_\delta^k f\|_{L_2(\Omega_{k\delta})}^2 &= \int_{\Omega_{k\delta}} \Big(\Delta_\delta^k \big(\sum_{i\in I} c_i\phi_i\big)\Big)^2 dx \\ &= \sum_{j\in J} \int_{T_j\cap\Omega_{k\delta}} \Big(\sum_{i\in I} c_i \Delta_\delta^k \phi_i\Big)^2 dx \\ &= \sum_{j\in J} \int_{T_j\cap\Omega_{k\delta}} \Big(\sum_{i\in I_j} c_i \Delta_\delta^k \phi_i\Big)^2 dx, \end{aligned}$$

where $I_j = \{i \in I : T_j \subset \operatorname{supp} \Delta_\delta^k(\phi_i)\}$.

Since $\{\phi_i\}_{i\in I}$ are locally supported we know by Lemma 2.3 the cardinality of I_j satisfies

$$\#I_j \le N_2.$$

Using the inequality

$$\left(\frac{1}{N_2}\sum_{i\in I_j} c_i \Delta_\delta^k \phi_i\right)^2 \le \frac{1}{N_2}\sum_{i\in I_j} c_i^2 (\Delta_\delta^k \phi_i)^2, \qquad j \in J,$$

for any real-valued c_i, we obtain

$$\left(\sum_{i\in I_j} c_i \Delta_\delta^k \phi_i\right)^2 \le N_2 \sum_{i\in I_j} c_i^2 (\Delta_\delta^k \phi_i)^2, \qquad j \in J.$$

Hence

$$\begin{aligned}
\|\Delta_\delta^k f\|_{L_2(\Omega_{k\delta})}^2 &\le \sum_{j\in J} \int_{T_j\cap\Omega_{k\delta}} N_2 \sum_{i\in I_j} c_i^2 (\Delta_\delta^k \phi_i)^2 dx \\
&= N_2 \sum_{j\in J}\sum_{i\in I_j} c_i^2 \int_{T_j\cap\Omega_{k\delta}} (\Delta_\delta^k \phi_i)^2 dx \\
&= N_2 \sum_{i\in I} c_i^2 \sum_{j: i\in I_j} \int_{T_j\cap\Omega_{k\delta}} (\Delta_\delta^k \phi_i)^2 dx \\
&= N_2 \sum_{i\in I} c_i^2 \int_{\operatorname{supp}\Delta_\delta^k(\phi_i)} (\Delta_\delta^k \phi_i)^2 dx \\
&= N_2 \sum_{i\in I} c_i^2 \left\|\Delta_\delta^k \phi_i\right\|_{L_2(\Omega_{k\delta})}^2.
\end{aligned}$$

Hence we get

$$I_k(f,\delta)^2 \lesssim \sum_{i\in I} c_i^2 I_k(\phi_i,\delta)^2, \qquad f = \sum_{i\in I} c_i \phi_i.$$

□

Theorem 2.5 (Bernstein Inequality)**.** *Suppose that $S \subset S_d^r(\Delta)$ has a stable local basis $\{\phi_i\}_{i\in I}$. Then for any $f \in S$,*

$$\|f\|_{H^s(\Omega)} \lesssim h_\Delta^{-s} \|f\|_{L_2(\Omega)}, \qquad 0 < s < r + \frac{3}{2}, \tag{2.3.2}$$

where the bounding constant depends only on $s, r, d, \beta_\Delta, \gamma_\Delta$ and the parameters m, C_1, C_2 of the stable local basis.

Under slightly different assumptions on S, a proof of the Bernstein inequality can be found in [50], see also [52]. We provide a proof based on the following lemma.

Lemma 2.6 ([33, Lemma 2.2])**.** *Let $f \in S_d^r(\Delta)$. Then $f \in H^s(\Omega)$ for all $s < r + \frac{3}{2}$, and*

$$\|f\|_{H^s(\Omega)} \lesssim h_\Delta^{-s} \|f\|_{L_2(\Omega)}, \qquad 0 < s < r + \frac{3}{2}, \tag{2.3.3}$$

where the bounding constant depends only on $s, r, d, \beta_\Delta, \gamma_\Delta$ and the number of triangles $T \in \Delta$ in the support of f.

Proof Theorem 2.5. Since $\{\phi_i\}_{i\in I}$ is a stable local basis, the functions $\psi_i = |\operatorname{supp} \phi_i|^{-1/2}\phi_i$, $i \in I$, form an L_2-stable basis for S. In particular $\|\psi_i\|_{L_2(\Omega)} \le M$, where M depends only on the parameters m, C_1, C_2 of the stable local basis.

Let $f = \sum_{i\in I} c_i\psi_i$ for some $c_i \in \mathbb{R}$, so that $\|f\|_{L_2(\Omega)}^2 \sim \sum_{i\in I} c_i^2$. Choose an integer $k > s$. Since the basis $\{\psi_i\}_{i\in I}$ is m-local, by Lemma 2.4 we have

$$I_k(f,\delta)^2 \lesssim \sum_{i\in I} c_i^2 I_k(\psi_i,\delta)^2, \quad \text{where } I_k(f,\delta) := \|\Delta_\delta^k f\|_{L_2(\Omega_{k\delta})}, \quad \delta \in \mathbb{R}^2.$$

Hence,

$$\omega_k(f,t)_2^2 \lesssim \sum_{i\in I} c_i^2 \omega_k(\psi_i,t)_2^2,$$

and by (2.2.4),

$$|f|_{H^s(\Omega)}^2 \lesssim \sum_{i\in I} c_i^2 \int_0^\infty (t^{-s}\omega_k(\psi_i,t)_2)^2 \frac{dt}{t} \sim \sum_{i\in I} c_i^2 |\psi_i|_{H^s(\Omega)}^2.$$

By applying the Bernstein inequality (2.3.3) to the locally supported functions ψ_i and using the L_2-stability of the basis $\{\psi_i\}_{i\in I}$, in particular, uniform L_2-boundedness of ψ_i, we obtain

$$\|f\|_{H^s(\Omega)}^2 \lesssim h_\Delta^{-2s} \sum_{i\in I} c_i^2 \|\psi_i\|_{L_2(\Omega)}^2 \lesssim h_\Delta^{-2s} \sum_{i\in I} c_i^2 \lesssim h_\Delta^{-2s} \|f\|_{L_2(\Omega)}^2,$$

which completes the proof. □

2.3.2 Jackson inequality for macro-element spline spaces

We restrict our attention to the macro-element spaces, see Section 1.3.4, because of the availability of boundary conforming interpolation operators that allow appropriate treatment of subspaces with zero boundary conditions. The notations used in this section are inherited from Section 1.3.2 and 1.3.4.

The proof of the following version of the Jackson inequality follows the scheme used in [7, Section 4.4], where it is proved for *finite elements*, thus making an assumption of *affine equivalence* of the spaces $S|_K$, $K \in \Delta$. In place of affine equivalence, we only assume that the nodal basis is uniformly bounded, see (2.3.4).

Theorem 2.7 (Jackson Inequality)**.** *Let $S \subset S_d^r(\Delta_R)$ be a macro-element space such that $\mathbb{P}_k \subset S$ for some $1 \le k \le d$, and $\kappa(S) \le k-1$. Assume that its nodal basis $\{s_i\}_{i=1}^N$ satisfies*

$$\|s_i\|_{L_\infty(\Omega)} \le C_2, \qquad i = 1, \dots, N. \tag{2.3.4}$$

Then for every $f \in H^{k+1}(\Omega)$,

$$\|f - \Pi f\|_{H^\nu(\Omega)} \le C h_\Delta^{k+1-\nu} |f|_{H^{k+1}(\Omega)}, \quad \nu = 0, \dots, \min\{r, k\} + 1, \tag{2.3.5}$$

where C depends only on d, β_{Δ_R}, ν_{Δ_R}, χ_Δ and C_2.

Proof. Recall that by Sobolev embedding theorem any function $f \in H^{k+1}(\Omega)$ belongs (after possible modification on a set of zero measure) to $C^{k-1}(\Omega)$. This implies that Πf is well defined for all $f \in H^{k+1}(\Omega)$, and $f - \Pi f \in H^{r+1}(\Omega)$ since $S_d^r(\Delta_R) \subset H^{r+1}(\Omega)$.

Given any $K \in \Delta$, we define

$$\hat{K} := \left\{ \frac{x}{\operatorname{diam}(K)} : x \in K \right\}.$$

Then $\operatorname{diam} \hat{K} = 1$ and hence $|\hat{K}| \le \pi/4$. For any function g defined on K we set $\hat{g}(y) := g(\operatorname{diam}(K) y)$, $y \in \hat{K}$. The functions

$$\hat{s}_i := \widehat{s_i|_K}, \qquad \text{for all } i \text{ such that } \lambda_i \in \mathcal{N}_K,$$

form a basis for the spline space $\hat{S}_K := \{\hat{s} : s \in S|_K\}$ on $\hat{K}$, with its dual basis given by the linear functionals $\hat{\lambda}_i(\hat{g}) := \lambda_i(g)$, $g \in C^{k-1}(K)$. Since $\operatorname{diam}(T_i) \sim \operatorname{diam}(K)$, we have

$$\hat{\lambda}_i \hat{g} = \operatorname{diam}(T_i)^{\nu+\mu} \frac{\partial^{\nu+\mu} g}{\partial\sigma^\nu \partial\tau^\mu}(\eta) \sim \frac{\partial^{\nu+\mu} \hat{g}}{\partial\sigma^\nu \partial\tau^\mu}(\operatorname{diam}(K)^{-1}\eta),$$

and it follows that

$$|\hat{\lambda}_i(g)| \le \hat{C}_1 \|g\|_{C^{k-1}(\hat{K})}, \quad g \in C^{k-1}(\hat{K}), \quad \lambda_i \in \mathcal{N}_K, \tag{2.3.6}$$

where $\hat{C}_1$ depends only on β_{Δ_R}, ν_{Δ_R} and d. Note that by Sobolev inequality [7, Section 4.3],

$$\|g\|_{C^{k-1}(\hat{K})} \lesssim \|g\|_{H^{k+1}(\hat{K})}, \quad g \in H^{k+1}(\hat{K}) \subset C^{k-1}(\hat{K}), \tag{2.3.7}$$

where the bounding constant depends only on k and the chunkiness parameter $\chi_{\hat{K}}$ $(= \chi_K)$.

We define the interpolation operator $\Pi_{\hat{K}} : C^{k-1}(\hat{K}) \to \hat{S}_K$ by

$$\Pi_{\hat{K}} g := \sum_{i:\, \lambda_i \in \mathcal{N}_K} \hat{\lambda}_i(g) \hat{s}_i.$$

By (2.3.4) we get

$$\|\hat{s}_i\|_{L_2(\hat{K})} \le \frac{\sqrt{\pi}}{2} \|\hat{s}_i\|_{L_\infty(\hat{K})} \le \frac{\sqrt{\pi}}{2} C_2,$$

which in view of the Bernstein inequality (2.3.3) leads to

$$\|\hat{s}_i\|_{H^{r+1}(\hat{K})} \le \hat{C}_2, \tag{2.3.8}$$

where $\hat{C}_2$ depends only on d, r, β_{Δ_R}, $|K_R|$ and C_2.

The inequalities (2.3.6) and (2.3.8) imply that the operator $\Pi_{\hat{K}} : C^{k-1}(\hat{K}) \to H^{r+1}(\hat{K})$ is bounded, i.e.,

$$\|\Pi_{\hat{K}} g\|_{H^{r+1}(\hat{K})} \le \hat{C}_3 \|g\|_{C^{k-1}(\hat{K})}, \tag{2.3.9}$$

where the constant $\hat{C}_3$ depends only on $\hat{C}_1$, $\hat{C}_2$, d and $|K_R|$. Indeed, let $g \in C^{k-1}(\hat{K})$. Then $\Pi_{\hat{K}} g \in \hat{S}_K \subset W_\infty^{r+1}(\hat{K}) \subset H^{r+1}(\hat{K})$. Clearly, $\#\mathcal{N}_K$ does not

exceed a constant C' depending only on d and $|K_R|$. In view of (2.3.6) and (2.3.8),

$$\|\Pi_{\hat{K}} g\|_{H^{r+1}(\hat{K})} \leq \sum_{i:\, \lambda_i \in \mathcal{N}_K} |\hat{\lambda}_i(g)|\ \|\hat{s}_i\|_{H^{r+1}(\hat{K})} \leq C' \hat{C}_1 \hat{C}_2 \|g\|_{C^{k-1}(\hat{K})}.$$

We now show that for every $K \in \Delta$ and $g \in H^{k+1}(K)$,

$$|g - \Pi_K g|_{H^\nu(K)} \lesssim \operatorname{diam}(K)^{k+1-\nu} |g|_{H^{k+1}(K)}, \quad 0 \leq \nu \leq \min\{r, k\} + 1, \tag{2.3.10}$$

where the constant in the bound depends only on d, β_{Δ_R}, ν_{Δ_R}, χ_K and C_2. If $g \in H^{k+1}(K)$, then $\hat{g} \in H^{k+1}(\hat{K})$ and, by the Bramble-Hilbert lemma [7, Section 4.3] there exists a polynomial $p \in \mathbb{P}_k$ such that

$$\|\hat{g} - p\|_{H^\ell(\hat{K})} \lesssim |\hat{g}|_{H^{k+1}(\hat{K})}, \qquad 0 \leq \ell \leq k+1, \tag{2.3.11}$$

where the bounding constant depends only on k and the chunkiness parameter $\chi_{\hat{K}}$ $(= \chi_K)$. Let $m = \min\{r, k\}$. Since $\Pi_{\hat{K}} p = p$, we have by (2.3.9), (2.3.7) and (2.3.11),

$$\begin{aligned}
\|\hat{g} - \Pi_{\hat{K}} \hat{g}\|_{H^{m+1}(\hat{K})} &\leq \|\hat{g} - p\|_{H^{m+1}(\hat{K})} + \|\Pi_{\hat{K}}(p - \hat{g})\|_{H^{m+1}(\hat{K})} \\
&\lesssim \|\hat{g} - p\|_{H^{k+1}(\hat{K})} + \|p - \hat{g}\|_{C^{k-1}(\hat{K})} \\
&\lesssim \|\hat{g} - p\|_{H^{k+1}(\hat{K})} + \|p - \hat{g}\|_{H^{k+1}(\hat{K})} \\
&\lesssim |\hat{g}|_{H^{k+1}(\hat{K})},
\end{aligned}$$

and (2.3.10) follows since

$$|g - \Pi_K g|_{H^\nu(K)} = \operatorname{diam}(K)^{1-\nu} |\hat{g} - \Pi_{\hat{K}} \hat{g}|_{H^\nu(\hat{K})},$$

$|\hat{g} - \Pi_{\hat{K}} \hat{g}|_{H^\nu(\hat{K})} \lesssim \|\hat{g} - \Pi_{\hat{K}} \hat{g}\|_{H^{m+1}(\hat{K})}$, and

$$|\hat{g}|_{H^{k+1}(\hat{K})} = \operatorname{diam}(K)^k |g|_{H^{k+1}(K)}.$$

The estimate (2.3.5) follows from (2.3.10) because

$$\|f - \Pi f\|^2_{H^\nu(\Omega)} = \sum_{K \in \Omega} \sum_{i=0}^{\nu} |f|_K - \Pi_K f|_K|^2_{H^i(K)}, \quad |f|^2_{H^{k+1}(\Omega)} = \sum_{K \in \Omega} |f|_K|^2_{H^{k+1}(K)}$$

and $h_\Delta = \max_{K \in \Delta} \operatorname{diam}(K)$. □

Note that the estimate

$$\inf_{g\in S}\|f-g\|_{H^\nu(\Omega)}\le Ch_\Delta^{k+1-\nu}|f|_{H^{k+1}(\Omega)},\quad f\in H^{k+1}(\Omega),$$

can be obtained by using quasi-interpolation operators for any spline spaces S with a stable local basis, see [36] or [18]. Even though Theorem 2.7 is only applicable to macro-element spaces, its importance for the results below about Riesz bases in $H_0^s(\Omega)$ is that it leads to the estimate

$$\inf_{g\in S_{0,\sigma}}\|f-g\|_{H^\nu(\Omega)}\le Ch_\Delta^{k+1-\nu}|f|_{H^{k+1}(\Omega)},\quad f\in H_0^{k+1}(\Omega), \tag{2.3.12}$$

as soon as the interpolation operator Π is boundary conforming of some order $\sigma\le r$, which is normally the case for the macro-elements.

Corollary 2.8. *In addition to the assumptions of Theorem 2.7 suppose that the interpolation operator* Π *is boundary conforming of order* $\sigma\le r$. *Then the estimate* (2.3.12) *holds for all* $\nu=0,\dots,\min\{r,k\}+1$, *where* C *depends only on* d, β_{Δ_R}, ν_{Δ_R}, χ_Δ *and* C_2.

2.4 General theory of hierarchical Riesz bases

Recall that a basis $\{\phi_n\}_{n=1}^\infty$ for a Hilbert space H is said to be a *Riesz basis* if for any real-valued $c_n\in\ell_2$,

$$\Big\|\sum_{n=1}^\infty c_n\phi_n\Big\|_H\sim\Big(\sum_{n=1}^\infty c_n^2\Big)^{1/2}.$$

Suppose that S_n, $n=0,1,2\dots$, is a *nested sequence* of finite dimensional subspaces of a Hilbert space H, that is

$$S_0\subset S_1\subset\ldots\subset S_n\subset\ldots\quad n=0,1,2,\dots. \tag{2.4.1}$$

We assume that $\cup_{n=0}^\infty S_n$ is dense in H and set $S_{-1}:=\{0\}$. Then every element $f\in H$ can be represented as a convergent series $\sum_{n=0}^\infty f_n$ in H with $f_n\in S_n$. For $n=0,1,2,\dots$, let P_n be a linear projection from S_n onto S_{n-1}, and let W_n be the

complement space, that is, $P_n(W_n) = \{0\}$ and $S_n = S_{n-1} + W_n$. In particular, $W_0 = S_0$.

We will use the following general result about construction of Riesz bases for certain subspaces of H using stable bases of W_n.

Theorem 2.9 ([34]). *Assume that for some $v > 0$ and $\rho > 1$,*

$$\|P_{n+1} \cdots P_m f\|_H \lesssim \rho^{v(m-n)} \|f\|_H, \qquad f \in S_m, \tag{2.4.2}$$

for all $m, n = 0, 1, 2, \ldots$ with $n < m$. Let $s > v$ and let H_s be a linear subspace of H which itself is a Hilbert space with norm $\|\cdot\|_{H_s}$ satisfying

$$\|f\|_{H_s} \sim \inf_{f_n \in S_n:\, f = \sum_{n=0}^{\infty} f_n} \Big(\sum_{n=0}^{\infty} \big[\rho^{ns} \|f_n\|_H\big]^2 \Big)^{1/2}, \qquad f \in H_s. \tag{2.4.3}$$

Suppose that for each $n = 0, 1 \ldots$, $W_n \subset H_s$ and there is a stable basis $\{\phi_k^{(n)}\}_{k \in K_n}$ for W_n in the sense that

$$\Big\| \sum_{k \in K_n} c_k \phi_k^{(n)} \Big\|_H \sim \Big(\sum_{k \in K_n} c_k^2 \Big)^{1/2}, \tag{2.4.4}$$

with constants of equivalence independent of n. Then $\bigcup_{n=0}^{\infty} \{\rho^{-ns} \phi_k^{(n)}\}_{k \in K_n}$ is a Riesz basis for H_s.

Assumption (2.4.3) of Theorem 2.9 can often be verified with the help of the following theorem. Although it can be derived from more general results in e.g. [8, 40] (see also [51]), we provide here a short and self-contained proof based on arguments similar to those in [50, Theorem 6] and [13, Corollary 5.2].

Theorem 2.10. *Let H and $H' \subset H$ be Hilbert spaces with norms $\|\cdot\|_H$ and $\|\cdot\|_{H'} = \|\cdot\|_H + |\cdot|_{H'}$, where $|\cdot|_{H'}$ is a seminorm. Suppose that for some $\alpha > 1$ and $0 < \lambda < 1$ nested finite dimensional linear subspaces $S_n \subset H$ satisfy the Jackson inequality*

$$\inf_{s \in S_n} \|f - s\|_H \lesssim \alpha^{-n} |f|_{H'}, \quad f \in H', \qquad n = 0, 1, \ldots, \tag{2.4.5}$$

and the Bernstein inequality in the norm $\|\cdot\|_{\lambda;K}$ *of the interpolation space* $[H, H']_\lambda$,

$$\|s\|_{\lambda;K} \lesssim \alpha^{n\lambda}\|s\|_H, \qquad s \in S_n. \tag{2.4.6}$$

Then for any $0 < \theta < \lambda$,

$$\|f\|_{\theta;K} \sim \inf_{f_n \in S_n:\, f=\sum_{n=0}^\infty f_n} \Big(\sum_{n=0}^\infty \big[\alpha^{n\theta}\|f_n\|_H\big]^2\Big)^{1/2}, \quad f \in [H, H']_\theta, \tag{2.4.7}$$

where the constants of equivalence depend only on α, *the difference* $\lambda - \theta$ *and the bounding constants in* (2.4.5) *and* (2.4.6).

Proof. Recall from (2.2.2) that

$$\|f\|_{\theta;K} \sim \|f\| := \|f\|_H + \Big(\sum_{n=0}^\infty \big[\alpha^{n\theta}K_{H,H'}(f, \alpha^{-n})\big]^2\Big)^{1/2}.$$

We will show that $\|f\| \sim \|f\|^*$, where $\|f\|^*$ denotes the right hand side of (2.4.7).

We first prove that $\|f\|^* \lesssim \|f\|$. Let $f \in H$. It follows from (2.4.5) by Lemma 2.1 that there exists a sequence of elements $f_n \in S_n$ such that

$$\|f - f_n\|_H \lesssim K_{H,H'}(f, \alpha^{-n}), \qquad n = 0, 1, \ldots.$$

Then

$$\|f_n - f_{n-1}\|_H \le \|f_n - f\|_H + \|f_{n-1} - f\|_H \lesssim K_{H,H'}(f, \alpha^{-n}), \quad n \ge 1,$$

and $\|f_0\|_H \lesssim \|f\|_H + K_{H,H'}(f, 1)$. If $\|f\| < \infty$, then $\|f - f_n\|_H \to 0$ when $n \to \infty$ and hence

$$f = \sum_{n=0}^\infty (f_n - f_{n-1}), \qquad f_{-1} = 0,$$

where $f_n - f_{n-1} \in S_n$ since $S_{n-1} \subset S_n$, which implies

$$\|f\|^* \le \Big(\sum_{n=0}^\infty \big[\alpha^{n\theta}\|f_n - f_{n-1}\|_H\big]^2\Big)^{1/2} \lesssim \|f\|.$$

We now proceed to showing the opposite inequality $\|f\| \lesssim \|f\|^*$. Let $f = \sum_{n=0}^\infty f_n$ with some $f_n \in S_n$. By (2.4.6) we have for $t \in [\alpha^{-(j+1)}, \alpha^{-j}]$,

$$K_{H,H'}(f_n, t)^2 \le K_{H,H'}(f_n, \alpha^{-j})^2 \lesssim \alpha^{-2\lambda j}|f_n|^2_{\lambda,K} \lesssim (t\alpha^n)^{2\lambda}\|f_n\|^2_H. \tag{2.4.8}$$

Let $0 < \theta < \lambda$. Then

$$\sum_{j=0}^{\infty} \alpha^{2\theta j} K_{H,H'}(f, \alpha^{-j})^2 \leq 2(A + B),$$

where

$$A = \sum_{j=0}^{\infty} \alpha^{2j\theta} \Big(\sum_{n=0}^{j} K_{H,H'}(f_n, \alpha^{-j}) \Big)^2, \quad B = \sum_{j=0}^{\infty} \alpha^{2j\theta} \Big(\sum_{n=j+1}^{\infty} K_{H,H'}(f_n, \alpha^{-j}) \Big)^2.$$

By (2.4.8) and Cauchy-Schwarz inequality,

$$\begin{aligned} A &\lesssim \sum_{j=0}^{\infty} \alpha^{2j\theta} \Big(\sum_{n=0}^{j} \alpha^{(n-j)\lambda} \|f_n\|_H \Big)^2 \\ &= \sum_{j=0}^{\infty} \alpha^{2j(\theta-\lambda)} \Big(\sum_{n=0}^{j} \alpha^{n(\lambda-\theta)} \alpha^{n\theta} \|f_n\|_H \Big)^2 \\ &\leq \sum_{j=0}^{\infty} \alpha^{2j(\theta-\lambda)} \sum_{n=0}^{j} \alpha^{n(\lambda-\theta)} \sum_{n=0}^{j} \alpha^{n(\lambda-\theta)} \alpha^{2n\theta} \|f_n\|_H^2. \end{aligned}$$

Since

$$\sum_{n=0}^{j} \alpha^{n(\lambda-\theta)} = \frac{\alpha^{(j+1)(\lambda-\theta)} - 1}{\alpha^{(\lambda-\theta)} - 1} \leq \frac{\alpha^{(\lambda-\theta)}}{\alpha^{(\lambda-\theta)} - 1} \cdot \alpha^{j(\lambda-\theta)},$$

we get

$$\begin{aligned} A &\lesssim \sum_{j=0}^{\infty} \alpha^{-j(\lambda-\theta)} \sum_{n=0}^{j} \alpha^{n(\lambda-\theta)} \alpha^{2n\theta} \|f_n\|_H^2 \\ &= \sum_{n=0}^{\infty} \sum_{j=n}^{\infty} \alpha^{-(j-n)(\lambda-\theta)} \alpha^{2n\theta} \|f_n\|_H^2. \end{aligned}$$

Let $k = j - n$, then

$$\begin{aligned} A &\lesssim \sum_{n=0}^{\infty} \sum_{k=0}^{\infty} \alpha^{-k(\lambda-\theta)} \alpha^{2n\theta} \|f_n\|_H^2 \\ &= C_1 \sum_{n=0}^{\infty} \alpha^{2n\theta} \|f_n\|_H^2 \end{aligned}$$

where $C_1 = \sum_{k=0}^{\infty} \alpha^{-k(\lambda-\theta)} = \frac{1}{1-\alpha^{-(\lambda-\theta)}}$.

The bound $K_{H,H'}(f_n, \alpha^{-j}) \le \|f_n\|_H$ and the Cauchy-Schwarz inequality imply

$$\begin{aligned} B &\le \sum_{j=0}^{\infty} \alpha^{2j\theta} \Big(\sum_{n=j+1}^{\infty} \|f_n\|_H \Big)^2 \\ &= \sum_{j=0}^{\infty} \alpha^{2j\theta} \Big(\sum_{n=j+1}^{\infty} \alpha^{\frac{-n\theta}{2}} \alpha^{\frac{-n\theta}{2}} \alpha^{n\theta} \|f_n\|_H \Big)^2 \\ &\le \sum_{j=0}^{\infty} \alpha^{2j\theta} \sum_{n=j+1}^{\infty} \alpha^{-n\theta} \sum_{n=j+1}^{\infty} \alpha^{-n\theta} \alpha^{2n\theta} \|f_n\|_H^2 \\ &= \frac{\alpha^{-\theta}}{1-\alpha^{-\theta}} \sum_{n=1}^{\infty} \sum_{j=0}^{n-1} \alpha^{(j-n)\theta} \alpha^{2n\theta} \|f_n\|_H^2 \\ &\le C_2 \sum_{n=0}^{\infty} \alpha^{2n\theta} \|f_n\|_H^2, \end{aligned}$$

where $C_2 = \frac{\alpha^{-\theta}}{(1-\alpha^{-\theta})(\alpha^{\theta}-1)}$. Combining the above estimates for A and B yields $\|f\| \lesssim \|f\|^*$. □

We will use Theorems 2.9 and 2.10 with $H = L_2(\Omega)$ and $H_s = H^s(\Omega)$ or $H_0^s(\Omega)$, where $\Omega \subset \mathbb{R}^2$ is an arbitrary polygonal domain, and $\{S_n\}_{n=0}^{\infty}$ is a nested sequence of macro-element spline spaces.

A sequence of triangulations $\{\Delta_n\}_{n=0}^{\infty}$ of Ω is said to be *nested* if each Δ_{n+1} is a refinement of Δ_n, that is Δ_{n+1} is obtained from Δ_n by subdividing the triangles of Δ_n. Then obviously $S_d^r(\Delta_n) \subset S_d^r(\Delta_{n+1})$, so that $\{S_d^r(\Delta_n)\}_{n=0}^{\infty}$ is a nested sequence of spaces. However, certain subspaces $S_n \subset S_d^r(\Delta_n)$ may also be nested, see for example [17, 19, 24].

Recall that a sequence of triangulations $\{\Delta_n\}_{n=0}^{\infty}$ of Ω is *regular* if the minimum angle of all Δ_n remains bounded below by a positive constant $\beta > 0$ independent of n, and the triangulations Δ_n are quasi-uniform in the sense that there exist constants $\rho > 1$ and $c_1, c_2 > 0$ independent of n such that

$$c_1 \rho^{-n} \le \operatorname{diam} T \le c_2 \rho^{-n}, \qquad T \in \Delta_n. \tag{2.4.9}$$

The parameter ρ will be called the *refinement factor* of $\{\Delta_n\}_{n=0}^{\infty}$.

Recall that a finite set $\Xi \subset \Omega$ is said to be a *Lagrange interpolation set* for a finite dimensional linear space S of functions on Ω if $\#\Xi = \dim S$ and for each

$\xi \in \Xi$ there is a unique function $B_\xi \in S$ satisfying $B_\xi(\eta) = \delta_{\xi,\eta}$ for all $\xi, \eta \in \Xi$, where $\delta_{\xi,\eta} = 1$ if $\xi = \eta$ and $\delta_{\xi,\eta} = 0$ otherwise. The set $\{B_\xi\}_{\xi\in\Xi}$ is a basis for S called the *Lagrange basis*.

A sequence of Lagrange interpolation sets $\{\Xi_n\}_{n=0}^\infty$ for the corresponding spaces S_n is said to be *nested* if

$$\Xi_0 \subset \Xi_1 \subset \ldots \subset \Xi_n \subset \ldots. \tag{2.4.10}$$

We are ready to formulate the main result of this chapter.

Theorem 2.11. *Let $\{S_n\}_{n=0}^\infty$ be a nested sequence of spaces $S_n \subset S_d^r(\Delta_n)$, $r \geq 0$, with respect to a regular nested sequence of triangulations $\{\Delta_n\}_{n=0}^\infty$ of a polygonal domain $\Omega \subset \mathbb{R}^2$, with refinement factor $\rho > 1$, and let $\{\Xi_n\}_{n=0}^\infty$ be a nested sequence of Lagrange interpolation sets for the spaces S_n, with the corresponding Lagrange basis $\{B_\xi^{(n)}\}_{\xi\in\Xi_n}$ for S_n. Assume that the bases $\{B_\xi^{(n)}\}_{\xi\in\Xi_n}$ are uniformly local and bounded, that is they are m-local and satisfy $\|B_\xi^{(n)}\|_{L_\infty(\Omega)} \leq M$, $\xi \in \Xi_n$, for some m, M independent of n.*

(a) Assume that the spaces S_n satisfy the Jackson inequality

$$\inf_{g\in S_n} \|f - g\|_{L_2(\Omega)} \lesssim \rho^{-n(k+1)} |f|_{H^{k+1}(\Omega)}, \quad f \in H^{k+1}(\Omega), \tag{2.4.11}$$

For some $k \in \mathbb{N}$ with $r < k \leq d$. Then for any $s \in (1, r + \frac{3}{2})$ the set

$$\mathcal{B}_s := \bigcup_{n=0}^\infty \{\rho^{n(1-s)} B_\xi^{(n)}\}_{\xi\in\Xi_n\setminus\Xi_{n-1}}$$

is a Riesz basis for $H^s(\Omega)$.

(b) Moreover, if the spaces S_n, $n = 0, 1, \ldots$, satisfy the homogeneous boundary conditions of order $\sigma \leq r$, that is

$$\frac{\partial^{\nu+\mu} g}{\partial x^\nu \partial y^\mu} = 0 \text{ on } \partial\Omega, \text{ for all } \nu, \mu \geq 0,\ \nu + \mu \leq \sigma, \quad g \in S_n,$$

and (2.4.11) holds for all $f \in H_0^{k+1}(\Omega)$ rather than for all $f \in H^{k+1}(\Omega)$, then $\mathcal{B}_s$ is a Riesz basis for $H_0^s(\Omega)$ if $s \in (1, \sigma + \frac{3}{2}) \setminus (\mathbb{Z} + \frac{1}{2})$.

Proof. Under the assumptions of the theorem, the bases $\{B_\xi^{(n)}\}_{\xi\in\Xi_n}$ are stable and local in the sense of the definition in Section 1.3.2. Since $\operatorname{diam}(T)\sim\rho^{-n}$, $T\in\Delta_n$, the bases $\{\rho^n B_\xi^{(n)}\}_{\xi\in\Xi_n}$ are L_2-stable, which implies

$$\Big\|\sum_{\xi\in\Xi_n} c_\xi B_\xi^{(n)}\Big\|_{L_2(\Omega)} \sim \rho^{-n}\Big(\sum_{\xi\in\Xi_n} c_\xi^2\Big)^{1/2}, \tag{2.4.12}$$

for any real numbers c_ξ, with constants of equivalence independent of n.

Let $0<s<r+\frac{3}{2}$. We choose a number $\bar s$ such that $s<\bar s<r+\frac{3}{2}$. By Theorem 2.5, since the spaces S_n possess stable local bases, we obtain the Bernstein inequality

$$\|g\|_{H^{\bar s}(\Omega)} \lesssim \rho^{n\bar s}\|g\|_{L_2(\Omega)}, \qquad g\in S_n.$$

By Theorem 2.10, applied with $\alpha=\rho^{k+1}$, $\lambda=\bar s/(k+1)<1$ and $\theta=s/(k+1)$, we see that under the assumptions of part (a) condition (2.4.3) of Theorem 2.9 is satisfied for $H=L_2(\Omega)$, $H'=H^{k+1}(\Omega)$ and $H_s=H^s(\Omega)=[L_2(\Omega),H^{k+1}(\Omega)]_\theta$. Similarly, under the assumptions of part (b) condition (2.4.3) follows from Theorem 2.10 with $H=L_2(\Omega)$, $H'=H_0^{k+1}(\Omega)$ and $H_s=[L_2(\Omega),H_0^{k+1}(\Omega)]_\theta$.

We now verify the other assumptions of Theorem 2.9. The density of $\cup_{n=0}^\infty S_n$ in $H=L_2(\Omega)$ follows from the Jackson inequality (2.4.11) since both $H^{k+1}(\Omega)$ and $H_0^{k+1}(\Omega)$ are dense in $L_2(\Omega)$. Furthermore, let $I_n: C(\Omega)\to S_n$, $n=0,1,\dots$, be the Lagrange interpolation operator

$$I_n f := \sum_{\xi\in\Xi_n} f(\xi) B_\xi^{(n)}.$$

We set $P_n := I_{n-1}|_{S_n}$, $n\ge 1$, and $P_0:=0$. Then $P_n: S_n\to S_{n-1}$ is a linear projection, and, in view of the nestedness (2.4.10) of $\{\Xi_n\}_{n=0}^\infty$, we have $P_{n+1}\cdots P_m = I_n|_{S_m}$ for all $m>n$. Let $g\in S_m$ and $h:=P_{n+1}\cdots P_m g$. Then $g=\sum_{\xi\in\Xi_m} g(\xi)B_\xi^{(m)}$ and $h=\sum_{\xi\in\Xi_n} g(\xi)B_\xi^{(n)}$. By (2.4.12) and (2.4.10) we obtain

$$\begin{aligned}\|h\|_{L_2(\Omega)}^2 &\lesssim \rho^{-2n}\sum_{\xi\in\Xi_n}|g(\xi)|^2 \le \rho^{-2n}\sum_{\xi\in\Xi_m}|g(\xi)|^2\\ &\lesssim \rho^{2(m-n)}\|g\|_{L_2(\Omega)}^2,\end{aligned}$$

which implies (2.4.2) with $H = L_2(\Omega)$ and $v = 1$. Because of (2.4.10) the sets

$$\big\{\rho^n B_\xi^{(n)} : \xi \in \Xi_n \setminus \Xi_{n-1}\big\}, \quad n = 0, 1, \dots \quad (\Xi_{-1} = 0)$$

form L_2-stable bases for the complement spaces W_n. Since $W_n \subset S_n \subset H^s(\Omega)$ for all $s < r + \frac{3}{2}$ by Theorem 2.5, an application of Theorem 2.9 with $v = 1$ completes the proof of part (a). Under the assumptions of part (b) it is easy to see that $S_n \subset \tilde{H}^s(\Omega) = H_0^s(\Omega)$ for all $s < \sigma + \frac{3}{2}$, $s \notin \mathbb{Z} + \frac{1}{2}$, and Theorem 2.9 implies that $\mathcal{B}_s$ is a Riesz basis for $[L_2(\Omega), H_0^{k+1}(\Omega)]_{s/(k+1)}$ for all $1 < s < \sigma + \frac{3}{2}$. The statement of part (b) follows in view of the description (2.2.5) of these interpolation spaces in Section 2.2. □

Note that in the case $r = \sigma = 0$ the condition (2.4.3) of Theorem 2.9 for $H = L_2(\Omega)$ and $H_s = H_0^s(\Omega)$, $s < \frac{3}{2}$, can be verified with the help of [48, Corollary 3] without using interpolation spaces.

The argumentation of Theorem 2.11 for $\Omega \subset \mathbb{R}^d$ would lead to the Riesz basis for $H^s(\Omega)$ with the expectable range $\frac{d}{2} < s < r + \frac{3}{2}$. Indeed, (2.4.12) then holds with $\rho^{-\frac{dn}{2}}$ replacing ρ^{-n}, and hence Theorem 2.9 is applicable with $v = \frac{d}{2}$.

The standard C^0 piecewise linear hierarchical basis [57] is, after appropriate scaling, a Riesz basis of $H^s(\Omega)$ $s \in (1, \frac{3}{2})$ in two dimensions, see [39]. Clearly, Theorem 2.11 applies to this case, where the triangulations Δ_n are obtained by the uniform refinement of an initial triangulation of Ω, $\rho = 2$, S_n is either $S_1^0(\Delta_n)$ (for $H^s(\Omega)$) or its subspace $\{s \in S_n : s|_{\partial\Omega} = 0\}$ (for $H_0^s(\Omega)$), and Ξ_n is either the set of all vertices of Δ_n or the set of all interior vertices, respectively. The Jackson inequality (2.4.11) for $k = 1$ follows from Theorem 2.7 since $S_1^0(\Delta_n)$ are macro-element spaces with uniformly bounded basis functions, $\mathbb{P}_1 \subset S_1^0(\Delta_n)$, and the interpolation operator Π is boundary confirming of order $\sigma = 0$.

In the next section we provide a brief review of the existing constructions of C^1 Lagrange type hierarchical Riesz bases for Sobolev spaces $H^s(\Omega)$, $s \in (1, \frac{5}{2})$, and $H_0^s(\Omega)$, $s \in (1, \frac{3}{2}) \cup (\frac{3}{2}, \frac{5}{2})$. Note that C^1 hierarchical bases of Hermite type are also known [14, 49]. They form Riesz bases for $H^s(\Omega)$, $s \in (2, \frac{5}{2})$.

2.5 C^1 Lagrange hierarchical Riesz bases for Sobolev spaces

Spline spaces $S_n \subset S_d^r(\Delta_n)$ and Lagrange interpolation sets Ξ_n satisfying the hypotheses of Theorem 2.11 give rise to hierarchical Riesz bases for $H^s(\Omega)$, $s \in (1, r+\frac{3}{2})$, respectively $H_0^s(\Omega)$, $s \in (1, \sigma+\frac{3}{2})\backslash(\mathbb{Z}+\frac{1}{2})$. However, specific constructions are only available for $r = 0, 1$. In this section we review such constructions of the spaces S_n in the case $r = 1$. We do not describe the corresponding sets Ξ_n as they are quite technical, and the interested reader is instead referred to the original literature.

2.5.1 Piecewise cubics on triangulated quadrangulations

The first construction of C^1 Lagrange hierarchical bases has been suggested in [21], where the nested spline spaces are the macro element spaces of C^1 piecewise cubic polynomials on the triangulations (see [36, Section 6.5]) obtained by adding two diagonals to the quadrilaterals of a *checkerboard* quadrangulation of any polygonal domain, which means that all interior vertices of the quadrangulation are of degree 4 and quadrilaterals can be coloured black and white in such a way that any two quadrilaterals sharing an edge have opposite colours. The corresponding nodal basis satisfies (2.3.4) with a constant C_2 dependent only on the minimum angle of the triangles $T \in \Delta_R$ and the interpolation operator Π is boundary conforming of order 1.

Nested spaces are obtained by the *triadic refinement* of the quadrilaterals and their subtriangles illustrated in Figures 2.2 and 2.3. More precisely, Let $Q = \langle v_1, v_2, v_3, v_3\rangle$ be a quadrilateral and let $p_1 = 1/3(2v_1 + v_2)$, $p_2 = 1/3(v_1 + 2v_2)$, $p_3 = 1/3(2v_2 + v_3)$, $p_4 = 1/3(v_2 + 2v_3)$, $p_5 = 1/3(2v_3 + v_4)$, $p_6 = 1/3(v_3 + 2v_4)$, $p_7 = 1/3(2v_4 + v_1)$, $p_8 = 1/3(v_4 + 2v_1)$, $p_9 = 1/3(v_1 + 2\bar{v})$, $p_{10} = 1/3(v_2 + 2\bar{v})$, $p_{11} = 1/3(v_3 + 2\bar{v})$, $p_{12} = 1/3(v_4 + 2\bar{v})$, where $\bar{v}$ is the point of intersection of the

diagonals of Q. The refinement is obtained by connecting the points p_1 and p_8 to p_9, p_2 and p_3 to p_{10}, p_4 and p_5 to p_{11}, p_6 and p_7 to p_{12}, and finally connecting the points $p_9, p_{10}, p_{11}, p_{12}$ together, as shown in Figure 2.2. Each of the 9 quadrilaterals is subdivided into 4 triangles by its diagonals as in Figure 2.3.

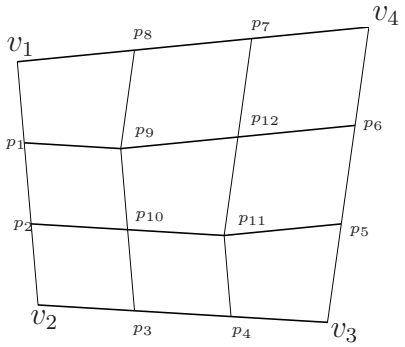

Figure 2.2: A triadic refinement $\diamondsuit_Q$ of a quadrilateral Q.

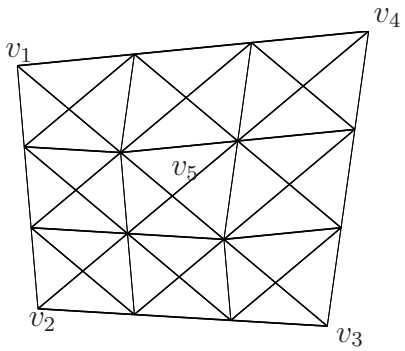

Figure 2.3: The triangulation Δ_Q of $\diamondsuit_Q$.

Given an initial quadrangulation $\diamondsuit_0$ of Ω, this method generates a sequence of successively refined quadrangulations $\diamondsuit_0, \diamondsuit_1, \ldots, \diamondsuit_n, \ldots$, and triangulations $\Delta_0, \Delta_1, \ldots, \Delta_n, \ldots$, and the nested macro-element spaces are $S_n = S_3^1(\Delta_n)$. While the nestedness of the sequence of triangulations $\{\Delta_n\}_{n=0}^{\infty}$ is obvious, its regularity, which has not been fully addressed in [21], follows from Proposition 2.12 below. For the nested sequence of Lagrange interpolation sets $\{\Xi_n\}_{n=0}^{\infty}$ described in [21]

all assumptions of Theorem 2.11 (b) are satisfied, with $r = \sigma = 1$, $k = 3$ and $\rho = 3$, which leads to a Riesz basis for $H_0^s(\Omega)$, $s \in (1, \frac{3}{2}) \cup (\frac{3}{2}, \frac{5}{2})$.

Proposition 2.12. *Each triangle $T \in \Delta_n$, $n \geq 2$, is similar to a triangle in Δ_1 with the scaling factor $\frac{1}{3^{n-1}}$.*

Proof. Consider the quadrangulation $\diamondsuit_Q$ of a quadrilateral Q obtained by the triadic refinement. It is easy to see that the quadrilateral $\langle p_9, p_{10}, p_{11}, p_{12}\rangle$ is similar to the parent quadrilateral $Q = \langle v_1, v_2, v_3, v_4\rangle$, whereas $\langle p_1, p_2, p_{10}, p_9\rangle$ is a parallelogram with side length $\frac{1}{3}$ of the size of the parent edge $\langle v_1, v_2\rangle$, see Figure 2.2. Three other children of Q in similar position are also parallelograms.

Let Δ_Q be the triangulation of $\diamondsuit_Q$ shown in Figure 2.3. We observe that there are 8 different types of similar triangles in Δ_Q as shown in Figure 2.4. The triangles of types $1, 2, 3$ and 4 are similar to their parent triangles (obtained from Q by splitting along its diagonals) with the coefficient $\frac{1}{3}$. The triangles of types $5, 6, 7$ and 8 will be referred to as "median" triangles because each of them has a side parallel to the median of its parent triangle and of length $\frac{2}{3}$ of that median, as illustrated in Figure 2.5, where the section $\langle v_1, v_2, v_5\rangle$ of the triangulations Δ_Q of Figure 2.3 is shown separately.

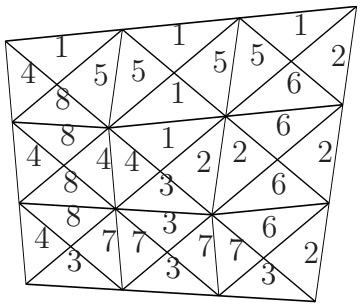

Figure 2.4: Eight types of similar triangles in Δ_Q.

We now apply the next refinement step and look at the median subtriangle $\langle a, b, c\rangle$ of the median triangle in Δ_Q as shown in Figure 2.6. We note that the

dotted line $\langle q_1, q_2\rangle$ is of length $\frac{2}{3}$ of the side $\langle p_1, p_9\rangle$ of the parent which is parallel to the median $\langle m, v_5\rangle$ of the grandparent. Hence the median of the median triangle $\langle a, b, c\rangle$ is of length $\frac{1}{4} \times \frac{2}{3} \times \frac{2}{3} = \frac{1}{9}$ of the median $\langle m, v_5\rangle$ of the grandparent $\langle v_1, v_2, v_5\rangle$. Therefore, the median subtriangle $\langle a, b, c\rangle$ is similar to the grandparent $\langle v_1, v_2, v_5\rangle$ with coefficient $\frac{1}{9}$.

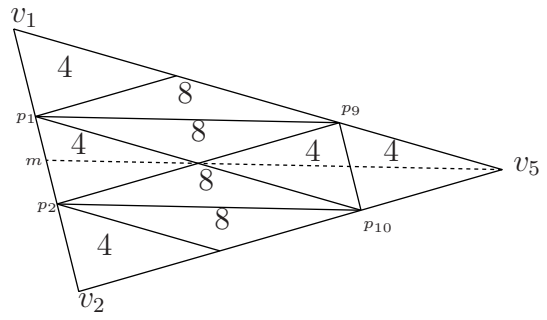

Figure 2.5: The triangle $\langle v_1, v_2, v_5\rangle$, its median $\langle m, v_5\rangle$ and 9 children.

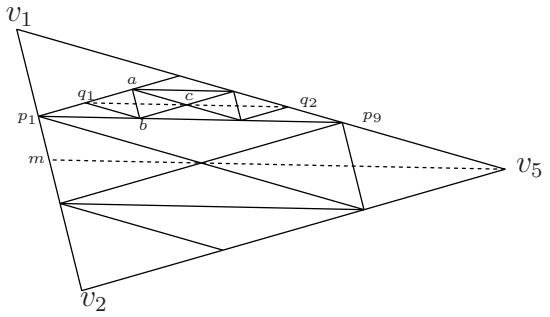

Figure 2.6: The triangle $\langle a, b, c\rangle$ is similar to the grandparent $\langle v_1, v_2, v_5\rangle$ with coefficients $\frac{1}{9}$.

Let $T \in \Delta_n$, with $n \geq 2$. By applying the above observations recursively, we have two following cases: 1) T is similar to an ancestor $\tilde{T} \in \Delta_1$ with coefficient $\frac{1}{3^{n-1}}$. 2) T is similar to an ancestor $\hat{T} \in \Delta_0$ with coefficient $\frac{1}{3^n}$. But $\hat{T}$ has a child $\tilde{T} \in \Delta_1$ which is similar to $\hat{T}$ with coefficient $\frac{1}{3}$ and this implies that T is similar to $\tilde{T}$ with coefficient $\frac{1}{3^{n-1}}$. □

2.5.2 Piecewise quadratics on Powell-Sabin-6 splits

C^1 piecewise quadratic hierarchical bases are considered in [41]. Here, an initial checkerboard quadrangulation of Ω is first turned into a triangulation by adding one diagonal of each quadrilateral, and then each triangle is subdivided using a Powell-Sabin-6 (PS-6) split. To obtain a nested sequence of triangulations $\{\Delta_n\}_{n=0}^{\infty}$, a triadic refinement of the PS-6 split [56] is performed, see Figure 2.7. The nested spline spaces S_n are the C^1 piecewise quadratic Powell-Sabin macro-elements [36, Section 6.3]. Lagrange interpolation sets Ξ_n with the required properties are selected using a scheme which can be seen as a specific realisation of the interpolation method described in [47]. It is shown in [41] that this construction leads to a Riesz basis for $H^s(\Omega)$, $1 < s < \frac{5}{2}$, under the assumption that the triangulation sequence $\{\Delta_n\}_{n=0}^{\infty}$ is regular. Indeed, in this case Theorem 2.11 is applicable with $r = \sigma = 1$ and $k = 2$. We note however that this assumption does not seem easy to verify unless Δ_0 is a uniform triangulation, in which case $\rho = 3$. It is an open question whether an arbitrary polygonal domain Ω admits an initial triangulation such that the sequence of triangulations obtained by the triadic refinement of its PS-6 split is regular.

2.5.3 Piecewise quadratics on mixed PS-6/PS-12 splits

In Chapter 3 we construct C^1 piecewise quadratic hierarchical bases on arbitrary polygonal domains using nested sequences of triangulations and spline spaces introduced in [33]. Beginning with an arbitrary triangulation Δ_0 of Ω, a nested sequence of triangulations $\{\Delta_n\}_{n=0}^{\infty}$ is obtained by the standard uniform refinement, where the middle points of edges are connected to each other. An edge of Δ_n is said to be regular if it is shared by two triangles that form a parallelogram. Clearly, all boundary edges are irregular, but an interior edge may only be irregular if it overlaps a part of an edge of Δ_0. Furthermore, let Δ_n^* be the triangulation obtained by subdividing each triangle $T \in \Delta_n$ using the Powell-Sabin-6 split if all

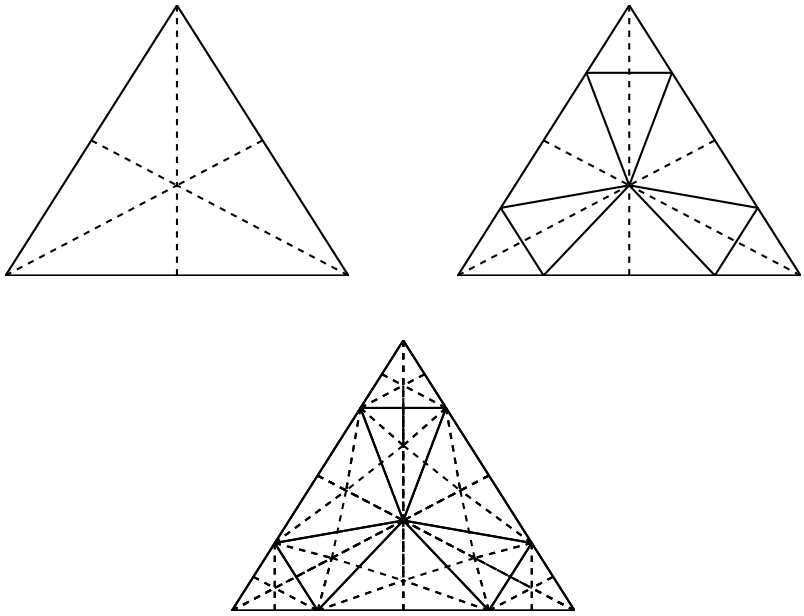

Figure 2.7: The triadic refinement of the PS-6 split: A new vertex is placed at the position of the interior point in the PS-6 split and two new vertices on each edge.

edges of T are regular, or the Powell-Sabin-12 split [36, Section 6.4] otherwise. For both PS-6 and PS-12 splits the central vertex is chosen at the barycentre of the triangle and the edge splitting vertices are at the midpoints of the edges. Then $\{\Delta_n^*\}_{n=0}^{\infty}$ is also a nested sequence of triangulations, as illustrated in Figure 2.8. It is obviously regular, with refinement factor $\rho = 2$.

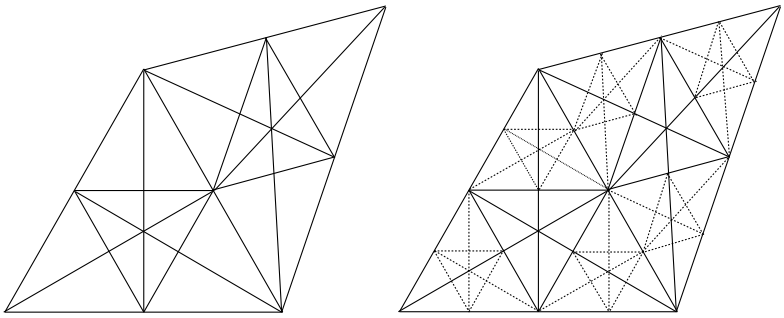

Figure 2.8: An example to illustrate that Δ_{n+1}^* is a refinement of Δ_n^*.

The spline spaces are defined by

$$S_n = \big\{ s \in S_2^1(\Delta_n^*) : \frac{\partial s}{\partial e^\perp}\big|_e \text{ is linear for each irregular edge } e \text{ of } \Delta_n \big\},$$

where $\frac{\partial s}{\partial e^\perp}$ denotes the normal derivative of s on e. It is easy to see that $\{S_n\}_{n=0}^\infty$ are nested macro-element spaces, their interpolation operators are boundary conforming of order 1, and $\mathbb{P}_2 \subset S_n$, $n = 0, 1, \ldots$. Let $P_n : S_n \to S_{n-1}$ be the orthogonal projector with respect to the inner product defined by

$$(f, g) = \sum_{e \in \mathcal{E}_n} (f, g)_e,$$

where $\mathcal{E}_n$ is the set of all edges of Δ_n and, for $e = \langle v_1, v_2 \rangle$,

$$\begin{aligned}(f, g)_e := \frac{1}{2^{2n}} \Big[& f(v_1)g(v_1) + \Big(f(v_1) + \frac{1}{4}\frac{\partial f}{\partial e}(v_1)\Big)\Big(g(v_1) + \frac{1}{4}\frac{\partial g}{\partial e}(v_1)\Big) \\ & + f(v_2)g(v_2) + \Big(f(v_2) - \frac{1}{4}\frac{\partial f}{\partial e}(v_2)\Big)\Big(g(v_2) - \frac{1}{4}\frac{\partial g}{\partial e}(v_2)\Big)\Big].\end{aligned}$$

It is shown in [33] that the projectors P_n satisfy (2.4.2) with

$$v = \log_2 \Big(\frac{2(1 + \sqrt{13})}{3}\Big) \approx 1.618,$$

and thus lead to a construction of Riesz bases in $H^s(\Omega)$ for $v < s < \frac{5}{2}$.

In Chapter 3 we present a construction of nested Lagrange interpolation sets for S_n and their subspaces with homogeneous boundary conditions of order 1, which leads to a Riesz basis for $H^s(\Omega)$, $s \in (1, \frac{5}{2})$ and $H_0^s(\Omega)$, $s \in (1, \frac{3}{2}) \cup (\frac{3}{2}, \frac{5}{2})$, by applying Theorem 2.11 with $r = \sigma = 1$, $k = 2$ and $\rho = 2$.

Chapter 3

C^1 Piecewise Quadratic Hierarchical Bases

3.1 Introduction

In this chapter we construct Lagrange hierarchical bases for the spaces of C^1 piecewise quadratic polynomials on the combination of Powell-Sabin-6 and Powell-Sabin-12 triangulations which are available for any polygonal domain. These hierarchical bases generate Riesz bases for the Sobolev spaces $H^s(\Omega)$ for $s \in (1, \frac{5}{2})$, and $H_0^s(\Omega)$ for $s \in (1, 3/2) \cup (3/2, 5/2)$.

Hierarchical bases were constructed first by Yserentant in [57], based on piecewise linear functions on general triangulations in the finite element applications to second order elliptic boundary value problems. For domains in $\mathbb{R}^2$ they give rise to Riesz bases for $H^s, s \in (1, 3/2)$. In [14] Oswald constructed hierarchical bases using C^1 quadratic and cubic spline spaces. It was demonstrated that the hierarchical bases are suboptimal for the condition numbers of the corresponding discretisation matrices related to fourth-order elliptic equations. In [49] hierarchical bases were constructed for C^1 quintic spline spaces. These C^1 hierarchical bases are of Hermite type and so they generate Riesz bases for $H^s(\Omega), s \in (2, 5/2)$. In [32] Hong and Schumaker also constructed C^1 hierarchical bases of Hermite

type for cubic splines and these bases are employed for surface compression.

For arbitrary polygonal domains $\Omega \in \mathbb{R}^2$, the first C^1 hierarchical Riesz bases of Lagrange type were constructed by Davydov and Stevenson [21], for $H^s(\Omega)$ with $s \in (1, \frac{5}{2})$ using C^1 piecewise cubic polynomials on certain triangulations obtained from checkerboard quadrangulations. Different C^1 piecewise quadratic hierarchical bases of Lagrange type were constructed in [41]. They are based on the triadic refinement of the Powell-Sabin-6 split of a special initial triangulation and lead to Riesz bases for $H^s(\Omega)$ with $s \in (1, \frac{5}{2})$ only under the assumption that the resulting nested sequence of triangulations is quasi-uniform. In [33] Jia and Liu constructed Riesz bases of spline wavelets based on orthogonal projection operators which give the range of stability $s \in (1.618, \frac{5}{2})$, but with an advantage of that it is applied to general triangulations of any polygonal domain Ω. On the unit square, Jia and Zhao [34] recently constructed wavelet Riesz bases for $H^s(\Omega), s \in (1, 5/2)$ and investigated their applications to numerical solutions of the biharmonic equation and general elliptic equations of fourth-order.

It is expected that the C^1 Lagrange hierarchical bases constructed in this chapter and also those bases constructed in [21, 33, 41] are suitable for surface compression, see [25, 32, 42]. These bases also will have applications to numerical solutions of partial differential equations. These bases are particular suitable for the biharmonic equation since they are H^2-stable (see the discussion in [49, 21, 41]). The condition numbers of the corresponding discretisation matrices are uniformly bounded.

We note that our hierarchical Riesz bases have a larger range of stability compared to the Hermite type hierarchical bases of [14, 49] and the wavelet bases of [33]. Our construction is available on general triangulations of the polygonal domains and it does not require any special initial partition as needed in [33, 41]. Our method can be applied to any polygonal domain compared to [34] where it is only available on the unit square. We also note that numerical schemes based on the Riesz bases of [21, 41, 33] have yet to be implemented. We have implemented

our bases and investigated their applications to surface compression and numerical solutions of the biharmonic equation. Numerical results are presented in Chapter 4.

In Section 3.2 we discuss the nested sequence of C^1 piecewise quadratic spline spaces of Powell-Sabin and in Section 3.3 we construct local Lagrange interpolation sets for the spaces and prove that the corresponding Lagrange bases are stable and local. The most challenging part is to ensure the Lagrange interpolation sets of consecutive refinement levels are nested so that the corresponding hierarchical bases can be constructed. In Section 3.4 we use the general theory established in Chapter 2 to show that the Lagrange hierarchical bases, properly scaled, give rise to Riesz bases for $H^s(\Omega)$ for $s \in (1, 5/2)$, and $H_0^s(\Omega)$ for $s \in (1, 3/2) \cup (3/2, 5/2)$.

3.2 Refinable Spaces of C^1 Piecewise Quadratics

We now describe the refinable spaces of C^1 piecewise polynomials we are going to use for our construction of hierarchical bases. This space is introduced by Jia and Liu [33] for the construction of C^1 spline wavelets.

Let Ω be a bounded connected polygonal domain in $\mathbb{R}^2$. Suppose that some initial triangulation Δ_0 of Ω is given such that the union of the triangles of Δ_0 is Ω and the intersection of two triangles of Δ_0 either consists of a common edge or a common vertex of both triangles or is empty.

Beginning with Δ_0 we construct a nested sequence $\Delta_0, \Delta_1, \Delta_2, \ldots$ of triangulations of Ω, i.e.,

$$\Delta_n \subset \Delta_{n+1} \quad n = 0, 1, \ldots. \tag{3.2.1}$$

The triangulation Δ_{n+1} is obtained from Δ_n by subdividing any triangle of Δ_n into four equal subtriangles by joining the midpoints of the three edges with each other as shown in Fig.3.1. We call this procedure the uniform refinement (T_U) of any triangle T.

The sequence $\{\Delta_n\}$ satisfies the minimum angle condition, i.e., the minimum

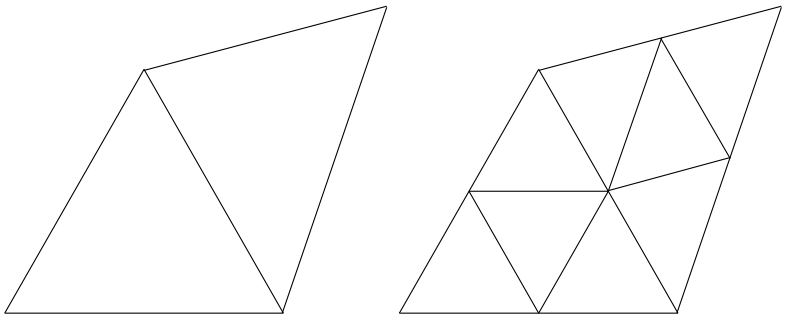

Figure 3.1: The uniform refinement procedure.

angle of any triangle in any Δ_n remains bounded away from zero (all triangles are similar to one of the triangles of level 0 so minimum angle in level n is the same as the minimum angle in level 0) and is quasi-uniform (all triangles in Δ_n have comparable sizes), i.e.,

$$C_1 \cdot 2^{-n} \leq \operatorname{diam} T \leq C_2 \cdot 2^{-n}, \quad T \in \Delta_n, \quad n = 0, 1, \ldots. \tag{3.2.2}$$

with absolute constants C_1, C_2.

Two triangles $T, T' \in \Delta_n$ are said to be neighbours if T and T' share a common edge. A triangle T is called *regular* if T and its any neighbouring triangle T' form a parallelogram. Otherwise T is called *irregular*. An edge shared by two triangles is said to be regular if and only if the two triangles form a parallelogram, and all other edges are said to be irregular. All edges of Δ_n which are not part of an edge of Δ_0 are regular. For example a triangle of Δ_2 may be irregular only if one of its edges is a part of an interior edge of Δ_0. These triangles are shown as shaded in Fig.3.2. All other triangles of Δ_2 are regular.

Starting from (3.2.1) we introduce further subdivisions by subdividing any regular triangle of Δ_n into six subtriangles by joining the midpoints of the three edges with the opposite vertex and subdividing any irregular triangle of Δ_n into twelve triangles by joining the midpoints of the three edges with each other and with the opposite vertex. We call these the Powell-Sabin-6 split (T_{PS6}) and Powell-Sabin-12 split (T_{PS12}) of any triangle T, respectively. See Fig.3.3. Clearly, T_{PS12} is a refinement of both T_U and T_{PS6}. Moreover, if each of the triangle of T_U is

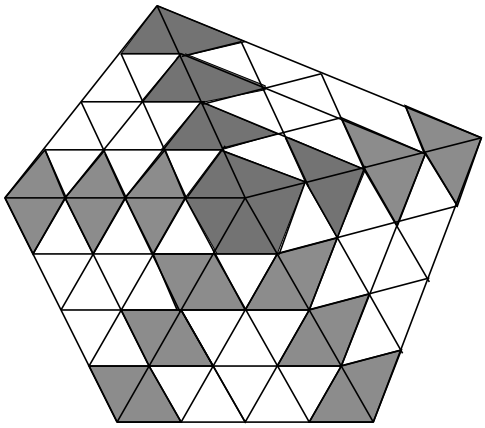

Figure 3.2: The irregular triangles are shaded.

divided into six smaller triangles by Powell-Sabin-6 split then it is also clear that the resulting triangulation is a refinement of T_{PS12}.

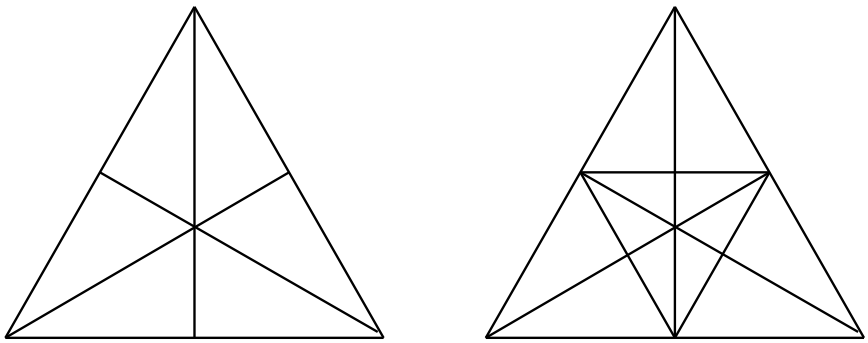

Figure 3.3: Powell-Sabin-6 split and Powell-Sabin-12 split of a triangle.

Let Δ_n^{reg} be the collection of all regular triangles of Δ_n, and $\Delta_n \setminus \Delta_n^{reg}$ the collection of all irregular triangles of Δ_n. We write the resulting triangulation Δ_n^* of Δ_n

$$\Delta_n^* := \Big(\bigcup_{T \in \Delta_n^{reg}} T_{PS6} \Big) \cup \Big(\bigcup_{T \in \Delta_n \setminus \Delta_n^{reg}} T_{PS12} \Big).$$

The sequence of triangulations $\Delta_0^*, \Delta_1^*, \Delta_2^*, \ldots$ satisfies

$$\Delta_n^* \subset \Delta_{n+1}^* \ldots, \quad n = 0, 1, \ldots, \tag{3.2.3}$$

$$C_3 \cdot 2^{-n} \leq \operatorname{diam} T^* \leq C_4 \cdot 2^{-n}, \quad T^* \in \Delta_n^*, \quad n = 0, 1, \ldots$$

with absolute constants C_3, C_4.

An example of property (3.2.3) is illustrated in Fig.3.4.

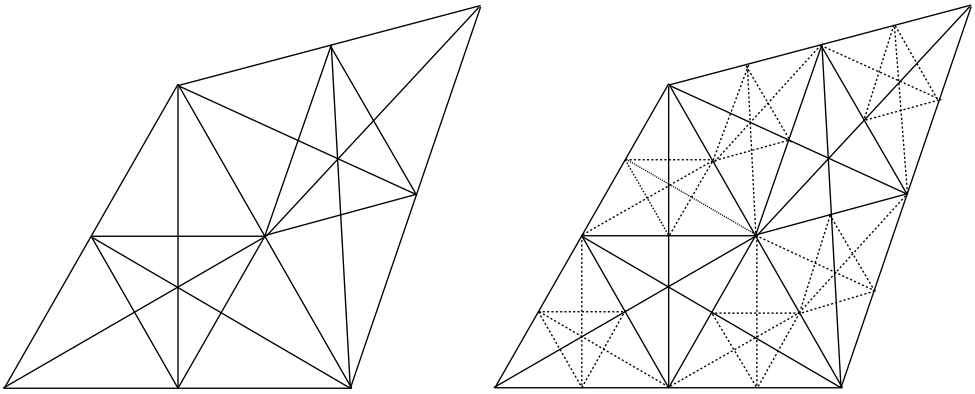

Figure 3.4: An example to illustrate that Δ_{n+1}^* is a refinement of Δ_n^*.

For $n = 0, 1, \ldots$, we define the space $S_2^1(\Delta_n^*)$ of C^1 quadratic piecewise polynomials, i.e.

$$S_2^1(\Delta_n^*) := \{s \in C^1(\Omega) : s|_T \in \mathbb{P}_2 \text{ for all } T \in \Delta_n^*\},$$

where $\mathbb{P}_2$ is the space of polynomials of degree at most 2.

We now consider a subspace S_n of $S_2^1(\Delta_n^*)$ defined by

$$S_n = \big\{s \in S_2^1(\Delta_n^*) : \frac{\partial s}{\partial e^\perp}\big|_e \text{ is linear for all irregular edges } e \text{ of } \Delta_n\big\},$$

where $\frac{\partial s}{\partial e^\perp}\big|_e$ is the normal derivative of s on e.

Suppose $s \in S_n$ and e is an irregular edge of Δ_{n+1}. Then the normal derivative of s on e is a linear function since all irregular edges of Δ_{n+1} are edges of Δ_n^*. This shows that

$$S_n \subset S_{n+1}, \quad n = 0, 1, 2, \ldots.$$

Theorem 3.1. *The dimension of S_n is given by*

$$\dim S_n = 3\#\mathcal{V}_n,$$

where $\mathcal{V}_n$ is the set of all vertices of Δ_n. Moreover, the spline $s \in S_n$ is uniquely defined by its function values $s(v)$ and gradients $\{\frac{\partial s}{\partial x}(v), \frac{\partial s}{\partial y}(v)\}$ at the vertices $v \in \mathcal{V}_n$ of Δ_n.

Proof. Suppose $T \in \Delta_n^{reg}$. Then T is a PS-6 split triangle. Let $s \in S_n$. It is known [53] that given function and gradient values at the vertices of T, the C^1 piecewise quadratic function $s|_T$ is uniquely determined. Moreover, the function $s|_e$ and the gradient of $s|_T$ on the edge e of T are defined by the function and gradient values at the two endpoints of e. This argument relies on the fact that the directional derivative along the line joining the midpoint of e to the barycentre of T evaluated on e is a linear function. Thus any function defined on two adjacent triangles of this type will be differentiable across their common edge if the line joining the barycentres of the two triangles intersects at the midpoint of their common edge. We also note that this condition is always satisfied by our construction since any two PS-6 split triangles together form a parallelogram.

Now suppose $T' \in \Delta_n \setminus \Delta_n^{reg}$. Then T' is a PS-12 split triangle. The edges of T' are either irregular or they are shared by PS-6 split triangles. If an edge e' of T' is irregular then the normal derivative of $s|_{T'}$ at the midpoint of e' is the average of the normal derivatives computed at the two endpoints of e' since the normal derivative is a linear function on e'. Thus any function defined on two PS-12 split triangles will be differentiable across their common edge e'. If an edge e of T' is shared by a PS-6 split triangle T, e is a regular edge of Δ_n and $T' \cup T$ forms a parallelogram. The directional derivative along the line joining the the midpoint of e to the barycentre of T' evaluated on e is a linear function. Then the normal derivative of $s|_{T'}$ at the midpoint w of e is determined from $s|_T$ since $s|_T$ and $s|_{T'}$ are differentiable across their common edge e (See Remark 3.2 and 3.3). The normal derivative of $s|_{T'}$ at w is the linear combinations of the directional derivative of $s|_T$ along the edge e evaluated at w and the directional derivative of $s|_T$ along the line connecting the midpoint of e to the barycentre of T evaluated at w. These two directional derivatives of $s|_T$ are defined by the function and gradients values at the two endpoints of e. Given function and gradient values at the vertices of T', and the normal derivatives at the midpoints of the edges of T', it is known [53] that the C^1 piecewise quadratic function $s|_{T'}$ is uniquely determined.

Thus from the above discussion we deduce that $s|_{T'}$ is uniquely determined only by the function and gradient values at the vertices of T'.

Since given function and gradient values uniquely determine s on each triangle of Δ_n of Ω, and hence on all of Ω, it follows that the dimension of the spline space $S_n(\Delta)$ is $3\#\mathcal{V}_n$. Furthermore, we obtain a piecewise quadratic function that is continuous and whose first derivative is continuous throughout the triangulation.

□

Remark 3.2. *Suppose we extend a PS-6 split triangle $T \in \Delta_n$ to a PS-12 split triangle and put a condition such that the directional derivatives along the line joining the midpoint of the regular edges to the barycentre of the triangle of the spline function $s|_T$, evaluated along the edges, are linear. We know from [53] the spline function $s|_T$ where T is PS-6 split triangle satisfies the linearity of these directional derivatives. Then any spline $s|_T$ and the gradient of s on such an edge are uniquely defined by the function and gradient values of s at its two endpoints when T is either the PS-6 split or PS-12 split triangle. So $s|_T$ is equivalent when T is either a PS-6 split or PS-12 split triangle. Hence if we extend all the PS-6 split triangles of Δ_n to PS-12 split triangles we obtain the same spline space. Moreover, the spline space is now a subspace of the classical Powell-Sabin-12 C^1 macro-element space.*

Remark 3.3. *Consider the edge shared by two triangles T_1, T_2, where T_1 is a PS-6 split and T_2 is a PS-12 split. Let $s_1 = s|_{T_1}$ and $s_2 = s|_{T_2}$. Along a common edge e, the restriction of each of the two bivariate C^1 piecewise quadratic polynomials $s_1|_e$ and $s_2|_e$ to the common edge e gives a univariate C^1 piecewise quadratic polynomials on the edge. Each of the univariate C^1 piecewise quadratic polynomials $s_1|_e$ and $s_2|_e$ is determined uniquely by two function values and first order derivatives at the two endpoints of the edge. These values are common to the two triangles so $s_1|_e$ and $s_2|_e$ are identical. Hence s_1 and s_2 are C^0 continuous across the common edge e. Now to show that it is C^1 continuous, it is enough to consider the*

continuity of the directional derivatives along the line joining the midpoint m_e of the common edge to the barycentre v_T of the triangle, evaluated along the common edge e, denoted by $D_{v_{T_1}-m_e}s_1|_e$ and $D_{v_{T_1}-m_e}s_2|_e$ for s_1 and s_2, respectively. It is known [53] that $D_{v_{T_1}-m_e}s_1|_e$ is a linear function and $D_{v_{T_1}-m_e}s_2|_e$ is a piecewise linear function. Also $D_{v_{T_1}-m_e}s_2|_e$ is determined by three data values, that is, it's two function values at each endpoint of e and at the midpoint of e. Since s_1 and s_2 are continuous across e, their gradients at the midpoint of e coincide and hence $D_{v_{T_1}-m_e}s_1|_e$ and $D_{v_{T_1}-m_e}s_2|_e$ evaluated at the midpoint m_e of e coincide. Since these data are common to the two triangles, then $D_{v_{T_1}-m_e}s_1|_e$ and $D_{v_{T_1}-m_e}s_2|_e$ are identical and they are linear functions. Hence s_1 and s_2 are C^1 continuous across the common edge e.

Let $N_n = 3\#\mathcal{V}_n$ be the dimension of S_n. We now describe a basis for S_n. For each $v \in \mathcal{V}_n$, let λ_v, λ_v^x and λ_v^y be the point-evaluation functionals defined on the space $C^1(\Omega)$ by

$$\lambda_v s = s(v), \quad \lambda_v^x s = \frac{\partial s}{\partial x}(v), \quad \lambda_v^y s = \frac{\partial s}{\partial y}(v). \tag{3.2.4}$$

Then by Theorem 3.1 the set of linear functionals

$$\mathcal{N}_n = \{\lambda_i^{(n)}\}_{i=1}^{N_n} = \bigcup_{v\in\mathcal{V}_n} \{\lambda_v, \lambda_v^x, \lambda_v^y\} \tag{3.2.5}$$

is a nodal minimal determining set (NMDS) for S_n. Then for $\mathcal{N}_n$, the (Hermite) nodal basis $\Phi_n = \{s_i^{(n)}\}_{i=1}^{N_n}$ for S_n will be defined uniquely by the duality

$$\lambda_i^{(n)} s_j^{(n)} = \begin{cases} 1, & i = j, \\ 0, & \text{otherwise.} \end{cases}$$

Theorem 3.1 shows that for every function $f \in C^1(\Omega)$, there is a unique spline $s \in S_n$ that solves the Hermite interpolation problem

$$s(v) = f(v), \quad \frac{\partial s}{\partial x}(v) = \frac{\partial f}{\partial x}(v), \quad \frac{\partial s}{\partial y}(v) = \frac{\partial f}{\partial y}(v), \quad \text{for all } v \in \mathcal{V}_n. \tag{3.2.6}$$

Since $\lambda_i^{(n)}$ are function evaluations or derivatives of at most first order, they lead to the Hermite interpolation operator $\Pi_n : C^1(\Omega) \to S_n$ defined by

$$\Pi_n f = \sum_{i=1}^{N_n} \lambda_i^{(n)}(f) s_i^{(n)}. \tag{3.2.7}$$

By the duality of the basis functions s_i, it is clear that the spline $\Pi_n s$ reproduces s, i.e.,

$$\Pi_n s = s, \quad \text{all } s \in S_n.$$

Now since $\mathbb{P}_2 \subset S_n$, Π_n reproduces the quadratic polynomials $\mathbb{P}_2$, i.e.,

$$\Pi_n p = p \quad \text{all } p \in \mathbb{P}_2.$$

Now we want to show that the NMDS $\mathcal{N}_n$ for S_n is stable and local. Given a triangle $T \in \Delta_n$, we can see from the formulae of B-coefficients (3.2.11) for $s \in S_n$ on T that these coefficients are computed from the nodal data at the vertices of T. This shows that $\mathcal{N}_n$ is local. Similarly, from the formulae (3.2.11) we can easily check that if the coefficient c_ξ of s is computed from the gradients then

$$|c_\xi| \le K_1 \sum_{\nu=0}^{1} \operatorname{diam}(T)^\nu |s|_{W^\nu_\infty(T)}, \tag{3.2.8}$$

where K_1 is a constant depending on the smallest angle in Δ_n. Since the computation of all other coefficients from the smoothness conditions is a stable process, it follows that (3.2.8) holds for all coefficients of s on T. This verifies the stability of $\mathcal{N}_n$. Since NMDS $\mathcal{N}_n$ is stable and local, it implies that the corresponding Hermite basis Φ_n is stable and local in the sense of the definition of Section 1.3.2.

Lemma 3.4. *Let $T \in \Delta_n$ be a triangle with vertices v_1, v_2, v_3. Then for every $s \in S_n$, we have*

$$\|s\|_{L_\infty(T)} \lesssim \max\left\{ |s(v_j)|, 2^{-n}\left|\frac{\partial s}{\partial x}(v_j)\right|, 2^{-n}\left|\frac{\partial s}{\partial y}(v_j)\right|,\ 1 \le j \le 3 \right\}, \tag{3.2.9}$$

where the bounding constants depend only on the smallest angle in Δ_n.

Proof. Since Φ_n is a stable local basis, $\{s_i^{(n)}\}_{i=1}^9$ is a stable basis for the L_∞-norm, that is for $\mathbf{c} = (c_1, \ldots, c_9)$

$$\|\sum_{i=1}^{9} c_i s_i^{(n)}\|_{L_\infty(T)} \sim \|\mathbf{c}\|_{l_\infty} \tag{3.2.10}$$

with bounding constant depending only on the smallest angle of Δ_n. By construction of Π_n we have

$$\|s\|_{L_\infty(T)} = \|\sum_{i=1}^{9} \lambda_i^{(n)} s_i^{(n)}\|_{L_\infty(T)}.$$

Then by (3.2.10),

$$\|s\|_{L_\infty(T)} \lesssim \max_i |\lambda_i^{(n)}|, \quad i = 1, \cdots, 9.$$

The lemma immediately follows from (3.2.4) with proper scaling of the linear functionals involving derivatives, that is $\gamma \frac{ds}{dx}(v_j)$ and $\gamma \frac{ds}{dy}(v_j)$ where $\gamma = \text{diam}(T)$, and we have $\text{diam}(T) \sim 2^{-n}$ from (3.2.2). □

We now write the set of linear functionals $\mathcal{N}_n$ for S_n in a different way. Let

$$\mathcal{N}_0 = \{\lambda_i^{(0)}\}_{i=1}^{n_0=N_0} = \bigcup_{v \in \mathcal{V}_0} \{\lambda_v, \lambda_v^x, \lambda_v^y\}$$

and for each $1 \le k \le n$, set

$$\Gamma_k = \{\lambda_i^{(k)}\}_{i=1}^{n_k} = \bigcup_{v \in \mathcal{V}_k \setminus \mathcal{V}_{k-1}} \{\lambda_v, \lambda_v^x, \lambda_v^y\}, \quad n_k = N_k - N_{k-1}.$$

Then for each $0 \le m \le n$, the set of linear functionals

$$\mathcal{N}_m = \mathcal{N}_0 \cup \bigcup_{k=1}^{m} \Gamma_k$$

is clearly a nodal minimal determining set for S_m.

We now construct a hierarchical basis for S_n. Let $\{s_i^{(0)}\}_{i=0}^{N_0}$ be the nodal basis for S_0. In addition, for each $1 \le m \le n$ and each $1 \le i \le n_m$, let $s_i^{(m)}$ be the unique spline in S_m such that

$$\lambda_j^{(m)} s_i^{(m)} = \begin{cases} 1, & i = j, \quad j = 1, \ldots, n_m, \\ 0, & \text{otherwise.} \end{cases}$$

and

$$\lambda_j^{(k)} s_i^{(m)} = 0, \quad j = 1, \ldots, n_k, \quad k = 1, \ldots, m-1.$$

Theorem 3.5. *For each $0 \le m \le n$, the set of splines*

$$\mathcal{B}_m = \bigcup_{k=0}^{m} \bigcup_{i=1}^{n_k} \{s_i^{(k)}\}$$

form a basis for S_m.

Proof. Since the splines in $\mathcal{B}_m$ belongs to S_m by the construction and they are also linear independent. The cardinality of $\mathcal{B}_m$ is equal to $n_0 + n_1 + \ldots + n_m$, which is the dimension of the space S_m. The proof is complete. □

Theorem 3.5 shows that $\mathcal{B}_n$ is a hierarchical basis for S_n, which means that every spline $s \in S_n$ can be written as a unique hierarchical representation

$$s = \sum_{m=0}^{n} \sum_{i=1}^{n_m} c_i^{(m)} s_i^{(m)}.$$

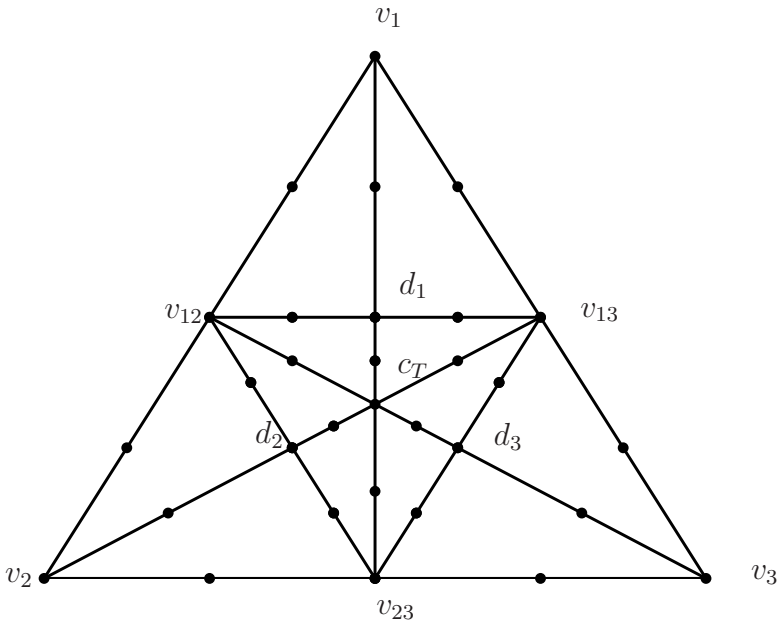

Figure 3.5: Powell-Sabin-12 split of a triangle and its domain points.

For the convenience of writing a program to compute the spline s satisfying (3.2.6), we now give explicit formulae for all the B-coefficients of $s \in S_n$ in terms

of function and gradient values at the vertices of $T \in \Delta_n$. For T regular, i.e. T is a PS-6 split, the formulae for the B-coefficients for s can be found in [36, (6.5)] and they are written in terms of function and gradient values at the vertices of T. We will now concentrate on the case where T is irregular, i.e. T is a PS-12 split. Following the notation used in [2], if v is a vertex of T, we write $C(v)$ for the B-coefficient associated with the domain point v, and if $[u, v]$ is an edge of T, we write $C(u, v)$ for the B-coefficient associated with the domain point at the midpoint of e. For a typical macro triangle $T = \langle v_1, v_2, v_3 \rangle$, see Fig.3.5, we write v_{12} for the midpoint of the $[v_1, v_2]$, with the similar notation for the other edges of T. Let $c_T = (v_1+v_2+v_3)/3$ be the barycenter of T, and let $d_1 = (2v_1+v_2+v_3)/4$ be the midpoint of the edge $[v_{12}, v_{13}]$, with similar definitions for d_2 and d_3. Then by the standard Bernstein Bézier techniques, we can compute the following formulae for the B-coefficients of s on T where T is irregular:

$$\begin{aligned}
C(v_1) &= s(v_1), \\
C(v_1, v_{12}) &= C(v_1) + \big[(x_{12} - x_1)\frac{\partial s}{\partial x}(v_1) + (y_{12} - y_1)\frac{\partial s}{\partial y}(v_1)\big]/2, \\
C(v_{12}) &= [C(v_1, v_{12}) + C(v_2, v_{12})]/2, \\
C(v_1, d_1) &= [C(v_1, v_{12}) + C(v_1, v_{13})]/2, \\
C(v_{12}, d_1) &= [3C(c_T, v_{12}) + C(v_1, v_{12})]/4, \\
C(d_1) &= [C(d_1, v_{12}) + C(d_1, v_{13})]/2, \\
C(c_T, d_1) &= [C(c_T, v_{12}) + C(c_T, v_{13})]/2, \\
C(c_T) &= [C(c_T, v_{12}) + C(c_T, v_{13}) + C(c_T, v_{23})]/3, \\
C(d_1, c_T) &= [C(v_{12}, c_T) + C(v_{13}, c_T)]/2.
\end{aligned} \tag{3.2.11}$$

It is now remaining to find the formula for $C(c_T, v_{12})$. We first consider the case where the edge $e = [v_1, v_2]$ is regular. We assume that the B-coefficients on all regular triangles (PS-6 split) are first computed. Then the gradient $\frac{\partial}{\partial x}s(v_{12}), \frac{\partial}{\partial y}s(v_{12})$ at v_{12} can be easily computed from the B-coefficients on the PS-6 macro triangle

sharing an edge with T. The coefficient $C(c_T, v_{12})$ can then be written as

$$C(c_T, v_{12}) = C(v_{12}) + \big[(x_{c_T} - x_{12})\frac{\partial s}{\partial x}(v_{12}) + (y_{c_T} - y_{12})\frac{\partial s}{\partial y}(v_{12})\big]/2.$$

Next we consider the case where the edge $e = [v_1, v_2]$ is irregular. Let n_e be the unit vector perpendicular to e and pointing into T. To find the formula for $C(c_T, v_{12})$, we make use of the requirement that the derivative $D_{n_e}s$ should be linear along the edge e. We first write

$$\begin{aligned} n_e &= \alpha_1(v_{12} - v_1) + \beta_1(v_{13} - v_1), \\ &= \alpha_2(v_{12} - v_2) + \beta_2(v_{23} - v_2), \\ &= \alpha_{12}(v_2 - v_{12}) + \beta_{12}(c_T - v_{12}). \end{aligned} \tag{3.2.12}$$

See Remark 3.6 for details on how to get the $\alpha's$ and $\beta's$. We make use of these equations to get the formulae for $D_{n_e}s$ at certain points on T. We note that for any two vertices u, v of a triangulation Δ_n, the directional derivative associated with the vector $u - v$ of a quadratic spline defined on Δ_n is

$$D_{u-v}s(v) = 2\delta(u, v)$$

where

$$\delta(u, v) = C(u, v) - C(v).$$

This then leads to

$$\begin{aligned} D_{n_e}s(v_1) &= 2[\alpha_1\delta(v_{12}, v_1) + \beta_1\delta(v_{13}, v_1)], \\ D_{n_e}s(v_2) &= 2[\alpha_2\delta(v_{12}, v_2) + \beta_2\delta(v_{23}, v_2)], \\ D_{n_e}s(v_{12}) &= 2[\alpha_{12}\delta(v_2, v_{12}) + \beta_{12}\delta(c_T, v_{12})]. \end{aligned} \tag{3.2.13}$$

The requirement that $D_{n_e}s$ is linear on e can be written as

$$D_{n_e}s(v_{12}) = [D_{n_e}s(v_1) + D_{n_e}s(v_2)]/2.$$

Now substituting the equations (3.2.13) and solving for $C(c_T, c_{12})$, we get

$$\begin{aligned} C(c_T, v_{12}) &= C(v_{12}) + [-2\alpha_{12}\delta(v_2, v_{12}) + D_{n_e}s(v_{12})]/(2\beta_{12}) \\ &= C(v_{12}) + \big[-2\alpha_{12}\delta(v_2, v_{12}) + [D_{n_e}s(v_1) + D_{n_e}s(v_2)]/2\big]/(2\beta_{12}) \\ &= C(v_{12}) + \big[-2\alpha_{12}\delta(v_2, v_{12}) + \alpha_1\delta(v_{12}, v_1) + \beta_1\delta(v_{13}, v_1) \\ &+ \alpha_2\delta(v_{12}, v_2) + \beta_2\delta(v_{23}, v_2)\big]/(2\beta_{12}). \end{aligned}$$

Remark 3.6. *To find α_i and β_i in the equation (3.2.12), we first compute a so that*

$$[a(v_{12} - v_1) + (v_{13} - v_1)] \circ (v_{12} - v_1) = 0$$

This is one equation for the unknown a.

In the next section we will construct suitable Lagrange bases for the spaces $S_n, n = 0, 1, \ldots$. We begin the construction on the coarsest level Δ_0 and then progress to the next level and so forth. In particular, we construct a nested Lagrange interpolation sets $\{\Xi_n\}_{n=0}^{\infty}$ so that a corresponding Lagrange hierarchical basis can be constructed.

3.3 Stable Local Lagrange Bases

Recall that a finite set $\Xi \subset \Omega$ is said to be a *Lagrange interpolation set* for a finite dimensional linear space S of functions on Ω if $\#\Xi = \dim S$ and for each $\xi \in \Xi$ there is a unique function $B_\xi \in S$ satisfying $B_\xi(\eta) = \delta_{\xi,\eta}$ for all $\xi, \eta \in \Xi$, where $\delta_{\xi,\eta} = 1$ if and only if $\xi = \eta$. The set $\big\{B_\xi\big\}_{\xi\in\Xi}$ is a basis for S called the *Lagrange basis*. A sequence of Lagrange interpolation sets $\{\Xi_n\}_{n=0}^{\infty}$ for the corresponding spaces S_n is said to be *nested* if $\Xi_0 \subset \Xi_1 \subset \ldots \subset \Xi_n \subset \ldots$.

In Algorithm 1 below we construct the set of interpolation points for the spline space S_0. We use an algorithm similar to one introduced by Nürnberger and Zeilfelder [47] for the construction of local Lagrange interpolation sets for C^1 quadratic splines on arbitrary triangulations with Powell-Sabin 6-splits. The construction of

local Lagrange interpolation sets is based on adding successively Lagrange interpolation points in the interior of the edges of Δ_0 to $\mathcal{V}_0$, the set of vertices of Δ_0. In [47] interpolation points on the edges are chosen at distance $\frac{|d|}{2}$, where $|d|$ is the distance from the endpoints to the interior knots of Powell-Sabin 6-splits on the edges. In contrast to [47], we choose the interpolation points at distance $\frac{|e|}{4}$ from the endpoints of the edges, where $|e|$ denotes the length of the edges. We shall see later that this is particularly important in order to get a nested interpolation sets. We also prove the Lagrange interpolation set is local.

Algorithm 1 [Interpolation set for S_0]

Let Δ_0 be the initial triangulation. In the algorithm the vertices of Δ_0 are marked whenever the interpolation points are chosen near the vertices. We say that an interpolation point ξ is *assigned* to a vertex $v \in \mathcal{V}_0$ if either $\xi = v$ or v is the closest endpoint of the edge containing ξ. We add successively Lagrange interpolation points in the interior of the edges of Δ_0 such that three interpolation points are assigned to every vertex of Δ_0.

Step 1. *Let $T_1, T_2, \ldots, T_n$ be the triangles of Δ_0. First, on $T_1 = \langle u, v, w\rangle$, the points*

$$u, v, w, \frac{3}{4}u + \frac{1}{4}v, \frac{3}{4}u + \frac{1}{4}w, \frac{3}{4}v + \frac{1}{4}u, \frac{3}{4}v + \frac{1}{4}w, \frac{3}{4}w + \frac{1}{4}u, \frac{3}{4}w + \frac{1}{4}v, \qquad (3.3.1)$$

are chosen and the vertices u, v, w are marked, see Fig.3.6a. The algorithm then proceeds by induction as follows. Assume that the triangles $T_1, T_2, \ldots, T_i$ have been considered. Next, the triangle T_{i+1} is considered, and again its vertices are denoted by u, v, w. If all vertices u, v, w are not yet marked, then the points (3.3.1) are chosen and the vertices u, v, w are marked. Otherwise, T_{i+1} is omitted and T_{i+2} is considered. This is repeated until all the m triangles of Δ_0 are considered.

Step 2. *After $T_1, T_2, \ldots, T_n$ are processed in Step 1, the unmarked vertices are denoted by $u_1, u_2, \ldots, u_m$. The algorithm proceeds by induction as follows. For $i = 1, \ldots, m$ consider two cases. If an unmarked vertex u_j, $j \geq i + 1$, exists such*

that $[u_i, u_j]$ *is an edge of* Δ_0*, then an arbitrary triangle* $T \in \Delta_0$ *is chosen with vertices* u_i, u_j, u*. Note that its third vertex* u *is necessarily already marked in Step 1. In this case, the interpolation points*

$$u_i, u_j, \frac{3}{4}u_i + \frac{1}{4}u, \frac{3}{4}u_i + \frac{1}{4}u_j, \frac{3}{4}u_j + \frac{1}{4}u, \frac{3}{4}u_j + \frac{1}{4}u_i,$$

are chosen and vertices u_i, u_j *are marked, see Fig.3.6b. Otherwise, an arbitrary triangle* T *with vertex* u_i *is chosen. Its two other vertices* u, v *are already marked. In this case, the interpolation points*

$$u_i, \frac{3}{4}u_i + \frac{1}{4}u, \frac{3}{4}u_i + \frac{1}{4}v,$$

are chosen and the vertex u_i *is marked, see Fig.3.6c.*

We call the triangle in Fig.3.6a the *filled triangle*. We call the triangle T in Fig.3.6b the *edge triangle*, the edge $[u, v]$ the *filled edge* and the vertex w the *dependent* vertex of T. We call the triangle T in Fig.3.6c the *vertex triangle*, the vertex u the *isolated vertex* and v, w the *dependent* vertices of T. We call a triangle which is not a filled triangle, an edge triangle or a vertex triangle, *an empty triangle*.

Let Ξ_0 be the interpolation set consisting of all points chosen in Algorithm 1. By the above construction it is clear that three interpolation points are assigned to every vertex of Δ_0 and hence Ξ_0 consists of $3\#\mathcal{V}_0$ interpolation points. An example for Ξ_0 is given in Fig.3.7.

Discussion. From the above construction it is clear that the dependent vertex of any edge triangle belongs to a filled triangle. The dependent vertices of any vertex triangle belong to either a filled triangle or an edge triangle. This it true since no two isolated vertices are connected by an edge of Δ_0, see Lemma 3.7 below. Also we note that any vertex of an empty triangle belongs to either a vertex, an edge or a filled triangle.

Lemma 3.7. *No two isolated vertices are connected by an edge of* Δ_0*.*

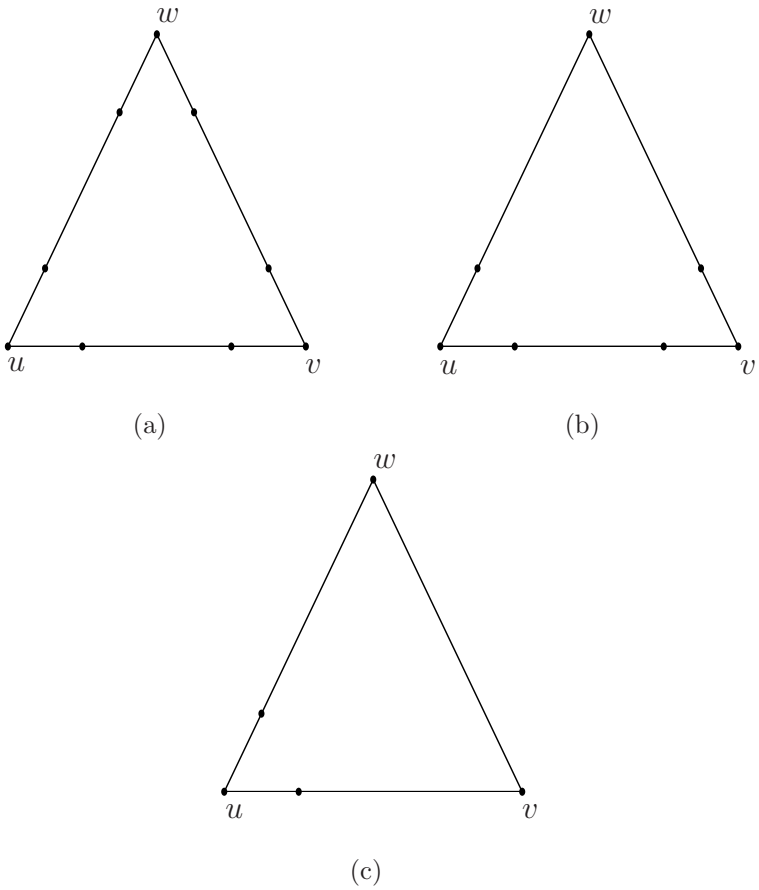

Figure 3.6: (a) Filled triangle, (b) Edge triangle and (c) Vertex triangle

Proof. From Step 2 of Algorithm 1 we understand that if a vertex u_j is connected to an isolated vertex u_k by an edge and $j < k$, then u_j cannot be isolated as by construction u_k could have been chosen as a pair to u_j at the j-th step to form an edge triangle. □

Lemma 3.7 immediately implies the following.

Lemma 3.8. *If $T \in \Delta_0$ is a vertex triangle then only its neighbour opposite to its isolated vertex maybe a non-empty triangle.*

Theorem 3.9. *The set Ξ_0 is a local interpolation set for S_0. The supports of the Lagrange basis functions $B_\xi^{(0)},\ \xi \in \Xi_0$ satisfy*

$$\operatorname{supp}(B_\xi^{(0)}) \subseteq \operatorname{star}^3(T),$$

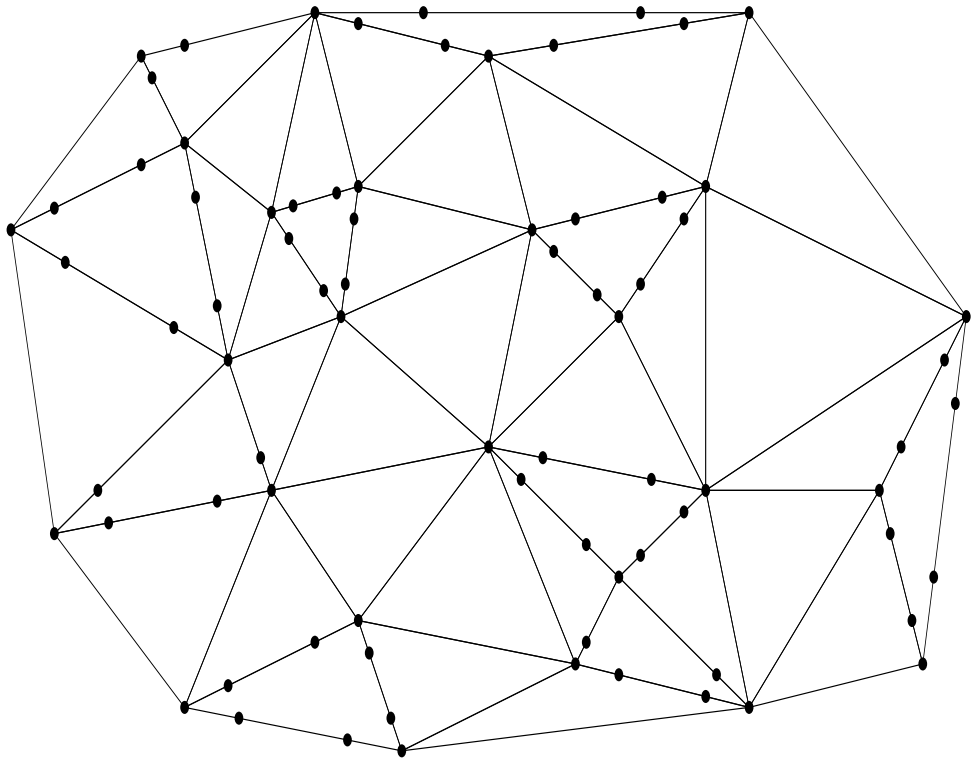

Figure 3.7: Construction of interpolation points in the two steps of the Algorithm 1. The interpolation points are indicated by black circles.

where $T \in \Delta_0$ is any triangle containing ξ.

Proof. Let $s \in S_0$. The set Ξ_0 is an interpolation set for S_0 if and only if the point evaluation functionals

$$s(\xi), \quad \xi \in \Xi_0,$$

form a basis for the dual space $(S_0)^*$. Since $\#\Xi_0 = 3\#\mathcal{V}_0 = \dim S_0$, this will follow once we show that these functionals span $(S_0)^*$, i.e., the condition $s(\xi) = 0,\ \xi \in \Xi_0$, implies $s \equiv 0$.

The idea of the proof is to assume $s(\xi) = 0,\ \xi \in \Xi_0$ and show that the gradient of s vanishes for all vertices v of Δ_0. Then it follows from Theorem 3.1 that $s \equiv 0$.

Before we proceed with the proof we observe that from the above construction each vertex of Δ_0 belongs to either a filled triangle, an edge triangle or a vertex triangle. If we can show that the gradient of s vanishes at the vertices of all the three types of triangle by assuming s is zero at the interpolations points, then the proof is complete.

First we consider the filled triangle. Clearly each edge of any filled triangle contains exactly four points of Ξ_0. It follows from the Schoenberg-Whitney Theorem in the univariate spline theory that

$$\Big\{a, \frac{1}{4}(3a+b), \frac{1}{4}(a+3b), b\Big\}$$

is a Lagrange interpolation set for the space of C^1 quadratic splines on $[a, b]$ with a knot at the midpoint. Therefore, it follows that $s|_e \equiv 0$ holds for all edges e of Δ_0 containing four Lagrange interpolation points. This shows that $s|_e \equiv 0$ for all edges of any filled triangle. Hence the gradient of s vanishes at the vertices of any filled triangle.

Next we look at the edge triangles. Let u, v, w and $e_1 = [v, u], e_2 = [u, w], e_3 = [w, v]$ be the vertices and edges respectively of an edge triangle and e_1 is the filled edge. We know that the dependent vertex w of the edge triangle belongs to a filled triangle, so the gradient of s vanishes at u. Since e_1 contains four points of Ξ_0, we have $s|_{e_1} \equiv 0$. Moreover, by Rolle's Theorem we can easily show that $s|_{e_2} \equiv 0$ and $s|_{e_3} \equiv 0$. This implies that the gradient of s also vanishes at v, w.

Finally we look at the vertex triangles. Let u, v, w and $e_1 = [v, u], e_2 = [u, w], e_3 = [w, v]$ be the vertices and edges of a vertex triangle respectively, and let u be the isolated vertex. We know that the dependent vertices v, w of the vertex triangle belong to either a filled triangle or an edge triangle. Hence the gradient of s vanishes at v, w. Thus by Rolle's theorem, we show that $s|_{e_1} \equiv 0$ and $s|_{e_2} \equiv 0$. This implies that gradient of s vanishes at u. Since we have considered all the three types of triangles of Δ_0 and also we have shown that the gradient of s vanishes on their vertices. Thus the gradient of s vanishes at all the vertices of

Δ_0. The proof to show that Ξ_0 is an interpolation set for S_0 is now complete.

Next we show that Ξ_0 is local. Let T be a filled triangle. Assume s satisfies zero interpolation conditions on T. Then from the above argument zero interpolation conditions on $T = \text{star}^0(T)$ imply zero function and gradient values at vertices of T. Hence $s|_T \equiv 0$. Suppose T is an edge triangle. Then there exists a filled triangle $T_F \in \text{star}(T)$ such that the dependent vertex v of T belongs to T_F. Zero interpolation conditions for s on $\text{star}(T)$ imply $s|_{T_F} \equiv 0$ and so the gradient of s vanishes at v, and hence at the other two vertices of T. Zero function and gradient values at vertices of T now imply $s|_T \equiv 0$. Now suppose T is a vertex triangle. Then there exists either a filled triangle T_F or an edge triangle T_E belongs to $\text{star}(T)$ such that the dependent vertices u, v of T belong to either T_F or T_E. Zero interpolation conditions for s on $\text{star}^2(T)$ imply $s|_{T_F} \equiv 0$ and $s|_{T_E} \equiv 0$ and so the gradient of s vanishes at u, v and hence at the other vertex of T. Since function and gradient values vanish at all vertices of T, we have $s|_T \equiv 0$. Finally, we suppose T is an empty triangle. Then the vertices v_1, v_2, v_3 of T belong to either a filled triangle T_F, an edge triangle T_E or a vertex triangle T_V where T_F, T_E, T_V belong to $\text{star}(T)$. Thus zero interpolation conditions for s on $\text{star}^3(T)$ imply $s|_{T_F} \equiv 0, s|_{T_E} \equiv 0, s|_{T_V} \equiv 0$ and so the gradient of s vanishes at all vertices of T. Zero function and gradient values at all vertices of T now imply $s|_T \equiv 0$. We therefore conclude that if T is a filled triangle, an edge triangle, a vertex triangle, an empty triangle then zero interpolation values of s on $T = \text{star}^0(T)$, $\text{star}^1(T)$, $\text{star}^2(T)$, $\text{star}^3(T)$, respectively imply $s|_T \equiv 0$.

Using the arguments above we now analyse the maximum size of supports of Lagrange basis functions $B_\xi^{(0)}$. If we choose triangles $T, T' \in \Delta_0$ such that T' is not in $\text{star}^3(T)$, then the Lagrange basis function $B_\xi^{(0)}|_{T'} \equiv 0$ if the corresponding interpolation point $\xi \in T$. Indeed, $B_\xi^{(0)}$ satisfies the zero interpolation condition in $\text{star}^2(T')$ since $\text{star}^2(T') \cap T = \emptyset$. This shows that the supports of $B_\xi^{(0)}$ satisfy

$$\text{supp}(B_\xi^{(0)}) \subseteq \text{star}^3(T).$$

This completes the proof. □

Corollary 3.10. *The supports of the Lagrange basis functions* $B_\xi^{(0)},\ \xi \in \Xi_0$ *satisfy*

$$\mathrm{supp}(B_\xi^{(0)}) = \begin{cases} \mathrm{star}^3(T), & \text{if } T \text{ is a filled triangle,} \\ \mathrm{star}^2(T), & \text{if } T \text{ is an edge triangle,} \\ \mathrm{star}(T), & \text{if } T \text{ is a vertex triangle.} \end{cases}$$

where $T \in \Delta_0$ *is any triangle containing* ξ.

An illustration on the maximal propagation of the Lagrange basis functions is given in Fig.3.8.

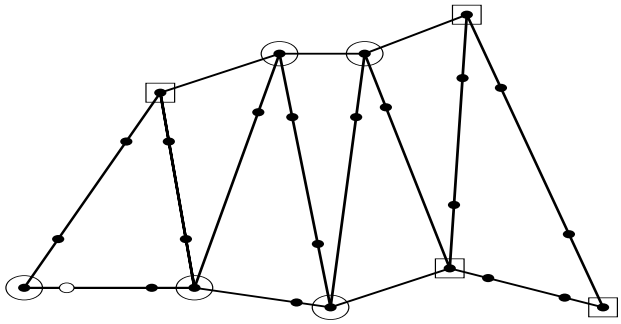

Figure 3.8: Maximal propagation along the edge of Δ_0. The white circle indicates the interpolation point associated with the Lagrange basis function. The circles indicate derivatives of the basis function which are possible non-zero, while the squares indicate zero derivatives of the basis function at the vertices.

Algorithm 2 [Interpolation sets for $S_n,\ n \geq 1$]

Next we describe an algorithm to construct Lagrange interpolation sets for S_n, $n \geq 1$. Using the same principle of Algorithm 1 we want to construct sets of filled, edge, vertex and empty triangles on Δ_n. Before we begin to describe the algorithm we first introduce some terminologies and put down some preliminary discussions which are necessarily useful later.

We recall that an interpolation point $\xi \in \Xi_n$ is *assigned* to a vertex $v \in \mathcal{V}_n$ if either $\xi = v$ or v is the closest end-point of the edge containing ξ. We add successively Lagrange interpolation points on the edges of Δ_n such that we have three interpolation points assigned to every vertex of Δ_n.

As we repeat the refinements, there are new born triangles and so are new vertices at every new level. We need to add new interpolation points at every new level and preserve all the interpolation points of the previous levels. We call the interpolation points from the previous levels on the *n-th* level the *inherited points* in Δ_n.

We note that some inherited points in Δ_n may be closer to a new vertex than to the vertex where they were assigned to in Δ_{n-1}. These points are thus assigned to different vertices in Δ_n. We call this the *reassignment* of interpolation points. Initially the point is located at distance $\frac{|e|}{4}$ from an endpoint of an edge e. First refinement does not lead to reassignment but relative distance increases to $\frac{1}{2}$. Each subsequent refinement produces reassignment of this point. Interpolation points assigned to a vertex $v \in \Delta_{n-1}$ are said to be *lost* if the points are now reassigned to new vertices in Δ_n. We *replace* the lost points by assigning new interpolation points to v at distance $\frac{|e|}{4}$ from v on the edges where the points were lost. To clarify this better, we illustrate an example here. Fig.3.9a shows a vertex triangle $T = \langle u, v, w\rangle$ on Δ_0 with the interpolation points u, p, p' where $p = \frac{3}{4}u + \frac{1}{4}v$ and $p' = \frac{3}{4}u + \frac{1}{4}w$ (p and p' are at distance $\frac{|e|}{4}$ from u on $[u, v]$ and $[u, w]$ respectively). The interpolation points u, p, p' are assigned to the vertex u in Algorithm 1. Fig.3.9b shows the same triangle T in Δ_1 with the middle triangle $\tilde{T} = \langle a, b, c\rangle$. We see that the same interpolation points u, p, p' are now contained in a new triangle $T_1 = \langle u, b, a\rangle$ on Δ_1 and, $p = \frac{1}{2}u + \frac{1}{2}b$ and $p' = \frac{1}{2}u + \frac{1}{2}a$ on T_1. The points p, p' are still remain assigned to u (p and p' are now at distance $\frac{|e|}{2}$ from u on $[u, a]$ and $[u, b]$ respectively). Next we see in Fig.3.9c the same triangle T in Δ_2. Clearly, the same interpolation points u, p, p' are now contained in a new triangle $T_2 = \langle u, e, d\rangle$ on Δ_2 and, the points p, p' are now located at e, d respectively in T_2.

We say two interpolation points p, p' are lost from u. Since we require each vertex of Δ_2 to be assigned with three interpolation points, clearly we need to add new interpolation points to the vertices u, e, d to achieve this.

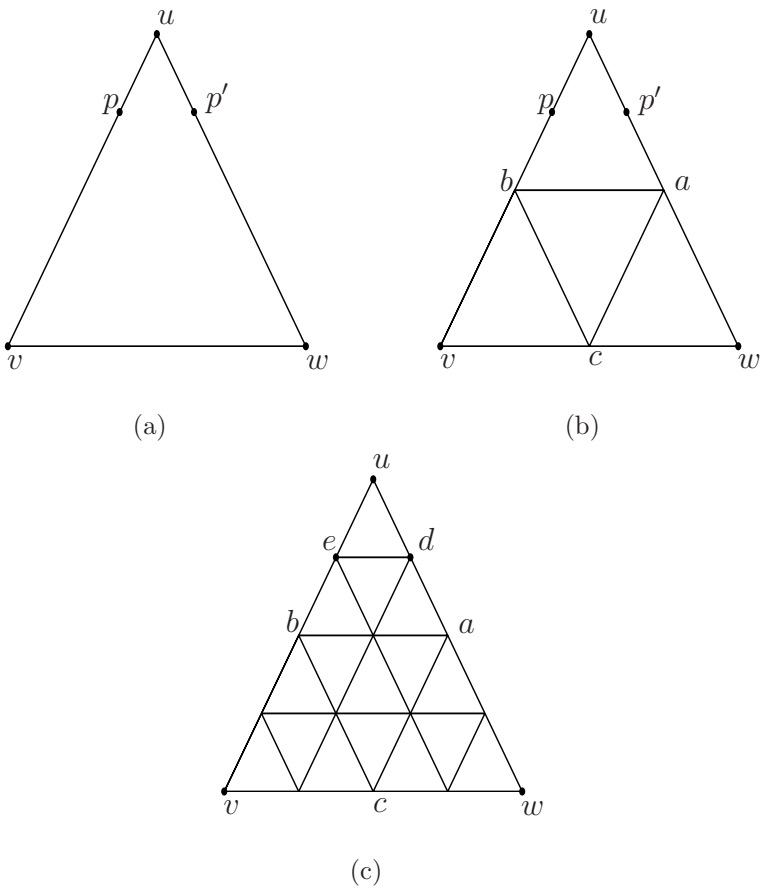

Figure 3.9: Example of reassignments of interpolation points.

We observe that each triangle $T \in \Delta_{n-1}$ for $n \geq 1$ is refined in Δ_n as shown in Fig.3.10a. We call the shaded triangle $\tilde{T} \in \Delta_n$ the *middle triangle* of T in Δ_n. We also see that each triangle $T \in \Delta_{n-2}$ for $n \geq 2$ is doubly refined in Δ_n as shown in Fig.3.10b. We call the shaded triangle $\hat{T} \in \Delta_n$ the *middle triangle* of T in Δ_n in this case.

The vertices of Δ_{n-1} remain marked and the vertices in $\Delta_n \backslash \Delta_{n-1}$ are unmarked initially. We recall that Δ_0 is made up of the filled, edge, vertex and empty triangles by the construction of Algorithm 1.

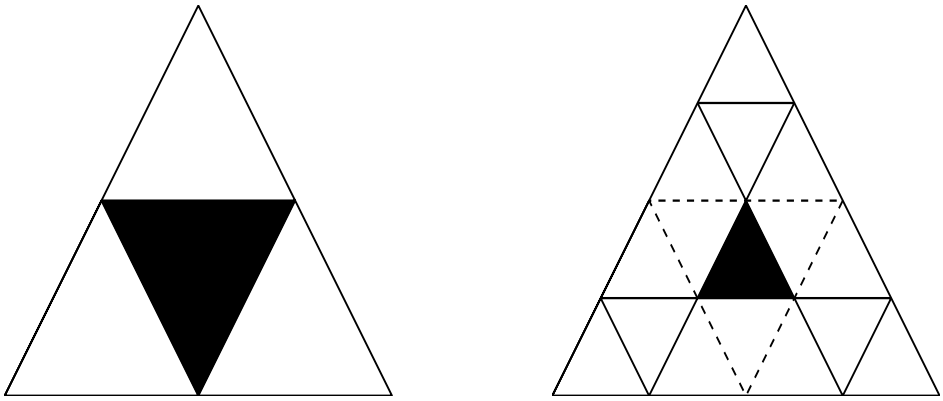

(a) (b)

Figure 3.10: Middle triangle of $T \in \Delta_{n-1}$ is shaded in (a). Middle triangle of $T \in \Delta_{n-2}$ is shaded in (b).

Step 1. *For each $T \in \Delta_0$, we choose interpolation points on its middle triangle $\tilde{T} \in \Delta_1$ in the following steps (a)-(d).*

(a) *For each filled triangle, each edge triangle, and each vertex triangle whose all neighbours are empty triangles in Δ_0, we make its middle triangle $\tilde{T} = \langle u, v, w \rangle$ in Δ_1 a fill triangle. i.e., we choose the points*

$$u, v, w, \frac{3}{4}u + \frac{1}{4}v, \frac{3}{4}u + \frac{1}{4}w, \frac{3}{4}v + \frac{1}{4}u, \frac{3}{4}v + \frac{1}{4}w, \frac{3}{4}w + \frac{1}{4}u, \frac{3}{4}w + \frac{1}{4}v, \quad (3.3.2)$$

and mark the vertices u, v, w. See Fig.3.11.

Discussion. All points produced in this step are different since no filled and edge triangles share an edge.

We know from Lemma 3.8 that only one neighbour of a vertex triangle $T \in \Delta_0$ maybe a filled triangle, an edge triangle or a vertex triangle, namely the triangle sharing with T the edge opposite to its isolated vertex.

(b) *For each pair T_1, T_2 of vertex triangles sharing an edge, we make the middle triangle of one of them a fill triangle and make the middle triangle of the other one an edge triangle.*

Let $\tilde{T}_1 = \langle u, v, w\rangle$ and $\tilde{T}_2 = \langle u, v', w'\rangle$ be the middle triangle of T_1 and T_2, respectively. Suppose we make $\tilde{T}_1$ a filled triangle and $\tilde{T}_2$ an edge triangle. i.e., for $\tilde{T}_1$ we choose the points (3.3.2) and for $\tilde{T}_2$ we choose the points

$$v', w', \frac{3}{4}v' + \frac{1}{4}u, \frac{3}{4}v' + \frac{1}{4}w', \frac{3}{4}w' + \frac{1}{4}u, \frac{3}{4}w' + \frac{1}{4}v'$$

and mark the vertices u, v, w, v', w'. See Fig.3.12.

Let $\mathcal{T}_V$ be the set of all remaining vertex triangles (those sharing an edge with a filled or an edge triangle).

(c) *For each $T \in \mathcal{T}_V$, we make the middle triangle $\tilde{T} = \langle u, v, w\rangle$ of T an edge triangle. i.e., we choose the points*

$$u, v, \frac{3}{4}u + \frac{1}{4}w, \frac{3}{4}u + \frac{1}{4}v, \frac{3}{4}w + \frac{1}{4}u, \frac{3}{4}w + \frac{1}{4}v$$

and mark u, v. Note that the dependent vertex w is necessarily already marked in step (a). See Fig.3.13 and 3.14.

At this stage it is clear that the remaining unmarked vertices now belong to the middle triangle of the empty triangles.

Let $\mathcal{T}_E$ be the set of middle triangles of all the empty triangles.

(d) *Let $T_1, T_2, \ldots, T_n$ be the triangles of $\mathcal{T}_E$. Starting with $T_1 = \langle u, v, w\rangle$, if the vertices u, v, w are unmarked then we choose the points (3.3.2) and make T_1 a fill triangle and mark u, v, w. Otherwise, T_1 is omitted and T_2 is considered. This is repeated until all n triangles of $\mathcal{T}_E$ are considered.*

(e) *After $T_1, T_2, \ldots, T_n$ have been processed in (d), the unmarked vertices are denoted by $u_1, u_2, \ldots, u_m$. The algorithm proceeds by induction. For $i = 1, \ldots, m$ consider two cases. If an unmarked vertex u_j, $j \geq i+1$ exists such that $[u_i, u_j]$ is an edge of $T = \langle u_i, u_j, u\rangle \in \mathcal{T}_E$, we make T an edge triangle. i.e., we choose the points*

$$u_i, u_j, \frac{3}{4}u_i + \frac{1}{4}u, \frac{3}{4}u_i + \frac{1}{4}u_j, \frac{3}{4}u_j + \frac{1}{4}u, \frac{3}{4}u_j + \frac{1}{4}u_i,$$

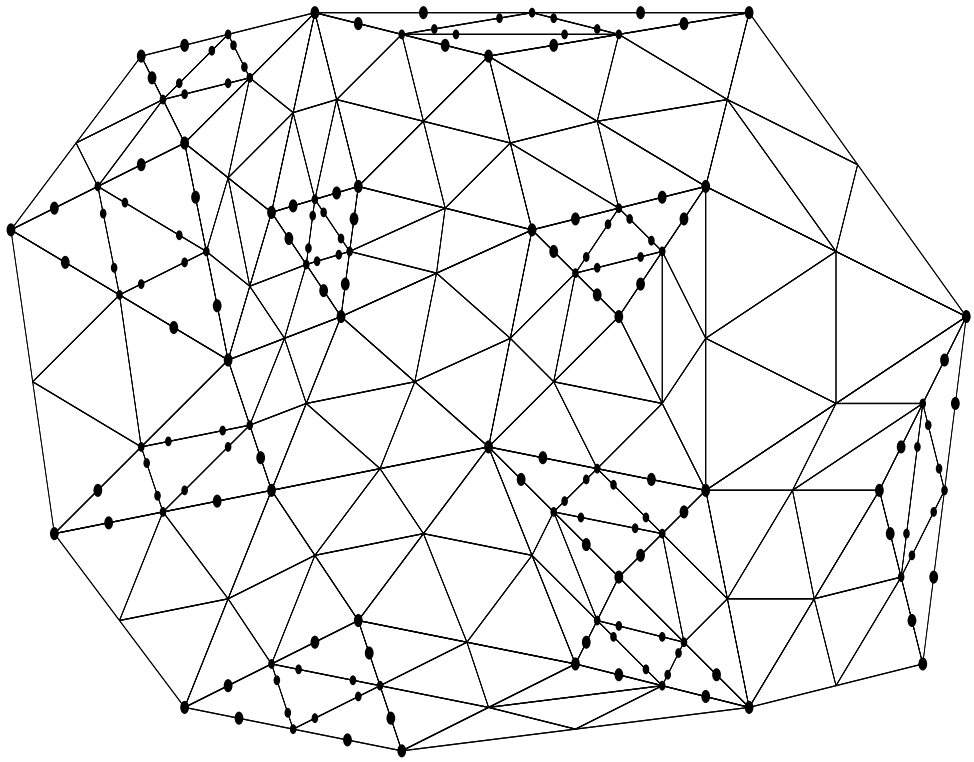

Figure 3.11: Construction of interpolation points in the two steps of Algorithm 1 and Step 1(a) of Algorithm 2. The interpolation points are indicated by black circles.

and mark u_i, u_j. Note that the third vertex u of T is necessarily marked before. Otherwise, $T \in \mathcal{T}_E$ with vertex u_i is made a vertex triangle since its two other vertices u, v are already marked. i.e, we choose the points

$$u_i, \frac{3}{4}u_i + \frac{1}{4}u, \frac{3}{4}u_i + \frac{1}{4}v$$

and mark u_i.

We also note that steps (d) and (e) are the same as the steps in Algorithm 1.

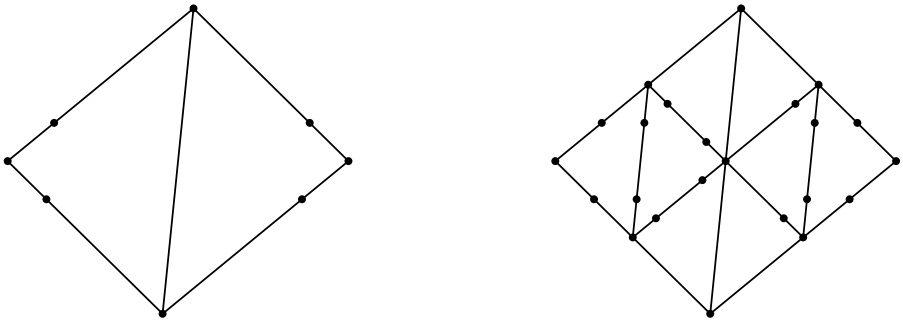

(a) (b)

Figure 3.12: (a) A vertex triangle with a vertex triangle as neighbour in Δ_0. (b) One of the middle triangle is made a filled triangle and the other one is made an edge triangle in Δ_1.

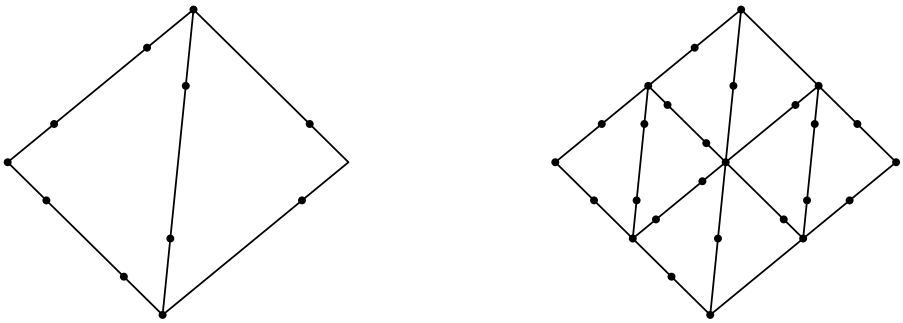

(a) (b)

Figure 3.13: (a) A vertex triangle with a filled triangle as a neighbour in Δ_0. (b) The middle triangle of the filled triangle is made a filled triangle and the middle triangle of the vertex triangle is made an edge triangle in Δ_1.

Let Ξ_1 be the interpolation set consisting of all points chosen in Algorithm 1 and Step 1 of Algorithm 2. An example for Ξ_1 is given in Fig.3.15.
For $\Delta_n, n \geq 2$, we choose the interpolation points in the following steps:
Step 2 (Middle Triangles). *For each $T \in \Delta_{n-2}$ we make its middle triangle $\hat{T} = \langle u, v, w \rangle$ in Δ_n a fill triangle, i.e., we choose the points (3.3.2) and mark the*

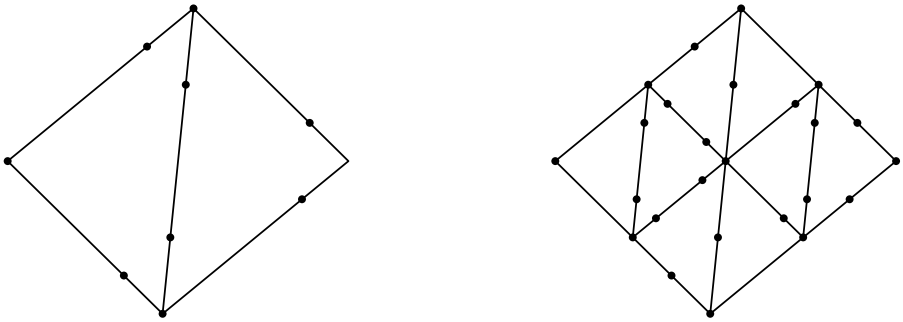

(a) (b)

Figure 3.14: (a) A vertex triangle with an edge triangle as a neighbour in Δ_0. (b) The middle triangle of the edge triangle is made a filled triangle and the middle triangle of the vertex triangle is made an edge triangle in Δ_1.

vertices u, v, w.

Discussion. Step 2 is possible since no inherited point is assigned in Δ_n to the vertices of $\hat{T}$, even after reassignment. This is because the vertices of Δ_{n-1} may have inherited points assigned to them in Δ_{n-1} but these points are not on the dotted edges as shown in Fig.3.10b since these edges did not exist in Δ_{n-2}. Hence any points on dotted edges assigned to these vertices in Δ_{n-1} are at distance $\frac{|e|}{4}$ from the vertices on $(n-1)st$ level and so they are not reassigned to other vertices in Δ_n.

Step 3 (Vertices of Δ_{n-1}). *For each vertex v of Δ_{n-1} which has no inherited points assigned in Δ_n, let $T \in \Delta_{n-1}$ be the triangle containing 3 interpolation points assigned to v in Δ_{n-1}. In fact each of these points is located at the vertices of $T' = \langle v_1, v_2, v_3 \rangle$ with $v_1 = v$ and T' is the child of T. We choose*

$$\frac{3}{4}v_1 + \frac{1}{4}v_2, \frac{3}{4}v_2 + \frac{1}{4}v_1, \frac{3}{4}v_2 + \frac{1}{4}v_3, \frac{3}{4}v_3 + \frac{1}{4}v_2, \frac{3}{4}v_1 + \frac{1}{4}v_3, \frac{3}{4}v_3 + \frac{1}{4}v_1$$

and mark v_2, v_3, see Fig.3.16b.

Discussion. Step 3 will replace two lost points and add four new points on T'. This makes T' a filled triangle and this is possible since for T' the vertex v belongs to Δ_{n-2} and hence the triangle T' is separated from filled triangles of Step 2.

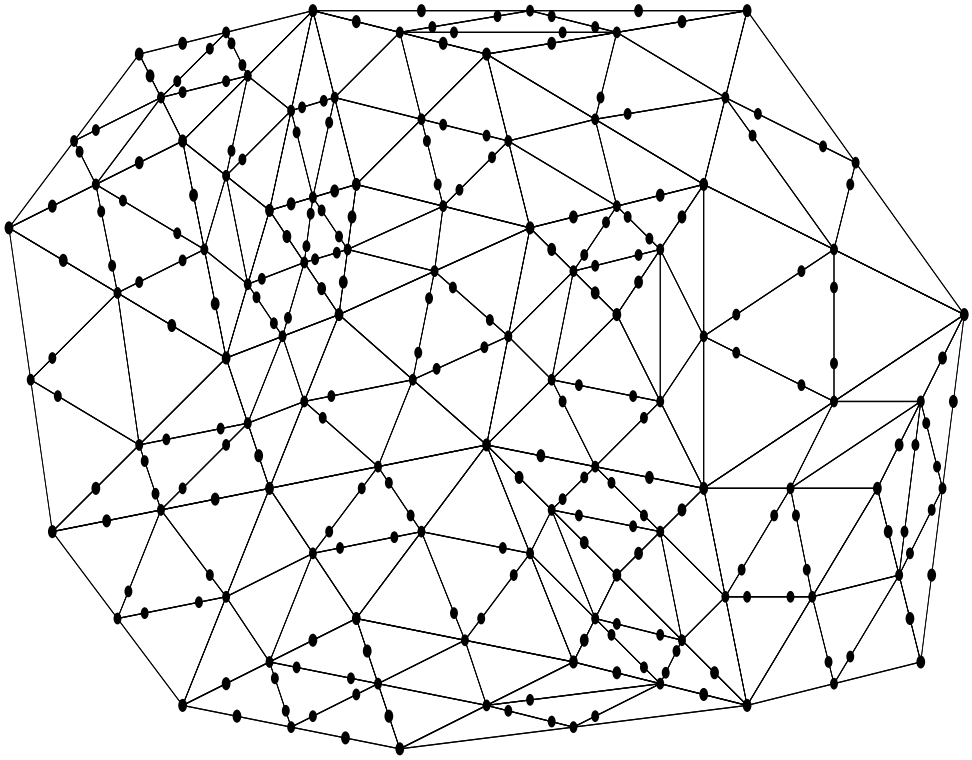

Figure 3.15: Construction of interpolation points in the two steps of the Algorithm 1 and Step 1 of Algorithm 2. The interpolation points are indicated by black circles.

After Step 2 and Step 3 are carried out, the remaining unmarked vertices of Δ_n now lie on the boundary of $\text{star}^1(v)$ where v is a vertex of Δ_{n-2}. This is illustrated in Fig.3.17. Clearly the marked vertices of the boundary of $\text{star}^1(v)$ are those which have received reassigned inherited points in step 3.

Step 4 (Vertices of Δ_{n-2}) *For each vertex of $v \in \Delta_{n-2}$, we denote the unmarked vertices connected to v by $u_1, u_2, \ldots, u_m$. The algorithm proceeds by induction as follows. For $i = 1, \ldots, m$ we consider two cases. If an unmarked vertex u_j, $j \geq i+1$ exists such that $[u_i, u_j]$ is an edge of Δ_n, then the triangle $T = \langle u_i, u_j, u \rangle$ is made an edge triangle where u is already marked and belongs to a filled triangle*

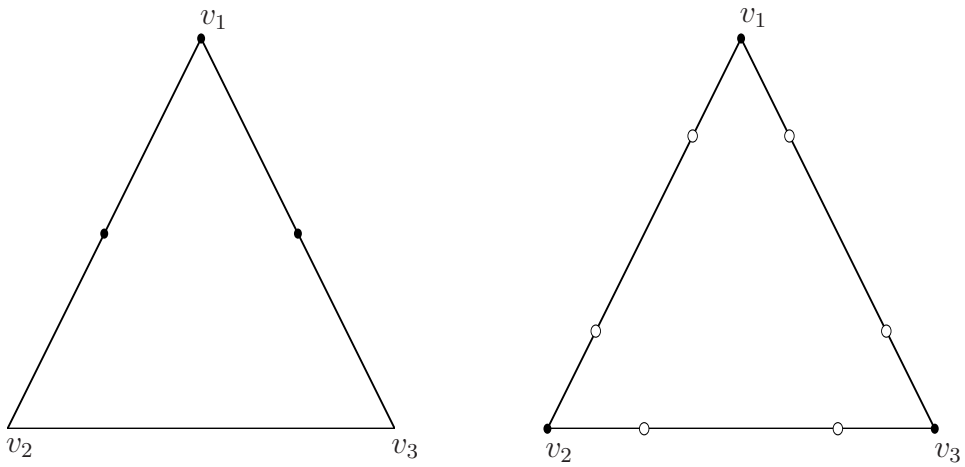

(a) (b)

Figure 3.16: Inherited points are indicated by black circles. New interpolation points assigned in Step 3 are indicated by white circles. (a) Three inherited points assigned to v_1 (no reassignment). (b) Inherited points are located at v_2 and v_3. Each v_1, v_2, v_3 get 2 newly assigned points.

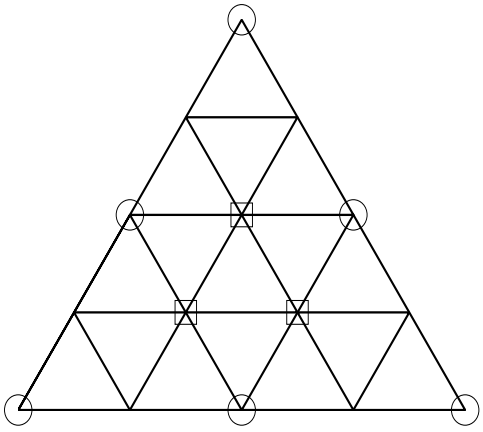

Figure 3.17: Vertices indicated by squares are processed in Step 2. Vertices indicated by circles are vertices of Δ_{n-1} processed in Step 3. The remaining vertices belong to the boundary of $\text{star}^1(v)$ for $v \in \Delta_{n-2}$.

of step 2. i.e., we choose

$$u_i, u_j, \frac{3}{4}u_i + \frac{1}{4}u_j, \frac{3}{4}u_i + \frac{1}{4}u, \frac{3}{4}u_j + \frac{1}{4}u_i, \frac{3}{4}u_j + \frac{1}{4}u$$

and mark u_i, u_j. *Otherwise,* T *with vertex* u_i *is made a vertex triangle. Of its two dependent vertices* p, q *one belongs to a filled triangle of step 2 and one belongs to the boundary of* $\mathrm{star}^1(v)$. *The vertices* p, q *are already marked. We choose the points*

$$u_i, \frac{3}{4}u_i + \frac{1}{4}p, \frac{3}{4}u_i + \frac{1}{4}q$$

and mark u_i. *An illustration is given in Fig.3.18.*

Discussion. The unmarked vertices mentioned above clearly do not belong to any filled triangle of step 2 but they are connected to such triangle since this is true for all vertices in $\mathcal{V}_n \setminus \mathcal{V}_{n-2}$.

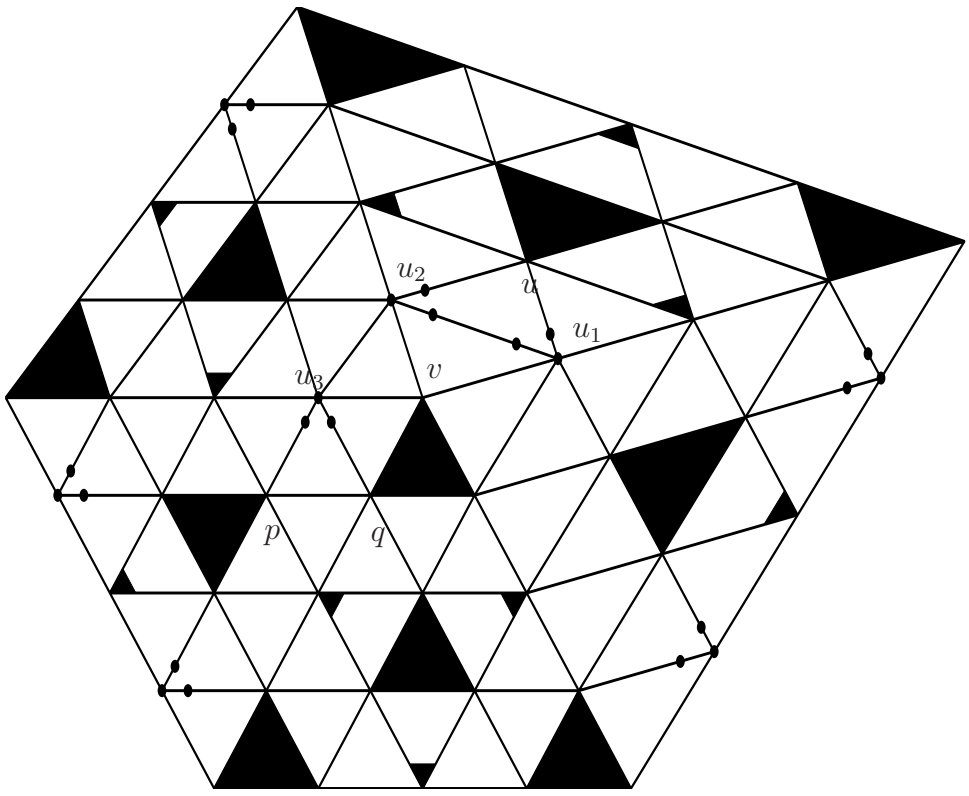

Figure 3.18: Black circles are interpolation points assigned in Step 4. The filled, edge and vertex triangles produced before Step 4 are appropriately shaded.

Let Ξ_n be the interpolation set consisting of all points chosen in Algorithm 1 or 2. It is again clear that by our construction three interpolation points are assigned to every vertex of Δ_n and hence the number of interpolation points of Ξ_n equals $3\#\mathcal{V}_n$, where $\#\mathcal{V}_n$ is the number of vertices of Δ_n.

We will now discuss the definite structures obtained from each step of the above construction. The discussion will be useful when we discuss the support of the Lagrange basis functions later.

In step 1(a) we get sets of filled and vertex triangles. Each of these vertex triangles shared an edge with a filled triangle. In step 1(b) and (c) we get sets of filled and edge triangles. The dependent vertex of each of these edge triangles belongs to a filled triangle. Consequently, we get vertex triangles sharing an edge with an edge triangle. Step 1(d) and (e) are similar to Algorithm 1. In conclusion, step 1 gives Δ_1 the same structure as Δ_0.

In Step 2 it is clear that we get a set of filled triangles and consequently we get a set of vertex triangles where each of these vertex triangles has interpolation points at distance $\frac{|e|}{2}$ and shares the edge opposite to its isolated vertex with a filled triangle. In addition, we get the followings when step 3 is performed. Filled triangles with interpolation points at distance $\frac{|e|}{4}$.

In addition to what we obtained above from step 2 and step 3, we get the following structures when step 4 is carried out. From the initial step of Step 4, we get edge triangles with points at the distance $\frac{|e|}{4}$ attached to the filled triangle of step 2. Otherwise we get vertex triangles with points at the distance $\frac{|e|}{4}$ with their dependent vertices one belong to the middle filled and the other one belongs to an edge triangle created from the initial step. The latter could also belong to a filled triangle produced in Step 3 since this vertex belongs to the boundary of $\text{star}^1(v)$ for $v \in \Delta_{n-2}$.

Remark 3.11. *Let $T_1, T_2 \in \Delta_{n-2}$ be two neighbouring triangles. Let T_{gc} be the grandchildren of T_1 in Δ_n intersect with the grandchildren of T_2 in Δ_n. Then every triangle of T_{gc} is contained in the* $\text{star}^2(T_m)$ *where T_m is the middle triangle of T_2*

in Δ_n. We can see this clearly from Fig.3.18, for example.

Remark 3.12. *In Step 4 we get a vertex triangle $T \in \Delta_n$ with its dependent vertices $u, v \in \mathcal{V}_n$ one belonging to the middle filled of step 2 and one belonging to a filled triangle T_F of Step 3, where T_F has a vertex of Δ_{n-2}. It is clear that T and T_F are grandchildren of T' and T'' respectively, where $T', T'' \in \Delta_{n-2}$ and T', T'' are neighbouring triangles. Since T and T_F share a vertex then T belongs to* $\text{star}^2(T_m)$ *where T_m is the middle filled triangle of T'' in Δ_n, see Remark 3.11.*

We also see that for any vertex $v \in \Delta_{n-2}$, v could be a vertex of a filled triangle of type 3 or vertex triangle with points at $\frac{|e|}{2}$. These triangles are processed in step 3. The remaining triangles in the $\text{star}^1(v)$ are necessary empties. For any vertex $u \in \mathcal{V}_{n-1} \setminus \mathcal{V}_{n-2}$, u could be a vertex of a vertex triangle with points at $\frac{|e|}{2}$ but not a filled triangle since all the triangles in $\text{star}^1(u)$ have a vertex of the filled triangle of step 2. The remaining triangles in the $\text{star}^1(u)$ are necessary empties.

Theorem 3.13. *The set Ξ_n is a local interpolation set for $S_n,\ n = 1, 2, \ldots$. The supports of the Lagrange basis functions $B_\xi^{(n)},\ \xi \in \Xi_n$ satisfy*

$$\text{supp}(B_\xi^{(n)}) \subseteq \text{star}^3(T),$$

where $T \in \Delta_n$ is any triangle containing ξ.

Proof. Clearly that from the above construction, $\Delta_n,\ n = 1, 2, \ldots$ consist of the filled, edge, vertex and empty triangles. Using the same argument as in the proof of Theorem 3.9, we can show that by assumming zero interpolation values, gradient of s vanishes for all vertices of Δ_n. The similar argument also shows that the supports of $B_\xi^{(n)}$ satisfy

$$\text{supp}(B_\xi^{(n)}) \subseteq \text{star}^3(T),$$

and Corollary 3.10 holds for $B_\xi^{(n)}$.

□

Theorem 3.14. *Let Ξ_n be the local interpolation set described above for S_n, $n = 0, 1, 2 \ldots$. For any arbitrary function f in $C(\Omega)$ and its corresponding unique Lagrange interpolating spline $s \in S_n$, we have*

$$\|s\|_{L_\infty(T)} \lesssim \max\big\{|f(\xi)| : \xi \in \Xi_n \cap \mathrm{star}^i(T)\big\}, \quad T \in \Delta_n, \tag{3.3.3}$$

where $i = 0, 1, 2, 3$ when T is a filled, an edge, a vertex, or an empty triangle, respectively. The bounding constant depending only on the smallest angle in the triangulation Δ_n.

Proof. We denote the vertices of T as $v_i = (x_i, y_i), i = 1, 2, 3$. Let $e_{12} = v_2 - v_1 = (x_2 - x_1, y_2 - y_1)$ and $e_{13} = v_3 - v_1 = (x_3 - x_1, y_3 - y_1)$ define two vectors. Then the directional derivatives of s at $(x, y) \in T$ with respect to the directions e_{12} and e_{13} are given respectively by

$$\begin{aligned}
\frac{\partial}{\partial e_{12}} s(x,y) &= (x_2 - x_1)\frac{\partial}{\partial x} s(x,y) + (y_2 - y_1)\frac{\partial}{\partial y} s(x,y), \\
\frac{\partial}{\partial e_{13}} s(x,y) &= (x_3 - x_1)\frac{\partial}{\partial x} s(x,y) + (y_3 - y_1)\frac{\partial}{\partial y} s(x,y).
\end{aligned} \tag{3.3.4}$$

We find that

$$\left|\frac{\partial}{\partial e_{12}} s(x,y)\right| \le |x_2 - x_1|\left|\frac{\partial}{\partial x} s(x,y)\right| + |y_2 - y_1|\left|\frac{\partial}{\partial y} s(x,y)\right|,$$

$$\left|\frac{\partial}{\partial e_{13}} s(x,y)\right| \le |x_3 - x_1|\left|\frac{\partial}{\partial x} s(x,y)\right| + |y_3 - y_1|\left|\frac{\partial}{\partial y} s(x,y)\right|,$$

and hence

$$\begin{aligned}
\left|\frac{\partial}{\partial e_{12}} s(x,y)\right| &\lesssim \max\left\{\left|\frac{\partial}{\partial x} s(x,y)\right|, \left|\frac{\partial}{\partial y} s(x,y)\right|\right\}, \\
\left|\frac{\partial}{\partial e_{13}} s(x,y)\right| &\lesssim \max\left\{\left|\frac{\partial}{\partial x} s(x,y)\right|, \left|\frac{\partial}{\partial y} s(x,y)\right|\right\}.
\end{aligned} \tag{3.3.5}$$

With $\mathrm{diam}(T)$ being the diameter of T, we get

$$\begin{aligned}
|e_{12}|\left|\frac{\partial}{\partial e_{12}} s(x,y)\right| &\lesssim \max\left\{\mathrm{diam}(T)\left|\frac{\partial}{\partial x} s(x,y)\right|, \mathrm{diam}(T)\left|\frac{\partial}{\partial y} s(x,y)\right|\right\}, \\
|e_{13}|\left|\frac{\partial}{\partial e_{13}} s(x,y)\right| &\lesssim \max\left\{\mathrm{diam}(T)\left|\frac{\partial}{\partial x} s(x,y)\right|, \mathrm{diam}(T)\left|\frac{\partial}{\partial y} s(x,y)\right|\right\}.
\end{aligned} \tag{3.3.6}$$

Solving (3.3.4) simultaneously gives

$$\frac{\partial}{\partial x}s(x,y) = \frac{(y_3-y_1)\frac{\partial}{\partial e_{12}}s(x,y) - (y_2-y_1)\frac{\partial}{\partial e_{13}}s(x,y)}{x_1y_2+x_2y_3+x_3y_1-x_1y_3-x_2y_1-x_3y_2},$$

$$\frac{\partial}{\partial y}s(x,y) = \frac{(x_2-x_1)\frac{\partial}{\partial e_{13}}s(x,y) - (x_3-x_1)\frac{\partial}{\partial e_{12}}s(x,y)}{x_1y_2+x_2y_3+x_3y_1-x_1y_3-x_2y_1-x_3y_2}.$$

We find that

$$\left|\frac{\partial}{\partial x}s(x,y)\right| \le \frac{|y_3-y_1|}{2\text{Area}(T)}\left|\frac{\partial}{\partial e_{12}}s(x,y)\right| + \frac{|y_2-y_1|}{2\text{Area}(T)}\left|\frac{\partial}{\partial e_{13}}s(x,y)\right|,$$

$$\left|\frac{\partial}{\partial y}s(x,y)\right| \le \frac{|x_2-x_1|}{2\text{Area}(T)}\left|\frac{\partial}{\partial e_{13}}s(x,y)\right| + \frac{|x_3-x_1|}{2\text{Area}(T)}\left|\frac{\partial}{\partial e_{12}}s(x,y)\right|,$$

and hence

$$\left|\frac{\partial}{\partial x}s(x,y)\right| \lesssim \max\left\{\left|\frac{\partial}{\partial e_{12}}s(x,y)\right|, \left|\frac{\partial}{\partial e_{13}}s(x,y)\right|\right\},$$

$$\left|\frac{\partial}{\partial y}s(x,y)\right| \lesssim \max\left\{\left|\frac{\partial}{\partial e_{12}}s(x,y)\right|, \left|\frac{\partial}{\partial e_{13}}s(x,y)\right|\right\}.$$

With $\text{diam}(T)$ being the diameter of T, we get

$$\begin{aligned}\text{diam}(T)\left|\frac{\partial}{\partial x}s(x,y)\right| &\lesssim \max\left\{|e_{12}|\left|\frac{\partial}{\partial e_{12}}s(x,y)\right|, |e_{12}|\left|\frac{\partial}{\partial e_{13}}s(x,y)\right|\right\},\\ \text{diam}(T)\left|\frac{\partial}{\partial y}s(x,y)\right| &\lesssim \max\left\{|e_{12}|\left|\frac{\partial}{\partial e_{12}}s(x,y)\right|, |e_{13}|\left|\frac{\partial}{\partial e_{13}}s(x,y)\right|\right\},\end{aligned} \tag{3.3.7}$$

with the bounding constant depending only on the smallest angle of the triangulation Δ_n.

We will prove (3.3.3) in several steps. We will make use of the classical *Markov Inequality*

$$\|p'\|_{L_\infty(0,1)} \le 2q^2\|p\|_{L_\infty(0,1)}$$

which is valid for all univariate polynomials of degree q, and we often apply this inequality in the following way: Let e be a line segment in $\mathbb{R}^2$ with endpoints v, w,

and let s be a bivariate polynomial of total degree q. With $\frac{\partial s}{\partial e}(v)$ we denote the derivative of s at v in the direction $w-v$. Defining $p(t) = s(v+t(w-v))$, we have $\frac{\partial s}{\partial e}(v) = \frac{p'(0)}{|e|}$ and Markov inequality shows that

$$\left|\frac{\partial s}{\partial e}(v)\right| \leq \frac{2q^2}{|e|}\|s\|_{L_\infty(e)}. \tag{3.3.8}$$

From our construction we have interpolation points on the line segments $e_i = [v_i, w_i]$, $1 \leq i \leq 4$,

$$\begin{aligned}
\Xi_{e_1} &= \{v_1, w_1, \frac{3}{4}v_1 + \frac{1}{4}w_1, \frac{3}{4}w_1 + \frac{1}{4}v_1\},\\
\Xi_{e_2} &= \{v_2, w_2, \frac{3}{4}v_2 + \frac{1}{4}w_2\},\\
\Xi_{e_3} &= \{v_3, w_3, \frac{1}{2}v_3 + \frac{1}{2}w_3\},\\
\Xi_{e_4} &= \{v_4, w_4\}.
\end{aligned}$$

We shall now classify Ξ_{e_1} as type 1, $\{\Xi_{e_2}, \Xi_{e_3}\}$ as type 2 and Ξ_{e_4} as type 3 interpolation points on the line segments.

The univariate C^1 quadratic splines $p_i(t) = s(tw_i + (1-t)v_i)$, $1 \leq i \leq 4$ satisfy the interpolation conditions

$$\begin{aligned}
&p_1(0) = s(v_1), \quad p_1(\frac{1}{4}) = s(\frac{3}{4}v_1 + \frac{1}{4}w_1), \quad p_1(\frac{3}{4}) = s(\frac{3}{4}w_1 + \frac{1}{4}v_1), \quad p_1(1) = s(w_1),\\
&p_2(0) = s(v_2), \quad p_2(\frac{1}{4}) = s(\frac{3}{4}v_2 + \frac{1}{4}w_2), \quad p_2(1) = s(w_2), \quad p_2'(1) = |e_2|\left|\frac{\partial s}{\partial e_2}(w_2)\right|,\\
&p_3(0) = s(v_3), \quad p_3(\frac{1}{2}) = s(\frac{1}{2}v_3 + \frac{1}{2}w_3), \quad p_3(1) = s(w_3), \quad p_3'(1) = |e_3|\left|\frac{\partial s}{\partial e_3}(w_3)\right|,\\
&p_4(0) = s(v_4), \quad p_4'(0) = |e_4|\left|\frac{\partial s}{\partial e_4}(v_4)\right|, \quad p_4(1) = s(w_4), \quad p_4'(1) = |e_4|\left|\frac{\partial s}{\partial e_4}(w_4)\right|.
\end{aligned}$$

The well-posedness of such a C^1 quadratic spline interpolation scheme implies that

$$\|s\|_{L_\infty(e_1)} \lesssim \max\{|s(\xi)| : \xi \in \Xi_{e_1}\}, \tag{3.3.9}$$

$$\|s\|_{L_\infty(e_j)} \lesssim \max\{|s(\xi)|, |e_j|\left|\frac{\partial s}{\partial e_j}(w_j)\right| : \xi \in \Xi_{e_j}\}, \quad 2 \leq j \leq 3, \tag{3.3.10}$$

and

$$\|s\|_{L_\infty(e_4)} \lesssim \max\{|s(\xi)|, |e_4|\left|\frac{\partial s}{\partial e_4}(v_4)\right|, |e_4|\left|\frac{\partial s}{\partial e_4}(w_4)\right| : \xi \in \Xi_{e_4}\}.$$

Let $T \in \Delta_n$ with vertices v_1, v_2, v_3. We put $e_1 = [v_1, v_2]$, $e_2 = [v_2, v_3]$, $e_3 = [v_3, v_1]$. Three univariate C^1 quadratic splines, $p_1(t) = s(tv_2 + (1-t)v_1), p_2(t) = s(tv_2 + (1-t)v_3), p_3(t) = s(tv_3 + (1-t)v_1)$, $t \in [0,1]$ will play an important role below.

Step 1: Suppose $T \in \Delta_n$ is a filled triangle. Then the interpolation points on each e_i, $i = 1, 2, 3$ are of type 1. Therefore, using the estimate (3.3.9) and Markov inequality give

$$|e_1|\left|\frac{\partial s}{\partial e_1}(v_1)\right| = |p_1'(0)| \lesssim \max\{|s(\xi)| : \xi \in \Xi_n \cap e_1\},$$

$$|e_3|\left|\frac{\partial s}{\partial e_3}(v_1)\right| = |p_3'(1)| \lesssim \max\{|s(\xi)| : \xi \in \Xi_n \cap e_3\},$$

$$|e_1|\left|\frac{\partial s}{\partial e_1}(v_2)\right| = |p_1'(1)| \lesssim \max\{|s(\xi)| : \xi \in \Xi_n \cap e_1\},$$

$$|e_2|\left|\frac{\partial s}{\partial e_2}(v_2)\right| = |p_2'(0)| \lesssim \max\{|s(\xi)| : \xi \in \Xi_n \cap e_2\},$$

$$|e_2|\left|\frac{\partial s}{\partial e_1}(v_3)\right| = |p_2'(1)| \lesssim \max\{|s(\xi)| : \xi \in \Xi_n \cap e_2\},$$

$$|e_3|\left|\frac{\partial s}{\partial e_3}(v_3)\right| = |p_3'(0)| \lesssim \max\{|s(\xi)| : \xi \in \Xi_n \cap e_3\}.$$

With $\operatorname{diam}(T) \sim 2^{-n}$ and (3.3.7), we conclude that

$$\max\left\{2^{-n}\left|\frac{\partial s}{\partial x}(v_i)\right|, 2^{-n}\left|\frac{\partial s}{\partial y}(v_i)\right|\right\} \lesssim M_i, \quad 1 \le i \le 3,$$

where

$$M_1 = \max\big\{|s(\xi)| : \xi \in \Xi_n \cap (e_1 \cup e_3)\big\},$$

$$M_2 = \max\big\{|s(\xi)| : \xi \in \Xi_n \cap (e_1 \cup e_2)\big\},$$

$$M_3 = \max\big\{|s(\xi)| : \xi \in \Xi_n \cap (e_2 \cup e_3)\big\},$$

with a constant depending only on the smallest angle in T. Lemma 3.4 applied to T shows that

$$\|s\|_{L_\infty(T)} \lesssim \max\{|s(\xi)| : \xi \in \Xi_n \cap T\}, \tag{3.3.11}$$

with a constant depending only on the smallest angle of the triangulation Δ_n.

Step 2: Suppose $T \in \Delta_n$ is an edge triangle. Then there exists a triangle $T_1 \in \mathrm{star}(T) \setminus T$ where T_1 is a filled triangle. Let v_3 be the dependent vertex of T and it is also the common vertex of T and T_1. We also note that interpolation points on e_1 is of type 1 and e_2, e_3 are of type 2.

Using the estimates (3.3.9) and (3.3.10) and Markov inequality imply that

$$|e_1|\left|\frac{\partial s}{\partial e_1}(v_1)\right| = |p_1'(0)| \lesssim \max\{|s(\xi)| : \xi \in \Xi_n \cap e_1\},$$

$$|e_3|\left|\frac{\partial s}{\partial e_3}(v_1)\right| = |p_3'(1)| \lesssim \max\left\{|s(\xi)| : \xi \in \Xi_n \cap e_3, |e_3|\left|\frac{\partial s}{\partial e_3}(v_3)\right|\right\},$$

$$|e_1|\left|\frac{\partial s}{\partial e_1}(v_2)\right| = |p_1'(1)| \lesssim \max\{|s(\xi)| : \xi \in \Xi_n \cap e_1\},$$

$$|e_2|\left|\frac{\partial s}{\partial e_2}(v_2)\right| = |p_2'(0)| \lesssim \max\left\{|s(\xi)| : \xi \in \Xi_n \cap e_2, |e_2|\left|\frac{\partial s}{\partial e_2}(v_3)\right|\right\}.$$

With $\mathrm{diam}(T) \sim 2^{-n}$ and (3.3.7), we conclude that

$$\max\left\{2^{-n}\left|\frac{\partial s}{\partial x}(v_1)\right|, 2^{-n}\left|\frac{\partial s}{\partial y}(v_1)\right|\right\} \lesssim \max\left\{|s(\xi)| : \xi \in \Xi_n \cap (e_1 \cup e_3), |e_3|\left|\frac{\partial s}{\partial e_3}(v_3)\right|\right\},$$

$$\max\left\{2^{-n}\left|\frac{\partial s}{\partial x}(v_2)\right|, 2^{-n}\left|\frac{\partial s}{\partial y}(v_2)\right|\right\} \lesssim \max\left\{|s(\xi)| : \xi \in \Xi_n \cap (e_1 \cup e_2), |e_2|\left|\frac{\partial s}{\partial e_2}(v_3)\right|\right\}.$$

With $\mathrm{diam}(T) \sim 2^{-n}$ and (3.3.6), we get

$$\max\left\{|e_2|\left|\frac{\partial s}{\partial e_2}(v_3)\right|, |e_3|\left|\frac{\partial s}{\partial e_3}(v_3)\right|\right\} \lesssim \max\left\{2^{-n}\left|\frac{\partial s}{\partial x}(v_3)\right|, 2^{-n}\left|\frac{\partial s}{\partial y}(v_3)\right|\right\}.$$

We now make use of the Markov inequality for bivariate polynomial on triangle, we deduce that

$$\left\{2^{-n}\left|\frac{\partial s}{\partial x}(v_3)\right|, 2^{-n}\left|\frac{\partial s}{\partial y}(v_3)\right|\right\} \lesssim \|s\|_{L_\infty(T_1)}$$

and

$$\max\left\{|e_2|\left|\frac{\partial s}{\partial e_2}(v_3)\right|, |e_3|\left|\frac{\partial s}{\partial e_3}(v_3)\right|\right\} \lesssim \|s\|_{L_\infty(T_1)}.$$

Lemma 3.4 applied to T and taking into account of the estimate (3.3.11) for s on T_1 shows that

$$\|s\|_{L_\infty(T)} \lesssim \max\{|s(\xi)| : \xi \in \Xi_n \cap \mathrm{star}(T)\}, \tag{3.3.12}$$

with the bounding constant depends only on the smallest angle of the triangulation Δ_n.

Step 3: Suppose $T \in \Delta_n$ is a vertex triangle. Then the dependent vertices v_2, v_3 of T belong to to T_2, T_3, respectively (which allows $T_2 = T_3$) in $\mathrm{star}(T) \setminus T$. Each of T_2, T_3 is either a filled or an edge triangle. We note that interpolation points on e_1, e_2 are of type 2 and e_3 can be either type 1 or type 4.

Using the estimate (3.3.10) and Markov inequality imply that

$$|e_1|\left|\frac{\partial s}{\partial e_1}(v_2)\right| = |p_1'(0)| \lesssim \max\left\{|s(\xi)| : \xi \in \Xi_n \cap e_1, |e_1|\left|\frac{\partial s}{\partial e_1}(v_2)\right|\right\},$$

$$|e_3|\left|\frac{\partial s}{\partial e_3}(v_3)\right| = |p_3'(1)| \lesssim \max\left\{|s(\xi)| : \xi \in \Xi_n \cap e_3, |e_3|\left|\frac{\partial s}{\partial e_3}(v_3)\right|\right\},$$

and so with $\mathrm{diam}(T) \sim 2^{-n}$ being the diameter of T, we conclude that

$$\begin{aligned}&\max\left\{2^{-n}\left|\frac{\partial s}{\partial x}(v_1)\right|, 2^{-n}\left|\frac{\partial s}{\partial y}(v_1)\right|\right\}\\ &\quad\lesssim \max\left\{|s(\xi)| : \xi \in \Xi_n \cap (e_1 \cup e_3), |e_1|\left|\frac{\partial s}{\partial e_1}(v_2)\right|, |e_3|\left|\frac{\partial s}{\partial e_3}(v_3)\right|\right\},\end{aligned}$$

With $\mathrm{diam}(T) \sim 2^{-n}$ and (3.3.6), we get

$$|e_1|\left|\frac{\partial s}{\partial e_1}(v_2)\right| \lesssim \max\left\{2^{-n}\left|\frac{\partial s}{\partial x}(v_2)\right|, 2^{-n}\left|\frac{\partial s}{\partial y}(v_2)\right|\right\}$$

and

$$|e_3|\left|\frac{\partial s}{\partial e_3}(v_3)\right| \lesssim \max\left\{2^{-n}\left|\frac{\partial s}{\partial x}(v_3)\right|, 2^{-n}\left|\frac{\partial s}{\partial y}(v_3)\right|\right\}.$$

Making use of the Markov inequality for bivariate polynomial, we deduce that

$$\left\{2^{-n}\left|\frac{\partial s}{\partial x}(v_2)\right|, 2^{-n}\left|\frac{\partial s}{\partial y}(v_2)\right|\right\} \lesssim \|s\|_{L_\infty(T_2)}$$

and

$$\left\{2^{-n}\left|\frac{\partial s}{\partial x}(v_3)\right|, 2^{-n}\left|\frac{\partial s}{\partial y}(v_3)\right|\right\} \lesssim \|s\|_{L_\infty(T_3)},$$

and hence

$$|e_1|\left|\frac{\partial s}{\partial e_1}(v_2)\right| \lesssim \|s\|_{L_\infty(T_2)}$$

$$|e_3|\left|\frac{\partial s}{\partial e_3}(v_3)\right| \lesssim \|s\|_{L_\infty(T_3)}.$$

Case 1: The dependent vertices v_2, v_3 belong to two different triangles where both are filled triangles or they belong to the same triangle which is a filled triangle ($T_2 = T_3$).

Lemma 3.4 applied to T and taking into account of the estimate (3.3.11) on T_2 and T_3 show that

$$\|s\|_{L_\infty(T)} \lesssim \max\{|s(\xi)| : \xi \in \Xi_n \cap \mathrm{star}(T)\}.$$

Case 2: The dependent vertices v_2, v_3 belong to two different triangles where both are edge triangles or they belong to the same triangle which is a edge triangle ($T_2 = T_3$).

Lemma 3.4 applied to T and taking into account of the estimate (3.3.12) on T_2 and T_3 show that

$$\|s\|_{L_\infty(T)} \lesssim \max\{|s(\xi)| : \xi \in \Xi_n \cap \mathrm{star}^2(T)\}.$$

Case 3: The dependent vertices v_2, v_3 belong to two different triangles of different types (T_2 edge and T_3 filled triangle).

Lemma 3.4 applied to T and taking into account of the estimates (3.3.11) on T_3 and (3.3.12) on T_2 show that

$$\|s\|_{L_\infty(T)} \lesssim \max\{|s(\xi)| : \xi \in \Xi_n \cap \mathrm{star}^2(T)\}.$$

Step 4: Suppose T is an empty triangle. Since empty triangle is attached to either the filled, edge or vertex triangle, in view of the above argument for step 1, 2 and 3, using Markov inequality on T and then apply Lemma 3.4 to T, we hereby conclude that

$$\|s\|_{L_\infty(T)} \lesssim \max\{|s(\xi)| : \xi \in \Xi_n \cap \mathrm{star}^3(T)\}.$$

This completes the proof. □

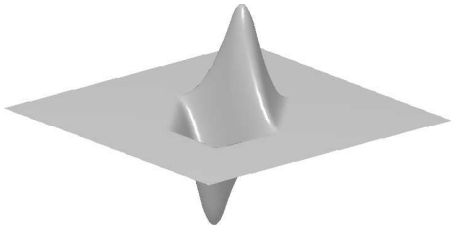

(a)

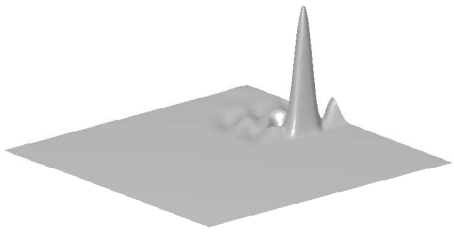

(b)

Figure 3.19: (a) Basis function B_ξ with ξ corresponding to a vertex in Δ_n (b) Basis function B_ξ with ξ corresponding to a vertex in $\Delta_{n+1} \setminus \Delta_n$.

By Theorem 3.14, the bases $\{B_\xi^{(n)}\}_{\xi\in\Xi_n}$ are well-defined, and so we have

$$\left\|B_\xi^{(n)}\right\|_{L_\infty(\Omega)} \lesssim 1, \quad \xi \in \Xi_n, \tag{3.3.13}$$

where the bounding constant depends only on the smallest angle of the triangulation Δ_n. Since uniform refinement does not change angles, the constant depends only on the smallest angle in Δ_0.

Finally, by construction since we used all point of Ξ_n when constructing Ξ_{n-1}, Algorithms 1 and 2 give us a nested interpolation set, i.e.

$$\Xi_n \subset \Xi_{n+1},\ n = 0, 1, 2, \ldots$$

Figures 3.20a, 3.20b, 3.21a, 3.21b and 3.22 provide some illustrations.

For each $n = 0, 1, 2, \ldots$, we are also interested in the multilevel spaces $\tilde{S}_n \subset S_n$ satisfying the homogeneous boundary conditions, i.e.,

$$\tilde{S}_n := \left\{ s \in S_n : s = \frac{\partial s}{\partial x} = \frac{\partial s}{\partial y} = 0 \text{ on } \partial\Omega \right\}.$$

It is clear that the splines spaces $\tilde{S}_n$ are nested, i.e.

$$\tilde{S}_n \subset \tilde{S}_{n+1}, \quad n = 0, 1, 2 \ldots.$$

Let $\tilde{\Xi}_n = \Xi_n \setminus \Xi_n^b$ with Ξ_n^b being the set of interpolation points assigned to the boundary vertices of Δ_n. It is also clear that the interpolation set $\tilde{\Xi}_n$ is nested, i.e.,

$$\tilde{\Xi}_n \subset \tilde{\Xi}_{n+1}, \quad n = 0, 1, 2, \ldots.$$

Theorem 3.15. *The set $\tilde{\Xi}_n$ is a Lagrange interpolation set for $\tilde{S}_n$. The maximal supports of the Lagrange basis functions $\tilde{B}_\xi^{(n)},\ \xi \in \tilde{\Xi}_n$ satisfy*

$$\operatorname{supp}\left(\tilde{B}_\xi^{(n)}\right) \subseteq \operatorname{star}^3(T),$$

if the corresponding interpolation point $\xi \in \tilde{\Xi}_n$ lies on $T \in \Delta_n$.

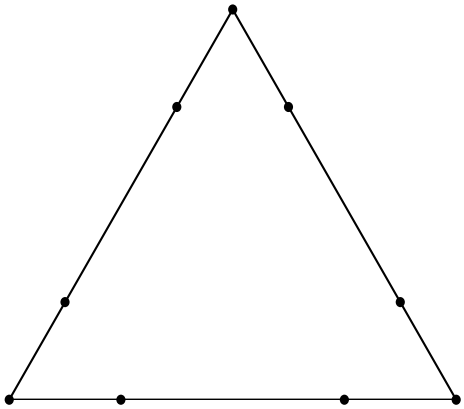

(a)

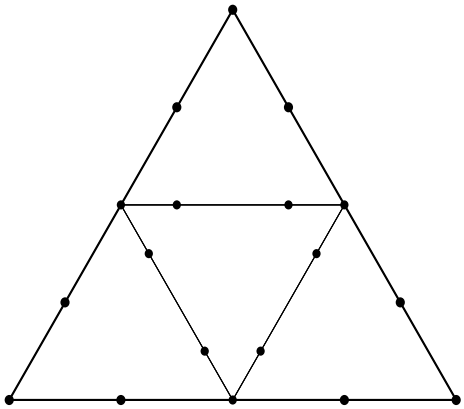

(b)

Figure 3.20: (a) Ξ_T for some $T \in \Delta_n$ and (b) $\bigcup \left\{ \Xi_{\tilde{T}} : \tilde{T} \in \Delta_{n+1}, \tilde{T} \subset T \right\}$

Proof. The spline spaces $\tilde{S}_n$ satisfy homogeneous boundary conditions; therefore we find that $\dim \tilde{S}_n = 3\#\mathcal{V}_n^I = \#\tilde{\Xi}_n$ where $\mathcal{V}_n^I$ is the set of all interior vertices of Δ_n. We need to show that for $s \in \tilde{S}_n$ with $s(\xi) = 0$, $\xi \in \tilde{\Xi}_n$ implies $s \equiv 0$. Indeed, using the same argument as in the proof of Theorem 3.9 and 3.13 with three interpolation conditions on every boundary vertex replaced with the homogeneous boundary conditions, we can show that $s|_e \equiv 0$ for all edges of Δ_n. Therefore we deduce that the function value and the gradient of s vanish at all vertices of Δ_n. Thus $s \equiv 0$ by Theorem 3.1. It is also clear that the maximum size of supports of

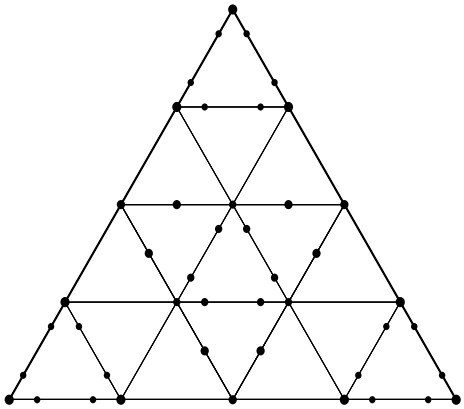

(a)

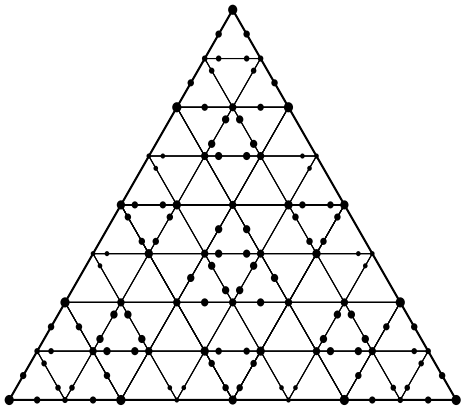

(b)

Figure 3.21: (a) $\bigcup\{\Xi_{\hat{T}} : \hat{T} \in \Delta_{n+2}, \hat{T} \subset \tilde{T} \subset T\}$ and (b) $\bigcup\{\Xi_{T^*} : T^* \in \Delta_{n+3}, T^* \subset \hat{T} \subset \tilde{T} \subset T\}$

the basis functions $\tilde{B}_\xi^{(n)},\ \xi \in \tilde{\Xi}_n$ satisfy $\text{supp}\left(\tilde{B}_\xi^{(n)}\right) \subseteq \text{star}^3(T)$. □

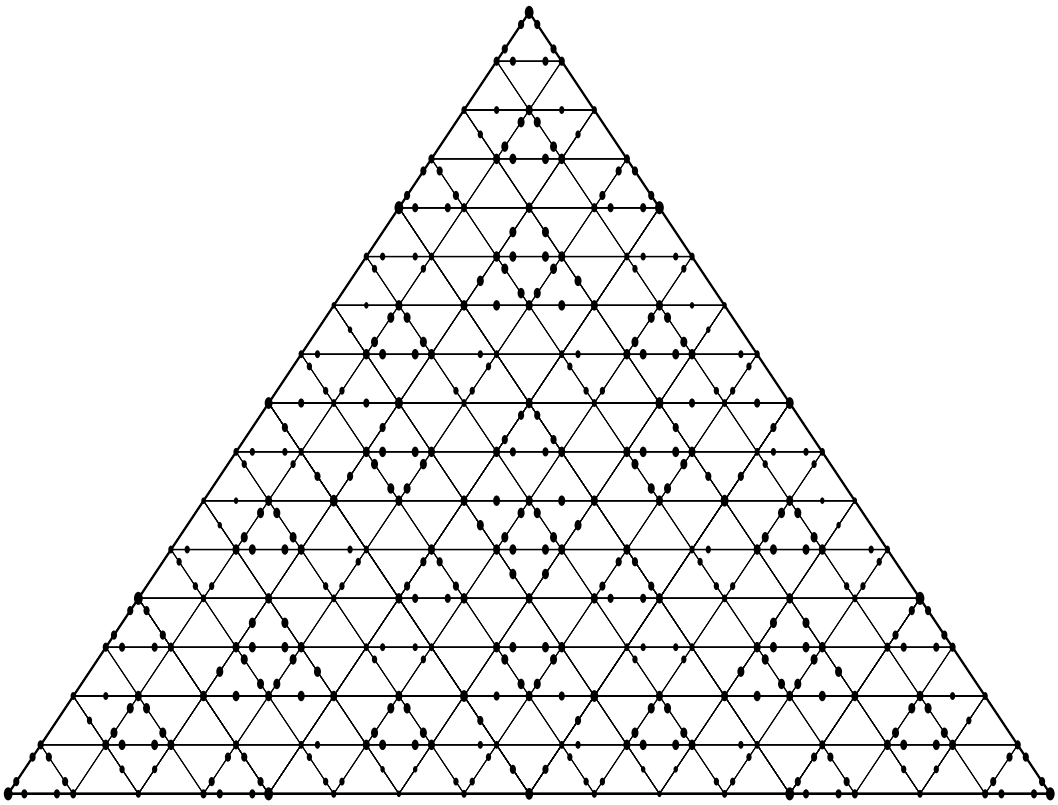

Figure 3.22: $\bigcup \{\Xi_{\dot{T}} : \dot{T} \in \Delta_{n+4}, \dot{T} \subset T^* \subset \hat{T} \subset \tilde{T} \subset T\}$

3.4 Hierarchical Riesz Bases

For any $K \in \mathbb{N},\ K \geq 1$, it can be easily checked that the set

$$\bigcup_{n=0}^{K} \{B_\xi^{(n)}\}_{\xi \in \Xi_n \setminus \Xi_{n-1}}$$

is a *hierarchical basis* for S_K.

Under the guidance of the general theory for macro-element hierarchical Riesz bases developed in Chapter 2, in the next theorem we show that the properly scaled hierarchical bases give rise to Riesz bases for certain Sobolev spaces on Ω.

Theorem 3.16. *Let*

$$\mathcal{B}^s := \bigcup_{n=0}^{\infty} \{2^{n(1-s)} B_\xi^{(n)}\}_{\xi \in \Xi_n \setminus \Xi_{n-1}}, \qquad \mathcal{B}_0^s := \bigcup_{n=0}^{\infty} \{2^{n(1-s)} \tilde{B}_\xi^{(n)}\}_{\xi \in \tilde{\Xi}_n \setminus \tilde{\Xi}_{n-1}}.$$

Then $\mathcal{B}^s$ is a Riesz basis for $H^s(\Omega)$ for any $s \in (1, \frac{5}{2})$. Moreover, $\mathcal{B}_0^s$ is a Riesz basis for $H_0^s(\Omega)$ for any $s \in (1, \frac{3}{2}) \cup (\frac{3}{2}, \frac{5}{2})$.

Proof. By Lemma 3.4, we see that the nodal basis $\{s_i^{(n)}\}_{i=1}^{N_n}$ is uniformly bounded. Then by Theorem 2.7, for $k = 2$, $h_{\Delta_n} \sim 2^{-n}$, we obtain the Jackson estimate

$$\inf_{s \in S_n} \|f - s\|_{L_2(\Omega)} \lesssim 2^{-3n} |f|_{H^3(\Omega)}, \quad f \in H^3(\Omega). \tag{3.4.1}$$

Moreover, the corresponding Lagrange interpolation sets for S_n are nested and the Lagrange basis functions $B_\xi^{(n)}$ are uniformly local and bounded (see Theorem 3.14 and (3.3.13)). Then by Theorem 2.11, applied with $\rho = 2, k = 2$ and $r = 1$, $\mathcal{B}^s$ leads to a Riesz basis for $H^s(\Omega)$ for any $s \in (1, \frac{5}{2})$. This completes the proof for the first part.

For the second part, we recall that the spaces $\tilde{S}_n \subset S_n$ satisfies homogeneous boundary conditions of order 1. We also note that the operators Π_n (3.2.7) are boundary conforming of order 1, that is

$$f = \frac{\partial f}{\partial x} = \frac{\partial f}{\partial y} = 0 \text{ on } \partial\Omega$$

implies $\Pi_n f \in \tilde{S}_n$. Then by Corollary 2.8 we get the estimate

$$\inf_{s \in \tilde{S}_n} \|f - s\|_{L_2(\Omega)} \lesssim 2^{-3n} |f|_{H^3(\Omega)}, \quad f \in H_0^3(\Omega). \tag{3.4.2}$$

We have now verified the assumptions of part (b) of Theorem 2.11. Hence $\mathcal{B}_0^s$ is a Riesz basis for $H_0^s(\Omega)$ for any $s \in (1, \frac{3}{2}) \cup (\frac{3}{2}, \frac{5}{2})$. □

As the result, we say for $K \in \mathbb{N}$,

$$\bigcup_{n=0}^{K} \{2^{n(1-s)} B_\xi^{(n)}\}_{\xi \in \Xi_n \setminus \Xi_{n-1}}$$

and

$$\bigcup_{n=0}^{K} \{2^{n(1-s)} \tilde{B}_\xi^{(n)}\}_{\xi \in \tilde{\Xi}_n \setminus \tilde{\Xi}_{n-1}}$$

are uniformly H^s-stable bases for S_K and $\tilde{S}_K$, respectively.

The above constructed Lagrange hierarchical bases can be used for surface compression, see [32, 42]. For this application, our basis of Lagrange type has a larger range of stability than the Hermite type will have its advantage here. Furthermore, Lagrange basis has another advantage that only Lagrange data of the surface is needed.

The hierarchical bases can also be used to solve boundary value problems of fourth order. For example, consider the biharmonic equation

$$\Delta^2 u = f \text{ on } \Omega, \quad u = \frac{\partial u}{\partial n} = 0 \text{ on } \partial\Omega, \tag{3.4.3}$$

where $\partial\Omega$ denotes the boundary of the polygonal domain Ω. As usual, Δ stands for the Laplace operator: $\Delta = \frac{\partial^2}{\partial x^2} + \frac{\partial^2}{\partial y^2}$, and $\frac{\partial}{\partial n}$ represents the normal derivative. The biharmonic equation appears as result of the modelling of plate bending problems.

After switching to a variational formulation, the Ritz-Galerkin approximation $u_K \in S_K$ solves

$$a(u_K, v_K) = (f, u_K)_{L_2(\Omega)}, \quad v_K \in S_K,$$

where

$$a(u, v) = \int_\Omega \sum_{i,j} \partial_{ij}^2 u \partial_{ij}^2 v dx.$$

Since $a(v, v) \sim \|v\|^2_{H_0^2(\Omega)}$, then using the properly scaled hierarchical basis

$$\bigcup_{n=0}^{K} \{2^{-ns} \tilde{B}_\xi^{(n)}\}_{\xi \in \tilde{\Xi}_n \setminus \tilde{\Xi}_{n-1}}$$

will lead to uniformly well-conditioned stiffness matrices. For comparison, note that standard, single scale bases for S_K give rise to stiffness matrices with condition numbers of the order $h_{\Delta_K}^{-4}$ with $h_{\Delta_K} = 2^{-K}$.

Remark 3.17. *The hierarchical bases constructed in Section 1 are of Hermite type. The functionals defining the bases involve both the function values and derivatives, so by Sobolev embedding thereom, the corresponding interpolation operator* Π_n *is only well defined for* $H^s(\Omega)$ *when* $s > 2$. *As a consequence, properly scaled, these bases generate Riesz basis for* $H^s(\Omega)$ *for* $2 < s < 5/2$. *This is a suboptimal result in the case of* $s = 2$ *thus using these bases to solve the biharmonic equation will lead to logarithmically growing condition numbers of stiffness matrices, see [49, 14].*

Chapter 4

Applications

4.1 Introduction

In this chapter we consider the applications of hierarchical bases constructed in the previous chapter. In particular, we explore the use of our hierarchical bases of Lagrange type in surface compression and also in solving the biharmonic equation.

Hierarchical bases of Lagrange type were constructed in [21, 41]. However, numerical schemes based on these hierarchal bases have yet to be implemented. Therefore it is important here for us to explore the use of hierarchical basis of this type in applications.

The application of hierarchical bases in surface compression was first proposed in [32]. In [32] a surface compression method was constructed for the space of C^1 cubic splines defined on triangulations obtained from convex quadrangulations. Later, Maes and Bultheel [42] construct a compression method for the space of C^1 quadratic splines on Powell-Sabin-6 triangulations. The hierarchical basis of [32] is of Hermite type and the hierarchical basis of [42] is constructed using quasi-interpolation schemes. Surface compression using C^2 quadratic wavelets of certain box-spline spaces was discussed in [25]. For this application, the fact that our basis is of Lagrange type, instead of the Hermite basis as employed in [32], has the obvious practical advantage that only Lagrange data of the surface is needed. Also

the larger range of stability of our Lagrange basis extends its applicability here. As mentioned in the previous chapter our Lagrange hierarchical basis is suitable as a preconditioner for fourth order elliptic equations.

We note for the same spline spaces that we have used in our construction of Lagrange hierarchical bases, Jia and Liu [33] constructed spline wavelet bases which lead to Riesz bases for $H^s(\Omega), 1.618 < s < 5/2$. These wavelet bases can also be used in surface compression but they are stable for a smaller range of $H^s(\Omega)$ compared to our bases. Since these bases are H^2-stable, they can also be used in solving the biharmonic equation. However, no numerical scheme based on these wavelet bases has been implemented. Furthermore, we would like to note that the Lagrange hierarchical bases of [21, 41] are also applicable in surface compression and they can be used as preconditioners for solving the biharmonic equation.

In Section 4.2, we consider a very simple surface compression algorithm developed by [25] and employed in [32, 42]. We formulated two functions and numerically compare the compression results obtained by employing Lagrange hierarchical basis with the results obtained by using the Hermite hierarchical basis.

Section 4.3 is devoted to solving the biharmonic equation. In addition to hierarchical basis preconditioner we also consider a Bramble-Pasciak-Xu (BPX) preconditioner [6] that is optimal for the biharmonic equation. The BPX preconditioner is derived by using the nodal basis functions of all levels. In other words, the BPX works with a set of redundant basis functions instead of a basis. Moreover we numerically compare the BPX preconditioner with the hierarchical basis (HB) preconditioner based on both Lagrange and Hermite bases.

Overall, we show that our Lagrange hierarchical basis can be implemented and performs very well. Test results show that it has an advantage over Hermite hierarchical basis when applied to surface compression. However, test results also reveal that hierarchical preconditioner based on Lagrange basis is not favorable in use for solving the biharmonic equation.

4.2 Applications to Surface Compression

Some surfaces in Computer-Aided Geometric Design are often described by using millions of control parameters. These parameters can arise, for example, as measurements from a physical model. In order to effectively store and manipulate the computer representation of such surfaces, the process called *Surface Compression* can be used to reduce the amount of data while maintain accuracy. In [25] a surface compression algorithm was given by means of wavelet decompositions of surfaces into box splines. In this section we explore the use of our hierarchical bases of the previous chapter in surface compression as inspired by the work of Hong and Schumaker [32, 42]. Test results show that it can achieve good approximations with good compression rates. Test results also show that Lagrange hierarchical basis has advantage over the Hermite hierarchical basis in compressing surfaces.

4.2.1 Compression

In view of the previous chapter, a spline $s \in S_n$ is uniquely determined by the function values

$$\{s(\xi)\}_{\xi\in\Xi_n}, \tag{4.2.1}$$

where Ξ_n is the set of Lagrange interpolation set for S_n on level n.

A spline $s \in S_n$ can be represented as

$$s = \sum_{\xi\in\Xi_n} s(\xi) B_\xi^{(n)},$$

where $B_\xi^{(n)}$ is the Lagrange basis function corresponding to $\xi \in \Xi_n$. Then it is easy to show that the set of functions

$$\mathbf{B}_n = \{B_\xi^{(0)}\}_{\xi\in\Xi_0} \cup \{B_\xi^{(1)}\}_{\xi\in\Xi_1\setminus\Xi_0} \cup \ldots \cup \{B_\xi^{(n)}\}_{\xi\in\Xi_n\setminus\Xi_{n-1}}$$

is a hierarchical basis for S_n. Then every $s \in S_n$ can be written in the form

$$s = \sum_{k=0}^{n} \sum_{\xi\in\Xi_k\setminus\Xi_{k-1}} c_\xi^{(k)} B_\xi^{(k)}, \quad \Xi_{-1} = \emptyset. \tag{4.2.2}$$

The coefficients in (4.2.2) are given by

$$c_\xi^{(0)} = s(\xi), \quad \xi \in \Xi_0 \tag{4.2.3}$$

and

$$c_\xi^{(k)} = s(\xi) - s_{k-1}(\xi), \quad \xi \in \Xi_k \setminus \Xi_{k-1}, \quad k = 1 \dots n, \tag{4.2.4}$$

where

$$s_{k-1} = \sum_{j=0}^{k-1} \sum_{\xi \in \Xi_j \setminus \Xi_{j-1}} c_\xi^{(j)} B_\xi^{(j)}. \tag{4.2.5}$$

The discussion above can be turned into an algorithm for computing the coefficients in (4.2.2). The process of computing the coefficients in (4.2.2) from the values (4.2.1) is called *decomposition*, see Algorithm 1.

Algorithm 1 Decomposition

1: Use (4.2.3) to compute $\{c_\xi^{(0)}\}_{\xi \in \Xi_0}$ from functional $s(\xi),\ \xi \in \Xi_0$.
2: **for** $k = 1, \dots, n$ **do**
3: Form the spline s_{k-1} as in (4.2.5),
4: Compute $\{c_\xi^{(k)}\}_{\xi \in \Xi_k \setminus \Xi_{k-1}}$ as in (4.2.4).
5: **end for**

To discuss a compressed approximation of s, we can store (or transmit) only coefficients which are larger than some prescribed *threshold*. The ratio of the number of the retained coefficients to the original number of coefficients will then describe the *compression rate*.

Now we describe the thresholding algorithm, see Algorithm 2.

Algorithm 2 Thresholding

1: Choose some threshold ϵ.
2: **for** $k = 1, \dots, n$ **do**
3: Drop the coefficient $\{c_\xi^{(k)}\}_{\xi \in \Xi_k \setminus \Xi_{k-1}}$ if it is smaller than the threshold ϵ.
4: **end for**

The above discussion can be applied to Hermite basis, see [32], where in our case (see Section 1 of Chapter 3) the associated functionals are defined to be

$$\bigcup_{v\in\mathcal{V}_n}\{s(v),\ \frac{\partial s}{\partial x}(v),\ \frac{\partial s}{\partial y}(v)\}, \tag{4.2.6}$$

and $\mathcal{V}_n$ is the set of vertices of the triangulations Δ_n on level n.

4.2.2 Numerical Examples

Now we present some examples to illustrate the performance of the compression scheme. In all cases we choose Δ_0 as the triangulation that is constructed by dividing the unit square $[0,1]^2 \in \mathbb{R}^2$ into two triangles by drawing a single diagonal. For each test function f and approximating spline s, we measure both the relative maximum error L_∞-error:$= \|f-s\|_\infty/\|f\|_\infty$ and relative L_2-error:$= \|f-s\|_2/\|f\|_2$.

Instead of using the thresholding algorithm (Algorithm 2) to decide the number of coefficients to be retained in our implementation we choose the various numbers of coefficients we want to be retained, that is, the errors are computed for particular numbers of coefficients rather than particular sizes if we use the threshold algorithm above. For example, if we want to obtain a compressed function with say N number of coefficients, we order all its coefficients in a hierarchical basis according to the absolute values, starting with the largest. Then we retain the N coefficients in this order. This approach will later help us to get a better comparison of the compression results.

Now we formulate the test functions for surface compression. We first write the univariate functions

$$f_1(x) = \begin{cases} \psi(x+\frac{1}{2})-\frac{1}{2} & : 0 \le x < \frac{1}{2} \\ \frac{1}{2}\psi(2-2x) & : \frac{1}{2} \le x \le 1 \end{cases}$$

where

$$\psi(x) = \frac{\phi(x)}{\phi(x)+\phi(1-x)}$$

and

$$\phi(x) = \begin{cases} e^{-\frac{1}{x}} & : x > 0 \\ 0 & : x \le 0; \end{cases}$$

$$f_2(x) = \begin{cases} f_1(x) & : 0 \le x < 1 \\ -f_1(-x) & : -1 \le x \le 0; \end{cases}$$

$$g_{\rho,b}(y) = \begin{cases} e^{-\frac{-r_0^2}{(r_0^2-r^2)^2}} & : r < r_0 \\ 0 & : \text{otherwise} \end{cases}$$

where

$$r_0 = \frac{1}{\rho} \text{ and } r(y) = (y-b)^2.$$

We also define the bivariate function $p(x, y)$

$$p(x, y) = \sqrt{(1.5^2 - x^2 - y^2)}/1.5$$

and the bivariate version of the function $g_{\rho,b}(y)$, that is

$$\mathbf{g}_{\rho,a,b}(x, y) = \begin{cases} e^{-\frac{-r_0^2}{(r_0^2-r^2)^2}} & : r < r_0 \\ 0 & : \text{otherwise} \end{cases}$$

where

$$r_0 = \frac{1}{\rho} \text{ and } r(x, y) = (x-a)^2 + (y-b)^2.$$

1. *First example: A smooth function with a single spike.* Here we consider the function

$$q_1(x, y) = 0.5 \cdot f_2(150(x - 0.5))g_{\rho,b}(y) + p(x, y)$$

with $\rho = 20000$ and $a = 0.5$. The test function q_1 is shown in Fig.4.1.

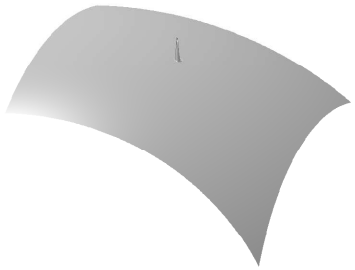

Figure 4.1: Test function q_1 of Example 1.

The test function is approximated by splines s_n based on both Lagrange and Hermite bases corresponding to levels $n = 1, \ldots, 8$ and by splines $\hat{s}$ which are compressed.

The surfaces corresponding to the splines s_n are plotted in Fig.4.5 and Fig.4.6, and the surfaces corresponding to the compressed splines $\hat{s}$ are plotted in Fig.4.3 and Fig4.4. We see that with as few as 20 coefficients, the compressed surface using Lagrange hierarchical basis functions has captured the spike of the original function while a compressed surface with 90 coefficients is virtually indistinguishable from the original. But for the case when a Hermite hierarchical basis is employed we notice the large artifacts with a smaller number of coefficients. However, we see that gradually with more coefficients the Hermite surfaces start to perform corrections and begin to reproduce the spike of the original function. Hermite compression with 90 coefficients has also captured the spike of the original function but not as close yet to the original compared to Lagrange. The above observation can be explained using the fact that Lagrange basis is more stable than Hermite in the hierarchical representation.

Now we do a comparison of the compressed approximations to the single level approximations. We see from Fig.4.5 that Lagrange single level approximations with small number of coefficients only approximate the smooth part of the surface and ignore the small feature, whereas compressed Lagrange approximations are already reasonable with 20 coefficients and capturing the shape of the original function. We also note that Hermite single level approximations do not give any good results until level 6, see Fig.4.6.

The numerical results are displayed in Tables 4.1 and 4.2. We have also plotted a log-log plot to compare the error results obtained above as shown in Fig.4.2. The errors for compressed Lagrange, compressed Hermite, single level Lagrange and single level Hermite approximations are represented

by line plots indicated by ComLag, ComHerm, SLLag and SLHerm, respectively, as shown on the legend of the graph. We clearly see from the graph that single level Hermite approximations do not give any good results until they reached to higher level. The plots show that at the beginning with small number of coefficients the single level Lagrange approximations give better errors than the compressed Lagrange approximations. But these results do not agree on what we have seen before on the figures of the approximations. We think that in this case the L_2 and L_∞ errors are not the right indication of the quality of approximations. We also see that compressed Lagrange is significantly better than compressed Hermite, most important for small number of coefficients which imply high compression rates but both approximation results are comparable from about 200 coefficients. However with more coefficients compressed Hermite might give a better approximation than Lagrange basis due to its smaller support of basis functions.

Table 4.1: Errors and number of coefficients N for the surface compression algorithm applied to the test function of Example 1

	Lagrange		Hermite	
N	L_2-error	L_∞-error	L_2-error	L_∞-error
10	1.33e-01	5.54e-01	2.09	4.84
20	6.71e-03	5.11e-02	1.59	4.89
30	6.70e-03	4.47e-02	1.06	2.69
40	5.59e-03	4.47e-02	7.87e-01	1.87
50	5.58e-03	3.13e-02	1.54e-01	6.25e-01
60	2.42e-03	3.13e-02	1.03e-01	3.33e-01
70	2.06e-03	3.08e-02	3.16e-02	2.04e-01
80	7.16e-04	2.91e-02	3.14e-02	7.88e-02
90	4.26e-04	2.88e-02	2.60e-02	4.70e-02
100	3.85e-04	2.87e-02	9.80e-03	3.73e-02
150	2.70e-04	2.88e-02	4.65e-04	2.49e-02
200	2.68e-04	2.88e-02	3.31e-04	2.49e-02

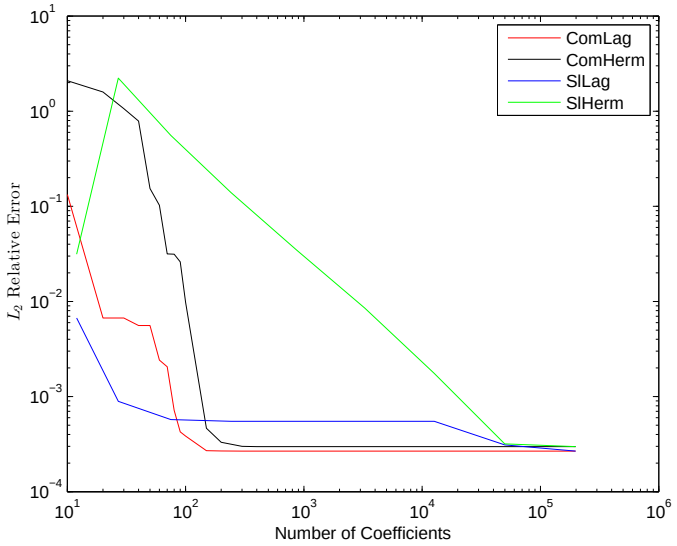

(a) Log-Log Plot for L_2-errors

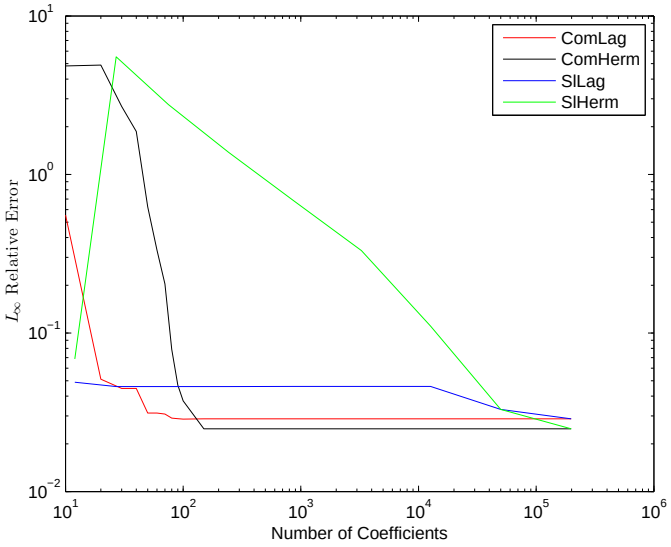

(b) Log-Log Plot for L_∞-error

Figure 4.2: Example 1. Log-Log Plot of the numerical results.

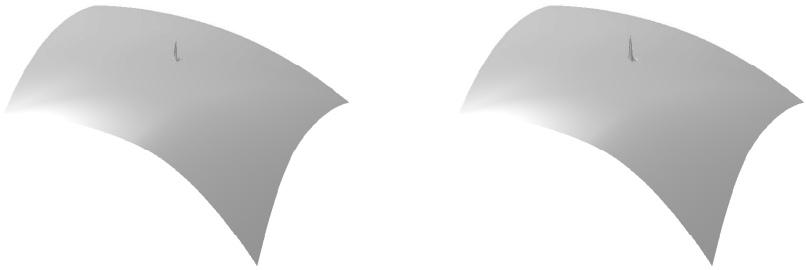

(a) 20 Coefficients

(b) 30 Coefficients

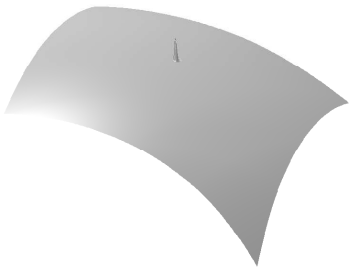

(c) 60 Coefficients

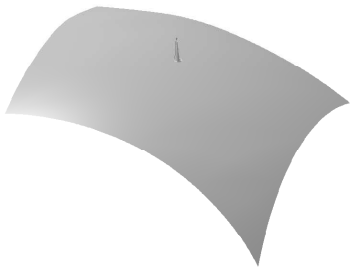

(d) 70 Coefficients

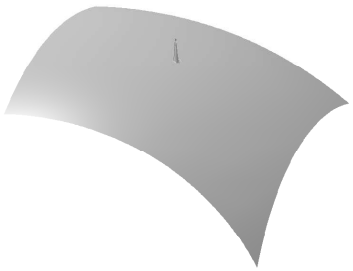

(e) 80 Coefficients

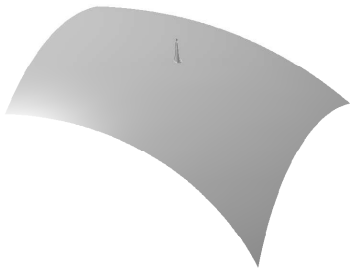

(f) 90 Coefficients

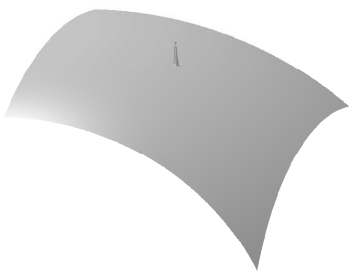

(g) 200 Coefficients

Figure 4.3: Example 1. The compressed approximations with various numbers of coefficients using Lagrange basis functions.

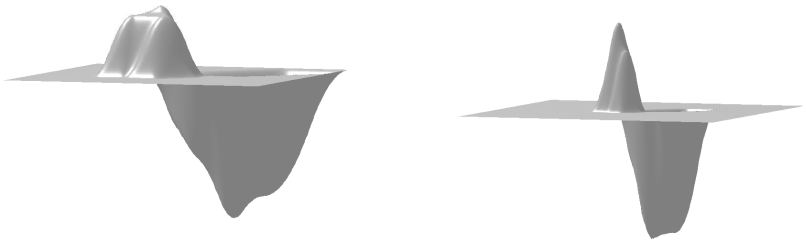

(a) 20 Coefficients

(b) 30 Coefficients

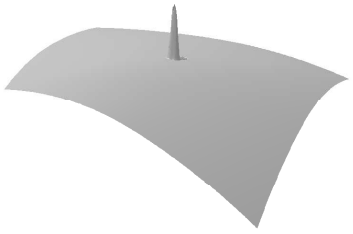

(c) 60 Coefficients

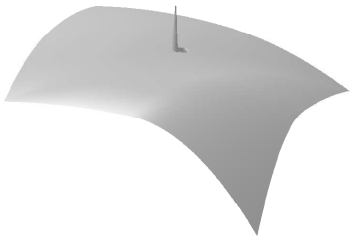

(d) 70 Coefficients

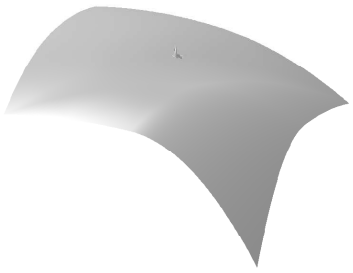

(e) 80 Coefficients

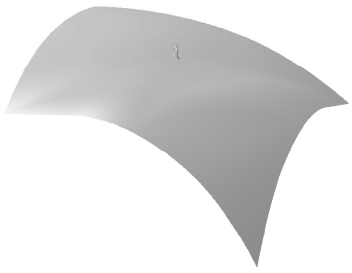

(f) 90 Coefficients

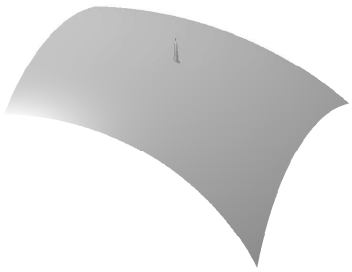

(g) 200 Coefficients

Figure 4.4: Example 1. The compressed approximations with various numbers of coefficients using Hermite basis functions.

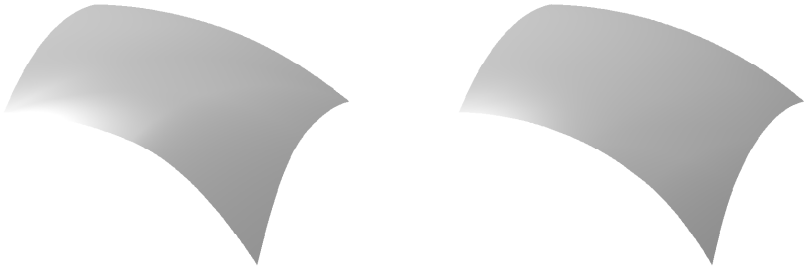

(a) Level 0

(b) Level 1

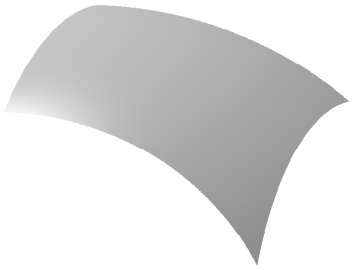

(c) Level 2

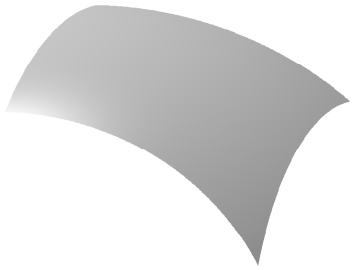

(d) Level 3

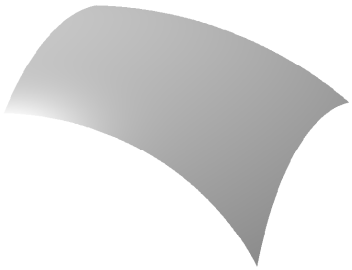

(e) Level 4

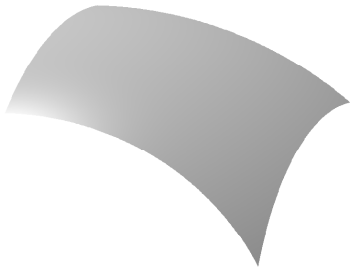

(f) Level 5

Figure 4.5: Example 1. The single level approximations using Lagrange basis functions.

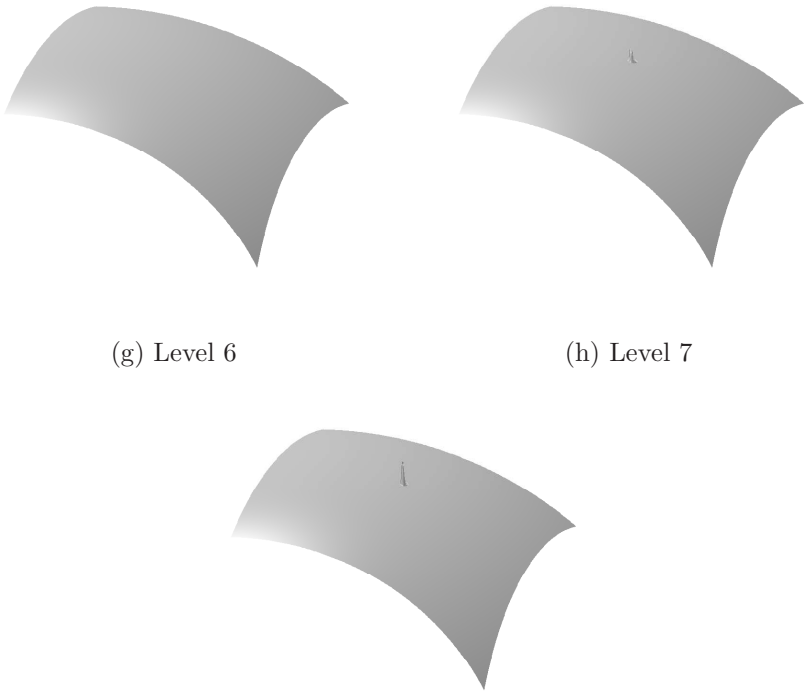

(g) Level 6

(h) Level 7

(i) Level 8

Figure 4.5: Example 1. Single level approximation using Lagrange basis functions.

(a) Level 0

(b) Level 1

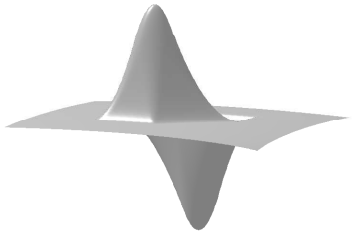

(c) Level 2

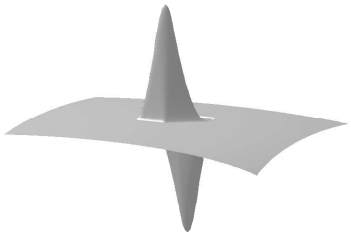

(d) Level 3

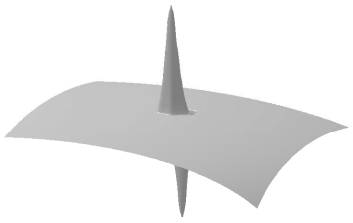

(e) Level 4

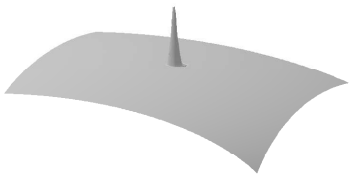

(f) Level 5

Figure 4.6: Example1. The single level approximations using Hermite basis functions.

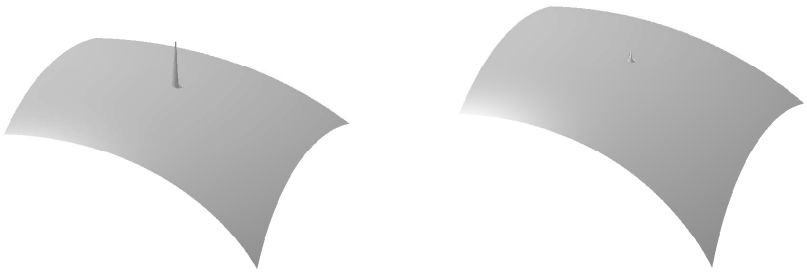

(g) Level 6

(h) Level 7

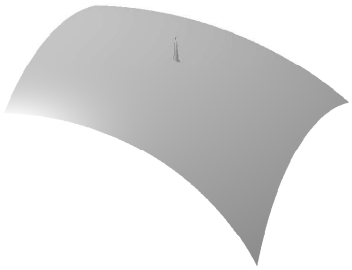

(i) Level 8

Figure 4.6: Example 1. Single level approximation using Hermite basis functions.

Table 4.2: Errors and number of coefficients N for single level approximations to Example 1

n	N	Lagrange		Hermite	
		L_2-error	L_∞-error	L_2-error	L_∞-error
0	12	6.71e-03	4.90e-02	3.15e-02	6.86e-02
1	27	8.93e-04	4.60e-02	2.23	5.52
2	75	5.72e-04	4.60e-02	5.57e-01	2.76
3	243	5.50e-04	4.60e-02	1.39e-01	1.38
4	867	5.50e-04	4.60e-02	3.48e-02	6.84e-01
5	3267	5.50e-04	4.60e-02	8.54e-03	3.31e-01
6	12675	5.50e-04	4.60e-02	1.75e-03	1.11e-01
7	49923	3.10e-04	3.30e-02	3.18e-04	3.30e-02
8	198147	2.67e-04	2.88e-02	2.97e-04	2.49e-02

2. *Second example: A smooth function with several spikes.* In this example we consider a function which is obtained by adding 4 more spikes of different sizes to the function of Example 1 and placed each at a different location of the domain as illustrated in Fig.4.7. The function is written explicitly as follows

$$\begin{aligned} q_2(x,y) = {} & s_1 \cdot f_2(c_1(x-a_1))g_{\rho_1,b_1}(y) + s_2 \cdot f_2(c_2(x-a_2))g_{\rho_2,b_2}(y) \\ & + s_3 \cdot f_2(c_3(x-a_3))g_{\rho_3,b_3}(y) + s_4 \cdot f_2(c_4(x-a_4))g_{\rho_4,b_4}(y) \\ & + s_5 \cdot \mathbf{g}_{\rho_5,a_5,b_5}(x,y) + p(x,y) \end{aligned}$$

where $\rho_1 = 20000, \rho_2 = 40000, \rho_3 = 20000, \rho_4 = 20000, \rho_5 = 40000, c_1 = 40, c_2 = 150, c_3 = 40, c_4 = 150, c_5 = 200, s_1 = 0.5, s_2 = 0.1, s_3 = 0.5, s_4 = 0.2, s_5 = 0.3$, and the values of a's and b's are chosen randomly from $(0, 1)$.

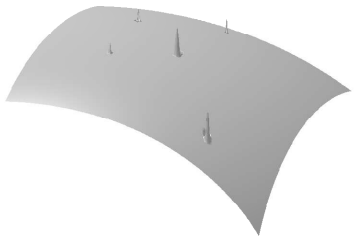

Figure 4.7: Test function q_2 of Example 2

Just like in Example 1 the test function is approximated by splines s_n based on both Lagrange and Hermite bases corresponding to levels $n = 1, \ldots, 8$ and by splines $\hat{s}$ which are compressed with various numbers of coefficients N.

The surfaces corresponding to the splines s_n are plotted in Fig.4.11 and Fig.4.12,and the surfaces corresponding to the compressed splines $\hat{s}$ are plotted in Fig.4.9 and Fig4.10. Here we see that as few as 100 coefficients, the

compressed surface using Lagrange basis functions has captured the feature of the original function and is a good approximation to the original, while a compressed surface with 500 coefficients is virtually indistinguishable from the original. But for Hermite case, just as we have observed in Example 1 we notice the large artifacts with smaller number of coefficients due to the instability of Hermite basis functions in the hierarchical representation.

Similarly in this example we also do a comparison of the compressed approximations to the single level approximations. We see that although $\hat{s}$ with 800 coefficients which is fewer than 867 coefficients of s_4, it does a much better job of approximation and capturing the shape of the original function. The similar result is also observed in the Hermite case. These results also show the effectiveness of the compression algorithm in this example.

The numerical results are shown in Table 4.3 and Table 4.4. We have also plotted a log-log plot to compare the results as shown in Fig.4.8. These plots exhibit the similar behaviour to what we have already seen in Example 1. The errors for compressed Lagrange, compressed Hermite, single level Lagrange and single level Hermite approximations are represented by line plots indicated by ComLag, ComHerm, SLLag and SLHerm, respectively, as shown on the legend of the graph. In this example we also see that single level Hermite approximations do not give any good results until they reached to higher level. The plots show that at the beginning with small number of coefficients the single level Lagrange approximations give better errors than the compressed Lagrange approximations. But these results do not agree on what we have seen before on the figures of the approximations. As in Example 1, we think that in this case the L_2 and L_∞ errors are not the right indication of the quality of approximations. We also see that compressed Lagrange is significantly better than compressed Hermite, most important for small number of coefficients which imply high compression rates but both

approximation results are comparable from about 1000 coefficients. However with more coefficients compressed Hermite might give a better approximation than Lagrange basis due to its smaller support of basis functions.

Table 4.3: Relative Errors and number of coefficients for the surface compression algorithm applied to the test function of Example 2

N	Lagrange		Hermite	
	L_2-error	L_∞-error	L_2-error	L_∞-error
50	7.43e-03	1.59e-01	2.12e-01	6.56e-01
100	7.24e-03	1.28e-01	5.56e-02	2.75e-01
150	7.12e-03	1.10e-01	3.54e-02	1.96e-01
200	7.05e-03	8.34e-02	2.73e-02	1.46e-01
250	6.89e-03	4.49e-02	2.62e-02	1.16e-01
300	6.81e-03	4.27e-02	2.61e-02	1.04e-01
400	5.66e-03	3.44e-02	9.83e-03	4.11e-02
500	3.05e-03	4.00e-02	7.42e-03	2.29e-02
800	8.36e-04	3.27e-02	3.01e-04	2.33e-02
1000	5.73e-04	3.19e-02	2.66e-04	2.33e-02

Table 4.4: Relative Errors for Single Level Approximations of Example 2

l	N	Lagrange		Hermite	
		L_2-error	L_∞-error	L_2-error	L_∞-error
0	12	7.17e-03	1.04e-01	3.16e-02	1.56e-01
1	27	2.65e-03	9.22e-02	5.94e-01	1.47
2	75	2.56e-03	9.20e-02	3.11e-01	1.30
3	243	2.56e-03	9.19e-02	8.24e-02	6.49e-01
4	867	2.56e-03	9.19e-02	2.03e-02	3.24e-01
5	3267	3.03e-03	1.10e-01	4.79e-03	1.62e-01
6	12675	2.68e-03	1.33e-01	2.36e-03	1.56e-01
7	49923	1.51e-03	1.03e-01	1.11e-03	7.71e-02
8	198147	4.94e-04	3.13e-02	2.65e-04	2.33e-02

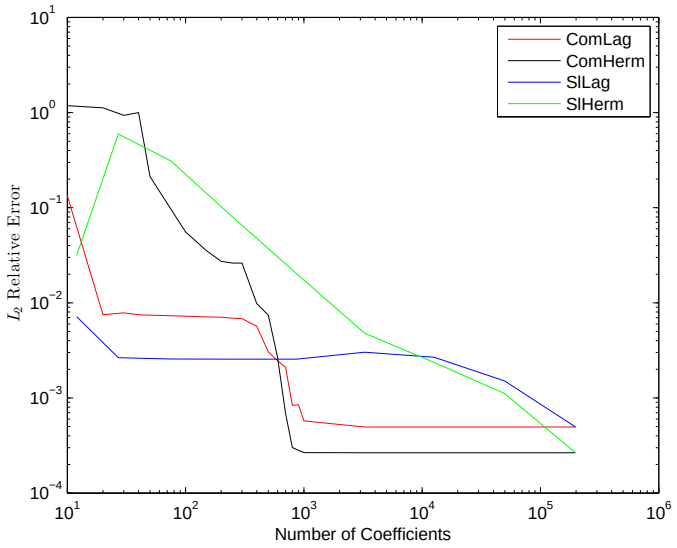

(a) Log-Log Plot for L_2-errors

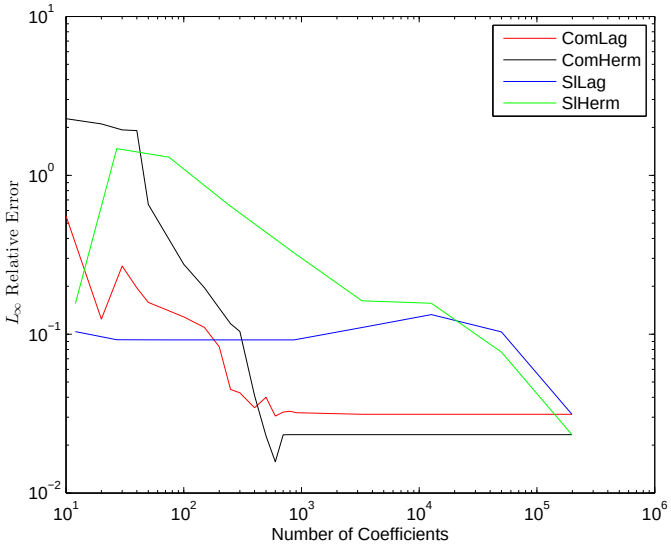

(b) Log-Log Plot for L_∞-error

Figure 4.8: Example 2. Log-Log Plot of the numerical results.

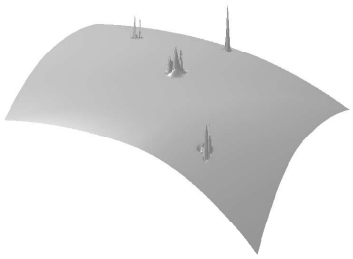

(a) 50 Coefficients

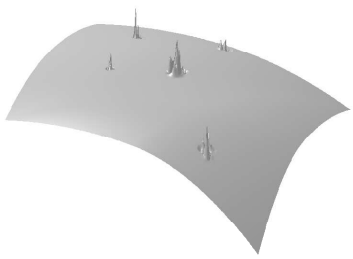

(b) 100 Coefficients

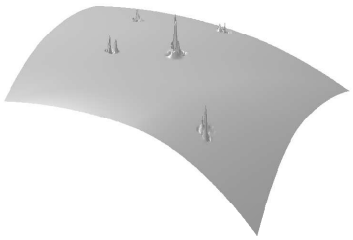

(c) 150 Coefficients

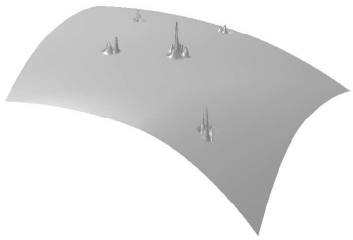

(d) 200 Coefficients

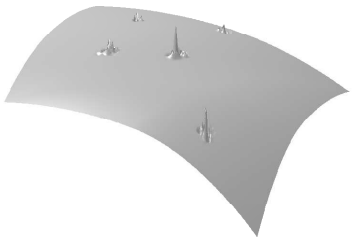

(e) 300 Coefficients

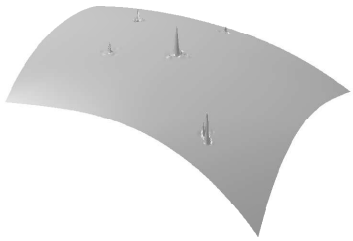

(f) 500 Coefficients

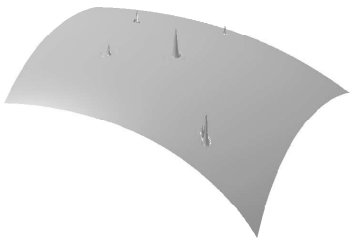

(g) 800 Coefficients

Figure 4.9: Example 2. The compressed approximations with various numbers of coefficients using Lagrange basis functions.

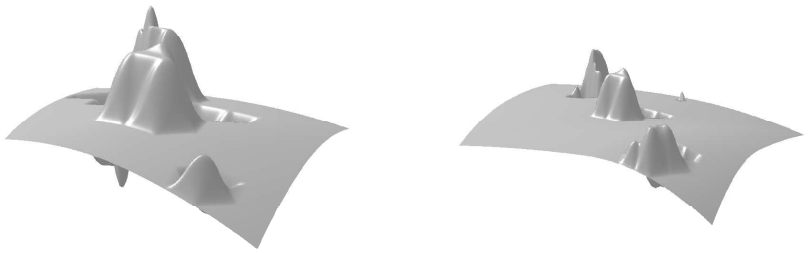

(a) 50 Coefficients

(b) 100 Coefficients

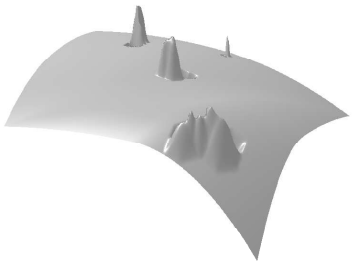

(c) 150 Coefficients

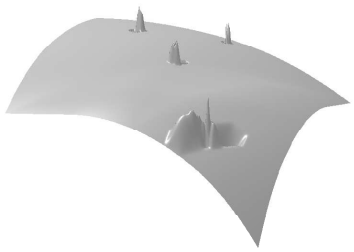

(d) 200 Coefficients

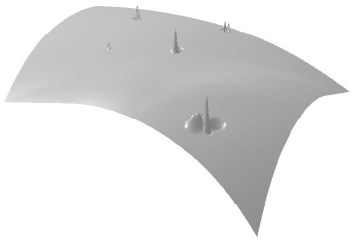

(e) 300 Coefficients

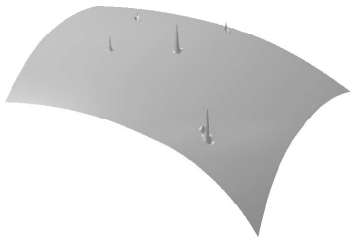

(f) 500 Coefficients

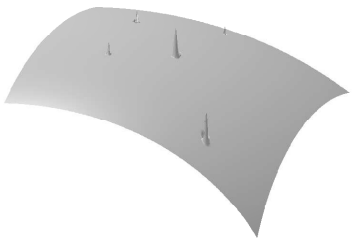

(g) 800 Coefficients

Figure 4.10: Example 2. The compressed approximations with various numbers of coefficients using Hermite basis functions.

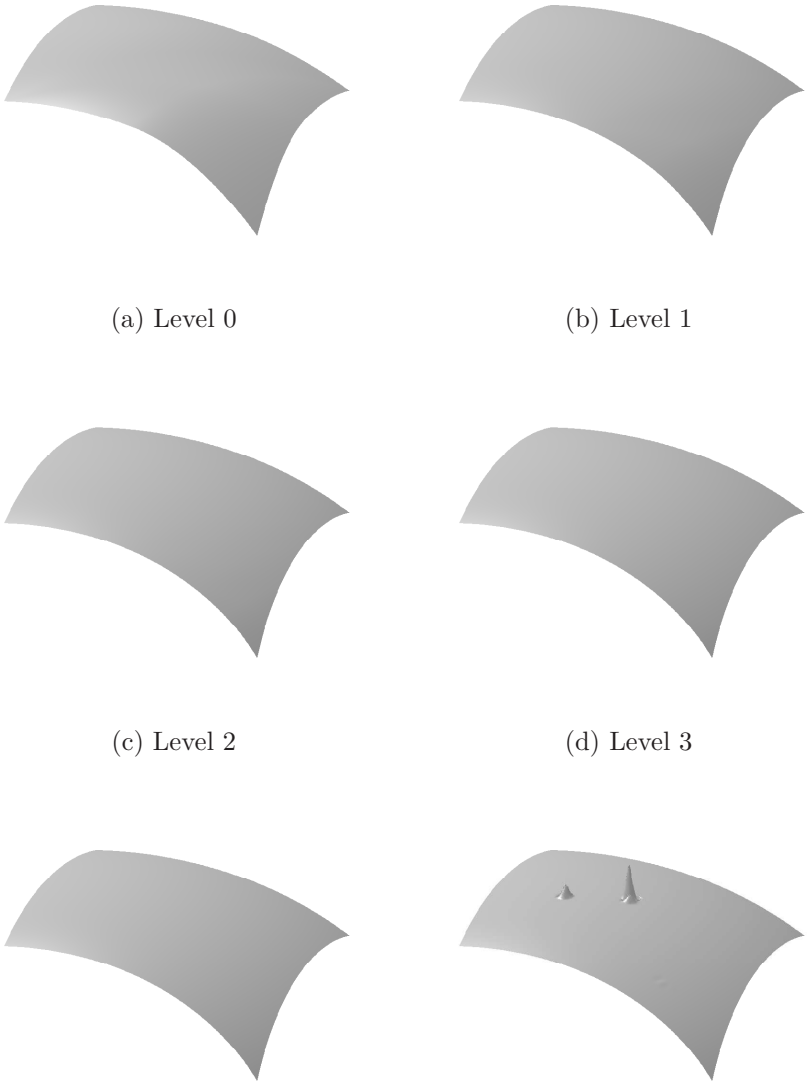

(a) Level 0 (b) Level 1

(c) Level 2 (d) Level 3

(e) Level 4 (f) Level 5

Figure 4.11: Example 2. Single level approximation using Lagrange basis functions.

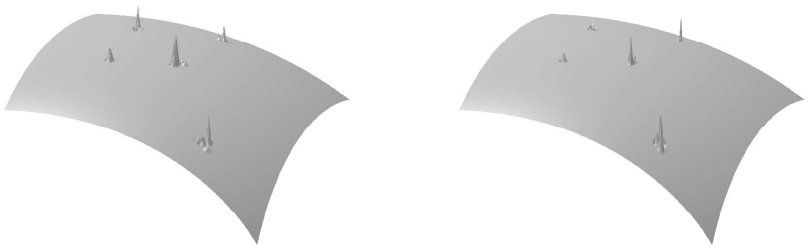

(g) Level 6 (h) Level 7

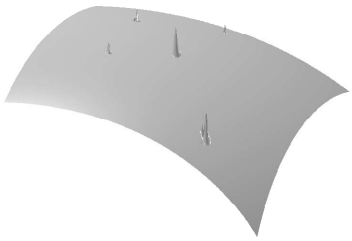

(i) Level 8

Figure 4.11: Example 2. Single level approximation using Lagrange basis functions.

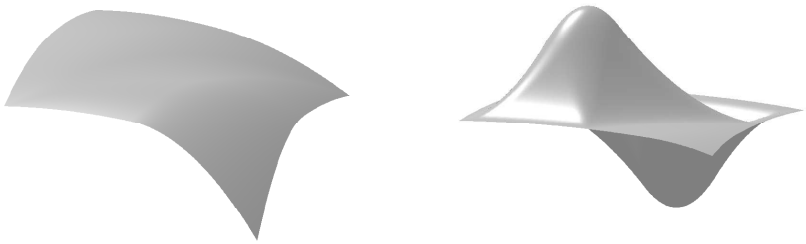

(a) Level 0

(b) Level 1

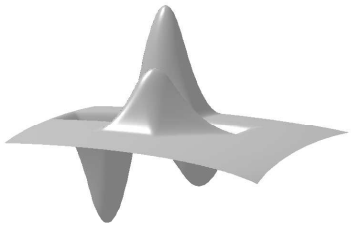

(c) Level 2

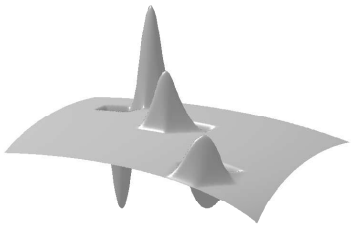

(d) Level 3

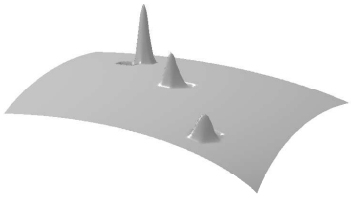

(e) Level 4

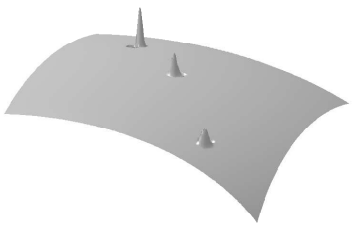

(f) Level 5

Figure 4.12: Example 2. Single level approximation using Lagrange basis functions.

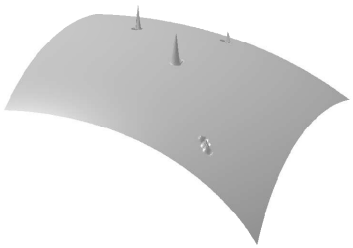

(g) Level 6

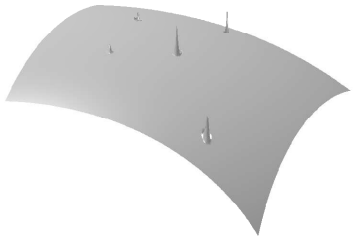

(h) Level 7

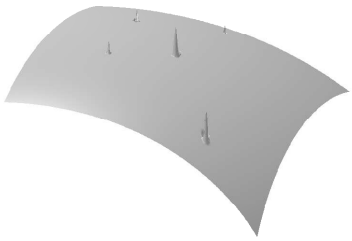

(i) Level 8

Figure 4.12: Example 2. The single level approximations using Lagrange basis functions.

3. *Third Example: Cusp function*

We take the test function

$$g_3(x, y) = \left[(2x-1)^2 + (2y-1)^2\right]^{1/4}$$

introduced in [25], as shown in Fig.4.13.

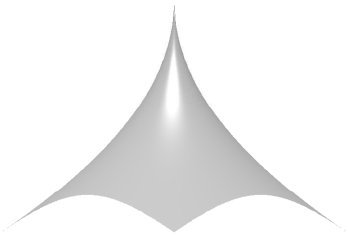

Figure 4.13: Cusps function of Example 3

This function has a cusp singularity at the point $(1/2, 1/2)$. Compressing this function using Hermite hierarhical basis functions is not well defined since the gradient ∇f is not defined at the point $(1/2, 1/2)$ and there is a possibility that a vertex might be located at this point. This example also exhibits another advantage of using Lagrange basis since only Lagrange data of the surface is needed. The surfaces corresponding to the Lagrange compressed splines $\hat{s}$ are plotted in Fig.4.14. Here we see that as few as 222 coefficients, the compressed surface has captured the shape of the original function, while a compressed surface with 463 coefficients is virtually indistinguishable from the original.

Table 4.5 presents the error of approximation produced by the compression algorithm for various numbers of coefficients. The errors we computed for this example are the absolute errors instead of relative errors computed for the previous two examples. This allows us to compare the results to the results in DeVore [25] where absolute errors are presented. We also extracted

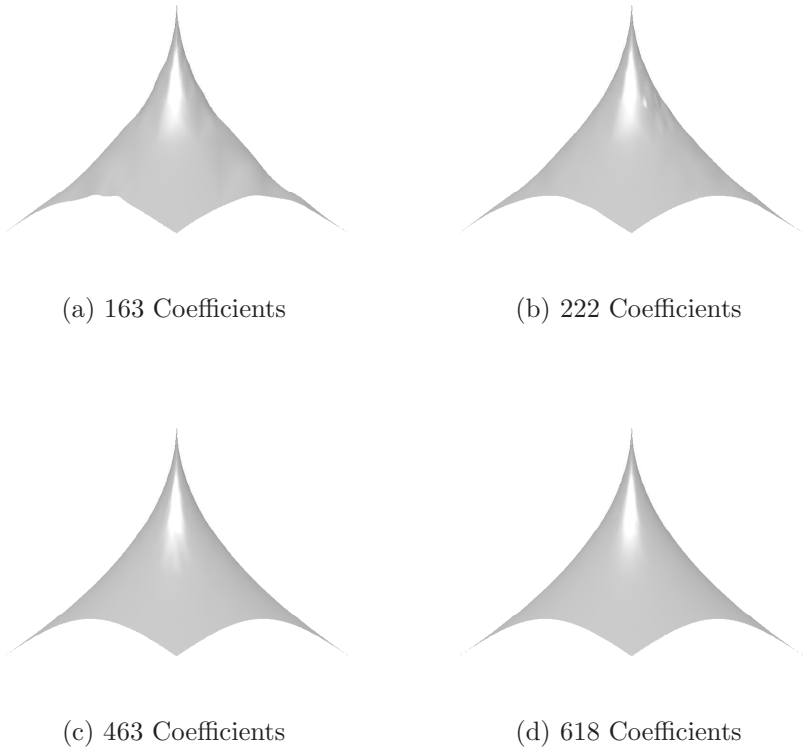

(a) 163 Coefficients

(b) 222 Coefficients

(c) 463 Coefficients

(d) 618 Coefficients

Figure 4.14: Example 3. The compressed approximations with various numbers of coefficients using Lagrange basis functions.

Table 4.5: Example 3. Compression comparing with [25].

Lagrange Compression			DeVore Compression
Number of Coefficients	L_2-error	L_∞-error	L_∞-error
70	4.34e-2	1.76e-1	1.05e-1
91	2.91e-2	1.30e-1	7.13e-2
163	3.89e-3	1.98e-2	2.69e-2
222	2.36e-3	9.19e-3	1.38e-2
463	4.05e-4	2.48e-3	2.76e-3
618	2.48e-4	1.29e-3	1.38e-3

the results from DeVore [25] and put them on the same table for easy comparison. We see that the errors are comparable even though we do not have a wavelet basis. Recall that our hierarchical basis is available on any polygonal domain whereas the box spline wavelets of [25] are only for $\mathbb{R}^2$.

In the last part of this section we would like to demonstrate the instability of Hermite bases in the hierarchical expansion which will also explain the observations we get in test functions of Examples 1 and 2.

In this experiment, we choose a Hermite basis function $B_{n,s} = 2^{n(1-s)}B_v^{(n)}$ (where $2^{n(1-s)}$ is the normalising factor in H^s-norm) from each level $n = 1, \ldots 9$ corresponding to the same point $v = (0.5, 0.5) \in \mathcal{V}_1$ of the coarse level with scaling factors $s \in (1, 5/2)$. Each of these function $B_{n,s}$ has a finite representation involving functions of levels up to n. We write each of these functions in the Hermite hierarchical representation and also in Lagrange hierarchical representation. We compute the l_2 norm of the coefficient vectors for each of these functions for different scaling factors. The results are displayed in Table 4.6.

For a better view of the results, we plotted a semi-log graph as shown in Fig.4.15 with semi-log y-axis representing the l_2 norm of coefficient vectors and x-axis representing the level n where the function comes from. The graphs are plotted with different colours for different scaling factors s. We clearly see from the graphs in the case where functions are written in the hierarchical Hermite basis

Table 4.6: The l_2 norm of coefficient vectors for functions $B_{n,s}$ with different scaling factors.

	s=1		s=1.25		s=1.5		s=1.75		s=2		s=2.25		s=2.5	
n	H	L	H	L	H	L	H	L	H	L	H	L	H	L
1	1	0.346	1	0.332	1	0.322	1	0.315	1	0.310	1	0.306	1	0.304
2	2.50	0.426	2.25	0.421	2.06	0.417	1.91	0.414	1.80	0.412	1.72	0.411	1.66	0.410
3	5.22	0.159	4.08	0.159	3.28	0.159	2.73	0.159	2.35	0.159	2.08	0.159	1.90	0.159
4	10.55	0.379	7.02	0.373	4.87	0.369	3.57	0.366	2.78	0.363	2.31	0.362	2.02	0.361
5	21.15	0.159	11.90	0.159	7.05	0.159	4.51	0.159	3.16	0.159	2.45	0.159	2.07	0.159
6	42.32	0.379	20.06	0.373	10.09	0.369	5.56	0.366	3.50	0.363	2.55	0.362	2.10	0.361
7	84.66	0.159	33.78	0.159	14.34	0.159	6.78	0.159	3.81	0.159	2.62	0.159	2.11	0.159
8	169.33	0.379	56.82	0.373	20.34	0.369	8.21	0.366	4.09	0.363	2.66	0.362	2.11	0.361
9	338.66	0.159	95.58	0.159	28.80	0.159	9.87	0.159	4.36	0.159	2.70	0.159	2.12	0.159

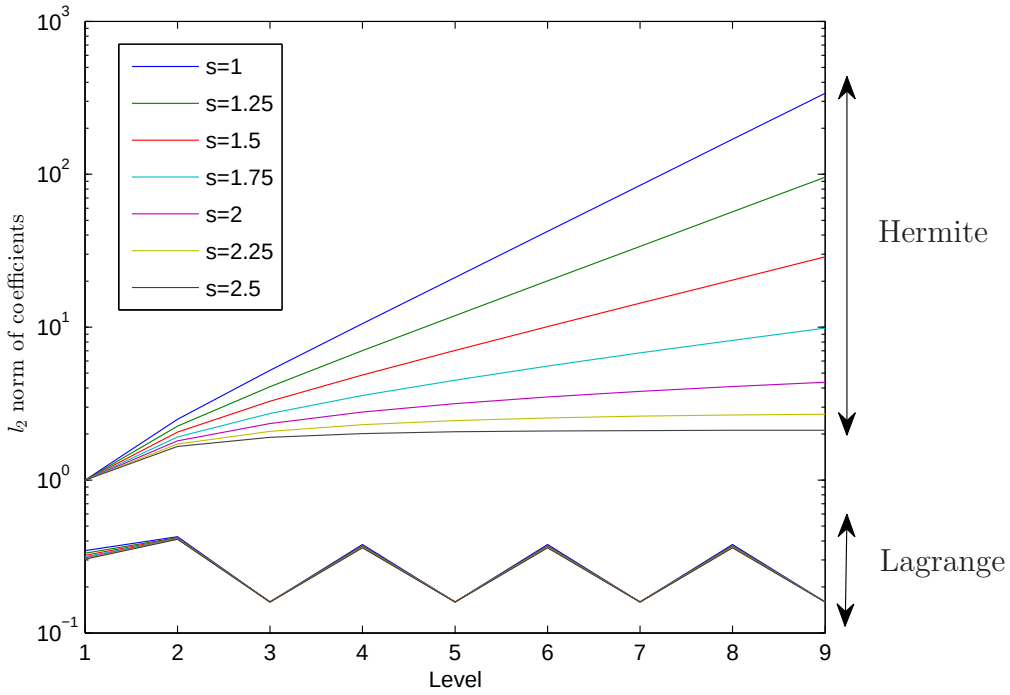

Figure 4.15: Semi-log graph of l_2 norm versus the level n where the function belongs to.

representations that the l_2 norms are large and growing with n, especially fast for

$1 < s < 2$. On the other hand, functions written in the Lagrange hierarchical basis representations have smaller l_2 norms and their values do not grow with n and they vary very little with scaling. In the case of Hermite hierarchical expansion, the results also show that the stability constants

$$K = \frac{\|\mathbf{c}\|_{l_2}}{\|B_{n,s}\|_{H^s(\Omega)}}, \quad 1 < s < 2$$

are growing with n and this implies the instability of the expansion. The results confirm the theory that we have already know about the stability of these hierarchical bases, that is, Lagrange hierarhical bases are stable for $H^s(\Omega)$, $1 < s < 5/2$ and Hermite hierarchical bases are stable for $2 < s < 5/2$. The H^1 and H^2 norms for $B_{n,1}$ and $B_{n,2}$, respectively, for $n = 1, \ldots 8$ are presented in Table 4.7.

Table 4.7: The H^1 norms for $B_{n,1}$ and H^2 norms for $B_{n,2}$.

n	H^1-norm	H^2-norm
1	6.23e-1	4.32
2	6.23e-1	4.32
3	6.23e-1	4.32
4	6.23e-1	4.31
5	6.24e-1	4.33
6	6.26e-1	4.23
7	6.39e-1	4.07
8	6.92e-1	3.53

4.3 Applications to the Biharmonic Equation

We consider the two dimensional biharmonic equation with homogeneous boundary conditions, that is,

$$\Delta^2 u = f \text{ on } \Omega, \quad u = \frac{\partial u}{\partial n} = 0 \text{ on } \partial\Omega, \tag{4.3.1}$$

where $\partial\Omega$ denotes the boundary of the polygonal domain Ω. As usual, Δ stands for the Laplace operator: $\Delta = \frac{\partial^2}{\partial x^2} + \frac{\partial^2}{\partial y^2}$, and $\frac{\partial}{\partial n}$ represents the normal derivative.

The variation formulation of the biharmonic equation (4.3.1) is to find $u \in H_0^2(\Omega)$ such that

$$a(u, v) = \langle f, v\rangle, \quad \forall v \in H_0^2(\Omega), \tag{4.3.2}$$

where $a(u, v) = \langle \Delta u, \Delta v\rangle$. For $u, v \in H_0^2(\Omega)$, it is easy to verify that $a(u, v) \leq \beta_1 \|u\|_{H_0^2(\Omega)} \|v\|_{H_0^2(\Omega)}$ (bounded) and $a(u, u) \geq \beta_2 \|u\|^2_{H_0^2(\Omega)}$ (coercieve) where β_1, β_2 are constants independent of u and v, see [34]. Hence $a(u, v)$ is bounded and coercive, and by the Lax-Milgram theorem (see [7]), existence and uniqueness of the solution are guaranteed for (4.3.2). This u is the weak solution to the biharmonic equation (4.3.1).

In order to solve the variation problem (4.3.2), we use finite dimensional subspaces to approximate $H_0^2(\Omega)$. Let V be a subspace of $H_0^2(\Omega)$ with $\{v_1, \ldots, v_m\}$ as its basis. We look for $y_1, \ldots, y_m \in \mathbb{R}$ such that $u = \sum_{k=1}^m y_k v_k$ satisfies the system of equations

$$\langle \Delta u, \Delta v_j\rangle = \langle f, v_j\rangle, \quad j = 1, \ldots, m,$$

which can be written as

$$\sum_{k=1}^m a_{jk} y_k = b_j, \quad j = 1, \ldots, m, \tag{4.3.3}$$

where $b_j = \langle f, v_j\rangle$ and $a_{jk} = \langle \Delta v_k, \Delta v_j\rangle, j, k \in \{1, \ldots, m\}$. We call $A = (a_{jk})_{1\leq j,k\leq m}$ the stiffness matrix and $b = (b_j)^T_{1\leq j\leq m}$ the load vector. Often $v_1, \ldots, v_m$ are chosen to be finite elements over a triangulation of Ω with mesh size $h > 0$.

It is well known that the linear system arising from usual discretisations of the biharmonic equation is ill conditioned. Under mesh refinement, the condition number of the stiffness matrix deteriorates rapidly like h^{-4} in general. Thus, it is a challenging problem to efficiently solve the large linear system. An ill-conditioned matrix usually results in very slow convergence for classical iterative methods. Thus, without preconditioning, it would be very difficult to solve the system of linear equations in (4.3.3) for small h.

4.3.1 Convergence Rates

In this section we established the convergence rates of the C^1 quadratic finite element method for the biharmonic equation in different norms. In particular, we will establish the suboptimal convergence rate in L_2 norm which does not seem to have been explicitly discussed in the literature.

Given $f \in L_2(\Omega)$, let $u \in H_0^2(\Omega)$ be the unique solution to the equation

$$a(u, v) = \langle f, v \rangle \quad \text{for all } v \in H_0^2(\Omega). \tag{4.3.4}$$

Here we assume that Ω is a bounded polygonal domain with inner angle ω at each boundary corner satisfying

$$\omega < 126.283696...^\circ$$

Then we have $u \in H^4(\Omega)$, by Blum and Rannacher [4]. Moreover,

$$\|u\|_{H^4(\Omega)} \leq C\|f\|_{L_2(\Omega)} \tag{4.3.5}$$

for some constant C independent of f.

Recall our spline spaces $\tilde{S}_n$ with homogenous boundary condition in Chapter 3. Let u_n be the unique solution in $\tilde{S}_n$ to the following equation

$$a(u_n, v) = \langle f, v \rangle \quad \text{for all } v \in \tilde{S}_n. \tag{4.3.6}$$

There is a standard trick, called the duality argument, for deriving an L_2 estimate from an energy norm estimate. This argument requires the elliptic regularity property (4.3.5).

Let $w \in H_0^2(\Omega)$ be the solution to the variation problem

$$a(w, v) = \langle u - u_n, v \rangle \quad \text{for all } v \in H_0^2(\Omega).$$

Since $u - u_n \in L_2(\Omega)$, the solution w belongs to $H_0^2(\Omega) \cap H^4(\Omega)$. Then

$$\begin{aligned} \|u - u_n\|_{L_2(\Omega)}^2 &= \langle u - u_n, u - u_n \rangle \\ &= a(w, u - u_n). \end{aligned}$$

Since the interpolant w_I belong to $\tilde{S}_n$,

$$a(u, w_I) = \langle f, w_I \rangle$$

and

$$a(u_n, w_I) = \langle f, w_I \rangle,$$

which implies that

$$a(u - u_n, w_I) = 0.$$

It follows that

$$a(w, u - u_n) = a(w - w_I, u - u_n)$$

and therefore we obtain

$$\begin{aligned} \|u - u_n\|_{L_2(\Omega)}^2 &= a(w - w_I, u - u_n) \\ &\leq \beta_1 \|u - u_n\|_{H^2(\Omega)} \|w - w_I\|_{H^2(\Omega)}. \end{aligned}$$

By the elliptic regularity assumption (4.3.5), $w \in H^3(\Omega)$ and therefore, by the Jackson estimate (2.3.5), there is a constant C such that

$$\|w - w_I\|_{H^2(\Omega)} \leq Ch|w|_{H^3(\Omega)}.$$

It follows that

$$\begin{aligned} \|u - u_n\|_{L_2(\Omega)}^2 &\leq C\beta_1 h \|u - u_n\|_{H^2(\Omega)} |w|_{H^3(\Omega)} \\ &\leq C\beta_1 h \|u - u_n\|_{H^2(\Omega)} |w|_{H^4(\Omega)}. \end{aligned}$$

By the elliptic regularity assumption, there is another constant C such that

$$|w|_{H^4(\Omega)} \leq \|w\|_{H^4(\Omega)} \leq C\|u - u_n\|_{L_2(\Omega)}.$$

Combining β_1 and the two constants denoted above by C into a new constant, also denoted by C, we get

$$\|u - u_n\|^2_{L_2(\Omega)} \leq Ch\|u - u_n\|_{H^2(\Omega)}\|u - u_n\|_{L_2(\Omega)}$$

and hence

$$\|u - u_n\|_{L_2(\Omega)} \leq Ch\|u - u_n\|_{H^2(\Omega)}. \tag{4.3.7}$$

In view of the fact that the finite element solution u_n is the orthogonal projection of u in $\tilde{S}_n$, then by the Cea's theorem [7, Theorem 2.8.1] and the Jackson estimate (2.3.5) we obtain the convergence in energy norm

$$\begin{aligned}\big\|u - u_n\big\|_{H^2(\Omega)} &\leq C \inf_{v\in\tilde{S}_n} \|u - v\|_{H^2(\Omega)} \\ &\leq C\|u - u_I\|_{H^2(\Omega)}, \quad u_I \in \tilde{S}_n,\end{aligned}$$

and hence

$$\big\|u - u_n\big\|_{H^2(\Omega)} \leq C'h|u|_{H^3(\Omega)}. \tag{4.3.8}$$

Finally, applying the estimate (4.3.8) in (4.3.7) for $\|u - u_n\|_{H^2(\Omega)}$, we obtain

$$\|u - u_n\|_{L_2(\Omega)} \leq Ch^2|u|_{H^3(\Omega)}. \tag{4.3.9}$$

Now by [7, Theorem 14.3.3] we get the error in H^1-norm below

$$\|u - u_n\|_{H^1(\Omega)} \leq Ch^2|u|_{H^3(\Omega)}. \tag{4.3.10}$$

With the above discussion we can now write the theorem below.

Theorem 4.1. *Given $f \in L_2(\Omega)$, let u be the unique solution in $H^2_0(\Omega)$ to the equation* (4.3.4)*. Let u_n be the unique solution in $\tilde{S}_n$ to the equation* (4.3.6)*. Then the estimates* (4.3.8)*,* (4.3.9) *and* (4.3.10) *hold, and their bounding constants are independent of f and n.*

Theorem 4.1 says that our C^1 piecewise quadratic finite element solutions converge to the exact solution of biharmonic equation in optimal order for H^1 and H^2 norms but suboptimal order $\mathcal{O}(h^2)$, not $\mathcal{O}(h^3)$ for error in L_2 norm. The numerical results displayed in Tables 4.8 and 4.9 confirm that these convergence rates cannot be improved.

The suboptimal convergence rate in L_2 norm for certain quadratic elements which are not C^1 continuous has been observed numerically in [55, 27]. Also in [27] the suboptimal convergence rate in L_2-norm was proved in the context of the discontinuous Galerkin method.

4.3.2 Hierarchical Basis Preconditioner

In this section we will discuss the use of our Lagrange type hierarchical basis in solving the biharmonic equation (4.3.1).

Recall that in order to solve the variational problem (4.3.2), we take the finite dimensional space $\tilde{S}_n$ to approximate $H_0^2(\Omega)$ and seek $u_n \in \tilde{S}_n$ such that

$$\langle \Delta u_n, \Delta v \rangle = \langle f, v \rangle \quad \forall v \in \tilde{S}_n. \tag{4.3.11}$$

Since our hierarchical basis

$$\bigcup_{k=0}^{\infty} \{2^{k(1-s)} \tilde{B}_\xi^{(k)}\}$$

is a Riesz basis for $H_0^s(\Omega)$ for any $s \in (1, \frac{3}{2}) \cup (\frac{3}{2}, \frac{5}{2})$, by exploiting the properly scaled hierarchical basis

$$\Psi_n = \bigcup_{k=0}^{n} \{2^{-k} \tilde{B}_\xi^{(k)}\}$$

we get uniformly well-conditioned stiffness matrices. For comparison, single scale bases for $\tilde{S}_n$ will give rise to stiffness matrices with condition numbers of the order 2^{4n}. Hence it would be difficult to solve the problem when n is large.

Let Φ_n denote the locally supported single scaled basis for S_n. Let $\mathcal{A}_n$ and A_n denote the stiffness matrices with respect to Ψ_n and Φ_n, respectively, and the associated linear systems

$$A_n y_n = b_n$$

and

$$\mathcal{A}_n y_n' = b_n' \tag{4.3.12}$$

respectively.

Since Φ_n and Ψ_n are two bases of $\tilde{S}_n$, there exists a unique matrix T_n, called the transformation matrix, which transform Ψ_n to Φ_n. Therefore,

$$\mathcal{A}_n = T_n^T A_n T_n$$

$$b_n' = T_n^T b_n.$$

Consequently, the linear system (4.3.12) is equivalent to

$$T_n^T A_n T_n y_n' = T_n^T b_n.$$

We can use conjugate gradient (CG) algorithm to solve $T_n^T A_n T_n y_n' = T_n^T b_n$, the iterations needed to reach a fixed tolerance τ would not increase as the mesh size decreases since the condition number of $\mathcal{A}_n$ is uniformly bounded.

By letting $y_n = T_n y_n'$, the CG algorithm for solving $T_n^T A_n T_n y_n' = T_n^T b_n$ is equivalent to the preconditioned conjugate gradient (PCG) algorithm for solving $A_n y_n = b_n$ using the preconditioner $T_n T_n^T$.

The conjugate gradient (CG) algorithm and preconditioned conjugate gradient (PCG) algorithm (see [28]) for solving the linear system are introduced in Algorithm 3 and Algorithm 4, respectively.

Algorithm 3 Conjugate Gradient Algorithm for $A_n y_n = b_n$

Given initial guess y_n^0
$r_0 = b_n - A_n y_n^0$
$p_0 = r_0$
for $k = 0, 1 \ldots$ **do**
    $\alpha_k = \frac{r_k^T r_k}{p_k^T A_n p_k}$
    $y_n^{k+1} = y_n^k + \alpha_k p_k$
    $r_{k+1} = r_k - \alpha_k A_n p_k$
    if $\|r_{k+1}\|_2 < \tau$ **then**
        stop
    end if
    $\beta_k = \frac{r_{k+1}^T r_{k+1}}{r_k^T r_k}$
    $p_{k+1} = r_{k+1} + \beta_k p_k$
end for

Algorithm 4 Preconditioned Conjugate Gradient Algorithm for $A_n y_n = b_n$ with preconditioner M

Given initial guess y_n^0
$r_0 = b_n - A_n y_n^0$
$z_0 = M^{-1} r_0$
$p_0 = z_0$
for $k = 0, 1 \ldots$ **do**
    $\alpha_k = \frac{r_k^T z_k}{p_k^T A_n p_k}$
    $y_n^{k+1} = y_n^k + \alpha_k p_k$
    $r_{k+1} = r_k - \alpha_k A_n p_k$
    if $\|r_{k+1}\|_2 < \tau$ **then**
        stop
    end if
    $z_{k+1} = M^{-1} r_{k+1}$
    $\beta_k = \frac{z_{k+1}^T r_{k+1}}{z_k^T r_k}$
    $p_{k+1} = z_{k+1} + \beta_k p_k$
end for

4.3.3 The BPX-Preconditioner

In the paper [30] Griebel shows that the conjugate gradient (CG) method for the semidefinite system that arises from the Galerkin scheme using the nodal basis functions of the finest level and of all coarser levels of discretisation, is equivalent to the Bramble-Pasciak-Xu (BPX) preconditioned CG method [6] for the linear system that arises from the Galerkin scheme using only the nodal basis functions of the finest level. We will briefly discuss this here. The interested reader is referred to [30] for further details.

Let $\Phi_n = \{\phi_1^n, \phi_2^n, \ldots, \phi_{N_n}^n\}$ be the nodal basis of level n (either Hermite or Lagrange type). Any function $s \in S_n$ can be expressed uniquely by

$$s = \sum_{i=1}^{N_n} u_i^n \phi_i^n, \tag{4.3.13}$$

with the column vector $u_n := (u_1^n, u_2^n, \ldots, u_{N_n}^n)^T$ of nodal values.

Instead of the expression in (4.3.13), the set of functions E_n is defined as the union of all different nodal bases Φ_k for the levels $k = 1, \ldots, n$

$$E_n = \Phi_1 \cup \Phi_2 \cup \ldots \cup \Phi_{n-1} \cup \Phi_n.$$

Then clearly E_n is a linearly dependent set of functions and it is no longer a basis for S_n but a generating system. Then any function $s \in S_n$ can be expressed in terms of the generating system by

$$s = \sum_{k=1}^{n} \sum_{i=1}^{N_k} w_i^k \phi_i^k$$

with the block vector $w_n^E := (w^1, w^2, \ldots, w^n)^T$, where

$$w^k = (w_1^k, w_2^k, \ldots, w_{N_k}^k), \quad k = 1, \ldots, n.$$

This represents a level-wise decomposition of s into functions $g^k \in S_k,\ k = 1, \ldots, n$, where

$$s = \sum_{k=1}^{n} g^k, \quad g^k = \sum_{i=1}^{N_k} w_i^k \phi_i^k.$$

We denote representation in terms of the generating system E_k by the superscript E. The length of w_n^E is

$$N_n^E = \sum_{k=1}^{n} N_k.$$

For a given representation w_n^E of s in E_n, we can easily compute its unique representation u_n with respect to Φ_n.

The transformation from w_n^E to u_n resembles a mapping

$$T_n^E : \mathbb{R}^{N_n^E} \to \mathbb{R}^{N_n},$$

which can be described by the product

$$\begin{aligned} T_n^E &= T_n^{n-1,E} \cdot T_{n-1}^{n-2,E} \cdot T_{n-2}^{n-3,E} \dots T_3^{2,E} \cdot T_2^{1,E} \\ &= \Pi_{k=n}^{2} T_k^{k-1,E} \end{aligned}$$

of sparse $(N_n^E - N_{k-1}^E) \times (N_n^E - N_{k-2}^E)$ matrices $T_k^{k-1,E}$. We then have

$$u_n = T_n^E w_n^E.$$

Since the spaces S_k are nested, there exists a transformation matrix P_{k-1}^k such that $\phi_{k-1} = \phi_k P_{k-1}^k$ or equivalently $u_k = P_{k-1}^k u_{k-1}$. The matrix P_{k-1}^k maps S_{k-1} to S_k, $k = n, \dots, 2$. The transformation matrices $T_k^{k-1,E}$, $k = n, \dots, 2$ can be expressed by

$$T_k^{k-1,E} = \begin{pmatrix} P_{k-1}^k & I_k & 0 \\ 0 & 0 & I_{n,k+1} \end{pmatrix}$$

where $I_{n,k+1}$ is the identity operator of dimension $\sum_{i=n}^{k+1} N_i$.

Using the nodal basis Φ_n at the fixed level n, the Galerkin approach leads to a linear system of equations

$$L_n u_n = f_n$$

where $(L_n)_{(i,j)} = a(\phi_i^n, \phi_j^n)$ and $(f_n)_{(j)} = \langle f, \phi_j^n \rangle$, $i, j = 1, \dots, N_n$. For the generating system E_n, the Galerkin approach leads to the system of equations

$$L_n^E w_n^E = f_n^E,$$

where $(L_n^E)^k_{(i_k,j_k)} = a(\phi^k_{i_k}, \phi^k_{j_k})$ and $(f_n^E)^k_{(j,k)} = \langle f, \phi^k_{j_k}\rangle$, $k = 1, \ldots, n$, $i_k, j_k = 1, \ldots, N_k$. The matrix L_n^E is singular symmetric positive semidefinite. It has the same rank as L_n. Thus $N^E_{n-1} = N^E_n - rank(L_n)$ eigenvalues are zero. The system is solvable but it has infinitely many solutions. For two different solutions $w_n^{E,1}$ and $w_n^{E,2}$

$$T_n^E w_n^{E,1} = T_n^E w_n^{E,2} = u_n$$

holds, where u_n is the unique solution of the system $L_n u_n = f_n$. This is direct consequences of (4.3.14). Therefore, it is sufficient to compute just one solution of the enlarged semidefinite system to obtain using T_n^E.

Since the transformation from E_n to Φ_n is expressed by $u_n = T_n^E w_n^E$, then

$$L_n^E = (T_n^E)^T L_n T_n^E, \quad f_n^E = (T_n^E)^T f_n. \tag{4.3.14}$$

Hence to compute L_n^E and f_n^E it is not necessary to explicit compute $a(\phi^k_{i_k}, \phi^k_{j_k})$ and $(f_n^E)^k_{(j,k)} = \langle f, \phi^k_{j_k}\rangle$. which involves integration on all levels $1, \ldots, n$, but instead the expression (4.3.14) can be used.

Now we consider the *diagonally preconditioned* conjugate gradient method for the enlarged semidefinite system. A major task is to compute the residual

$$r_n^E = f_n^E - L_n^E w_n^E$$

of the semidefinite system for a given w_n^E. Using the product representation (4.3.14) of L_n^E and f_n^E, we have

$$r_n^E = (T_n^E)^T f_n - (T_n^E)^T L_n T_n^E w_n^E,$$

and, with $u_n = T_n^E w_n^E$ and $r_n = f_n - L_n u_n$, we have

$$r_n^E = (T_n^E)^T (f_n - L_n u_n) = (T_n^E)^T r_n.$$

Let D_n^E be a diagonal matrix that we use as a preconditioner. With D_n^E preconditioning, we have to compute $(r_n^E)^T D_n^E r_n^E$ in the preconditioned conjugate gradient algorithm. Since $r_n^E = (T_n^E)^T r_n$, then

$$(r_n^E)^T D_n^E r_n^E = r_n^T T_n^E D_n^E (T_n^E)^T r_n.$$

Hence, the D_n^E preconditioned conjugate gradient algorithm for solving $L_n^E w_n^E = f_n^E$ is equivalent to the conjugate gradient algorithm with preconditioner $T_n^E D_n^E (T_n^E)^T$ for solving $L_n u_n = f_n$.

In [58], the finest level system $L_n u_n = f_n$ is treated by BPX preconditioners given by the matrix C_n^X defined as follows:

$$C_n^X := \sum_{k=0}^{n} \sum_{i=1}^{N_k} \frac{1}{d_i^k} \langle \cdot, \phi_i^k \rangle \phi_i^k$$

with the scaling factor $d_i^k = a(\phi_i^k, \phi_i^k)$. The preconditioner can now be expressed easily in terms of semi-definite system $L_n^E w_n^E = f_n^E$. Computation of the residual $r_n^E = f_n^E - L_n^E w_n^E$ gives

$$r_n^E = (T_n^E)^T r_n = (r^1 \quad r^2 \ldots r^{n-1} \quad r^n)^T,$$

where $(r^k)_i = \langle r_n, \phi_i^k \rangle \phi_i^k, \quad k = 0, \ldots, n, \quad i = 1, \ldots, N_k$. The BPX preconditioner resembles just a multiplication of the residual r_n^E of the enlarged system with the diagonal matrix D_n^E where the diagonal entries are given by the scaling factor $1/a(\phi_i^k, \phi_i^k)$. Therefore, in term of the enlarged system, BPX preconditioning is just the diagonal scaling of the residual.

Now we consider the condition number of the D_n^E preconditioned semidefinite system. In general, the conventional number is infinity because L_n^E is singular. In [30], it is shown that the condition numbers of the preconditioned enlarged and original systems are the same, provided a generalised condition number is used that considers the preconditioned matrix restricted to the orthogonal complement of its null space. The generalised condition number that we use is given by

$$\kappa(D_n^E L_n^E) = \lambda_{\max} / \lambda_{\min},$$

where $\lambda_{\max}$ denotes the largest eigenvalue of $D_n^E L_n^E$ and $\lambda_{\min}$ its smallest nonzero eigenvalue.

For hierarchical basis preconditioner we use a similar strategy. That is, the hierarchical basis preconditioner is just the diagonal matrix D_n^E where only the

diagonal entries associated with the functions appearing in the hierarchical basis are non-zero.

4.3.4 Numerical Results

We solve the biharmonic equation (4.3.1) for the unit square $\Omega = [0,1]^2$. The initial triangulation Δ_0 is constructed by drawing the two diagonals of Ω which divide Ω into four triangles as shown in Fig.4.16a.

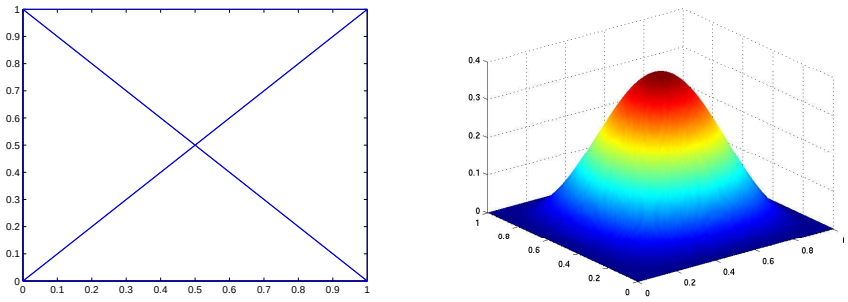

(a) Initial Triangulation (b) Approximate Solution

Figure 4.16: Initial triangulation and approximate solution to the biharmonic equation.

The right hand side f is chosen such that the exact solution is given by

$$u = (10x(1-x)y(1-y))^2.$$

The same problem has been investigated by Maes and Bultheel [43].

In Table 4.8 and 4.9, we display the errors between the exact solution and the finite element solutions at several levels. The order of convergence of the finite element is consistent with that stated in Theorem 4.1. The graph of the approximate solution on the level 8 of the triangulation is shown in Fig.4.16b.

We also solve the problem using the Lagrange type Hierarchical preconditioner, Hermite type Hierarchical preconditioner and also BPX preconditioners based on

Table 4.8: The convergence of finite element for the biharmonic solution based on Lagrange basis functions.

Level	Dim	L_2-error	Rate	L_∞-error	Rate	H^1-error	Rate	H^2-error	Rate
1	15	5.22e-02	-	1.49e-01	-	2.75e-01	-	3.32	-
2	75	8.65e-03	2.59	2.48e-02	2.58	4.87e-02	2.50	1.35	1.30
3	339	2.18e-03	1.99	6.12e-03	2.02	1.24e-02	1.98	6.83e-01	0.99
4	1443	5.35e-04	2.03	1.51e-03	2.02	3.04e-03	2.02	3.44e-01	0.99
5	5955	1.33e-04	2.01	3.75e-04	2.02	7.54e-04	2.01	1.69e-01	1.02
6	24195	3.30e-05	2.00	9.34e-05	2.01	1.88e-04	2.00	8.37e-02	1.02
7	97539	8.27e-06	2.00	2.34e-05	2.00	4.70e-05	2.00	4.21e-02	0.99
8	391683	2.37e-06	1.80	6.58e-06	1.83	1.30e-05	1.85	2.10e-02	1.00

Table 4.9: The convergence of finite element for the biharmonic solution based on Hermite basis functions.

Level	Dim	L_2-error	Rate	L_∞-error	Rate	H^1-error	Rate	H^2-error	Rate
1	15	5.22e-02	-	1.49e-01	-	2.75e-01	-	3.32	-
2	75	8.65e-03	2.59	2.48e-02	2.58	4.87e-02	2.50	1.35	1.30
3	339	2.18e-03	1.99	6.12e-03	2.02	1.24e-02	1.98	6.83e-01	0.99
4	1443	5.35e-04	2.03	1.51e-03	2.02	3.04e-03	2.02	3.44e-01	0.99
5	5955	1.33e-04	2.01	3.75e-04	2.01	7.54e-04	2.01	1.69e-01	1.02
6	24195	3.30e-05	2.01	9.34e-05	2.01	1.88e-04	2.00	8.37e-02	1.02
7	97539	8.24e-06	2.00	2.33e-05	2.00	4.69e-05	2.01	4.21e-02	0.99
8	391683	2.05e-06	2.01	5.81e-06	2.00	1.17e-05	2.00	2.10e-02	1.00

these two type of bases. We follow the approach outlined by Griebel [30] as discussed in the previous section to implement these preconditioners. For each preconditioner we compute the spectral condition number κ of the system matrix for the linear system of the equations that is solved. The condition numbers are listed in Table 4.10.

The numerical computation shows that BPX preconditioned matrices have smaller condition numbers compared to hierarchical preconditioned matrices for both Lagrange and Hermite versions. We also notice that despite knowing from the theory that the Lagrange hierarchical basis is a Riesz basis for the Sobolev space

Table 4.10: Condition numbers of single level discretisation matrices, BPX and hierarchical preconditioned matrices.

Level	Dim	Lagrange			Hermite		
		κ	κ-BPX	κ-Hie	κ	κ-BPX	κ-Hie
2	75	2.02e4	1080	1190	1.02e4	66	68
3	339	3.25e5	1530	4100	1.50e5	85	108
4	1443	5.35e6	1860	7060	2.34e6	99	193
5	5955	8.67e7	2120	9560	3.72e7	108	302
6	24195	1.37e9	2310	11330	5.95e8	115	437

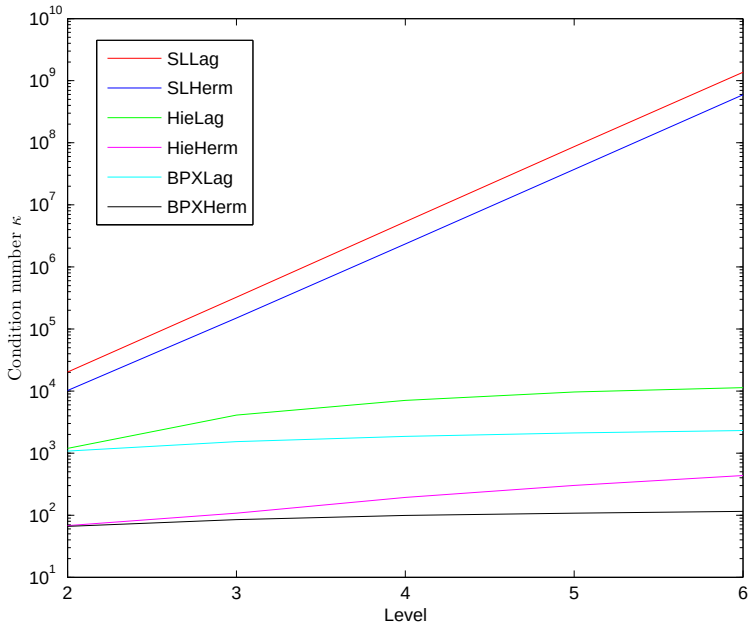

Figure 4.17: Semi-log graph of the condition number κ versus the level n.

$H_0^2(\Omega)$, the corresponding preconditioned matrices have larger condition numbers compared to the other preconditioned matrices. We have also plotted a semilog graph to illustrate the behaviour of these condition numbers, as shown in Fig. 4.17. We see from the graph that the condition numbers of the single level discretisation matrices are growing at a high rate with n, the condition numbers of Lagrange hierarchical preconditioned matrices and BPX preconditioned matrices of Lagrange and Hermite versions are stabilising and the condition numbers of

Hermite hierarchical preconditioned matrices are growing at a lower rate. These behaviours are consistent with the theory on these preconditioned matrices that we already know before.

Now we proceed to computing the solution at each level with the conjugate gradient method. The starting vector for each iteration is the zero vector. At each level we stop the conjugate gradient iteration when the residual $r \leq 0.1 * H^2$ single level discretisation error. The results are shown on Tables 4.11, 4.12, 4.13 and 4.14. The first column gives the maximum resolution level n. For each level, we display the residuals, the errors in different norms, and the number of iterations that is needed to reach the stopping criteria. The results clearly favor for Hermite based BPX preconditioner which requires the least number of iterations.

Table 4.11: Numerical Results - Using BPX preconditioner based on Lagrange basis functions.

Level	Dim	Its	Res	L_2-error	L_∞-error	H^1-error	H^2-error
2	75	22	6.30e-02	1.33e-02	3.37e-02	7.48e-02	1.59
3	339	35	6.25e-02	4.20e-03	1.23e-02	2.94e-02	8.36e-01
4	1443	46	2.66e-02	2.12e-03	6.29e-03	1.74e-02	4.94e-01
5	59550	58	1.52e-02	1.14e-03	3.20e-03	1.04e-02	2.83e-01
6	24195	69	6.78e-03	7.30e-04	1.98e-03	6.82e-03	1.75e-01
7	97539	78	3.89e-03	5.18e-04	1.44e-03	4.78e-03	1.18e-01
8	391683	87	2.13e-03	3.63e-04	1.00e-03	3.28e-03	8.07e-02

Table 4.12: Numerical Results - Using Hierarchical preconditioner based on Lagrange basis functions.

Level	Dim	Its	Res	L_2-error	L_∞-error	H^1-error	H^2-error
2	75	21	8.50e-02	1.25e-02	2.97e-02	6.97e-02	1.58
3	339	32	6.02e-02	6.53e-03	1.74e-02	4.74e-02	1.02
4	1443	46	3.02e-02	3.15e-03	1.01e-02	3.02e-02	6.77e-01
5	5955	61	1.62e-02	1.54e-03	5.32e-03	2.01e-02	4.52e-01
6	24195	83	8.20e-03	8.55e-04	2.92e-03	1.06e-02	2.56e-01
7	97539	97	4.05e-03	6.19e-04	1.93e-03	7.02e-03	1.79e-01
8	391683	113	2.18e-03	3.26e-04	1.03e-03	3.83e-03	1.17e-01

Table 4.13: Numerical Results - Using BPX preconditioner based on Hermite basis functions.

Level	Dim	Its	Res	L_2-error	L_∞-error	H^1-error	H^2-error
2	75	7	5.34e-02	8.85e-03	2.50e-02	4.88e-02	1.37
3	339	10	2.44e-02	2.41e-03	7.37e-03	1.43e-02	7.13e-01
4	1443	12	1.80e-02	6.88e-04	2.69e-03	5.22e-03	3.76e-01
5	5955	14	9.19e-03	2.58e-04	1.08e-03	3.09e-03	2.03e-01
6	24195	16	4.53e-03	1.43e-04	5.04e-04	2.21e-03	1.15e-01
7	97539	17	4.09e-03	1.22e-04	4.41e-04	2.02e-03	8.16e-02
8	391683	19	1.87e-03	8.83e-05	2.96e-04	1.50e-03	5.34e-02

Table 4.14: Numerical Results - Using Hierarchical preconditioner based on Hermite basis functions.

Level	Dim	Its	Res	L_2-error	L_∞-error	H^1-error	H^2-error
2	75	6	1.02e-01	9.71e-03	2.77e-02	5.75e-02	1.43
3	339	11	4.21e-02	2.82e-03	9.73e-03	1.76e-02	7.66e-01
4	1443	14	2.75e-02	9.99e-04	4.19e-03	7.71e-03	4.62e-01
5	5955	17	1.45e-02	4.17e-04	1.70e-03	3.97e-03	3.01e-01
6	24195	21	7.43e-03	2.02e-04	7.25e-04	2.38e-03	1.94e-01
7	97539	26	3.65e-03	9.18e-05	2.80e-04	9.69e-04	1.17e-01
8	391683	32	2.04e-03	4.58e-05	1.22e-04	5.06e-04	8.58e-02

The last experiment is to show the advantage of the C^1 piecewise quadratics finite element space we used in our construction compared to multilevel spaces of Powell-Sabin-6 split elements in [43].

In order to compare with the results obtained by [43], for each level we stop the conjugate gradient iteration when the residual r is less than equal to 0.001 times H^2 single level discretisation error. The results are displayed in Table 4.15. A comparison to the results obtained in [43] Table 1 reveals that even though we have a larger condition number (see Table 4.10) compared to the $\sqrt{3}$ PS-6 of [43], we achieve comparable residuals with similar number of iterations and our results are better than the ones obtained with the non-reduced PS-12 split method as shown in the same table of [43].

Table 4.15: Numerical Results for BPX-PCG based on Hermite basis functions with tolerance 0.001*H^2norm

Level	Dim	Its	Res	L_2-error	L_∞-error	H^1-error	H^2-error
2	75	10	4.67e-04	8.64e-03	2.48e-02	4.87e-02	1.35
3	339	14	6.10e-04	2.19e-03	6.16e-03	1.24e-02	6.84e-01
4	1443	18	2.83e-04	5.43e-04	1.50e-03	3.15e-03	3.45e-01
5	5955	22	1.16e-04	1.35e-04	3.56e-04	8.48e-04	1.70e-01
6	24195	25	6.28e-05	3.45e-05	9.66e-05	2.89e-04	8.44e-02
7	97539	27	4.09e-05	1.06e-05	4.16e-05	1.72e-04	4.29e-02
8	391683	30	1.66e-05	3.63e-06	1.45e-05	7.65e-05	2.19e-02

Chapter 5

Refinable C^2 Piecewise Quintic Polynomials on Powell-Sabin-12 Triangulations

5.1 Introduction

Nested spaces of smooth piecewise polynomials (splines) are used in multilevel algorithms for surface compression [25, 42], nonlinear approximation [15, 19] and preconditioning of spline based finite element system matrices [14, 21, 49]. If the triangulations Δ_n are obtained by successive refinements of a starting triangulation Δ_0, then the spaces $S_n = S_d^r(\Delta_n)$ of all C^r splines of degree at most d are nested. However, these spaces are known to possess stable local bases important for application only if d is relatively large, $d \geq 3r + 2$, see [20]. Therefore much attention is paid to the *macro-element* spaces [36, Chapter 6] whose degree can be kept much lower at the expense of requiring that Δ_n is obtained from a general triangulation by splitting each triangle into subtriangles by various methods such as Clough-Tocher split, Powell-Sabin-6 or Powell-Sabin-12 split. Some C^1 macro-elements [11, 21, 32, 33, 41] are refinable in the sense that nested spline spaces

with stable local bases can be constructed with their help. However, refinable macro-elements of higher smoothness have not been known.

In this chapter we propose a construction of refinable C^2 macro-elements, whose degree 5 is substantially lower than degree 8 of the C^2 splines of [20] and degree 9 of the refinable C^2 spline spaces with stable dimension suggested in [17]. On a single macro-triangle our spaces coincide with the C^2 quintic macro-element of [54], although we obtain a simpler description of it (important for nestedness) in the case when the central point of the Powell-Sabin-12 split is placed at the barycentre of the macro-triangle. The nestedness of the spaces is achieved as in [17] by relaxing the C^3 smoothness conditions at the vertices of macro-triangles, which allows to break the 'super-smoothness disks' at the vertices into half-disks. The proposed macro-elements are easy to implement in the framework of the Bernstein-Bézier techniques because we provide explicit formulas for all B-coefficients which are not computed directly by the standard smoothness conditions. The work in this chapter is published in the paper [24].

In Section 5.2 we construct the nested spaces and stable minimal determining sets (leading to a stable local basis). Section 5.3 is devoted to the proofs of the main results, whereas Section 5.4 provides a nodal minimal determining set and error bounds for the corresponding Hermite interpolation operator. We show that the nodal minimal determining set is stable and local and we also define the associated stable local basis. In the last part, we introduce a hierarchical basis for the nested spaces.

5.2 Refinable spaces of C^2 piecewise quintics

Let Ω be a bounded connected polygonal domain in $\mathbb{R}^2$. Suppose that some initial regular triangulation Δ_0 of Ω is given. Beginning with Δ_0 we construct a sequence $\{\Delta_n\}_{n=0}^{\infty}$ of triangulations of Ω by *uniform refinement*, that is Δ_{n+1} is obtained from Δ_n by subdividing any triangle T of Δ_n into four equal subtriangles by

joining the midpoints of the three edges with each other, as in Figure 5.1 (left). The uniform refinement of a single triangle T will be denoted T_U.

Starting from $\{\Delta_n\}_{n=0}^{\infty}$ we introduce further subdivisions by splitting each triangle of Δ_n into twelve triangles by joining the midpoints of the three edges with each other and with the opposite vertices. This *Powell-Sabin-12 split* T_{PS12} of a single triangle T is illustrated in Figure 5.1 (right). Clearly, T_{PS12} is a refinement of T_U. The triangulation obtained from Δ_n by applying the Powell-Sabin-12 split to each triangle will be denoted Δ_n^*. An important observation is that Δ_{n+1}^* is a *refinement* of Δ_n^*, in the sense that Δ_{n+1}^* can be obtained from Δ_n^* by subdividing its triangles.

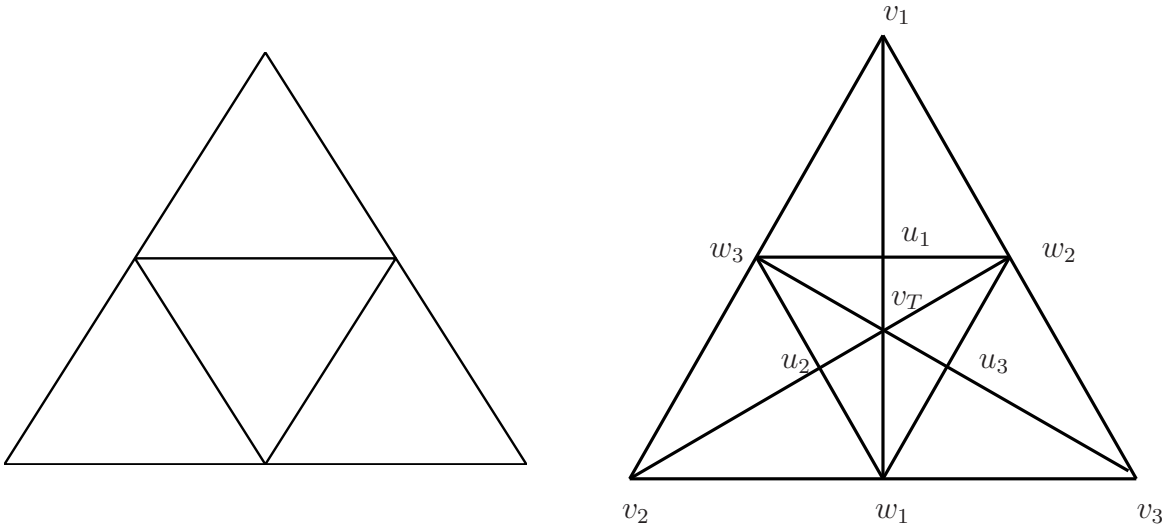

Figure 5.1: Uniform refinement T_U and Powell-Sabin-12 split T_{PS12} of a triangle.

For each $n = 0, 1, \ldots$, we denote by $\mathcal{V}_n$, $\mathcal{E}_n$, $\tilde{\mathcal{E}}_n$ and $\mathcal{W}_n$ the sets of all vertices, edges, interior edges and midpoints of edges of Δ_n, respectively. Given a triangle $T \in \Delta_n$, we denote the vertices of T_{PS12} by $v_1, v_2, v_3, w_1, w_2, w_3, u_1, u_2, u_3$ and v_T as shown in Figure 5.1. We refer to the edges of the form $[v_i, u_i]$ as *type-1 edges*, to edges of the form $[u_i, v_T]$ as *type-2 edges* and to edges of the form $[w_i, v_T]$ as *type-3 edges*. For $i = 1, 2, 3$, we write $\mathcal{E}_n^i$ for the set of all edges of Δ_n^* of type-i.

We set

$$\tilde{\mathcal{V}}_0 = \emptyset, \quad \tilde{\mathcal{V}}_n = (\mathcal{V}_n \cap \operatorname{Int}\Omega) \setminus \mathcal{V}_0, \quad n = 1, 2, \ldots.$$

Then

$$\mathcal{V}_n \setminus \tilde{\mathcal{V}}_n = \mathcal{V}_0 \cup (\mathcal{V}_n \cap \partial\Omega).$$

For any $v \in \bigcup_{n\in\mathbb{N}} \tilde{\mathcal{V}}_n$, let $n_v := \min\{n : v \in \tilde{\mathcal{V}}_n\}$. Clearly, there is a unique edge e_v of Δ_{n_v-1}, with adjacent triangles $T_v^+, T_v^- \in \Delta_{n_v-1}$, such that v lies at the midpoint of e_v. Since $\mathcal{W}_n \cap \operatorname{Int}\Omega \subset \tilde{\mathcal{V}}_{n+1}$, the triangles $T_w^+, T_w^- \in \Delta_n$ are well defined for any $w \in \mathcal{W}_n \cap \operatorname{Int}\Omega$.

For $n = 0, 1, \ldots$, let $S_5^2(\Delta_n^*)$ denote the space of C^2 quintic piecewise polynomials, i.e.

$$S_5^2(\Delta_n^*) := \{s \in C^2(\Omega) : s|_T \in \mathbb{P}_5 \text{ for all } T \in \Delta_n^*\}.$$

We consider the subspace S_n of $S_5^2(\Delta_n^*)$ defined by

$$\begin{aligned} S_n = \big\{ & s \in S_5^2(\Delta_n^*) : \\ & \text{(i) } s \in C^3(v) \quad \text{for all } v \in \mathcal{V}_0 \cup (\mathcal{V}_n \cap \partial\Omega) \text{ and all } v \in \mathcal{W}_n \cap \partial\Omega, \\ & \text{(ii) } s|_{T_v^+} \in C^3(v), s|_{T_v^-} \in C^3(v) \quad \text{for all } v \in \tilde{\mathcal{V}}_n \text{ and all } v \in \mathcal{W}_n \cap \operatorname{Int}\Omega, \text{ and} \\ & \text{(iii) } s \text{ is } C^3 \text{ across all edges in } \mathcal{E}_n^1 \cup \mathcal{E}_n^2 \cup \mathcal{E}_n^3 \big\}. \end{aligned}$$

One crucial property of the spaces S_n is their nestedness.

Theorem 5.1. *The spaces $S_n, n = 0, 1, \ldots$ are nested, that is,*

$$S_n \subset S_{n+1}, \quad n = 0, 1, 2, \ldots.$$

Proof. Let $n \geq 1$. We suppose $s \in S_{n-1}$ and show that $s \in S_n$. If $v \in \mathcal{V}_0 \cup (\mathcal{V}_n \cap \partial\Omega)$, then $v \in \mathcal{V}_0 \cup (\mathcal{V}_{n-1} \cap \partial\Omega)$ or $v \in \mathcal{W}_{n-1} \cap \partial\Omega$, so $s \in C^3(v)$ by Condition (i) in the definition of S_n. It is also clear that $s \in C^3(v)$ for $v \in \mathcal{W}_n \cap \partial\Omega$ since v lies in the interior of a boundary edge of Δ_{n-1}^*. If $v \in \tilde{\mathcal{V}}_n$, then either $v \in \tilde{\mathcal{V}}_{n-1}$, or $n_v = n$ and $v \in \mathcal{W}_{n-1} \cap \operatorname{Int}\Omega$, $T_v^+, T_v^- \in \Delta_{n-1}$ and v lies at the midpoint of the common edge e_v of these two triangles. By Condition (ii) in both cases $s|_{T_v^+}, s|_{T_v^-} \in C^3(v)$ as required. If $v \in \mathcal{W}_n \cap \operatorname{Int}\Omega$, then $n_v = n + 1$ and $T_v^+, T_v^- \in \Delta_n$, whereas v lies at the midpoint of the common edge $e_v \in \Delta_n$ of these two triangles. Moreover, for a triangle $T \in \Delta_{n-1}$, v is either the midpoint of the

edges $\langle v_1, w_2\rangle, \langle v_1, w_3\rangle, \langle v_2, w_1\rangle, \langle v_2, w_3\rangle, \langle v_3, w_1\rangle, \langle v_3, w_2\rangle$ or the vertices u_1, u_2, u_3 of T_{PS12}. In the first case, $s|_{T_v^+}, s|_{T_v^-} \in C^3(v)$ because v is not a vertex of Δ^*_{n-1}. In the second case, $s|_{T_v^+}, s|_{T_v^-} \in C^3(v)$ since s is C^3 across type 1 and type 2 edges, $e \in \mathcal{E}^1_{n-1} \cup \mathcal{E}^2_{n-1}$. If $e \in (\mathcal{E}^1_n \cup \mathcal{E}^2_n \cup \mathcal{E}^3_n)$ then either e is (a part of) an edge $\tilde{e} \in (\mathcal{E}^1_{n-1} \cup \mathcal{E}^2_{n-1} \cup \mathcal{E}^3_{n-1})$ since Δ^*_n is a refinement of Δ^*_{n-1} or e lies in the interior of some triangle $T \in \Delta^*_{n-1}$. In both cases, s is C^3 across e by Condition (iii). □

We now want to generate a stable local MDS for S_n. We will use the Bernstein-Bézeir techniques presented in Section 1.3.3 and also follow the notation introduced there.

For each $v \in \tilde{\mathcal{V}}_n$, let e_v in Δ_{n_v-1} be the unique edge with adjacent triangles $T_v^+, T_v^- \in \Delta_{n_v-1}$ such that v lies at the midpoint of e_v. For each $v \in \mathcal{V}_n$, we choose a triangle $\hat{T}_v \in \Delta^*_n$ with vertex at v. If $v \in \tilde{\mathcal{V}}_n$, we assume that $\hat{T}_v \subset T_v^+$ and we choose another triangle $\tilde{T}_v = \langle v, u, w\rangle \in \Delta^*_n$ attached to v such that $\tilde{T}_v \subset T_v^-$ and an edge of $\tilde{T}_v$ is a part of e_v. We now set $M_v := D_3(v) \cap \hat{T}_v$ for any $v \in \mathcal{V}_n$, and $\tilde{M}_v := M_v \cup \xi^{\tilde{T}_v}_{2,3,0}$ for any $v \in \tilde{\mathcal{V}}_n$. The set $\tilde{M}_v$ is illustrated in Figure 5.2.

Furthermore, for each edge e of Δ_n, let v_{T_e} be the barycentre of a triangle T_e in Δ_n attached to e, let w_e be the midpoint of e, let $T^3_e = \langle v_{T_e}, w_e, u\rangle$ be one of the triangles in Δ^*_n attached to the edge $\langle w_e, v_{T_e}\rangle$, of type 3, and let $M_e = \{\xi^{T^3_e}_{3,2,0}, \xi^{T^3_e}_{2,3,0}, \xi^{T^3_e}_{2,2,1}, \xi^{T^3_e}_{1,4,0}\}$. For each $w \in \mathcal{W}_n \cap \operatorname{Int}\Omega$, let T_e^+ and T_e^- be two triangles in Δ_n attached to the edge $e = \langle v_1, v_2\rangle$ in Δ_n, such that w is the midpoint of e, that is $w = w_e$. Let $v_{T_e^+}$ be the barycentre of T_e^+ and let $\hat{T}^3_e \subset T_e^+$ be some triangle in Δ^*_n attached to the edge $\langle w_e, v_{T_e^+}\rangle$ of type 3. Let $\tilde{T}_e = \langle w_e, u, v_1\rangle \subset T_e^-$ be one of the triangles in Δ^*_n with vertex w_e and such that one of its edges is a part of e. Let $\tilde{M}_e = \{\xi^{\hat{T}^3_e}_{3,2,0}, \xi^{\hat{T}^3_e}_{2,3,0}, \xi^{\hat{T}^3_e}_{2,2,1}, \xi^{\hat{T}^3_e}_{1,4,0}\} \cup \{\xi^{\tilde{T}_e}_{2,3,0}\}$. The domain points corresponding to $\tilde{M}_e$ are shown in Figure 5.3.

Theorem 5.2. *The dimension of S_n is given by*

$$\dim S_n = 10\#\mathcal{V}_n + \#\tilde{\mathcal{V}}_n + 4\#\mathcal{E}_n + \#\tilde{\mathcal{E}}_n. \tag{5.2.1}$$

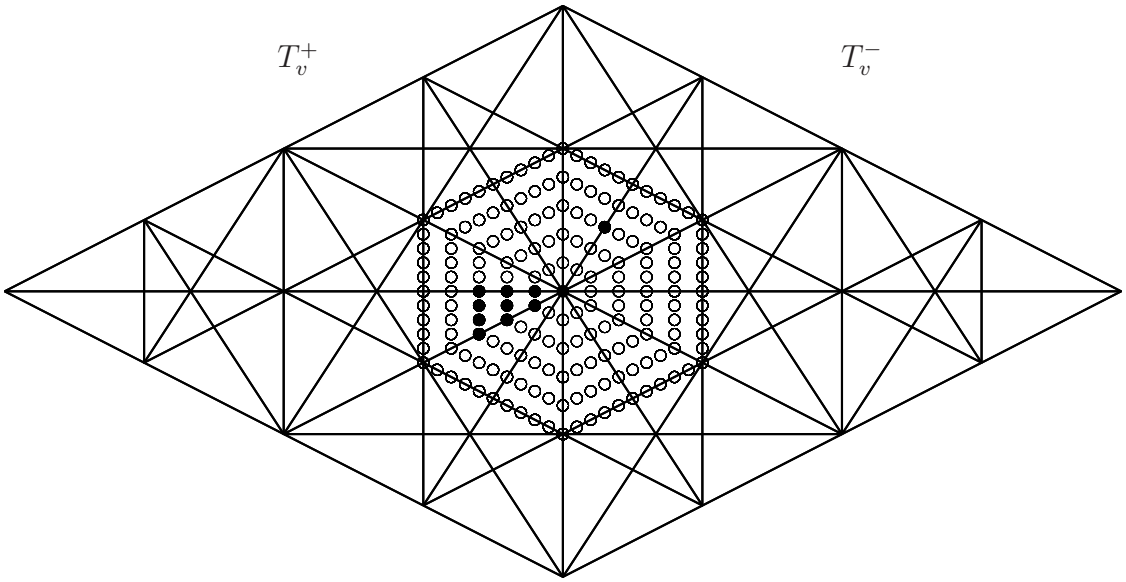

Figure 5.2: Domain points corresponding to $\tilde{M}_v$ are marked with filled circles.

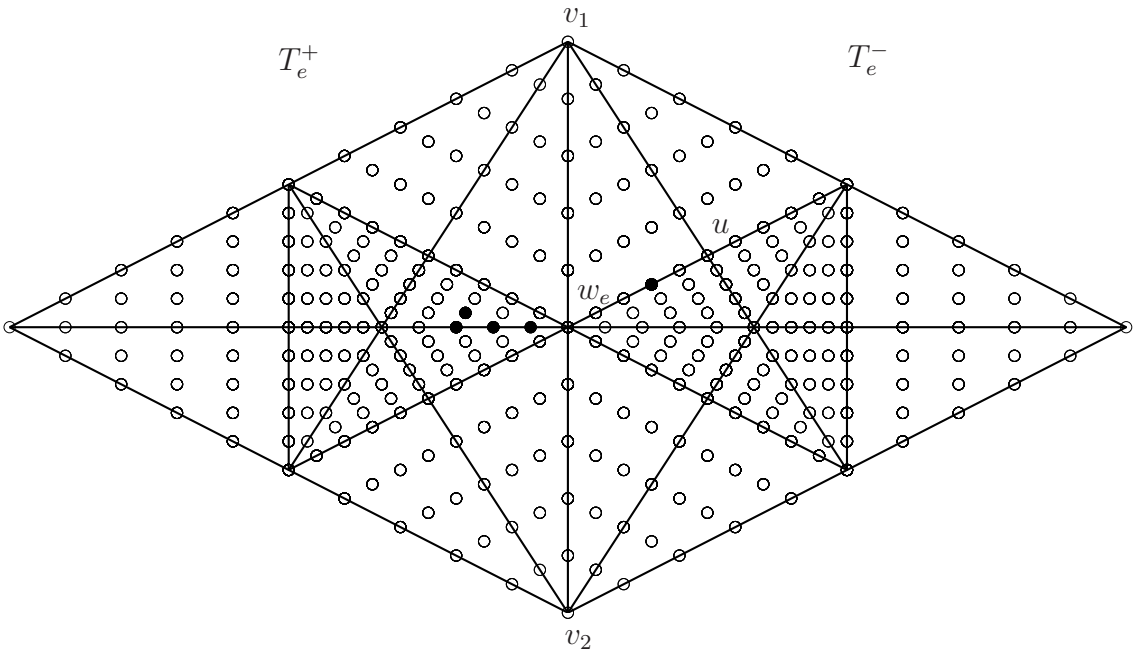

Figure 5.3: Domain points corresponding to $\tilde{M}_e$ are marked with filled circles.

Moreover, the set

$$M_n = \bigcup_{v\in\mathcal{V}_n\setminus\tilde{\mathcal{V}}_n} M_v \cup \bigcup_{v\in\tilde{\mathcal{V}}_n} \tilde{M}_v \cup \bigcup_{e\in\mathcal{E}_n\setminus\tilde{\mathcal{E}}_n} M_e \cup \bigcup_{e\in\tilde{\mathcal{E}}_n} \tilde{M}_e$$

is a stable local minimal determining set for S_n.

The proof of this theorem will be given in Section 5.3.

By restricting to a single Powell-Sabin-12 split T_{PS12}, we consider the space $S(T_{PS12})$ defined by

$$\begin{aligned} S(T_{PS12}) = \big\{ & s \in S_5^2(T_{PS12}) : \\ & s \in C^3(v_i) \text{ for all } i = 1,2,3, \\ & s \in C^3(w_i) \text{ for all } i = 1,2,3, \\ & s \text{ is } C^3 \text{ across the segment } \langle v_i, u_i\rangle, \langle u_i, v_T\rangle, \langle w_i, v_T\rangle, \text{ for all } i = 1,2,3\big\}, \end{aligned}$$

where v_i, u_i, w_i are as in Figure 5.1. Clearly, $S(T_{PS12}) = S_0$ if Δ_0 consists of just one triangle.

Let $T_1 = \langle v_1, w_3, u_1\rangle$, $T_2 = \langle v_2, w_1, u_2\rangle$, $T_3 = \langle v_3, w_2, u_3\rangle$, $T_4 = \langle v_T, w_2, u_1\rangle$, $T_5 = \langle v_T, w_3, u_2\rangle$, $T_6 = \langle v_T, w_1, u_3\rangle$, and let

$$M_v = \bigcup_{i=1}^{3} (D_3(v_i) \cap T_i), \qquad M_e = \bigcup_{i=4}^{6} \big\{\xi_{1,4,0}^{T_i}, \xi_{2,3,0}^{T_i}, \xi_{3,2,0}^{T_i}, \xi_{2,2,1}^{T_i}\big\}.$$

Theorem 5.2 specialised to the case of $S(T_{PS12})$ gives the following corollary, see Figure 5.4 for an illustration.

Corollary 5.3. *The dimension of $S(T_{PS12})$ is 42. Moreover, the set $M = M_v \cup M_e$ is a stable minimal determining set for $S(T_{PS12})$.*

Remark 5.4. The spaces $S(T_{PS12})$ can be used to define non-nested C^2 macro-element spaces which in fact coincide with the spaces of C^2 Powell-Sabin-12 macro-elements constructed in [54] when the v_T is the barycentre of T. Note that our definition of $S(T_{PS12})$ is simpler than the corresponding space $S_2(T_{PS12})$ in [54].

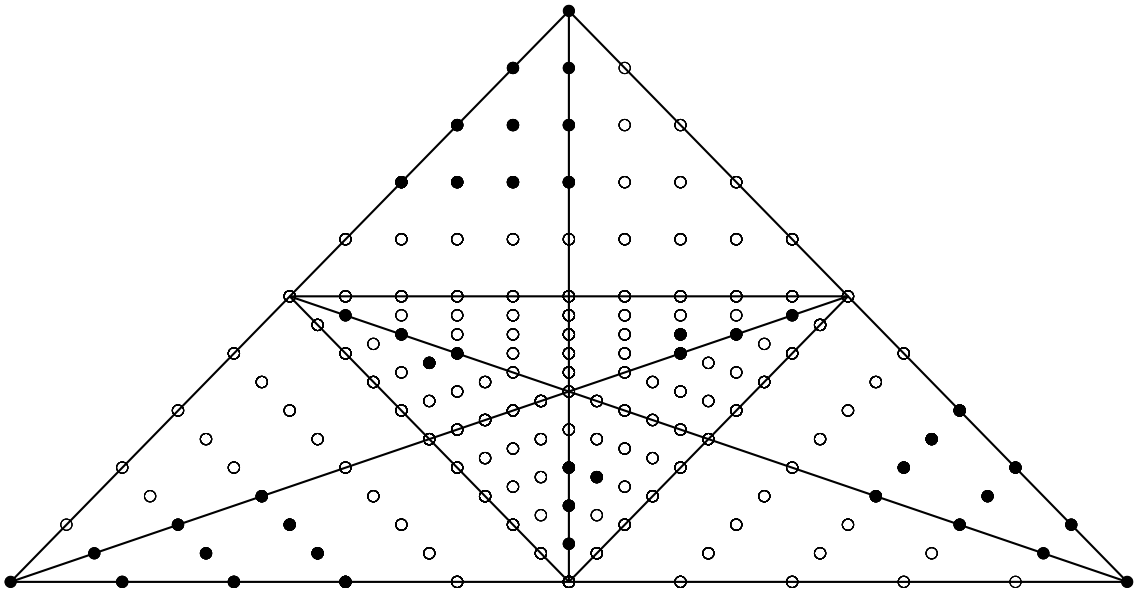

Figure 5.4: Minimal determining set for $S(T_{PS12})$ is indicated by filled circles.

5.3 Proof of Theorem 5.2

We start by providing two auxiliary results.

Let T_{PS6} be the Powell-Sabin-6 split of the triangle $T = \langle w_1, w_2, w_3 \rangle$ which lies inside the Powell-Sabin-12 split in Figure 5.1 and is shown separately in Figure 5.5 for convenience. Recall that u_i is the midpoint of the edge opposite to w_i for $i = 1, 2, 3$, and $v_T = (w_1 + w_2 + w_3)/3$ is the barycentre of T. We consider the space $S_5^3(T_{PS6})$ of all C^3 piecewise quintics on T_{PS6}.

Let $T_1 = \langle v_T, w_1, u_3 \rangle, T_2 = \langle v_T, w_2, u_1 \rangle$ and $T_3 = \langle v_T, w_3, u_2 \rangle$, and let

$$M = \bigcup_{i=1}^{3} (D_3(w_i) \cap T_i),$$

see Figure 5.6, where the points in M are marked with filled circles.

Lemma 5.5. *The dimension of $S_5^3(T_{PS6})$ is 30. Moreover, the above set M is a stable minimal determining set for $S_5^3(T_{PS6})$.*

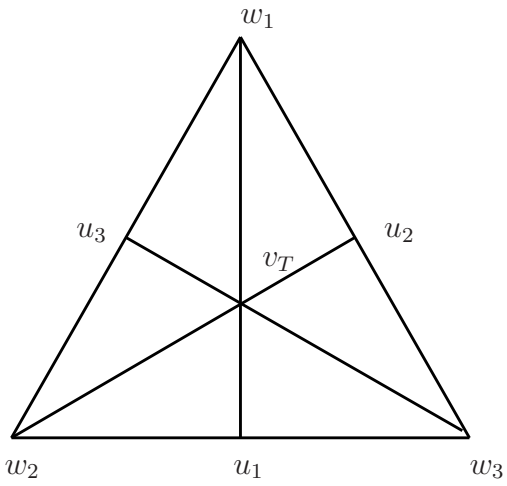

Figure 5.5: Powell-Sabin-6 Split

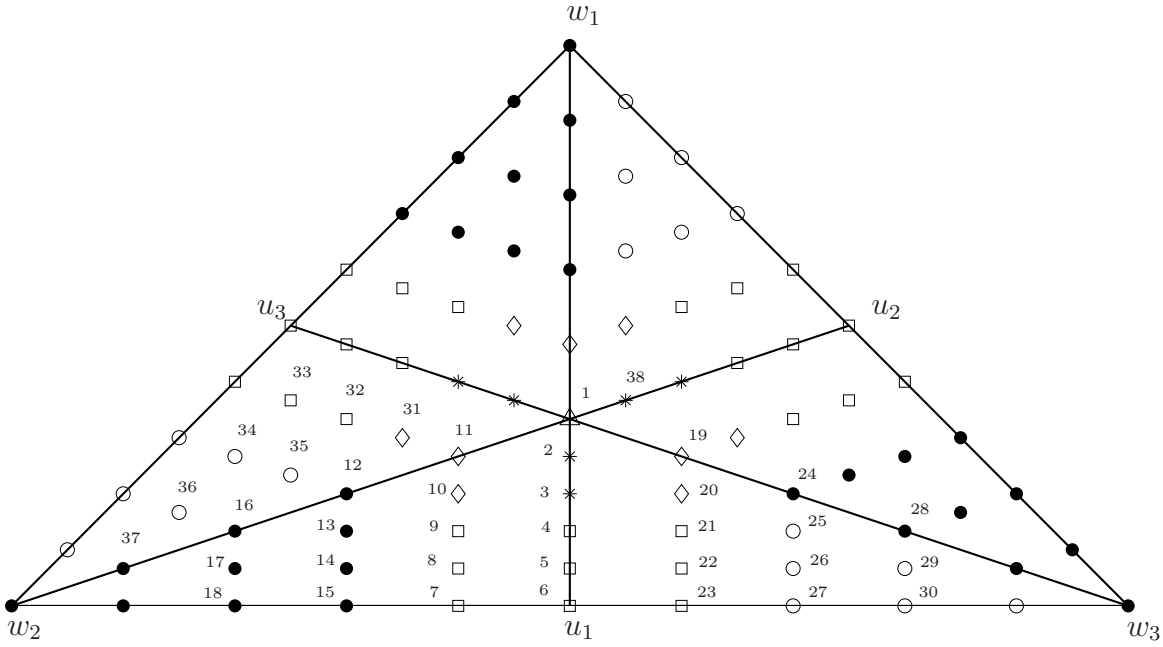

Figure 5.6: Minimal determining set M for $S_5^3(T_{PS6})$ is marked by filled circles.

Proof. The dimension of $S_5^3(T_{PS6})$ is easily obtained by [36, Theorem 9.3]. Let us show that M is a minimal determining set for $S_5^3(T_{PS6})$. For each $i = 1, 2, 3$, we use the C^3 smoothness at w_i to uniquely and stably compute the coefficients corresponding to all domain points in $D_3(w_i) \setminus M$ by [36, Lemma 5.10].

Next, for each edge $e_1 = \langle w_2, w_3 \rangle$, $e_2 = \langle w_1, w_3 \rangle$, $e_3 = \langle w_1, w_2 \rangle$ of T, we

use the C^3 smoothness across the edge $\langle v_T, u_1\rangle$, $\langle v_T, u_2\rangle$, $\langle v_T, u_3\rangle$, respectively, to determine the coefficients corresponding to domain points in the set

$$E_2(e_i) := \{\xi : \mathrm{dist}(\xi, e_i) \le 2,\ \xi \notin D_3(w_i) \cup D_3(w_{i+1})\}, \quad i = 1, 2, 3.$$

(These coefficients are indicated by squares in Figure 5.6.) The C^3 smoothness across the edge $\langle v_T, u_i\rangle$ gives three smoothness conditions involving these coefficients which uniquely determine them as solutions of the corresponding linear system. For example, the barycentric coordinates of w_3 relative to $\langle w_2, u_1, v_T\rangle$ are given by $(-1, 2, 0)$ since u_1 is the midpoint of the edge $\langle w_2, w_3\rangle$. Hence, the three smoothness conditions across the edge $\langle v_T, u_1\rangle$ involving the coefficients on the edge $\langle w_2, w_3\rangle$ are given by

$$\begin{aligned} C_{23} &= -C_7 + 2C_6, \\ C_{27} &= C_{15} - 4C_7 + 4C_6, \\ C_{30} &= -C_{18} + 6C_{15} - 12C_7 + 8C_6, \end{aligned}$$

where the coefficients C_i of a spline $s \in S_5^3(T_{PS6})$ are numbered as in Figure 5.6. By solving this linear system of equations with respect to C_7, C_{23} and C_6, we get

$$\begin{aligned} C_7 &= -\tfrac{1}{4}C_{18} - \tfrac{1}{4}C_{30} + C_{15} + \tfrac{1}{2}C_{27}, \\ C_{23} &= -\tfrac{1}{4}C_{18} - \tfrac{1}{4}C_{30} + \tfrac{1}{2}C_{15} + C_{27}, \\ C_6 &= -\tfrac{1}{4}C_{18} - \tfrac{1}{4}C_{30} + \tfrac{3}{4}C_{15} + \tfrac{3}{4}C_{27}. \end{aligned}$$

Similarly, we obtain

$$\begin{aligned} C_8 &= -\tfrac{1}{4}C_{17} - \tfrac{1}{4}C_{29} + C_{14} + \tfrac{1}{2}C_{26}, \quad C_{22} = -\tfrac{1}{4}C_{17} - \tfrac{1}{4}C_{29} + \tfrac{1}{2}C_{14} + C_{26}, \\ C_5 &= -\tfrac{1}{4}C_{17} - \tfrac{1}{4}C_{29} + \tfrac{3}{4}C_{14} + \tfrac{3}{4}C_{26}, \quad C_9 = -\tfrac{1}{4}C_{16} - \tfrac{1}{4}C_{28} + C_{13} + \tfrac{1}{2}C_{25}, \\ C_{21} &= -\tfrac{1}{4}C_{16} - \tfrac{1}{4}C_{28} + \tfrac{1}{2}C_{13} + C_{25}, \quad C_4 = -\tfrac{1}{4}C_{16} - \tfrac{1}{4}C_{28} + \tfrac{3}{4}C_{13} + \tfrac{3}{4}C_{25}. \end{aligned}$$

The other coefficients indicated by squares in Figure 5.6 can be found in the same way.

By taking into account the C^3 smoothness condition across the edges $\langle w_1, v_T\rangle$, $\langle w_2, v_T\rangle$, $\langle w_3, v_T\rangle$, we compute the yet unknown coefficients corresponding to the domain points on the rings $R_4(w_1), R_4(w_2)$ and $R_4(w_3)$, respectively. These coefficients are indicated by diamonds in Figure 5.6. For example, the barycentric coordinates of u_1 relative to $\langle u_3, w_2, v_T\rangle$ are $(-1, \frac{1}{2}, \frac{3}{2})$, and hence the three smoothness conditions across the edge $\langle w_2, v_T\rangle$ involving the coefficients in the ring $R_4(w_2)$ are given by

$$C_{10} = -C_{31} + \tfrac{1}{2}C_{12} + \tfrac{3}{2}C_{11}, \quad C_9 = C_{32} - C_{35} - 3C_{31} + \tfrac{1}{4}C_{16} + \tfrac{3}{2}C_{12} + \tfrac{9}{4}C_{11},$$
$$C_8 = -C_{33} + \tfrac{3}{2}C_{34} + \tfrac{9}{2}C_{32} - \tfrac{3}{4}C_{36} - \tfrac{9}{2}C_{35} - \tfrac{27}{4}C_{31} + \tfrac{1}{8}C_{37} + \tfrac{9}{8}C_{16} + \tfrac{27}{8}C_{12} + \tfrac{27}{8}C_{11}.$$

By solving the linear system involving the above equations, we get

$$C_{10} = \tfrac{4}{3}C_9 + \tfrac{2}{3}C_{32} - \tfrac{2}{3}C_{35} + \tfrac{1}{6}C_{16} - \tfrac{4}{9}C_8 - \tfrac{4}{9}C_{33} + \tfrac{2}{3}C_{34} - \tfrac{1}{3}C_{12} + \tfrac{1}{18}C_{37} - \tfrac{1}{3}C_{36},$$
$$C_{11} = \tfrac{4}{3}C_9 + \tfrac{4}{3}C_{32} + \tfrac{1}{3}C_{16} - \tfrac{16}{27}C_8 - \tfrac{16}{27}C_{33} + \tfrac{8}{9}C_{34} - \tfrac{4}{9}C_{36} + \tfrac{2}{27}C_{37} - \tfrac{4}{3}C_{35},$$
$$C_{31} = \tfrac{2}{3}C_9 + \tfrac{4}{3}C_{32} - \tfrac{4}{3}C_{35} + \tfrac{1}{2}C_{12} - \tfrac{4}{9}C_8 - \tfrac{4}{9}C_{33} + \tfrac{2}{3}C_{34} - \tfrac{1}{3}C_{36} + \tfrac{1}{18}C_{37} + \tfrac{1}{3}C_{16}.$$

By using C^1 smoothness across the edges $\langle u_1, v_T\rangle, \langle u_2, v_T\rangle, \langle u_3, v_T\rangle$ we compute the remaining undetermined coefficients corresponding to the domain points at distances three and four from $\langle w_1, w_2\rangle, \langle w_2, w_3\rangle, \langle w_3, w_1\rangle$. These coefficients are marked by stars in Figure 5.6. For instance, since that the coefficients C_{10}, C_{11}, C_{19} and C_{20} are already known, we compute C_2 and C_3 using the formulas

$$C_2 = \tfrac{1}{2}C_{11} + \tfrac{1}{2}C_{19}, \quad C_3 = \tfrac{1}{2}C_{10} + \tfrac{1}{2}C_{20}.$$

Finally, the only remaining undetermined coefficient at v_T, marked by a triangle in Figure 5.6, can be computed by using for example the univariate C^1 smoothness condition along the line $\langle u_2, w_2\rangle$, which gives

$$C_1 = \tfrac{2}{3}C_{11} + \tfrac{1}{3}C_{38}.$$

We have shown that M is a determining set for $S_5^3(T_{PS6})$. The set M is minimal since its cardinality is equal to the dimension of $S_5^3(T_{PS6})$. The stability of M is obvious in view of [36, Lemma 5.10] and the above explicit formulas. □

Remark 5.6. The space $S_5^3(T_{PS6})$ coincides with the space $S_2(T_{PS6})$ of [36, Theorem 7.9], where the vertex v_T is placed at the barycentre of T.

Lemma 5.7. *Let Δ be the triangulation shown in Figure 5.7 with six vertices $v_1, \ldots, v_6,$, where $v_4 = (v_3 + v_5)/2$, $v_2 = (3v_1 + v_3)/4$ and $v_6 = (3v_1 + v_5)/4$. Let $T = \langle v_1, v_4, v_6 \rangle$. Let $M = D_1(v_3) \cup D_1(v_5) \cup M_e \subset D_{3,\Delta}$, where*

$$M_e = \{\xi^T_{1,2,0}, \xi^T_{2,1,0}, \xi^T_{3,0,0}, \xi^T_{2,0,1}\}.$$

Then M is a stable minimal determining set for the space $\mathbb{P}_3$ of cubic polynomials regarded as a subspace of $S_3^0(\Delta)$.

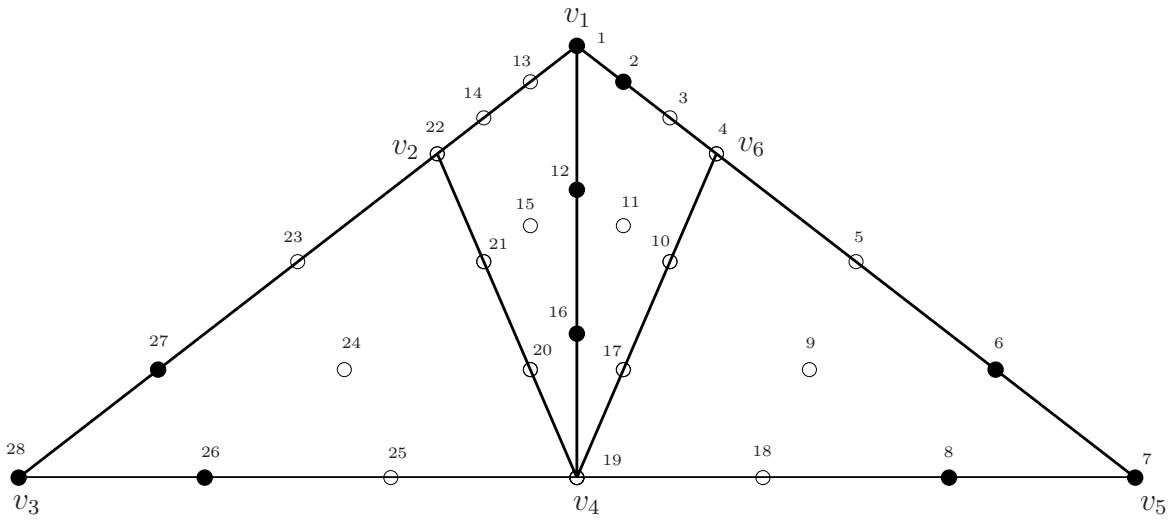

Figure 5.7: Triangulation of Lemma 5.7, where the minimal determining set M is indicated by filled circles.

Proof. The lemma follows from a more general statement given in [54, Lemma 4.1]. We provide a (somewhat different) proof in order to work out explicit formulas for the B-coefficients. We see that $\#M = \dim \mathbb{P}_3 = 10$. Hence we only need to show that if we set the coefficients of $s \in \mathbb{P}_3$ corresponding to $\xi \in M$, then all other

coefficients are stably determined. Suppose the coefficients of s are numbered as in Figure 5.7. Then using the C^1 smoothness across the common edge $\langle v_1, v_4\rangle$ of two triangle $T_1 = \langle v_2, v_4, v_1\rangle$ and $T_2 = \langle v_6, v_1, v_4\rangle$, where the barycentric coordinates of v_6 relative to T_1 are given by $(-1, \frac{1}{2}, \frac{3}{2})$, we obtain

$$C_{13} = \tfrac{1}{2}C_{12} + \tfrac{3}{2}C_1 - C_2.$$

By using the univariate C^1, C^2 and C^3 smoothness conditions along the edge $\langle v_1, v_3\rangle$, where the barycentric coordinates of v_3 relative to $\langle v_1, v_2\rangle$ are given by $(-3, 4)$ and solving the linear system involving the three equations, we obtain

$$\begin{aligned}
C_{14} &= -\tfrac{9}{16}C_1 - \tfrac{1}{48}C_{28} + \tfrac{3}{2}C_{13} + \tfrac{1}{12}C_{27},\\
C_{23} &= -\tfrac{27}{16}C_1 - \tfrac{1}{16}C_{28} + \tfrac{9}{4}C_{13} + \tfrac{1}{2}C_{27},\\
C_{22} &= -\tfrac{27}{32}C_1 - \tfrac{1}{32}C_{28} + \tfrac{27}{16}C_{13} + \tfrac{3}{16}C_{27}.
\end{aligned}$$

By symmetry, similar formulas hold for C_3, C_4 and C_5, and by using the univariate C^1, C^2 and C^3 smoothness conditions along the edge $\langle v_3, v_5\rangle$ and solving the corresponding linear system, we get the formulas

$$\begin{aligned}
C_{25} &= -\tfrac{1}{4}C_{28} - \tfrac{1}{4}C_7 + C_{26} + \tfrac{1}{2}C_8,\\
C_{18} &= -\tfrac{1}{4}C_{28} - \tfrac{1}{4}C_7 + \tfrac{1}{2}C_{26} + C_8,\\
C_{19} &= -\tfrac{1}{4}C_{28} - \tfrac{1}{4}C_7 + \tfrac{3}{4}C_{26} + \tfrac{3}{4}C_8.
\end{aligned}$$

In the next step we compute C_{20} and C_{17} by C^1 smoothness conditions across edges $\langle v_2, v_4\rangle$ and $\langle v_4, v_6\rangle$, respectively,

$$C_{20} = \tfrac{1}{4}C_{25} + \tfrac{3}{4}C_{16}, \quad C_{17} = \tfrac{1}{4}C_{18} + \tfrac{3}{4}C_{16}.$$

By the C^1 and C^2 smoothness conditions across the edge $\langle v_1, v_4\rangle$, as well as the C^2 smoothness conditions across the edges $\langle v_2, v_4\rangle$ and $\langle v_4, v_6\rangle$, we obtain the

system of equations

$$\begin{aligned}
C_{11} &= -C_{15} + \tfrac{1}{2}C_{16} + \tfrac{3}{2}C_{12},\\
C_{10} &= C_{21} - C_{20} - 3C_{15} + \tfrac{1}{4}C_{19} + \tfrac{3}{2}C_{16} + \tfrac{9}{4}C_{12},\\
C_{26} &= 9C_{12} - 24C_{15} + 16C_{21},\\
C_{8} &= 16C_{12} - 24C_{11} + 9C_{10},
\end{aligned}$$

which can be solved with respect to C_{10}, C_{11}, C_{15} and C_{21} to give

$$\begin{aligned}
C_{10} &= -\tfrac{1}{7}C_8 + C_{12} + \tfrac{12}{7}C_{16} + \tfrac{4}{7}C_{19} - \tfrac{16}{7}C_{20} + \tfrac{1}{7}C_{26},\\
C_{11} &= -\tfrac{2}{21}C_8 + \tfrac{25}{24}C_{12} + \tfrac{9}{14}C_{16} + \tfrac{3}{14}C_{19} - \tfrac{6}{7}C_{20} + \tfrac{3}{56}C_{26},\\
C_{15} &= \tfrac{2}{21}C_8 + \tfrac{11}{24}C_{12} - \tfrac{1}{7}C_{16} - \tfrac{3}{14}C_{19} + \tfrac{6}{7}C_{20} - \tfrac{3}{56}C_{26},\\
C_{21} &= \tfrac{1}{7}C_8 + \tfrac{1}{8}C_{12} - \tfrac{3}{14}C_{16} - \tfrac{9}{28}C_{19} + \tfrac{9}{7}C_{20} - \tfrac{1}{56}C_{26}.
\end{aligned}$$

Finally, using C^1 smoothness across the edges $\langle v_4, v_6\rangle$ and $\langle v_2, v_4\rangle$, we get

$$C_9 = -3C_{11} + 4C_{10}, \quad C_{24} = -3C_{15} + 4C_{21},$$

which completes the proof that M is a determining set for $\mathbb{P}_3$. The stability is again obvious in view of the explicit formulas used. □

Proof of Theorem 5.2. To see that M_n is a stable minimal determining set, we show that we can set the coefficients $\{c_\xi\}_{\xi\in M_n}$ of a spline $s \in S_n$ to arbitrary values, and that all other coefficients of s are then uniquely and stably determined.

First, we show how the coefficients in $\mathcal{D}_{5,\Delta_n^*} \setminus M_n$ can be computed. For each $v \in \mathcal{V}_n \setminus \tilde{\mathcal{V}}_n$, using C^3 smoothness conditions at v and the coefficients corresponding to M_v, we can uniquely compute the coefficients of s corresponding to all domain points in $D_3(v)$ by [36, Lemma 5.10]. For each $v \in \tilde{\mathcal{V}}_n$, using the C^3 smoothness of $s|_{T_v^+}$ at v and the coefficients in $M_v \cap T_v^+$, we compute the coefficients of s corresponding to all domain points in $D_3(v) \cap T_v^+$. By using C^2 smoothness across the common edge e_v of T_v^+ and T_v^-, we can compute the coefficients corresponding to $D_2(v) \cap T_v^-$. Then by C^3 smoothness at v inside T_v^- and the coefficient

corresponding to the domain point $\xi^{\tilde{T}_v}_{2,3,0}$ inside T_v^- we can compute the remaining coefficients corresponding to all domain points in $R_3(v) \cap T_v^-$.

For each $e = \langle u, v\rangle \in \mathcal{E}_n \backslash \tilde{\mathcal{E}}_n$, using the coefficients corresponding to M_e, we now apply Lemma 5.7 to determine the coefficients of s corresponding to domain points in the disk $D_3(w_e)$, where w_e is the midpoint of e. Due to the C^3 smoothness at w_e, we can regard the coefficients of s in the disk as coefficients of a polynomial g of degree 3. Lemma 5.7 ensures that we can set the coefficients of s corresponding to domain points in M_e to arbitrary values, and that all coefficients corresponding to the remaining domain points in $D_3(w_e)$ are uniquely and stably determined.

For each $e = \langle u, v\rangle \in \tilde{\mathcal{E}}_n$, using the C^3 smoothness of $s|_{T_e^+}$ at the midpoint w_e of e and the coefficients corresponding to $\left\{\xi^{\hat{T}^3_e}_{3,2,0}, \xi^{\hat{T}^3_e}_{2,3,0}, \xi^{\hat{T}^3_e}_{2,2,1}, \xi^{\hat{T}^3_e}_{1,4,0}\right\}$ inside T_e^+ we can compute the coefficients of s corresponding to domain points in the disk $D_3(w_e) \cap T_e^+$ by Lemma 5.7 as described previously. Using the C^2 smoothness across the common edge e of T_e^+ and T_e^- we can compute the coefficients corresponding to $D_2(w_e) \cap T_e^-$. Then using the C^3 smoothness condition supported inside T_e^- and the coefficient corresponding to the point $\xi^{\tilde{T}_e}_{2,3,0}$ we can compute the remaining coefficients corresponding to domain points in $R_3(w_e) \cap T_e^-$. For each type-1 edge $e = \langle u, v\rangle$, by taking account of the C^3 smoothness across the edge $e = \langle u, v\rangle$ we can now compute the three central coefficients in the ring $R_4(v)$. Note that in practice these coefficients can be more conveniently computed by using C^1 smoothness conditions across the edges of the form $\langle w_i, w_{i+1}\rangle$, see Remark 5.8.

We now show that the coefficients corresponding to the remaining domain points are uniquely determined. These remaining domain points lie inside triangles of the form $T = \langle w_1, w_2, w_3\rangle$, where $w_i \in \mathcal{W}_n$. Let T_{PS6} be the Powell-Sabin-6 split of T, see Figure 5.5. We have already determined all coefficients corresponding to domain points in the disks $D_3(w_i)$ for $i = 1, 2, 3$. Now we can apply Lemma 5.5 to uniquely and stably determine all coefficients of s corresponding to the remaining domain points in T.

We have thus shown that M is a determining set for S_n. To complete the proof,

we need to show that the six central C^1, C^2 smoothness conditions across the edges $\langle w_i, w_{i+1}\rangle$, $i = 1, 2, 3$ are satisfied. Indeed, all other smoothness conditions are either used in the above computation or are satisfied in view of Lemmas 5.5 and 5.7.

To check these conditions we will only look at the section $\langle v_1, w_3, v_T, w_2\rangle$ of the triangle $T = \langle v_1, v_2, v_3\rangle$ as shown in Figure 5.8, where we indicate the domain points of the 5×7 grid around u_1 by double integer indices (i, j) with the origin $(0, 0)$ at u_1 and the row of indices with $j = 0$ on the edge $\langle w_2, w_3\rangle$. The coefficient corresponding to (i, j) is denoted by $C_{i,j}$. All smoothness conditions that need verification are supported within this grid. The smoothness conditions on the other two sections of the triangle can be checked in the same way.

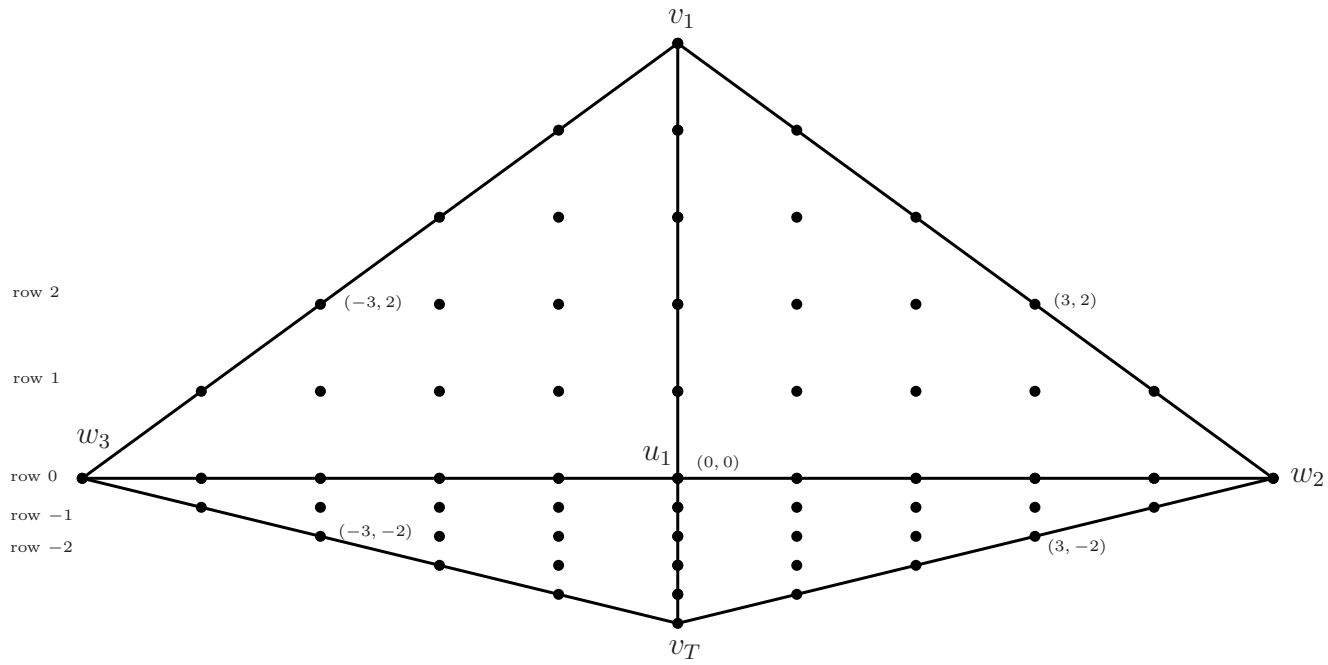

Figure 5.8: The 5×7 grid around u_1.

Let (γ, β, δ) be the barycentric coordinates of v_T relative to $\langle v_1, w_3, u_1\rangle$. Thus $\beta = 0$ and $v_T = \gamma v_1 + \delta u_1$ where $\gamma = -\frac{1}{3}$ and $\delta = \frac{4}{3}$. We first write down the

known C^1, C^2 and C^3 smoothness conditions in rows $j = -2, -1, 0, 1, 2$ of the grid,

$$\begin{aligned} C_{3,j} &= 8C_{0,j} - 12C_{-1,j} + 6C_{-2,j} - C_{-3,j}, \\ C_{2,j} &= 4C_{0,j} - 4C_{-1,j} + C_{-2,j}, \\ C_{1,j} &= 2C_{0,j} - C_{-1,j}. \end{aligned}$$

By solving this linear system for $C_{-1,j}, C_{0,j}, C_{1,j}$, we obtain for $j = -2, -1, 0, 1, 2$

$$C_{-1,j} = \tfrac{1}{4}(2C_{2,j} - C_{3,j} + 4C_{-2,j} - C_{-3,j}), \tag{5.3.1}$$

$$C_{0,j} = \tfrac{1}{4}(3C_{2,j} - C_{3,j} + 3C_{-2,j} - C_{-3,j}), \tag{5.3.2}$$

$$C_{1,j} = C_{2,j} - \tfrac{1}{4}C_{3,j} + \tfrac{1}{2}C_{-2,j} - \tfrac{1}{4}C_{-3,j}. \tag{5.3.3}$$

We write down the four known C^1 smoothness conditions across row 0 of the grid

$$C_{i,-1} = \gamma C_{i,1} + \delta C_{i,0}, \quad i = -3, -2, 2, 3. \tag{5.3.4}$$

By replacing $C_{-3,-1}, C_{-2,-1}, C_{2,-1}, C_{3,-1}$ in (5.3.1)–(5.3.3) with expressions in (5.3.4) and collecting the terms with coefficients γ and δ, we obtain

$$C_{i,-1} = \gamma C_{i,1} + \delta C_{i,0}, \quad i = -1, 0, 1,$$

which confirms the three remaining C^1 smoothness conditions across row 0. Similarly, by replacing $C_{3,2}, C_{2,2}, C_{-2,2}, C_{-3,2}$ in (5.3.1)–(5.3.3) with expressions in the four known C^2 smoothness conditions across row 0,

$$C_{i,2} = \gamma^2 C_{i,0} + 2\gamma\delta C_{i,-1} + \delta^2 C_{i,-2}, \quad i = -3, -2, 2, 3,$$

we verify the three remaining C^2 smoothness conditions across row 0,

$$C_{i,2} = \gamma^2 C_{i,0} + 2\gamma\delta C_{i,-1} + \delta^2 C_{i,-2}, \quad i = -1, 0, 1.$$

We have shown that M_n is a stable local minimal determining set for S_n. Hence, the dimension of S_n is equal to the cardinality of M_n, which is easily seen to be the number in (5.2.1). □

Since M_n is a minimal determing set for S_n, a basis can be constructed for S_n. Let $\{\gamma_\xi\}_{\xi\in M_n}$ be the linear functionals such that γ_ξ applied to S_n gives the B-coefficients C_ξ. Then the so-called M_n-basis $\Psi_n = \{\psi_\xi\}_{\xi\in M_n}$ for S_n can be defined uniquely using the conditions

$$\gamma_\eta\psi_\xi = \begin{cases} 1, & \xi = \eta, \\ 0, & \text{otherwise}, \end{cases}$$

for all $\xi, \eta \in M_n$. Moreover M_n is stable and local, it follows from [36, Theorem 5.21] that Ψ_n is a stable local basis for S_n.

Remark 5.8. Note that in practice the three central coefficients in the ring $R_4(v_1)$ are more conveniently computed by using C^1 smoothness conditions across the edge $\langle w_3, w_2\rangle$ rather than by C^1, C^2 and C^3 smoothness conditions across $\langle v_1, u_1\rangle$ according to the above proof. Indeed, in the notation of Figure 5.8 these coefficients are given by

$$C_{-1,1} = 4C_{-1,0} - 3C_{-1,-1}, \quad C_{0,1} = 4C_{0,0} - 3C_{0,-1}, \quad C_{1,1} = 4C_{1,0} - 3C_{1,-1}.$$

5.4 A nodal minimal determining set for S_n

As usual for macro-element spaces, we provide a stable nodal minimal determining set for S_n and an error bound for the corresponding Hermite interpolation operator.

Recall that a linear functional λ is called a *nodal functional* provided that λf is a combination of values and/or derivatives of f at some point η. A collection $\mathcal{N} = \{\lambda\}_{i=1}^N$ is called a *nodal determining set* for a spline space S if $\lambda s = 0$ for all $\lambda \in \mathcal{N}$ implies $s \equiv 0$. Moreover, $\mathcal{N}$ is called a *nodal minimal determining set* (NMDS) for S if there is no smaller nodal determining set.

Let (u_x, u_y) and (v_x, v_y) be the Cartesian coordinates of u and v, respectively. Then the directional derivative of s at $(x, y) \in T$ with respect to the (directed) edge e is given by

$$D_e s(x, y) = (v_x - u_x)D_x s(x, y) + (v_y - u_y)D_y s(x, y).$$

Let $e^\perp$ be the directed segment obtained rotating e ninety degrees in the counterclockwise direction. We write $D_{e^\perp}s$ for the directional derivative of s associated with $e^\perp$. The linear functional evaluating at $\xi \in \Omega$ any function f continuous at ξ will be denoted by δ_ξ.

Lemma 5.9. *Let Δ be the triangulation shown in Figure 5.7, where $v_4 = (v_3 + v_5)/2$, $v_2 = (3v_1 + v_3)/4$ and $v_6 = (3v_1 + v_5)/4$. The set*

$$\mathcal{N} = \mathcal{N}_{v_3} \cup \mathcal{N}_{v_4} \cup \mathcal{N}_{v_5}$$

is a nodal determining set for $\mathbb{P}_3$, where

1) $\mathcal{N}_{v_3} = \{\delta_{v_3}, \delta_{v_3}D_x, \delta_{v_3}D_y\}$,

2) $\mathcal{N}_{v_5} = \{\delta_{v_5}, \delta_{v_5}D_x, \delta_{v_5}D_y\}$,

3) $\mathcal{N}_{v_4} = \{\delta_{v_4}D_{e_1}, \delta_{v_4}D_{e_1}^2, \delta_{v_4}D_{e_2}D_{e_1}^2, \delta_{v_4}D_{e_1}^3\}$,

with $e_1 := \langle v_4, v_1\rangle$ and $e_2 := \langle v_4, v_5\rangle$.

Proof. It is clear that the cardinality of $\mathcal{N}$ is equal to the dimension of $\mathbb{P}_3$. Thus to prove that $\mathcal{N}$ is a nodal minimal determining set, we just need to show that given the values of $\{\lambda s\}_{\lambda\in\mathcal{N}}$ all B-coefficients of $s \in \mathbb{P}_3$ can be determined. Suppose the coefficients of $s \in \mathbb{P}_3$ are numbered as in Figure 5.7. Using the data $\{\delta_{v_3}s, \delta_{v_3}D_xs, \delta_{v_3}D_ys\}$ at v_3 we can compute the coefficients C_{26}, C_{27} and C_{28} by [36, Theorem 2.19]. Similarly, using the data $\{\delta_{v_5}s, \delta_{v_5}D_xs, \delta_{v_5}D_ys\}$ at v_5 we compute the coefficients C_6, C_7 and C_8. Using the data $\{\delta_{v_4}D_{e_1}s, \delta_{v_4}D_{e_1}^2s, \delta_{v_4}D_{e_1}^3s\}$ we can compute the coefficients C_{16}, C_{12} and C_1 by [36, Theorem 2.15], that is, using the formulas

$$\begin{aligned}
\delta_{v_4}D_{e_1}s &= -3C_{19} + 3C_{16},\\
\delta_{v_4}D_{e_1}^2s &= 6C_{19} - 12C_{16} + 6C_{12},\\
\delta_{v_4}D_{e_1}^3s &= -6C_{19} + 18C_{16} - 18C_{12} + 6C_1,
\end{aligned}$$

where C_{19} can be computed using the three univariate smoothness conditions along the edge $\langle v_3, v_5\rangle$ as in the proof of Lemma 5.7.

Let $e = \langle v_4, v_6\rangle$. Since $v_6 - v_4 = \frac{1}{4}(v_5 - v_4) + \frac{3}{4}(v_1 - v_4)$, according to [36, (2.36)], we can use the data $\delta_{v_4} D_{e_2} D_{e_1}^2 s$ to compute the coefficient C_2 from the relation

$$\frac{1}{4}\delta_{v_4} D_{e_2} D_{e_1}^2 s + \frac{3}{4}\delta_{v_4} D_{e_1}^3 s = \delta_{v_4} D_e D_{e_1}^2 s = -6C_{19} + 12C_{16} + 6C_{12} + 12C_{11} - 6C_{17} - 6C_2,$$

where the coefficients C_{11} and C_{17} are computed as in the proof of Lemma 5.7.

At this point we have determined all coefficients corresponding to domain points in the minimal determining set M of Lemma 5.7, and it follows from that lemma that all other coefficients are also determined. □

Theorem 5.10. *The set*

$$\mathcal{N}_n = \bigcup_{v\in\mathcal{V}_n\setminus\tilde{\mathcal{V}}_n} \mathcal{N}_v \cup \bigcup_{v\in\tilde{\mathcal{V}}_n} \tilde{\mathcal{N}}_v \cup \bigcup_{e\in\mathcal{E}_n\setminus\tilde{\mathcal{E}}_n} \mathcal{N}_e \cup \bigcup_{e\in\tilde{\mathcal{E}}_n} \tilde{\mathcal{N}}_e$$

is a nodal minimal determining set for S_n, where

1) $\mathcal{N}_v = \{\delta_v D_x^\alpha D_y^\beta,\ 0 \le \alpha + \beta \le 3\}$,

2) $\tilde{\mathcal{N}}_v = \{\delta_v D_{e_v}^\alpha D_{e_v^\perp}^\beta,\ 0 \le \alpha + \beta \le 3,\ \beta \le 2\} \cup \{\delta_v^+ D_{e_v^\perp}^3, \delta_v^- D_{e_v^\perp}^3\}$,

3) $\mathcal{N}_e = \{\delta_{w_e} D_{e^\perp}, \delta_{w_e} D_{e^\perp}^2, \delta_{w_e} D_e D_{e^\perp}^2, \delta_{w_e} D_{e^\perp}^3\}$,

4) $\tilde{\mathcal{N}}_e = \{\delta_{w_e} D_{e^\perp}, \delta_{w_e} D_{e^\perp}^2, \delta_{w_e} D_e D_{e^\perp}^2, \delta_{w_e}^+ D_{e^\perp}^3, \delta_{w_e}^- D_{e^\perp}^3\}$,

where $\delta_v^\pm f := \delta_v(f|_{T_v^\pm})$ *and* $\delta_{w_e}^\pm f := \delta_{w_e}(f|_{T_e^\pm})$, *and* w_e *denotes the midpoint of the edge* e.

Proof. It is clear that the cardinality of $\mathcal{N}_n$ is equal to the dimension of S_n as given in (5.2.1). Thus to prove that $\mathcal{N}_n$ is a nodal minimal determining set, we just need to show that given the values of $\{\lambda s\}_{\lambda\in\mathcal{N}_n}$ all B-coefficients of $s \in S_n$ can be determined.

For every vertex $v \in \mathcal{V}_n \setminus \tilde{\mathcal{V}}_n$, we can compute all coefficients corresponding to domain points in the disk $D_3(v)$ directly from the data in $\mathcal{N}_v$ by [36, Theorem 2.19].

For every vertex $v \in \tilde{\mathcal{V}}_n$, we can compute all the coefficients of s corresponding to domain points in the disk $D_3(v)$ from the data in $\tilde{\mathcal{N}}_v$. That is, using the data $\{\delta_v D_{e_v}^{\alpha} D_{e_v^{\perp}}^{\beta} s,\ 0 \le \alpha+\beta \le 3,\ \beta \le 2\} \cup \{\delta_v^+ D_{e_v^{\perp}}^3 s\}$, we can compute the coefficients corresponding to domain points in $D_3(v) \cap T_v^+$ by [36, Theorem 2.19]. Then using the coefficients corresponding to domain points in $D_3(v) \cap T_v^+$ and C^2 smoothness conditions across the edge e_v, we can compute the coefficients corresponding to domain points in $D_2(v) \cap T_v^-$. Now using the data $\{\delta_v^- D_{e_v^{\perp}}^3 s\}$ and C^3 smoothness conditions inside T_v^-, we can compute all the remaining coefficients corresponding to domain points in $R_3(v) \cap T_v^-$.

Given an edge $e = \langle v', v'' \rangle$ in $\mathcal{E}_n \backslash \tilde{\mathcal{E}}_n$, let w_e be its midpoint. We now compute all coefficients of s corresponding to domain points in $D_3(w_e)$. By the C^3 smoothness at w_e, as in the proof of Theorem 5.2, these coefficients can be regarded as the coefficients of a polynomial g of degree 3. Hence, it follows from Lemma 5.9 that all B-coefficients in $D_3(w_e)$ are determined by the known B-coefficients in the sets $D_3(w_e) \cap D_3(v')$ and $D_3(w_e) \cap D_3(v'')$ and the nodal data in $\mathcal{N}_e$.

Given an edge e in $\tilde{\mathcal{E}}_n$, we can compute the coefficients of s corresponding to the domain points in the disk $D_3(w_e)$ from the data in $\tilde{\mathcal{N}}_e$. That is, using the data $\{\delta_{w_e} D_{e^{\perp}} s, \delta_{w_e} D_e D_{e^{\perp}}^2 s, \delta_{w_e} D_{e^{\perp}}^2 s, \delta_{w_e}^+ D_{e^{\perp}}^3 s\}$, we can compute the B-coefficients corresponding to $D_3(w_e) \cap T_e^+$ using the same argument as above. Then using the coefficients corresponding to domain points in $D_3(w_e) \cap T_e^+$, and C^2 smoothness conditions across the edge e we can compute all the coefficients corresponding to domain points in $D_2(w_e) \cap T_e^-$. Finally, using $\{\delta_{w_e}^- D_{e^{\perp}}^3 s\}$ and C^3 smoothness conditions inside T_e^- we can compute all the remaining coefficients corresponding to domain points in $R_3(w_e) \cap T_e^-$. At this point we have determined all coefficients corresponding to domain points in the minimal determining set M_n of Theorem 5.2, and it follows from that theorem that all other coefficients are also determined. □

Corollary 5.11. *The set*

$$\mathcal{N} = \mathcal{N}_v \cup \mathcal{N}_e$$

is a nodal minimal determining set for $S(T_{PS12})$, where

1) $\mathcal{N}_v = \bigcup_{i=1}^3 \{\delta_{v_i} D_x^\alpha D_y^\beta,\ 0 \le \alpha+\beta \le 3\}$,

2) $\mathcal{N}_e = \bigcup_{i=1}^3 \left\{\delta_{w_{e_i}} D_{e_i^\perp}, \delta_{w_{e_i}} D_{e_i} D_{e_i^\perp}^2, \delta_{w_{e_i}} D_{e_i^\perp}^2, \delta_{w_{e_i}} D_{e_i^\perp}^3\right\}$,

v_i are the three vertices of T, $e_1 := \langle v_1, v_2\rangle$, $e_2 := \langle v_2, v_3\rangle$, $e_3 := \langle v_3, v_1\rangle$ and w_{e_i} denotes the midpoint of e_i.

By Theorem 5.10 for any function $f \in C^3(\Omega)$ and any $n = 0, 1, \ldots$, there exists a unique spline $s_n(f) \in S_n$ that solves the Hermite interpolation problem

$$\lambda s = \lambda f, \quad \lambda \in \mathcal{N}_n.$$

Given a triangle $T \in \Delta_n$ and a domain point $\xi \in T$ of $s_n(f)$, it is easy to see that if the coefficient c_ξ of $s_n(f)$ is computed from the derivatives as in the proof of Theorem 5.10, then

$$|c_\xi| \le K_1 \sum_{\nu=0}^{3} \operatorname{diam}(T)^\nu |f|_{W_\infty^\nu(T)}, \tag{5.4.1}$$

where K_1 is a constant depending only on the smallest angle in Δ_n. Since the computation of all other coefficients from the smoothness conditions is a stable process, it follows that (5.4.1) holds for all domain points ξ lying in T. Since the Bernstein basis polynomials form a partition of unity, (5.4.1) implies that

$$\|s_n(f)\|_{L_\infty(T)} \le K_1 \sum_{\nu=0}^{3} \operatorname{diam}(T)^\nu |f|_{W_\infty^\nu(T)}.$$

This verifies the stability of nodal minimal determining set $\mathcal{N}_n$.

The following error bound follows immediately by [36, Theorem 5.26] if we take into account that the uniform refinement used to generate the triangulation Δ_n halves the diameters of the triangles.

Theorem 5.12. *For every $f \in C^r(\Omega)$, with $3 \le r \le 6$,*

$$|f - s_n(f)|_{W_\infty^k(\Omega)} \le \frac{K}{2^{n(r-k)}} |f|_{W_\infty^r(\Omega)},$$

for all $0 \le k < r$, where K depends only on the maximum diameter and the smallest angle of the triangles of the initial triangulation Δ_0, and $|\cdot|_{W_\infty^r(\Omega)}$ denotes the standard Sobolev seminorm on Ω.

The nodal NMDS $\mathcal{N}_n$ of Theorem 5.10 provides another stable local basis for S_n, see pp. 144 and 491 of [36], in the sense of definition of Section 1.3.2. The basis $\Phi_n = \{\phi_j^{(n)}\}_{j=1}^{\#\mathcal{N}_n}$ is defined uniquely using the duality

$$\lambda_i \phi_j^{(n)} = \begin{cases} 1, & i = j, \\ 0, & \text{otherwise}, \end{cases}$$

where $\lambda_i \in \mathcal{N}_n$ and $i, j = 1, \ldots, \#\mathcal{N}_n$.

Now we write the nodal determining set $\mathcal{N}_n$ in a slightly different way. We set

$$\hat{\mathcal{V}}_n = (\mathcal{V}_n \cap \partial\Omega) \setminus \mathcal{V}_0, \quad n = 1, 2, \ldots.$$

For any $v \in \bigcup_{n\in\mathbb{N}} \hat{\mathcal{V}}_n$, let $n_v := \min\{n : v \in \hat{\mathcal{V}}_n\}$. Clearly, for any $v \in \hat{\mathcal{V}}_n$ there is a unique edge $\hat{e}_v \in \xi_{n_v-1} \setminus \tilde{\xi}_{n_v-1}$ such that v lies at the midpoint of $\hat{e}_v$. Let

$$\hat{\mathcal{N}}_v = \{\delta_v D^{\alpha}_{\hat{e}_v} D^{\beta}_{\hat{e}_v^{\perp}},\ 0 \le \alpha + \beta \le 3\}.$$

Then it can be easily checked that the set

$$\widehat{\mathcal{N}}_n = \bigcup_{v\in\mathcal{V}_0} \mathcal{N}_v \cup \bigcup_{v\in\hat{\mathcal{V}}_n} \hat{\mathcal{N}}_v \cup \bigcup_{v\in\tilde{\mathcal{V}}_n} \tilde{\mathcal{N}}_v \cup \bigcup_{e\in\mathcal{E}_n\setminus\tilde{\mathcal{E}}_n} \mathcal{N}_e \cup \bigcup_{e\in\tilde{\mathcal{E}}_n} \tilde{\mathcal{N}}_e$$

is also a stable local nodal determining set for S_n. Moreover, the nodal determining sets $\widehat{\mathcal{N}}_n$ are nested, that is, $\widehat{\mathcal{N}}_n \subset \widehat{\mathcal{N}}_{n+1}$, $n = 0, 1, 2, \ldots$. We now construct the hierarchical basis $\mathcal{B}_n$ by

$$\mathcal{B}_n = \tilde{\Phi}_0 \cup \tilde{\Phi}_1 \cup \cdots \cup \tilde{\Phi}_n, \quad \tilde{\Phi}_0 = \Phi_0$$

where $\tilde{\Phi}_k = \{\phi_j^{(k)}, j = \#\widehat{\mathcal{N}}_{k-1} + 1, \cdots, \#\widehat{\mathcal{N}}_k\}$ is the set of all those nodal basis functions from Φ_k corresponding to nodal minimal determing set $\widehat{\mathcal{N}}_k$ on Δ_k not yet used on Δ_{k-1} for $k = 1, 2, \ldots n$.

Remark 5.13. In developing the macroelement spaces of this chapter, we have used P. Alfeld's software for examining determining set for the spline spaces, available from `http://www.math.utah.edu/~alfeld`.

Chapter 6

Conclusions and Future Work

In this thesis, we investigated the construction of stable local bases for refinable spaces of spline functions on Powell-Sabin 12 triangulations. Here we would like to give a brief overview of our studies.

In Chapter 2, we proved that functions in subspaces of smooth splines $S_d^r(\Delta)$ possessing stable local bases satisfy a Bernstein type inequality. Furthermore, we established the Jackson inequality for macro-element spline spaces. We then proceed to present the general theory on hierarchical bases of Lagrange type to give rise to Riesz bases for Sobolev spaces $H^s(\Omega)$ and $H_0^s(\Omega)$. In the last part of this chapter, we reviewed the known C^1 macro-element spaces where Lagrange hierarchical bases were constructed. We also proved that the sequence of nested triangulations suggested in [21] is quasi-uniform. These results are published in the paper [23].

Then, in Chapter 3, we constructed Lagrange hierarchical bases for refinable C^1 piecewise quadratic polynomials on combination of Powell-Sabin 6 and Powell-Sabin 12 triangulations. Under the guidance of general theory established in Chapter 2, we proved that the hierarchical bases are stable for a larger range of Sobolev spaces $H^s(\Omega)$ and $H_0^s(\Omega)$ than the hierarchical basis of Hermite type and the wavelet type bases of [33] for the same spline space.

Chapter 4 was devoted to the applications of the hierarchical bases we con-

structed in Chapter 3. We formulated two test functions to demonstrate the performance of our bases in surface compression. We numerically compared the compression results based on the Lagrange hierarchical basis and Hermite hierarchical basis. Numerical results show that Lagrange hierarchical basis has an advantage over Hermite hierarchical basis in compressing surfaces. The second part of this chapter is devoted to solving the biharmonic equation. We numerically compared the hierarchical basis preconditioners and the BPX preconditioners based on both Hermite and Lagrange bases.

In Chapter 5 we presented a new construction of refinable C^2 spline spaces of degree 5 on Powell-Sabin-12 triangulations. We proved that the refinable spaces have stable local minimal determining sets which will lead to a stable local basis. Furthermore, we show that the spaces have nodal minimal determining sets. This leads to a stable local basis of Hermite type. At the end, we also provide the error bounds for the corresponding Hermite interpolation operators. These results are published in the paper [24]. We also constructed a hierarchical basis for the refinable spaces.

In terms of future work, we would like to address the following topics:

- We would like to extend the results of Chapter 3 to multilevel spline bases which would give rise to a larger range of stability for $H^s(\Omega)$. In particular, we are interested to construct a projection operator such that the range of stability of the corresponding bases can be extended to include $H^0(\Omega) = L_2(\Omega)$.

- It would also be interesting to investigate the use of our multilevel bases in the numerical solutions of fractional order elliptic PDEs. In particular, if the energy space of the variational formulation is the fractional Sobolev spaces $H^s(\Omega)$ for $3/2 < s < 2$, in 2D, then our hierarchical bases are stable in this range and hence they are suitable to be used as preconditioners for these type of problems. Recall that neither C^0 nor C^1 Hermite hierarchical bases

are stable for $H^s(\Omega),\ 3/2 < s < 2$.

- We have seen several constructions that generate Riesz bases for Sobolev spaces, see [21, 41, 33]. It would be interesting to implement the hierarchical bases of [21, 41] and the wavelet bases of [33] and to compare all these methods numerically. These multilevel bases might be useful for surface compression which is also interesting to investigate.

- Another interesting task is to implement the refinable C^2 macro-element spaces constructed in Chapter 5 and investigate the use of the corresponding multilevel bases for surface compression and numerical PDEs.

- Finally, we would also like to extend the results of Chapter 5 to macro-element spaces of higher smoothness.

Bibliography

[1] R. A. Adams and J. J. F. Fournier. *Sobolev Spaces, Second Edition*. Elsevier, 2003.

[2] P. Alfeld, L. Schumaker, and T. Sorokina. Two condensed macro-elements with full approximation power. Adv. Comput. Math., 32:381–391, 2010.

[3] J. Bergh and J. Löfström. *Interpolation Spaces: An Introduction*. Springer-Verlag, New York, 1976.

[4] H. Blum and R. Rannacher. On the boundary value problem of the biharmonic operator on domains with angular corners. Math. Mech. Appl. Sci, 2:556–581, 1980.

[5] J. Bramble. Interpolation between Sobolev spaces in Lipschitz domains with an application to multigrid theory. *Math. Comp.*, 64:1359–1365, 1995.

[6] J. H. Bramble, J. E. Pasciak, and J. Xu. Parallel multilevel preconditioners. Math. Comp., 55:1–22, 1990.

[7] S. C. Brenner and L. R. Scott. *The Mathematical Theory of Finite Element Methods, Third Edition*. Springer-Verlag, New York, 2008.

[8] P. L. Butzer and K. Scherer. *Approximationsprozesse und Interpolationsmethoden*. Bibliographisches Institut, Mannheim, 1968.

[9] C. K. Chui and T. X. He. Bivariate C^1 quadratic finite elements and vertex splines. Math. Comput, 54:169–187, 1990.

[10] E. Cohen, T. Lyche, and R. F. Riesenfeld. A B-Spline-Like basis for the Powell-Sabin 12-Split based on simplex splines. Math. Comput, 82:1667–1707, 2013.

[11] M. Daehlen, T. Lyche, and H-P. Seidel K. Morken, R. Schneider. Multiresolution analysis over triangles, based on quadratic Hermite interpolation. J. Comput. Appl. Math., 119:97–114, 2000.

[12] W. Dahmen. Multiscale analysis, approximation and interpolation spaces. In Charles K. Chui and Larry L. Schumaker (eds), editors, *Approximation Theory VIII, Vol. 2: Wavelets and Multilevel Approximation*, pages 47–88. World Scientific Publishing, 1995.

[13] W. Dahmen. Stability of multiscale transformations. *J. Fourier. Anal. Appl.*, 2:341–361, 1996.

[14] W. Dahmen, P. Oswald, and X.-Q. Shi. C^1-hierarchical bases. *J. Comput. Appl. Math.*, 51:37–56, 1994.

[15] W. Dahmen and P. Petrushev. "push-the-error" algorithm for nonlinear n-term approximation. *Constr. Approx.*, 23:261–304, 2006.

[16] O. Davydov. Stable local bases for multivariate spline spaces. *J. Approx. Theory*, 111:267–297, 2001.

[17] O. Davydov. Locally stable spline bases on nested triangulations. In L. L. Schumaker C. K. Chui and Eds. J. Stöckler, editors, *Approximation Theory X: Wavelets, Splines, and Applications*, pages 231–240. Vanderbilt University Press, 2002.

[18] O. Davydov. Smooth finite elements and stable splitting. In *Berichte "Reihe Mathematik" der Philipps-Universität Marburg*, pages 2007–4, 2007. An adapted version of this article has appeared as Section 4.2.6 "Smooth FEs

on polyhedral domains" of the book K. Böhmer, Numerical Methods for Nonlinear Elliptic Differential Equations: A Synopsis, Oxford University Press, Oxford, 2010.

[19] O. Davydov and P. Petrushev. Nonlinear approximation from differentiable piecewise polynomials. *SIAM J. Math. Anal.*, 35:708–758, 2003.

[20] O. Davydov and L. L. Schumaker. On stable local bases for bivariate polynomial spline spaces. *Constr. Approx.*, 18:87–116, 2002.

[21] O. Davydov and R. Stevenson. Hierarchical Riesz bases for $H^s(\Omega)$, $1 < s < \frac{5}{2}$. *Constr. Approx.*, 22:365–394, 2005.

[22] O. Davydov and W. P. Yeo. C^1 piecewise quadratic hierarchical bases, in preparation.

[23] O. Davydov and W. P. Yeo. Macro-element hierarchical Riesz bases, to appear in MMCS2012 proceedings.

[24] O. Davydov and W. P. Yeo. Refinable C^2 piecewise quintic polynomials on Powell-Sabin-12 triangulations. *J. Comput. Appl. Math.*, 240:62–73, 2013.

[25] R. DeVore, B. Jawerth, and B. Lucier. Surface compression. *Comput. Aided Geom. Design.*, 9:219–239, 1992.

[26] Nira Dyn and Tom Lyche. A Hermite subdivision scheme for the evaluation of the Powell-Sabin 12-split element. In C. Chui and L.L. Schumaker (eds), editors, *in Approximation Theory IX*.

[27] E. H. Georgoulis and P. Houston. Discontinuous Galerkin methods for the biharmonic problem. IMA Journal of Numerical Analysis, 29:573–594, 2009.

[28] M. Gockenbach. *Understanding and implementing the finite element method.* Philadelphia, PA : Society for Industrial and Applied Mathematics, 2006.

[29] T. Goodman and D. Hardin. Refinable multivariate spline functions. In K.Jetter et al. Eds., editor, *Topics in Multivariate Approximation and Interpolation*, pages 55–83. Elsevier, 2006.

[30] M. Griebel. Multilevel algorithms considered as iterative methods on semidefinite systems. SIAM Journal on Scientific Computing, 15:547–565, 1994.

[31] P. Grisvard. *Elliptic Problems in Nonsmooth Domains*. Pitman, 1985.

[32] D. Hong and L. L. Schumaker. Surface compression using a basis of C^1 cubic bivariate spline spaces. Computing, 72:79–92, 2004.

[33] R. Q. Jia and S. T. Liu. C^1 spline wavelets on triangulations. *Math. Comp.*, 77:287–312, 2008.

[34] R. Q. Jia and W. Zhao. Riesz bases of wavelets and applications to numerical solutions of elliptic equations. *Math. Comp.*, 80:1525–1556, 2011.

[35] M. J. Lai and L. L. Schumaker. On the approximation power of bivariate splines. Adv. Comput. Math., 9:251–279, 1998.

[36] M. J. Lai and L. L. Schumaker. *Spline Functions on Triangulations*. Cambridge University Press, Cambridge, 2007.

[37] M. J. Lai and P. Wenston. On multilevel bases for elliptic boundary value problems. J. Comput. Appl. Math., 71:95–113, 1996.

[38] J. L. Lions and E. Magenes. *Non-homogeneous Boundary Value Problems and Applications, Vol. I.* Springer-Verlag, Berlin, 1972.

[39] R. Lorentz and P. Oswald. Multilevel finite element Riesz bases for Sobolev spaces. In Eds. P. Bjorstad et al., editor, *Domain Decomposition Methods in Science and Engineering: 9th International Conference*, pages 178–187, Bergen, Norway, 1997. Domain Decomposition Press.

[40] U. Luther. Representation, interpolation, and reiteration theorems for generalized approximation spaces. *Annali di Matematica*, 182:161–200, 2003.

[41] J. Maes and A. Bultheel. C^1 hierarchical Riesz bases of Lagrange type on Powell-Sabin triangulations. *J. Comp. Appl. Math.*, 196:1–19, 2006.

[42] J. Maes and A. Bultheel. Surface compression with hierarchical Powell-Sabin B-splines. *Int. J. Wav. Multires. Inf. Proc.*, 4:177–196, 2006.

[43] J. Maes and A. Bultheel. Powell-Sabin spline based multilevel preconditioners for the biharmonic equation. Applied Numerical Mathematics, 60:527–530, 2010.

[44] G. Nürnberger, L. L. Schumaker, and F. Zeilfelder. Local Lagrange interpolation by bivariate C^1 cubic splines. In T. Lyche and L.L. Schumaker (eds), editors, *in Mathematical Methods for Curves and Surfaces III: Oslo 2000*, pages 393–404. Vanderbilt University Press, 2001.

[45] G. Nürnberger, L. L. Schumaker, and F. Zeilfelder. Lagrange interpolation by C^1 cubic splines on triangulations of separable quadrangulations. In T.Lyche C.K.Chui and L.L. Schumaker (eds), editors, *in Approximation Theory X: Splines, Wavelets, and Applications*, pages 405–424. Vanderbilt University Press, 2002.

[46] G. Nürnberger, L. L. Schumaker, and F. Zeilfelder. Lagrange interpolation by C^1 cubic splines on triangulated quadrangulations. Adv. Comput. Math, 21:357–380, 2004.

[47] G. Nürnberger and F. Zeilfelder. Local Lagrange interpolation on Powell-Sabin triangulations and terrain modelling. In M. Reimer (eds) W. Haussmann, K. Jetter, editor, *Recent Progress in Multivariate Approximation*, pages 227–244. Birhäuser, 2001.

[48] P. Oswald. On function spaces related to finite element approximation theory. *Z. Anal. Anwendungen.*, 9:43–64, 1990.

[49] P. Oswald. Hierarchical conforming finite element methods for the biharmonic equation. *SIAM J. Numer. Anal.*, 29:1610–1625, 1992.

[50] P. Oswald. *Multilevel Finite Element Approximation: Theory and Applications.* Stuttgart: B.G. Teubner, 1994.

[51] P. Oswald. Frames and space splittings in Hilbert spaces, manuscript. 1997. `http://www.faculty.jacobs-university.de/poswald/bonn1.pdf`.

[52] P. Oswald. Multilevel frames and Riesz bases in Sobolev spaces, manuscript. 1998. `http://www.faculty.jacobs-university.de/poswald/bonn2.pdf`.

[53] M. J. D. Powell and M. A. Sabin. Piecewise quadratic approximations on triangles. ACM Trans. on Math. Software, 3:316–325, 1977.

[54] L. L. Schumaker and T. Sorokina. Smooth macro-elements on Powell-Sabin-12 splits. Math. Comp., 75:711–726, 2006.

[55] E. Süli and I. Mozolevski. hp-version interior penalty DGFEMS for the biharmonic equations. Comput. Methods Appl. Mech. Eng., 196:1851–1863, 2007.

[56] E. Vanraes, J. Windmolders, A. Bultheel, and P. Dierckx. Automatic construction of control triangles for subdivided Powell-Sabin splines. *Computer Aided Geometric Design*, 21:671–682, 2004.

[57] H. Yserentant. On the multi-level splitting of finite element spaces. *Numer. Math.*, 49:379–412, 1986.

[58] H. Yserentant. Two preconditioners based on the multi-level splitting of finite element spaces. Numer. Math., 58(2):163–184, 1990.

[59] J.-L. Zolesio. Interpolation d'espaces de Sobolev avec conditions aux limites de type mêlé. *C. R. Acad. Sc. Paris, Série A*, 285:621–624, 1977.